

Aus dem Institut für Schlaganfall- und Demenzforschung
Klinikum der Universität München, Großhadern
Direktor: Prof Dr. med. Martin Dichgans



Interactions between MIF-family proteins and the classical chemokine ligand/receptor network

Dissertation
zum Erwerb des Doktorgrades der Naturwissenschaften
an der Medizinischen Fakultät der
Ludwig-Maximilians-Universität zu München

vorgelegt von
Markus Brandhofer

aus
München

Jahr
2022

Mit Genehmigung der Medizinischen Fakultät
der Universität München

Betreuer: Univ.-Prof. Dr. rer. nat. Jürgen Bernhagen
Zweitgutachterin: Prof. Dr. Sabine Marten-Steffens
Dekan: Prof. Dr. med. Thomas Gudermann
Tag der mündlichen Prüfung: 05. Oktober 2022

Affidavit



Eidesstattliche Versicherung

Brandhofer, Markus

Name, Vorname

Ich erkläre hiermit an Eides statt,

dass ich die vorliegende Dissertation mit dem Titel

Interactions between MIF-family proteins and the classical chemokine ligand/receptor network

selbständig verfasst, mich außer der angegebenen keiner weiteren Hilfsmittel bedient und alle Erkenntnisse, die aus dem Schrifttum ganz oder annähernd übernommen sind, als solche kenntlich gemacht und nach ihrer Herkunft unter Bezeichnung der Fundstelle einzeln nachgewiesen habe.

Ich erkläre des Weiteren, dass die hier vorgelegte Dissertation nicht in gleicher oder in ähnlicher Form bei einer anderen Stelle zur Erlangung eines akademischen Grades eingereicht wurde.

München, 17.10.2022

Ort, Datum

Markus Brandhofer

Unterschrift Doktorandin bzw. Doktorand

Table of Contents

Affidavit	iii
Table of Contents	v
List of Figures	vii
List of Tables	ix
Abbreviations	xi
List of publications	xiii
1. Introduction	1
1.1. Chemokines – chemotactic cytokines	1
1.1.1. Chemokines as mediators of inflammation	3
1.1.2. Chemokines and their receptors – the chemokine network	5
1.1.3. The chemokine interactome	7
1.1.4. Atypical chemokines expand the chemokine network	10
1.2. Macrophage migration inhibitory factor and MIF-family proteins	10
1.2.1. Macrophage migration inhibitory factor	10
1.2.2. Interaction of MIF with chemokine receptors	12
1.2.3. Non-mammalian MIF-family proteins	14
1.3. Aim of the doctoral thesis	15
1.3.1. Part I: Interaction interface of MIF and its non-cognate receptor CXCR4 .	15
1.3.2. Part II: Ability of <i>AtMDLs</i> to interact with human CKRs	16
2. Own contributions to the publications	17
2.1. Publication I: Lacy <i>et al.</i> , 2018	17
2.2. Publication II: Sinitski <i>et al.</i> , 2020	18
3. Summary	19
4. Zusammenfassung	21
5. Publication I: Lacy <i>et al.</i>, 2018	25
6. Publication II: Sinitski <i>et al.</i>, 2020	43
A. Appendix	63
A.1. Additional findings on MIF’s interaction with the chemokine network	63
A.1.1. Screening for MIF and MIF-2 interactors and the discovery of the ACK/CK interactome	63

Table of Contents

A.1.2. Investigation of the novel MIF/CXCL4L1 heterocomplex	68
A.1.3. Expression and purification of CXCL4L1 and isotope-labeled MIF for NMR spectroscopy studies	132
A.2. Supplementary data	146
A.2.1. Supplementary data for Lacy <i>et al.</i> , 2018	146
A.2.2. Supplementary data for Sinitski <i>et al.</i> 2020	159
A.2.3. Supplementary data for manuscript by Brandhofer <i>et al.</i> , 2022	176
References	182
Acknowledgements	196
Curriculum vitae	199

List of Figures

1.1. Typical chemokine structure	2
1.2. Dimeric structure of CCL5 and CXCL5	3
1.3. Chemokines and their receptors in atherogenesis	6
1.4. Chemokine/Receptor network	8
1.5. Schematic description of the chemokine interactome	9
1.6. 3D-structure of human MIF	11
1.7. Two-site binding of MIF to CXCR2	13
A.1. Screening for MIF interactors via solid phase assay	65
A.2. Screening for MIF-2 interactors via solid phase assay	66
A.3. Schematic summary of MIF-family protein interactions with CKs and ACKs	67
A.4. Final purification of recombinant CXCL4L1 via size exclusion chromatography	135
A.5. Purification of ¹⁵ N-MIF by anion exchange chromatography	136
A.6. Purification of ¹⁵ N-MIF by size exclusion chromatography	137
A.7. Double isotope labeling of ¹⁵ N- ¹³ C-MIF	138
A.8. Purification of ¹⁵ N- ¹³ C-MIF by anion exchange chromatography	140
A.9. Purification of ¹⁵ N- ¹³ C-MIF by size exclusion chromatography	141

List of Tables

1.1. Chemokines and their receptors in disease	5
A.1. Results of interaction screening via solid phase assay	67
A.2. CXCL4L1 yield after SEC	133
A.3. ¹⁵ N-MIF yield after anion exchange chromatography	133
A.4. ¹⁵ N-MIF yield after SEC	134
A.5. ¹⁵ N- ¹³ C-MIF yield after anion exchange chromatography	138
A.6. ¹⁵ N- ¹³ C-MIF yield after SEC	139

Abbreviations

AtMDL	<i>A. thaliana</i> MIF/ <i>D</i> -dopachrome-tautomerase-like protein
ACK	Atypical chemokine
CCL	CC-type chemokine ligand
CCR	CC-type chemokine receptor
CD74	Cluster of differentiation 74
CK	(Classical) Chemokine
CKR	Chemokine receptor
CXCL	CXC-type chemokine ligand
CXCR	CXC-type chemokine receptor
D-DT	<i>D</i> -dopachrome-tautomerase
DAMPs	Damage-associated molecular patterns
DC	Dendritic cell
DTT	Dithiothreitol
ECL	Extracellular loop
EDTA	Ethylenediaminetetraacetic acid
ELR motif	glutamine-leucine-arginine tripeptide motif
FPLC	Fast protein liquid chromatography
GAGs	Glycosaminoglycans
GPCR	G protein-coupled receptor
HBD3	Human β -defensin 3
HMGB1	High mobility group box 1
HNP1	Human neutrophil peptide 1
HPLC	High performance liquid chromatography
HRP	Horseradish peroxidase

List of abbreviations

ICAM-1	Intercellular adhesion molecule 1
ICL	Intracellular loop
IEP	Isoelectric point
IMAC	Immobilized metal affinity chromatography
IPTG	Isopropyl β -D-1-thiogalactopyranoside
LB	Lysogeny broth
MES	2-(N-morpholino)ethanesulfonic acid
MHC	Major histocompatibility complex
MIF	Macrophage migration inhibitory factor
MW	Molecular weight
NIR	Near infrared
NMR	Nuclear magnetic resonance
PDB	Protein data bank
RANTES	Regulated on activation, normal T cell expressed and secreted (CCL5)
SEC	Size exclusion chromatography
SELE	Selectin E
SELP	Selectin P
SELPLG	Selectin P ligand
TFA	Trifluoroacetic acid
VCAM-1	Vascular cell adhesion molecule 1
XCL	C-type chemokine ligand

List of Publications

Journal Articles

- M. Lacy*, C. Kontos*, **M. Brandhofer***, K. Hille, S. Groning, D. Sinitski, P. Bourilhon, E. Rosenberg, C. Krammer, T. Thavayogarajah, G. Pantouris, M. Bakou, C. Weber, E. Lolis, J. Bernhagen and A. Kapurniotu. Identification of an Arg-Leu-Arg tripeptide that contributes to the binding interface between the cytokine MIF and the chemokine receptor CXCR4. *Sci Rep* **8**, 5171, doi:10.1038/s41598-018-23554-5 (2018).
- D. Sinitski, K. Gruner, **M. Brandhofer**, C. Kontos, P. Winkler, A. Reinstadler, P. Bourilhon, Z. Xiao, R. Cool, A. Kapurniotu, F. J. Dekker, R. Panstruga and J. Bernhagen. Cross-kingdom mimicry of the receptor signaling and leukocyte recruitment activity of a human cytokine by its plant orthologs. *J Biol Chem* **295**, 850-867, doi:10.1074/jbc.RA119.009716 (2020).
- C. Krammer, C. Kontos, M. Dewor, K. Hille, B. Dalla Volta, O. El Bounkari, K. Taş, D. Sinitski, **M. Brandhofer**, R. T. A. Megens, C. Weber, J. R. Schultz, J. Bernhagen and A. Kapurniotu. A MIF-derived cyclopeptide that inhibits MIF binding and atherogenic signaling via the chemokine receptor CXCR2. *ChemBioChem* doi:10.1002/cbic.202000574 (2020)
- C. Kontos, O. El Bounkari, C. Krammer, D. Sinitski, K. Hille, C. Zan, G. Yan, S. Wang, Y. Gao, **M. Brandhofer**, R. T. A. Megens, A. Hoffmann, J. Pauli, Y. Asare, S. Gerra, P. Bourilhon, L. Leng, H. H. Eckstein, W. E. Kempf, J. Pelisek, O. Gokce, L. Maegdefessel, R. Bucala, M. Dichgans, C. Weber, A. Kapurniotu and J. Bernhagen. Designed CXCR4 mimic acts as a soluble chemokine receptor that blocks atherogenic inflammation by agonist-specific targeting. *Nat Commun* **11**, 5981, doi:10.1038/s41467-020-19764-z (2020)
- E. Hofmann, J. Soppert, T. Ruhl, G. Gousopoulos, S. Gerra, G. Storti, Y. Tian, **M. Brandhofer**, R. Schweizer, S.-Y. Song, N. Lindenblatt, N. Pallua, J. Bernhagen and B.-S. Kim. The Role of Macrophage Migration Inhibitory Factor in Adipose-Derived Stem Cells Under Hypoxia. *Front Physiol* **12**, 638448, doi:10.3389/fphys.2021.638448 (2021)
- **M. Brandhofer** and J. Bernhagen. Cytokine aerobics: Oxidation controls cytokine dynamics and function. *Structure* **30**, 787-790, doi:10.1016/j.str.2022.05.005 (2022)
- **M. Brandhofer***, A. Hoffmann*, X. Blanchet, E. Siminkovitch, A-K. Rohlfling, O. El Bounkari, J. Nestele, A. Bild, C. Kontos, K. Hille, V. Rohde, A. Fröhlich, J. Golemi, O. Gokce, C. Krammer, P. Scheiermann, N. Tsilimparis, N. Sachs, W. Kempf, L. Mägdefessel, M. K. Otabil, R. T. A. Megens, H. Ippel, R. Koenen, J. Luo, B. Engelmann, K. H. Mayo, M. Gawaz, A. Kapurniotu, C. Weber, P. von Hundelshausen and J. Bernhagen. Heterocomplexes between the atypical chemokine MIF and the CXC-Motif chemokine CXCL4L1 regulate inflammation and thrombus formation. *Cell Mol Life Sci.*, **79**, 512, doi:10.1007/s00018-022-04539-0 (2022)
- Y. Asare, M. Shnipova, L. Živković, C. Schlegl, F. Tosato, A. Aronova, **M. Brandhofer**, L. Strohm, N. Beaufort, R. Malik, C. Weber, J. Bernhagen and M. Dichgans. IKK β binds NLRP3 providing a shortcut to inflammasome activation for rapid immune responses. *Sig Transduct Target Ther* **7**, 355, doi:10.1038/s41392-022-01189-3 (2022)

- C. Zan, B. Yang, **M. Brandhofer**, O. El Bounkari and J. Bernhagen. D-dopachrome tautomerase in cardiovascular and inflammatory diseases – A new kid on the block or just another MIF? *FASEB J.* **36**, 11, doi:10.1096/fj.202201213R (2022)

Preprints and Manuscripts

- O. El Bounkari, C. Zan, J. Wagner, E. Bugar, P. Bourilhon, C. Kontos, M. Zarwel, D. Sinitiski, J. Milic, Y. Jansen, W. Kempf, L. Mägdefessel, A. Hoffmann, **M. Brandhofer**, R. Bucala, R. Megens, C. Weber, A. Kapurniotu, and J. Bernhagen. MIF-2/D-DT is an atypical atherogenic chemokine that promotes advanced atherosclerosis and hepatic lipogenesis. *bioRxiv*, doi:10.1101/2021.12.28.474328 (2021)

Conference Talks

- **M. Brandhofer**, X. Blanchet, A. Hoffmann, P. von Hundelshausen, C. Weber, J. Bernhagen. Novel interaction of MIF with CXCR3 ligand CXCL4L1. In: II Joint Meeting of the German Society for Immunology and the Italian Society of Immunology, Clinical Immunology and Allergology (48th Annual Meeting of the German Society for Immunology), Munich (Germany). September 10th to 13th, 2019.
- **M. Brandhofer**, A. Hoffmann, X. Blanchet E. Siminkovitch, A. Rohlfig, O. El Bounkari, J. Nestele, K. Hille, C. Kontos, V. Rohde, A. Fröhlich, J. Golemi, O. Gokce, P. Scheiermann, N. Tsilimparis, H. Ippel, R. Koenen, K. Mayo, M. Gawaz, A. Kapurniotu, C. Weber, P. von Hundelshausen, J. Bernhagen. Heterocomplexes between the Atypical Chemokine MIF and the CXC-Motif Chemokine CXCL4L1 Regulate Inflammation and Thrombus Formation. In: European Society for Microcirculation Online Meeting, Aarhus (Denmark); Online event. May 27th, 2021.

Poster Presentations

- **M. Brandhofer**, A. Hoffmann, X. Blanchet, C. Krammer, P. Bourilhon, C. Kontos, C. Weber, A. Kapurniotu, P. von Hundelshausen, J. Bernhagen. The atypical chemokine interactome as a novel regulatory cue in inflammation? In: Institute for Stroke and Dementia Research Retreat 2019, Herrsching (Germany). July 10th and 11th, 2019.
- **M. Brandhofer**, A. Hoffmann, X. Blanchet, C. Krammer, H. Ippel, K. H. Mayo, P. Bourilhon, C. Kontos, C. Weber, A. Kapurniotu, P. von Hundelshausen, J. Bernhagen. The atypical chemokine interactome as a novel regulatory cue in inflammation? In: ISD Advisory Board Meeting, Munich (Germany), July 30th, 2019.
- **M. Brandhofer**, A. Hoffmann, X. Blanchet, E. Siminkovitch, A.-K. Rohlfig, O. El Bounkari, J. A. Nestele, K. Hille, C. Kontos, V. Rohde, A. Fröhlich, J. Golemi, O. Gokce, P. Scheiermann, N. Tsilimparis, W. Kempf, L. Mägdefessel, H. Ippel, R. R. Koenen, K. H. Mayo, M. Gawaz, A. Kapurniotu, C. Weber, P. von Hundelshausen, J. Bernhagen. Heterocomplexes between the atypical chemokine MIF and the CXC-motif chemokine CXCL4L1 regulate inflammation and thrombus formation. In: 9th Cardiac Regeneration and Vascular Biology Conference, San Servolo, Venice (Italy). October 18th to 20th, 2021.

1. Introduction

1.1. Chemokines – chemotactic cytokines

Being able to sense signals from the surrounding environment and responding to them provides a crucial advantage even for comparatively simple, unicellular lifeforms. Basic examples are flagellated bacteria, greatly benefiting from the ability to sense nutrients and travel towards them, thereby demonstrating the essential principle of “chemotaxis”. Derived from “chemo-” and the ancient greek “τάξις” (τάξις), translating to “arrangement” or “order”, the term chemotaxis describes directed movement along the concentration gradient of a chemical stimulus, e.g., the movement of a bacterium towards a nutrient like glucose [1]. Signal input is not limited to purely chemical stimuli from nutrients, though. A more complex signal exchange can be exemplified by the mating of yeast cells, e.g., haploid cells of *Saccharomyces cerevisiae*, which are able to secrete mating pheromones that act on haploid *S. cerevisiae* cells of the opposing mating-type and induce them to undergo polarization in order to facilitate mating [2]. This concept of exchanging signals, and the subsequent processing of these signals, gets vastly more complex when we look at multicellular organisms. The exchange of information between cells is however vital for complex organisms in order to function by maintaining ordered cellular structures, tissues and organs and allowing these systems to work together [3].

Looking at chemotaxis, especially in the mammalian system, it is clear that this process needs to be well regulated, as there are numerous cellular functions where directed movement is essential. These encompass a vast variety of processes from embryogenesis and homeostasis to the response of the immune system to, e.g., invading pathogens like gram-negative bacteria, that can be detected by the lipopolysaccharides on their outer membrane [4]. While many substances, from comparatively simple chemical compounds to complex proteins, are able to function as cues to induce cellular responses or allow for the exchange of information between cells, one family of signaling compounds is of special importance: the cytokines [5, 6].

This group of signaling molecules consists of various small proteins – roughly 5 to 20 kDa in molecular weight – that can be secreted by one cell and induce a signaling cascade in another cell by activating their respective cytokine receptor. Based on their structure as well as their function, cytokines can again be divided into separate subgroups like interferons, interleukins, colony stimulating factors and chemokines. However, a clear distinction between those subgroups may not always be possible, as the exact same cytokine can be classified as both an interleukin and a chemokine, like for example the interleukin IL-8, which is also known as the chemokine CXCL8 [5, 7, 8].

This section of the introduction now will focus on the chemotactic subgroup of the cytokines, aptly named chemokines (CKs). These 8 to 12 kDa proteins are important inflammatory and homeostatic mediators, orchestrating the recruitment of immune cells to sites of injury or infection but also playing a regulatory role in immune surveillance [9–11]. They differ from other cytokines not only in their effect, but also in their structure and the receptors they engage to exert their function. As opposed to other cytokines that interact with type I, single pass transmembrane receptors (or oligomeric complexes thereof), chemokines are ligands

1. Introduction

for G protein-coupled receptors (GPCRs), also known as 7-pass transmembrane receptors [7, 10]. This receptor-ligand interaction will be explained further in section 1.1.2 of this chapter. Chemokines are also divergent from other cytokines in their 3D-structure, as they show a conformation generally known as the “chemokine fold”, depicted in figure 1.1. This conformation, with a conserved N-terminal cysteine motif, the β -sheet motif and an α -helix, is essential for GPCR interactions [12, 13]. Currently, there are roughly 50 human chemokines known, along with 23 chemokine receptors [10, 14–16].

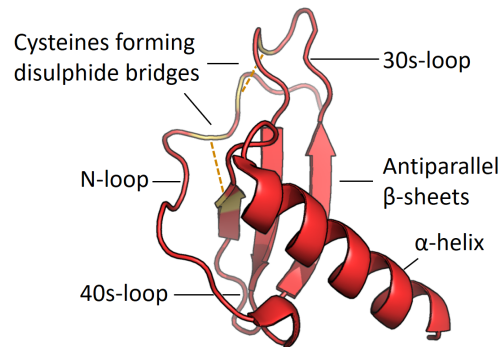


Figure 1.1.: Typical 3D-structure of classical chemokines, known as the “chemokine fold”, exemplified by human CXCL8 in its monomeric state. This structure with two disulphide bridges (one for XCL1 and XCL2) is highly conserved among chemokines and necessary for interaction with chemokine receptors [12, 13]. The 3D-structure was rendered with PyMOL based on PDB entry 4XDX [17].

This cysteine motif is also the basis for the systematic nomenclature of the classical chemokines, allowing a classification of these proteins into four different groups. Depending on the number of amino acids between the first two cysteine residues, they are referred to as C, CC, CXC and CX₃C-type chemokines – where in CC-type chemokines the first two cysteines are adjacent and one or three amino acids are between them for CXC- and CX₃C-type chemokines. C-type chemokines – XCL1 and XCL2 – are an exception here, having only two cysteine residues in total, one in the N-terminal region and the second further towards the C-terminus [13, 16]. CXC-type chemokines can again be divided into two subgroups, based on an N-terminal motif of adjacent Glu-Leu-Arg (ELR) residues, resulting in ELR⁺ and ELR⁻ CXC-type chemokines. This tripeptide motif also plays a role in the binding of these chemokines to their receptors [10, 13].

It is widely reported that chemokines can interact with their receptors as monomers to exert their function, even though they have the propensity to oligomerize as it has been shown in X-ray crystallography as well as via NMR spectroscopy in solution [11, 18–20]. Usually, chemokines form dimers, but also higher-order oligomers have been reported, for example in the case of the platelet-chemokine CXCL4L1, which is capable of forming tetrameric as well as dimeric complexes [21, 22]. The oligomerization of chemokines is seen as a way of modulating their activity, since by this process the concentration of CKs in their active state can be reduced – or the flexibility of chemokines, locked in the oligomeric state, altered to a level that interferes with receptor binding and activation [11, 13, 20]. On the example of the CXCR4-ligand CXCL12, present in both monomeric and dimeric conformation at physiological concentrations, it has been demonstrated that depending on the oligomerization state of the same chemokine, either β -arrestin- or G protein-dependent signaling can be favoured – underlying the complexity of the chemokine network with numerous mechanisms for adjustment and fine-tuning [23,

24]. Notably, even though CKs share a conserved 3D-structure, there are differences in dimer-formation between CC- and CXC-type chemokines. As depicted in figure 1.2, CC-type chemokines usually dimerize by interaction of their N-terminal region under formation of a β -sheet structure, while CXC-type chemokines form dimers by extending their pre-existing β -sheet motif [11, 20, 25]. These modes of dimerization are also named accordingly, and it has been observed that CC-type dimerization tends to enhance CK activity, while it is reduced for the CXC-type [26].

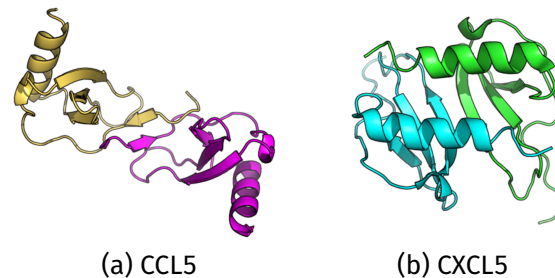


Figure 1.2.: Dimer formation differs between CC-type and CXC-type chemokines, shown on the example of homo-dimers of human CCL5 and CXCL5. Dimerization by the CC-type (a) yields a more elongated complex, formed by interaction the N-terminal regions of the chemokines, while the CXC-type dimer (b) results in a more globular shape with an extended β -sheet motif. Structures are visualized according to PDB IDs 5COY (CCL5) and 2MGS (CXCL5).

1.1.1. Chemokines as mediators of inflammation

Based on their function, it is clear that chemokines play an important physiological role, not only during immune surveillance but also in inflammation [9]. This complex task is, for example, controlled by the chemokine receptor profile, that is expressed in certain immune cell types and determines the cellular response to certain chemokines. Accordingly, cells secrete chemokines to their surrounding tissue – the extracellular space or, for example in the case of vascular endothelial cells, into the circulation – to generate a chemokine gradient, along which immune cells with the corresponding chemokine receptor can migrate towards their target [11, 27, 28]. This process is exemplified in the transendothelial migration of leukocytes, which is mediated by adhesion molecules and chemokines [29]. Such a haptotactic chemokine gradient can for example be formed on the cell surface of endothelial cells lining the vasculature, but also in the extracellular space. Essentially, the molecular entities that aid in immobilizing chemokines and forming haptotactic gradients are glycosaminoglycans (GAGs) and non-signaling chemokine receptors [30, 31].

While chemokines are known to act via their receptors, certain CKs like CXCL4 and CXCL8 were found to be able to bind to heparane sulfate and other GAGs, allowing for gradients of immobilized chemokines [32, 33]. This haptotactic – as opposed to a chemotactic – migration mechanism has indeed already been found in the example of neutrophils and CXCL8 by A. Rot in 1993 [34]. While the immobilization of chemokines is of great importance in the circulation, preventing them to be washed away under flow conditions and getting diluted below their active concentration, interaction with GAGs can also aid in the oligomerization of chemokines [30]. Thereby, GAG-interactions of chemokines are a way of modulating their function [12, 35]. An interesting observation regarding GAG-binding and chemokine structure was made by Je-Hung Kuo *et al.*, when they solved the X-ray structure of CXCL4L1. This CXCL4 homologue with a

1. Introduction

strong anti-angiogenic effect presented a novel, alternative conformation of its α -helix, that interferes with the GAG-binding ability of this chemokine. This in turn, they argue, enhances the ability for interactions with CXCR3, leading to the more potent anti-angiogenic effect [36]. However, the ability of chemokines to bind both GAGs and chemokine receptors, together with the observation that GAG-binding seems essential for the activity of certain chemokines *in vivo* but not *in vitro*, raised new questions. The seeming necessity of soluble, monomeric chemokines for receptor activation contrasts the current “bridge-model” of ternary GAG-CK-CKR complexes, leading to the proposed concept of a more loose, electrostatically bound *chemokine cloud* within the glycocalyx. Thus, the precise modes of chemokine presentation and their interaction with both GAGs and receptors, in addition to their oligomerization state, is still a matter of debate in the field [30, 37, 38].

Another way of sequestering chemokines is by the means of non-signaling chemokine receptors, also named *decoy-* or *scavenger-receptors* [31]. These GPCRs, matching the typical CKR nomenclature, are also referred to as atypical chemokine receptors (ACKRs) – especially since they can still be involved in ligand-dependent actions, *de facto* making them signaling receptors despite not inducing chemotactic effects in the same manner as classical CKRs [16]. One example of such an ACKR is ACKR3 or CXCR7 – a scavenger receptor for CXCL12 and CXCL11, that is capable of β -arrestin signaling and also a non-cognate receptor for the chemokine-like cytokine MIF, that will be covered in section 1.2 of this chapter [16, 39, 40]. Unlike GAGs, ACKRs do not seem to be involved in immobilizing chemokines in order to present them to other molecular entities. Furthermore, via internalization they can actively direct chemokines towards lysosomal degradation, offering another mechanism to regulate chemokine function by degradation [16, 41]. A more detailed overview of various chemokine receptors will be given in part 1.2.2 of this introduction.

The complex relationships between chemokines and their receptors, the affected immune cell subsets and their role in various diseases has been extensively studied [8–10, 42]. While a more detailed overview of chemokine/receptor interactions is given in the next section, a selection of chemokine receptors, their ligands, involved cell types and corresponding disease settings can be found in table 1.1. For example, chemokines are critically involved in inflammation of the central nervous system as well in the initiation and progression of atherosclerosis [43, 44]. Here it is important to note that chemokines, as regulators of immunity and inflammation, can play both beneficial and detrimental roles in a given disease context. In atherosclerosis, for example, distinct subsets of chemokines are involved in the recruitment of monocytes and neutrophils (e.g., CXCL1 and CCL20), while other chemokines play a role in homeostatic processes (e.g., CXCL5 and CXCL12) [42, 45]. Figure 1.3, taken from a review article from Weber and Noels, highlights the role of chemokines and their receptors in atherogenesis [46].

Despite their name, the function of chemokines is not strictly limited to chemotactic or haptotactic effects. Interestingly, CX₃CL1 (Fractalkine) exists not only as a soluble chemokine, but also as a membrane-anchored form that acts as an adhesion molecule during the adhesion and transmigration of leukocytes that express CX₃CR1 [16, 47]. Additionally, CX₃CL1 has been shown to be a survival factor for monocytes [48, 49]. On the example of atherosclerosis, chemokines also play certain non-chemotactic roles. Here, CXCL5 limits the formation of foam cells by upregulating a transporter protein responsible for cholesterol efflux from macrophages [42]. CXCL5 affects macrophages as well, promoting a shift to the more pro-inflammatory M4 phenotype [50]. Certain chemokines also show the ability to influence the cell differentiation, regulating for example T cell fate [51]. Other functions include angiogenesis, where ELR⁺ CXC-type chemokines generally promote angiogenesis, while their ELR⁻ counterparts have

Table 1.1.: Chemokines mediate immune cell recruitment via chemokine receptors expressed on distinct leukocyte types. This table combines data from multiple sources, providing selected examples for chemokine/receptor interactions in a disease context [10, 16, 42]. Ca: cancer cells, DCs: dendritic cells, ECs: endothelial cells, Ma: mast cells, Mono: monocytes, Neu: neutrophils, NHCs: non-hematopoietic cells.

Receptor	Chemokine	Cell type	Disease context
CXCR2	CXCL1, CXCL2, CXCL3, CXCL5, CXCL6, CXCL8	Mono, Neu, ECs, Ca	COPD, atherosclerosis, angiogenesis
CXCR3	CXCL4, CXCL4L1, CXCL9, CXCL10, CXCL11	T cells, B cells, ECs, Ma	Infl. skin disease, rheumatoid arthritis, mucosal immunity
CXCR4	CXCL12	Most leukocytes, NHCs	Atherosclerosis, tumor metastases
CCR6	CCL20	T cells, B cells, DCs, Mono	Atherosclerosis, T cell homing, mucosal immunity

mostly angiostatic effects [13]. Overall, the classical chemokines and their receptors play a role also in areas like cellular development, differentiation and survival, embryonic development, phagocytosis and others [41]. This demonstrates activities of chemokines well beyond their initial description as cytokines responsible for cellular movement.

1.1.2. Chemokines and their receptors – the chemokine network

As explained above, chemokines are important mediators of immunity, shaping its cellular response to insults by orchestrating recruitment of leukocytes. This important task relies on the interaction of CKs with their receptors. These receptors are named in a similar schematic as the chemokines, with the letter “R” for example in CXCR4 indicating the role as a receptor, as opposed to the “L” for ligand in, e.g., CXCL12 [16, 52]. CKRs are G protein-coupled receptors with 7 transmembrane-domains, which connect extra- and intracellular loops (ECLs and ICLs). They facilitate signal transmission across the cell membrane via conformational changes. Extracellular signaling events – binding of a ligand with the receptor’s N-terminus and ECLs, leading to receptor activation – induce conformation changes in the transmembrane domains, resulting in intracellular signaling via $G\alpha_i$ G-proteins or β -arrestins [41, 53].

The initiation of this process, the interaction of a chemokine with its receptor, is traditionally described by a two-step / two-site model. This model, dating back to the 1990s, provides a functional and spatial separation of ligand-binding. Numerous studies demonstrated the importance of the chemokine receptor’s N-terminus in recognizing the globular core-region of the chemokine, forming the site 1 interaction. Here, in place of the core region of the CK, the N-loop is mentioned in the literature as well [12]. From a functional aspect, this first step is seen to facilitate selective ligand binding. This is followed by receptor activation in the site 2 interaction, where residues of the chemokine’s unstructured N-terminus enter the ligand binding pocket of the receptor. This ligand binding pocket for the site 2 interaction reportedly consists of the receptor’s ECLs and/or transmembrane domain, depending on the CK receptor and the literature [12, 41, 54, 55].

In the light of recent crystallography studies and detailed molecular dynamics simulations, aimed at elucidating the intramolecular processes that go along with ligand binding and GPCR activation, it became more and more clear that the two-site model can be overly simplistic [23, 41]. As extensively reviewed by A. B. Kleist *et al.* in 2016, both site 1 and site 2 interactions show far more complexity under recent investigations. Site 2, for example, can again be divided into

1. Introduction

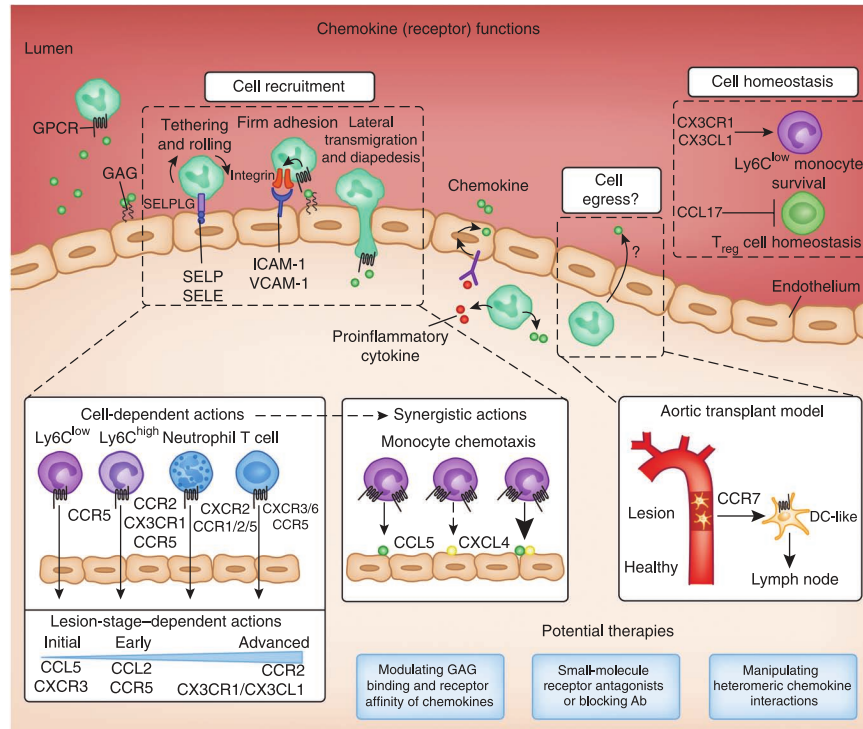


Figure 1.3.: Function of chemokines and their receptors in atherogenesis, with roles in both cell recruitment, as well as cellular homeostasis. Briefly, chemokines recruit leukocytes to sites of vascular inflammation, where immobilized CKs together with adhesion molecules aid in their transendothelial migration. Recruitment of cells is orchestrated by various chemokines in a both cell and disease-state dependent manner, using also synergistic CK effects and thereby exemplifying the robustness and complexity of the chemokine system. Potential therapeutic strategies to interfere in this system are presented in blue boxes. Used abbreviations: SELPLG: selectin P ligand, SELP: selectin P, SELE: selectin E, ICAM-1: intercellular adhesion molecule 1, VCAM-1: vascular cell adhesion molecule 1. Schematic taken from Weber and Noels, 2011 [46].

a major and a minor subpocket, each with its individual role for ligand interactions. In summary, this leads to numerous possible variables in chemokine/receptor interactions on every step of the ligand-binding and receptor-activation process, including specific interactions between residues, the orientation and binding-depth of the chemokine and allosteric effects, all affecting the final outcome of this interaction [55]. This is even further complicated by the dimerization of not only chemokines but also receptors, as the precise stoichiometry of CK-CKR-complexes is still incompletely understood and under debate [54, 55].

While some CKRs perform their function as homodimers (a dimer formed by two identical receptors), also heteromeric complexes exist, providing another regulatory mechanism in the chemokine network [20, 56]. For example, it has been reported that CXCR7, by hetero-complex formation, influences CXCL12/CXCR4-signaling by impairing G protein signaling via CXCR4 [57]. As stated above in section 1.1, there are roughly twice as many chemokines as there are chemokine receptors – this already indicates that in the chemokine network, receptor/ligand interactions are bound to show some extent of promiscuity. The fact that most chemokines interact with more than one chemokine receptor – and accordingly, many CKRs are targeted by

more than only one ligand – is a well-studied characteristic of this network, exemplified above in table 1.1, and figure 1.4 shows a comprehensive summary of chemokine/receptor interactions.

The already complex receptor/ligand network of chemokines also shows a certain level of redundancy, as many cells can produce numerous chemokines that are able to elicit the same effect, and also immune cells are known to express more than one specific chemokine receptor. This seeming redundancy however, in addition to providing a mechanism for fine-tuning of chemokine actions, adds to the robustness of the chemokine network [16, 41, 58]. Since the chemokine system is essential for key functions of, e.g., the immune system, a certain level of robustness is an evolutionary desirable feature. From that point of view, “securing” this system against disruptions, with another player of this system being able to at least partially take over, should, for example, genetic mutations rendering a certain CK or CKR non-functional, would be of great benefit [14, 58].

This level of robustness also comes into play when we look at defense mechanisms against parasites and pathogens. As the chemokine network is of crucial importance for immune functions, it is not surprising that pathogens evolved strategies to evade or modulate the hosts defensive mechanisms since, e.g., ticks employing chemokine-capturing proteins – evasins – in their saliva to interfere with the human chemokine and immune system [16, 41, 59, 60]. In addition to parasites, viral pathogens as well are known to exploit this regulatory system. Especially certain herpesviruses have been shown to exploit the chemokine network through *molecular mimicry* – by expressing viral mimics of CKs and CKRs – in order to enhance their pathogenicity [61, 62].

Generally, the complexity as well as redundancy of the human chemokine system can be explained by ligand-, receptor- and tissue-bias [63, 64]. Not only can different ligands have different affinities towards the same CKR, they might also elicit a different signaling response from the same receptor - a mechanism also called *biased agonism* [20]. The same CKR could thereby lead to G protein signaling, β -arrestin signaling or internalization, depending on which ligand activates the receptor, in a concept named *ligand-bias* [41, 63]. *Receptor-bias*, on the other hand, is a concept by which the same chemokine might induce different signaling outcomes in different receptors. For example, one chemokine could be an agonist of one CKR, but an antagonist of another [20, 63]. Lastly, there is the concept of tissue- or system-bias. This reflects expression patterns of chemokines and their receptors in various tissues and cell types, leading to situations where a chemokine effect might be tissue or organ dependent [63, 64].

1.1.3. The chemokine interactome

In section 1.1, it was already discussed that classical chemokines are able to form homodimers or higher oligomers, however also heteromeric complexes can be formed. These oligomers – usually dimers – can be formed within or across the chemokine-subtypes, giving rise to a vast amount of possible interactions, also referred to as the “chemokine interactome” [13, 14, 65]. While many heteromeric chemokine dimers have been reported, one of the most extensively studied ones is the CCL5/CXCL4-complex [66–68]. After it was discovered in 2005 that the platelet chemokines CCL5 (also known as RANTES) and CXCL4 could hetero-dimerize and thereby enhance the adhesion of monocytes on the endothelium, the role of this heteromer was studied further in the context of atherosclerosis. Here, the pro-inflammatory role of this complex in monocyte recruitment was investigated, including deployment of peptides, designed to interfere with CCL5/CXCL4-interaction. This showed that the targeting of chemokine/chemokine interactions could be a feasible therapeutic approach in atherosclerosis, in addition to targeting

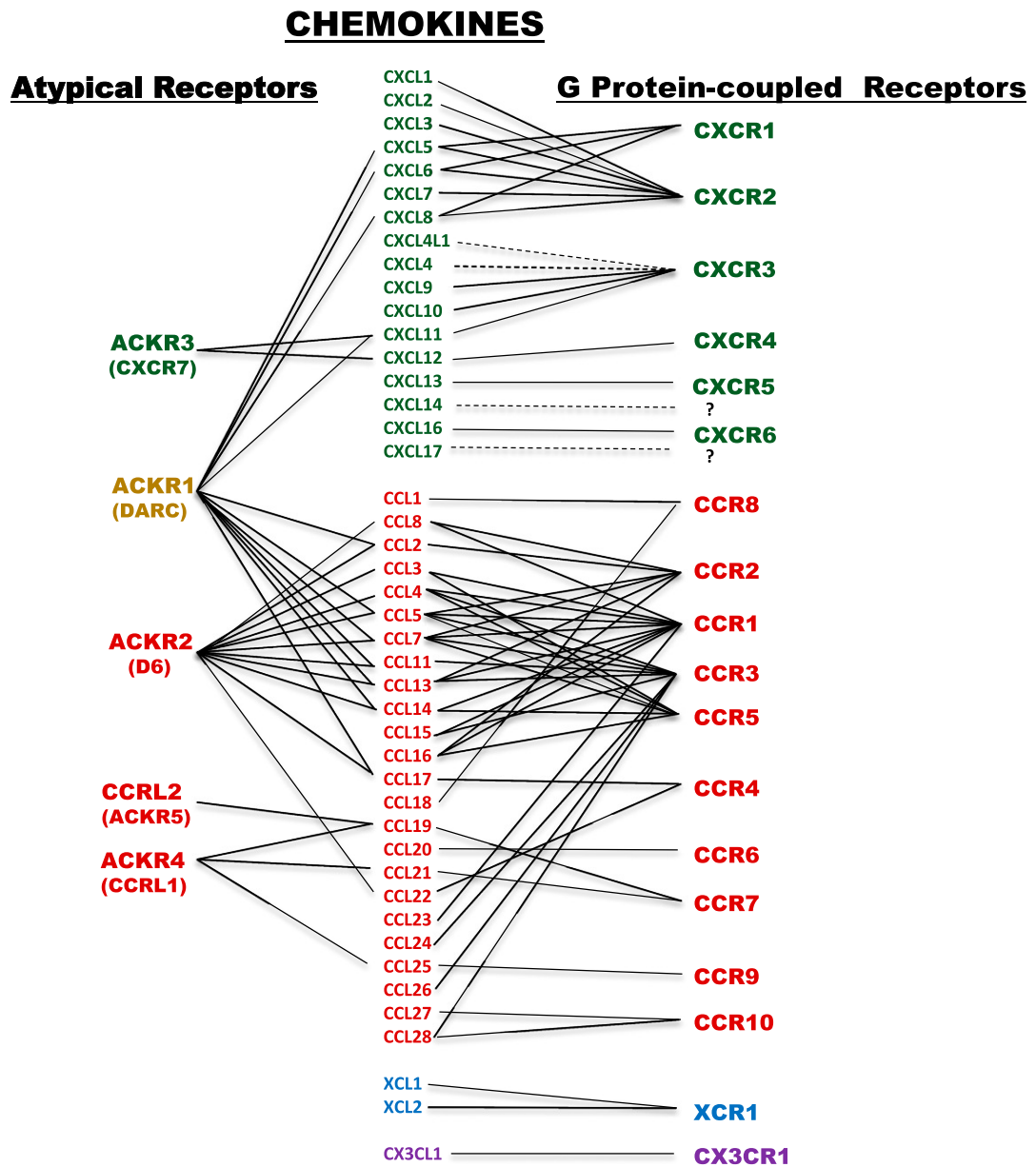


Figure 1.4.: The chemokine and chemokine receptor network. Receptor and ligand pairs are indicated with a solid line, putative interactions with a dotted line. The not yet identified receptors for CXCL14 and CXCL17 are indicated by a question mark. This schematic overview has been taken from F. Bachelierie *et al.* 2014 and slightly modified [16].

chemokine/receptor interactions [26, 65, 66, 69]. Inhibiting the formation of the CCL5/CXCL4 complex was also investigated in the context of acute lung injury, where this approach was beneficial as well, reducing tissue damage in a mouse model [70]. Additionally, the significance of this hetero-dimer was underlined by studies involving a covalently bound CCL5/CXCL4-complex [71]. Larger scale investigations on chemokine/chemokine interactions, using both *in vitro* as well as *in silico* approaches also show the prevalence of this chemokine interactome as regulatory and fine-tuning mechanism in the chemokine network [26, 72].

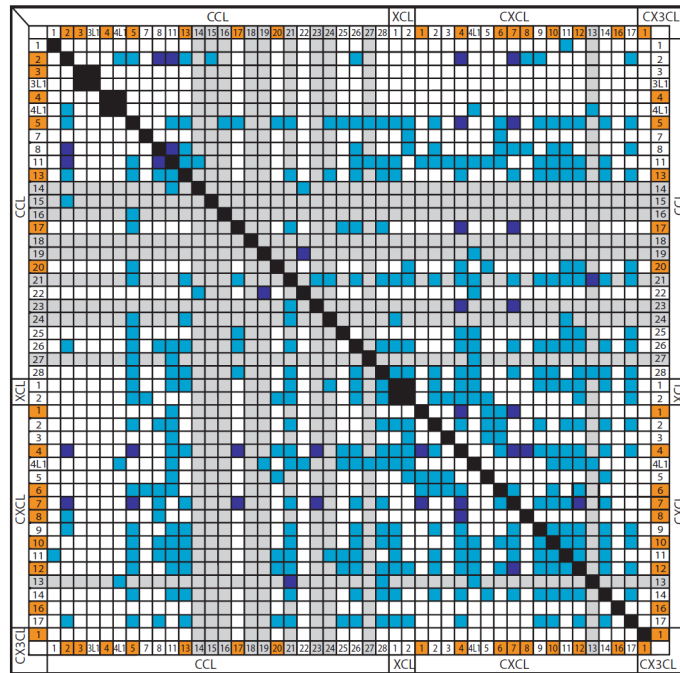


Figure 1.5.: The chemokine interactome, showing interactions among the classical chemokines. Light blue squares ■ indicate positive signal in bidirectional immunoligand blotting studies, dark blue squares ■ symbolize interactions that were previously identified by other experimental methods. White □ or grey □ squares indicate no interaction of chemokines, while chemokine-pairs where antibody binding could not distinguish between immobilized and soluble (complexed with immobilized) chemokine are shown in black ■. The chemokines with a known atherogenic role are highlighted in orange ■, while a grey color ■ marks nonmucosal, homeostatic chemokines. Taken from von Hundelshausen *et al.* 2017 [26].

While the focus of the chemokine interactome lies on interactions among chemokines, also some other proteins have been found to heteromerize with chemokines to modulate their function. One example of such an interaction was already mentioned above, with Evasin-3 – secreted in the saliva of the common brown dog tick (*Rhipicephalus sanguineus*) – found to exert anti-inflammatory effects by binding CXCL8 with nanomolar affinity and inhibiting chemokine/receptor interactions [60, 73]. In addition to Evasins, there are also viral proteins with a chemokine-binding ability that aid in evading the host immune system [16]. Another well known example of such an interaction, here within the human system, is HMGB1: This nuclear protein is able to function as a danger signal once released in the extracellular space [74]. In its fully reduced form, it is also able to heteromerize with CXCL12 to significantly enhance the CKs CXCR4-mediated signaling abilities [75, 76]. Another hetero-dimer that increases a CKs potential to recruit monocytes was found in a complex of CCL5 with the neutrophil-derived

1. Introduction

α -defensin HNP1 [77]. Recently, a systematic study found that both galectin-1 and galectin-3 are able to interact with XC-, CC-, and CXC-type chemokines and upon closer investigation, galectin-3 was shown to reduce CXCL12-mediated leukocyte recruitment and signaling via CXCR4 by formation of a heteromeric complex [78]. These examples highlight, that the chemokine network is also regulated on the level of protein-protein interactions without direct involvement of chemokine receptors – both via complex formation among chemokines, but also by interactions of chemokines with other proteins, that modulate chemokine effects in addition to their own unique function.

1.1.4. Atypical chemokines expand the chemokine network

While this section so far has focused on classical chemokines, it is important to note that there are also other proteins that can exert a chemokine-like function – so called *atypical chemokines* or ACKs [79]. Initially, it has been found that certain proteins have the ability to target classical chemokine receptors in order to facilitate chemotactic effects, even though these proteins do not share the conserved structure of CKs. Proteins that possess a chemokine-like function, commonly feature this as an additional “multitasking” role to other, e.g., intracellular, functions. One of these ACKs is the already mentioned HMGB1, a nuclear protein that also shows chemotactic abilities, but also other proteins like MIF (macrophage migration inhibitory factor, discussed in greater detail in the next section) or CKLF1 (chemokine-like factor 1) fall into this category [80, 81]. Thus, by employing chemokine receptors to mediate chemotactic effects, ACKs represent yet another functional and modulatory layer of the already complex chemokine network, despite deviating from the common chemokine structure.

1.2. Macrophage migration inhibitory factor and MIF-family proteins

Among the first cytokines discovered, described in 1966, is *macrophage migration inhibitory factor* (MIF). It is named after the observed inhibitory effect on random migration of macrophages, attributed to a soluble factor in the supernatant of T cells. This factor was then discovered to be the protein now known as MIF – although the initially studied supernatants likely also contained a mixture of numerous other migration modulating proteins, e.g., IL-4 and IFN- γ [82, 83]. Apart from its founding member, the MIF protein family also consists of the MIF paralog *D*-dopachrome tautomerase (D-DT or MIF-2) as well as many MIF-like orthologs of this evolutionary highly conserved protein, found in numerous species [84, 85].

MIF-2, the second discovered mammalian MIF-protein, even though sharing only a low amino acid homology to MIF, was found to exhibit a significant similarity to MIF regarding its 3D-structure [86]. Later studies showed MIF-2 to possess similar properties compared to MIF, regarding receptor binding and induced signaling pathways [84, 87].

MIF, which this work focuses on, will be introduced more thoroughly in the next section of this chapter, while the non-mammalian MIF orthologs will be briefly discussed in section 1.2.3 of this thesis.

1.2.1. Macrophage migration inhibitory factor

The various functions as well as the structure and properties of *macrophage migration inhibitory factor* have been extensively studied since its discovery more than five decades ago. MIF was not biochemically characterized until more than 20 years after its discovery, when cDNA of human MIF was successfully cloned [88]. Cloning and recombinant expression of both murine and

1.2. Macrophage migration inhibitory factor and MIF-family proteins

human MIF as well as the creation of a *Mif*-knockout mouse line greatly helped to advance research on this protein [88–90]. Structure elucidation via X-ray crystallography showed MIF to be a trimeric protein, with identical subunits of 114 amino acids and a molecular weight of 12.3 kDa. However, other studies reported an equilibrium of mono-, di- and trimeric states of MIF in solution under physiological conditions [91–94]. A visualization of human MIF in both monomeric and trimeric state is depicted in figure 1.6.

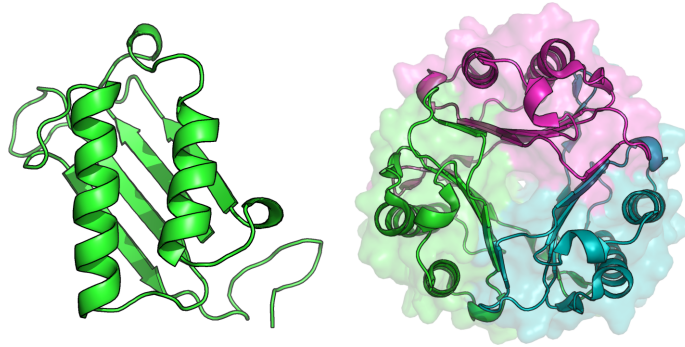


Figure 1.6.: 3D-structure of human MIF. Left: MIF monomer. Right: Trimeric MIF, visualized with half-transparent surface area. The subunits are depicted in cyan, green and magenta. Renderings, done with PyMOL, are based on PDB entry 3DJH [95].

Unlike many other pro-inflammatory cytokines, MIF is expressed not only in immune cells – including thrombocytes – but also by many other cell types like epithelial cells, fibroblasts and hepatocytes, resulting in an almost ubiquitous expression [88, 96, 97]. Macrophages and T cells, but also platelets, have been shown to store MIF in pre-formed pools to release it upon, e.g., pro-inflammatory, stimuli [98–100]. Recent studies show that under homeostatic conditions, MIF is constitutively released from immune cells but its secretion is upregulated upon cytotoxic stimuli, cellular damage and cell death, giving MIF characteristics of alarmins or DAMPs [101, 102]. While the precise secretion mechanism of MIF is not yet completely understood, a non-classical secretion involving p115 and JAB1/CSN5 has been demonstrated [103–105].

Overall, MIF was found to play a crucial role both in inflammatory processes and the regulation of innate immunity – underlined by its ability to exert an antagonistic effect on anti-inflammatory glucocorticoids, unique among cytokines [90, 106]. In accordance with its pro-inflammatory properties, in further studies MIF was identified to be a key player in numerous acute and chronic inflammatory conditions like sepsis, acute respiratory distress, rheumatoid arthritis, and atherosclerosis [107–110]. Due to the connection between chronic inflammation and cancer and MIFs pro-inflammatory activities, macrophage migration inhibitory factor is also believed to be part of the tumorigenic inflammatory microenvironment and contributing factor in cancerogenesis [111].

MIF exerts its functions – dependent on the tissue and physiological or disease context – by interaction with its various receptors: CD74 and the chemokine receptors CXCR2, CXCR4 and CXCR7 [39, 112, 113]. CD74, the cell surface expressed form of the invariant chain of the MHC class II complex, was the first described MIF receptor [112, 114]. However, the expression of this MIF receptor is not restricted to MHC class II positive, antigen-presenting, cells. It has been shown that also MHC-II negative cells can express CD74 on their surface after pro-inflammatory stimuli [115]. Additionally, MIF has been found to be a non-cognate ligand of chemokine receptors, an interaction that will be highlighted in greater detail in section 1.2.2. Despite being

1. Introduction

discovered as a cytokine, MIF shows also well-studied chemokine-like functions, facilitated by its ability to signal through chemokine receptors, ultimately leading to its classification as an atypical chemokine [79, 113]. A good example for this function again is atherosclerosis, where MIF mediates disease progression by facilitating monocyte and T-cell recruitment via CXCR2 and CXCR4, respectively [109, 116, 117]. Additionally, it has been demonstrated that MIF is able to signal through the atypical chemokine receptor CXCR7 (chemokine scavenger receptor ACKR3), promoting B-cell recruitment [39]. CXCR7, cognate receptor of CXCL11 and CXCL12, first believed to be a decoy- or scavenger-receptor without signaling activities, has been shown to be able of β -arrestin recruitment and activation of Akt as well as ERK, acting either alone or as a receptor complex with CXCR4 [16, 118]. This axis has also been implied in platelet function and more recently in prostate cancer [40, 119]. In the context of cardiovascular disease, circulating MIF has also been shown to act similar to an arrest chemokine, forming a gradient after being immobilized on the vascular endothelial surface [113]. As a consequence, numerous therapeutic approaches are focusing on MIF's role in atherosclerosis, yielding positive results with inhibition of MIF with small molecules or neutralizing antibodies, supported by studies on *Mif*-knockout mice with an atherosclerotic background [113, 120]. More recently, the specific inhibition of the MIF/CXCR axis using tailored peptides has proven to be a promising strategy [121–123].

Despite MIF being known for its atherogenic and pro-inflammatory properties, it also has to be noted that beneficial functions of MIF have been reported as well. This is, for example, the case in acute kidney injury or myocardial ischemia/reperfusion injury [124, 125]. In hepatotoxic models of liver injury MIF was found to exert an anti-fibrotic effect, while it shows pro-fibrotic properties in other hepatic pathologies [126, 127].

While these cytokine and chemokine-like functions of MIF are the physiologically most important ones, it was also shown to possess enzymatic activities. Possibly remnants of a previous function of this pleiotropic and evolutionary highly conserved protein, MIF shows both an tautomerase as well as an oxidoreductase activity [128, 129]. In fact, the MIF trimer shows a structural similarity to microbial enzymes including a 4-oxalocrotonate-isomerase, with its N-terminal proline residue being a key element of the enzymatic pocket and necessary for the conversion of phenylpyruvate by MIF. Even though no physiological relevance of this activity of MIF is known, enzyme-dead mutants of MIF, with an altered enzymatic pocket, also lack their chemokine function. While MIF's tautomerase activity itself might not be of great relevance for its physiological function, at least the conformation that is imposed on MIF by the corresponding residues, most importantly Pro-1, seems to be crucial for receptor interactions [88, 130–133]. This proline residue therefore is the target for many small molecule inhibitors of MIF [121, 134]. Apart from being an important target structure to modulate MIF's chemokine functions, the enzymatic capabilities of MIF have so far only been linked to a possible mechanism by which MIF could be involved in detoxification in neural tissues, as two publications from 1999 and 2000 show [135, 136].

1.2.2. Interaction of MIF with chemokine receptors

As described, MIF is the non-cognate ligand of certain CXC-type chemokine receptors despite lacking typical hallmarks of classical chemokines like the conserved cysteine motif or the chemokine fold structure. Nevertheless, MIF as an atypical chemokine mimics certain aspects of classical chemokines allowing it to engage in high-affinity interactions with e.g., CXCR2 and CXCR4. Given the importance of these receptors for MIF signaling, it is of no surprise that for them, these receptor-ligand interactions have been studied in great detail.

1.2. Macrophage migration inhibitory factor and MIF-family proteins

Structural comparison of MIF with the canonical CXCR2-ligand and classical chemokine CXCL8 provided first mechanistic insights into these interactions. Not only is there a structural similarity between a MIF monomer and a CXCL8 dimer, it was also shown that Arg-11 and Asp-44 residues of MIF have a similar spacing to the residues forming the ELR-motif of CXCL8. This motif, termed *pseudo-(E)LR* motif, proved to be crucial for receptor binding and MIF's chemotactic, CXCR2-mediated effects [137]. Building on this motif of the MIF/CXCR2 interface, further investigations shed more light on this interaction, based on the two-site binding model of classical chemokines and their receptors, asking whether the binding of MIF to CXCR2 would follow the same mechanic. Indeed, a two-site binding model was confirmed with site 1 interaction taking place between the N-terminal domain as well as parts of extracellular loop (ECL) 1 and 2 of CXCR2 and a newly identified N-like loop region of MIF (residues 47 to 56), mimicking the N loop of CXCL8. Site 2 binding was found to occur between the previously identified pseudo-(E)LR motif of MIF and a motif formed by the receptor's ECL2 and ECL3, as depicted in figure 1.7 [138]. Subsequently, this receptor/ligand interaction was also thoroughly studied by *in silico* approaches by Xu *et al.*, where they could confirm the two-site mode of interaction as well as the importance of MIF's pseudo-(E)LR motif and pinpoint numerous key residues of the binding interface [139]. This mimicking of binding motifs to facilitate signaling through chemokine receptors is not unique to MIF but a typical feature of ACKs.

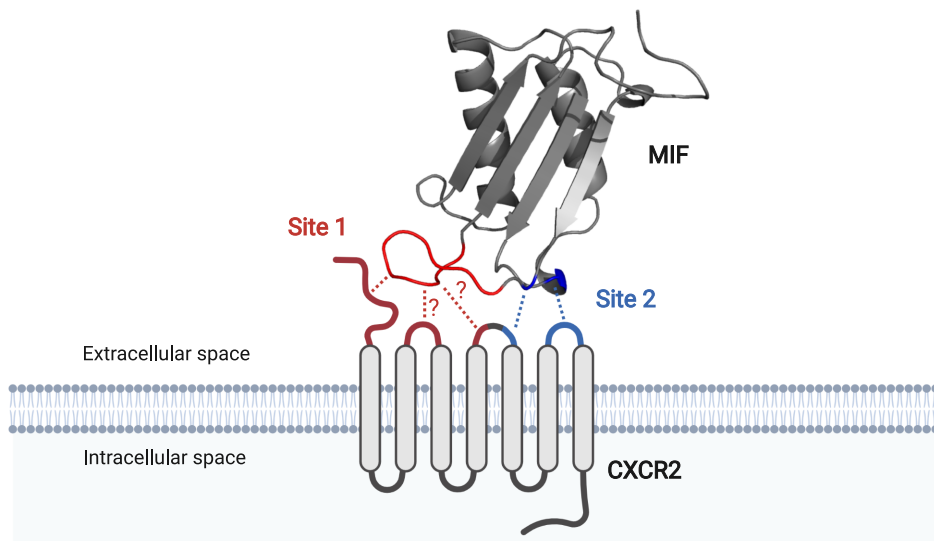


Figure 1.7.: Schematic depiction of two-site binding of MIF to CXCR2. Parts of MIF and extracellular parts of CXCR2 that contribute to site 1 interactions are depicted in red, while elements corresponding to site 2 are shown in blue. Question marks indicate interaction sites found for the MIF/CXCR2 interface, that differ from typical CK/CKR two-site interactions. As indicated, here site 1 is formed by the N-like loop of MIF and the flexible N-terminal parts, ECL1 and parts of ECL2 of CXCR2. Site 2 is comprised of MIF's pseudo-(E)LR motif and residues of CXCR2's ECL2 as well as ECL3. This figure was created with Biorender.com and is based on a summarizing schematic figure in S. Kraemer *et al.* 2011 [138].

More recently, also MIF's interaction with CXCR4 has been investigated in more detail. Rajasekaran *et al.* found that MIF's interaction with CXCR4 mostly differs from that with CXCR2 and – comparing the receptor binding and activation properties of MIF with the one of CXCR4's cognate chemokine ligand CXCL12 – found evidence of a partial allosteric agonism [133]. Briefly,

1. Introduction

MIF (with a region comprising residues 43 to 98, a larger N loop region compared to the one for interactions with CXCR2) competes with CXCL12 for binding at the N-terminus of CXCR4 but while CXCL12 also engages in interactions with the receptor's transmembrane cavity for receptor activation, this is not the case for MIF. Instead, formation of a cryptic pocket upon binding of MIF, in place of an interaction with the transmembrane cavity is suggested, followed by G protein signaling but not β -arrestin signaling. Furthermore, MIF's catalytic pocket is involved in the activation of CXCR4 – a potential opportunity to intervene with the MIF/CXCR4 axis without affecting CXCL12 effects [133]. While this study provided insights as to how MIF engages CXCR4, in comparison to typical chemokine receptor/ligand interactions, further research is needed for a complete understanding the MIF/CXCR4 interaction interface.

Even more is yet to be discovered about the interaction of MIF with CXCR7 – the cognate receptor of CXCL11 and CXCL12. First results, however, suggest MIF interacting with the N-terminal region of this chemokine receptor, leading to receptor internalization and that this interaction leads to a chemotactic response [39]. Details about the interaction interface and the involved motifs still need to be investigated more thoroughly.

1.2.3. Non-mammalian MIF-family proteins

While this section so far focused on human MIF and MIF-2, MIF-family proteins are not exclusive to mammals. In fact, genes coding for MIF-like proteins have been discovered in both eukaryotic and prokaryotic organisms, emphasizing the ancient origin and high conservation of the MIF-family proteins. Non-mammalian homologs of MIF or MIF-2 have for example been identified not only in bacteria but also in plants, fish, birds, nematodes, arthropods and various protozoa including dinoflagellates, with numerous organisms expressing multiple homolog MIF- or DDT-like proteins (MDLs). [85, 140–142]. Where the effect of these proteins has been investigated, the non-mammalian MIF-family proteins seem to be involved in mechanisms of immunity, stress response and host defense or parasite/host interactions [85].

Given the inflammatory and immune-modulating capabilities of their mammalian counterparts, these functions are not completely surprising. Intriguing is however the apparent cross-species reactivity, that can be observed for certain parasite or pathogen MIF-proteins, allowing them to interfere with the hosts defenses on a molecular level. For example, recombinantly expressed MIF of the lone star tick *Amblyomma americanum* was shown to have a similar inhibitory effect on the random migration of human macrophages as its human counterpart. Even though the precise function of this tick protein is unclear at this point, it can be speculated to be involved in protecting the parasite from the hosts immune system and demonstrates a cross-species reactivity of non-mammalian MIF proteins [143]. While it is known that ticks secrete other proteins to interfere with the hosts defenses on a molecular level, like Evasin-3 that inhibits CXCL8 via complex formation, the data suggesting *A. americanum* MIF mimicking its human counterpart to engage human chemokine receptors, presented by Jaworski *et al.* still is an intriguing concept [60]. In fact, signaling through human MIF receptors by non-mammalian MIF-family proteins, an ability most likely aided by the very similar 3D-structure of these highly conserved proteins, has also been reported for MDLs of *Leishmania major* and other protozoan parasites [144, 145].

Next to parasite- or pathogen-derived MIF-family proteins, also MDLs found in various plant species are of great interest as well. Of note, three genes coding for MIF-like proteins were identified in the plant model organism *Arabidopsis thaliana*. According to subsequent *in silico* analysis, two of them are constitutively expressed and all three are predicted to be structurally highly similar to human MIF [140]. This high similarity along with the *in silico* characterization

and rising interest in possible enzymatic or other activities of these proteins recently led to the development of methods to efficiently purify AtMDLs recombinantly, to facilitate further functional studies [146].

Taken together, since their discovery decades ago, MIF-family proteins have proven to be quite intriguing, multi-faceted modulators of immunity and context-dependent mediators of inflammation. Aptly described as “Most Interesting Factor”, MIF has been shown to have functionality beyond its initial characterization as a proinflammatory cytokine, readily engaging in the complex chemokine network [147]. Their highly conserved structure across kingdoms, paired with the aforementioned regulatory functions in the mammalian immune system and an enzymatic activity with a yet incompletely understood role make the MIF-family proteins undoubtedly an interesting and worthwhile target of future studies.

1.3. Aim of the doctoral thesis

MIF itself as well as the MIF-family proteins are recognized as chemokine-like cytokines or ACKs and the relationship of MIF and classical chemokine receptors has been extensively studied in the past, as outlined above. However, the precise mechanism through which MIF binds to CXCR4 and activates this non-cognate receptor, is still incompletely understood. Additionally, apart from the CKR-interactions of MIF, little is currently known about the extent to which MIF-family proteins are able to interfere with the complex human chemokine network. Such interference could be executed either by targeting chemokine receptors or by interfering with CKs directly, a mechanism not uncommon among classical chemokines.

Therefore, the abilities of MIF-family proteins to interact with the chemokine network to modulate its function were to be investigated more thoroughly in this project. This doctoral thesis is thus focused on two aspects of these interactions, including those of non-mammalian MIF proteins.

1.3.1. Part I: Interaction interface of MIF and its non-cognate receptor CXCR4

As outlined in section 1.2.2, the exact mechanism through which MIF engages in ligand/receptor interactions with CXCR4 as well as the involved residues of MIF, are currently not fully known. Based on our knowledge of MIFs interaction with CXCR2, which following a two-site binding model as well as previous data showing the involvement of MIF's N-like loop and proline-2 residue, the interaction of MIF with the chemokine receptor CXCR4 was to be investigated further. Since CXCR4 is the cognate receptor of the classical chemokine CXCL12 but is also targeted by MIF and HBD3, an important aspect of this study was to identify possible differences in the CXCR4 binding motifs of these ligands. Such differences could eventually provide crucial information necessary for designing MIF/CXCR4-specific inhibition strategies in further translational studies.

Here, multiple techniques like peptide-array based binding assays and targeted mutagenesis can be employed to first identify MIF residues possibly involved in CXCR4-binding, which then will have to be verified. In both biophysical as well as cell-culture based methods, backed by *in silico* approaches like molecular docking simulations, the importance of identified binding motifs of MIF can be assessed further, regarding both receptor binding and activation.

The function of MIF as an atypical chemokine, interacting with chemokine receptors, might additionally lead to the question whether MIF-family proteins are able to extend their interactions with the chemokine network further by modulating chemokine activity directly, e.g. in the form of complex formation. This has been reported for selected other ACKs like HMGB1 as described

1. Introduction

above, and previous findings also suggest heteromeric complexes of selected AtMDLs as well as human MIF. Such potential interactions could be identified by an unbiased solid-phase array approach using immobilized chemokines and ACKs, for example.

1.3.2. Part II: Ability of AtMDLs to interact with human CKRs

Based on previous findings, where *in silico* studies suggested a high structural similarity of plant-derived MIF-family proteins (see section 1.2.3, we wanted to investigate this further. Of special interest in this regard is the potential ability of AtMDLs to signal through human chemokine receptors, since for other non-mammalian MDLs an involvement in parasite/host interactions has been identified. While the parasite/host concept does not strictly apply to plant proteins and humans, it could nevertheless indicate the possibility of such proteins to have cross-species effects. Such novel interactions would therefore expand the effects of MIF-family proteins on the chemokine network across kingdom boundaries. In addition to CKR interactions, also the enzymatic activity of the AtMDLs was to be compared to human MIF, both in tautomerase assays as well as by employing computational methods, thereby investigating this pocket that is essential for these protein's enzymatic function in three-dimensional space as the enzymatic activity – as a remnant of MIF functions in early evolutionary stages – may have a relevance in plants.

2. Own contributions to the publications

This cumulative thesis is based on two scientific publications, in which various aspects of the interactions of MIF-family proteins with the chemokine network were investigated. How my work contributed to these publications will be laid out in this chapter.

2.1. Publication I: Lacy *et al.*, 2018

Identification of an Arg-Leu-Arg tripeptide that contributes to the binding interface between the cytokine MIF and the chemokine receptor CXCR4

M. Lacy*, C. Kontos*, M. Brandhofer*, K. Hille, S. Groning, D. Sinitski, P. Bourilhon, E. Rosenberg, C. Krammer, T. Thavayogarajah, G. Pantouris, M. Bakou, C. Weber, E. Lolis, J. Bernhagen and A. Kapurniotu

(*: Equally contributing, shared first authors)

DOI: 10.1038/s41598-018-23554-5

In this publication (see chapter 5, and section A.2.1 for supplementary data), we investigated the interaction of MIF with its non-cognate receptor CXCR4 in a detailed manner, building on our prior knowledge about the interaction interface of MIF and CXCR2. A better understanding of the MIF/CXCR4 interface would not only be helpful to explain binding and signaling of MIF via CXCR4 in contrast to the receptor's canonical ligand CXCL12, but could also aid in a directed targeting approach to develop specific inhibitors of the MIF/CXCR4 interaction.

As one of the equally contributing first authors of this paper, I contributed to writing the manuscript as well as to key experiments of the study. I was involved preparation of the figures and reviewed and edited the final manuscript. Regarding the experimental part, I provided supporting *in silico* data by performing the molecular docking studies between MIF and the receptor CXCR4. These protein-protein docking and refinement studies, giving similar results with and without restricting the interaction interface to residues 1–27 of the CXCR4 N-terminus, backed the data of our other experiments. This confirmed our hypothesis of the interaction interface between MIF and CXCR4, and thereby helped to illustrate the proposed interaction in a detailed manner, resulting in figure 6 of the publication.

I also significantly contributed to figures 7 and 8. Here, structural features of MIF were compared to those of CXCL12, the cognate ligand of CXCR4, as well as to human β -defensin 3 (HBD3) – an antagonist of CXCR4 that leads to receptor internalization without activation [148]. Figure 7 highlights the structure and position of residues forming motifs important for site 1 and site 2 receptor binding of these proteins where applicable, indicating a possible positive charge cluster formation by MIF's RLR-motif that could be comparable with similarly charged regions of CXCL12 and HBD3. These surface charge distributions and their similarities are then presented in figure 8, allowing a more detailed comparison. This comparison provides further evidence that the RLR-motif of MIF plays a role in binding to its receptor CXCR4.

2. Own contributions to the publications

Furthermore, I contributed to the data shown in supplementary figure 4 by Alexa Fluor 488 labeling of the R87A-L88A-R89A-MIF triple mutant, in which the RLR-motif was replaced with three alanines. This labeled MIF variant was used for fluorescence spectroscopy titrations in order to determine binding characteristics of the MIF mutant without the RLR-motif to the CXCR4(1–27)-peptide. As this mutant did not interact with the CKRs N-terminus, this further showed the RLR-motifs importance for the interaction of MIF with CXCR4.

2.2. Publication II: Sinitski et al., 2020

Cross-kingdom mimicry of the receptor signaling and leukocyte recruitment activity of a human cytokine by its plant orthologs

D. Sinitski, K. Gruner, **M. Brandhofer**, C. Kontos, P. Winkler, A. Reinstadler, P. Bourilhon, Z. Xiao, R. Cool, A. Kapurniotu, F. J. Dekker, R. Panstruga and J. Bernhagen

DOI: 10.1074/jbc.RA119.009716

This publication (see chapter 6, and section A.2.2 for supplementary data) describes the interaction of MIF orthologs found in *Arabidopsis thaliana* (*A. thaliana* MIF/*D*-dopachrome-tautomerase-like proteins or *AtMDLs*) across kingdom boundaries with human chemokine receptors. Here we showed the ability of *AtMDLs* to signal through the chemokine receptor CXCR4 to induce cell migration, thereby mimicking effects of classical chemokines. Also the structure of these proteins was investigated, in the context of the enzymatic activities that MIF possesses.

In figure 2 of this publication, we investigated the tautomerase activity of *AtMDLs* and compared them to human MIF. Here, I contributed subfigures C and D. I first performed a multiple sequence alignment of these proteins and highlighted the amino acid residues forming the catalytic pocket of MIF, comparing them to the corresponding residues of the plant orthologs (figure 2C). Also, depicted in supplementary figure 1A, this alignment was color-coded by the percentage of identity between the sequences. This investigation of the tautomerase pocket was also carried out in the 3D-space, for which 3D-models of the *AtMDLs* were necessary. Since the structure of these proteins had not been elucidated so far, I employed the PHYRE² algorithm for homology modeling. Here, running the program on the corresponding webserver in extensive mode to allow for multi-template and *ab initio* modeling, the structure of these proteins was predicted, complete with their C-terminal 6×His-tag as well as tagged human MIF for comparison. These predicted structures were then visualized and examined more closely, also regarding their surface charge distribution, via PyMOL, depicted in figure 2D. In the supplementary figure 1B, these predicted structures are also compared to the structure of native human MIF resolved by X-ray crystallography, highlighting their overall similarity. Together this indicates a crucial change in the catalytic pocket, caused by the substitution of asparagine to lysine for residue 98 in the *AtMDLs*. The importance of this change in amino acids was then confirmed by generating a N98K-mutant of MIF.

To facilitate a better understanding of the *AtMDL*'s binding and activation of MIF receptors, I performed a multiple sequence alignment, comparing *AtMDLs* to human MIF and the classical chemokine and CXCR4 ligand CXCL12. Here, residues of MIF involved in interactions with CD74, CXCR2 and CXCR4 and the other protein's corresponding residues are highlighted and color-coded by their properties to allow a detailed comparison of potential interaction motifs.

Additionally, I was involved in curation and formal analysis of the data as well as the visualization of our findings.

3. Summary

By providing signals for the migration of immune and other cell types, chemokines and their receptors are key regulators of both inflammation and homeostasis. While the group of classical chemokines is well defined and studied, also other proteins that diverge from the conserved chemokine structure are able to elicit chemotactic responses, by engaging chemokine receptors (CKRs). These mediators with a chemokine-like function are therefore described as *atypical* chemokines (ACKs). Macrophage migration inhibitory factor (MIF), one of the first cytokines described, and founding member of the MIF protein family, is such an atypical chemokine. MIF has been shown to be a key mediator in inflammatory processes by signaling through CKRs CXCR2 and CXCR4. Due to MIF's pro-inflammatory function, it plays a pivotal role, e.g., in cardiovascular diseases like atherosclerosis. Furthermore, MIF and MIF-like proteins are expressed not only in mammals but also in many other species including plants, where they are often involved in immunity and host/pathogen interactions.

In the course of this work, several aspects of the interplay between MIF-family proteins and the human chemokine network were investigated. We studied the interaction interface of human MIF with its non-cognate receptor CXCR4 and also extended the MIF/CKR interaction studies to recently characterized non-mammalian MIF-family proteins.

In Lacy *et al.*, 2018, we studied how MIF binds to the chemokine receptor CXCR4 and were able to expand the known MIF/CXCR4 interaction interface by identifying a tripeptide-motif (arginine-leucine-arginine, RLR) on MIF that extends its site 1 binding to this receptor. With the motif disabled, MIF lost the ability to signal through CXCR4 and induce chemotactic effects. Alanine-scanning of the motif and the surrounding region, in conjunction with peptide-based binding assays revealed the importance of this newly identified RLR-motif for interaction with the N-terminal region of CXCR4, which engages in site 1 binding with MIF's N-like loop region according to the two-site binding model of chemokine receptors and their ligands. These findings were backed by *in silico* studies comparing MIF with CXCL12 and HBD3, that emphasized the importance of the net positive surface charge of this region for binding to the CXCR4 N-terminus. This data leads to a more complete picture of how MIF is able to interact with its non-cognate receptor as an atypical chemokine. This allows to differentiate between the binding mechanism of CXCR4 with MIF and with its cognate ligand CXCL12, the CXCR4 antagonist HBD3, or the interaction of MIF with other chemokine receptors. This, in turn, is crucial knowledge required for developing strategies to specifically inhibit the MIF/CXCR4-axis, while leaving other ligand/receptor interactions unchanged. Similar to CXCR4, where activation can lead to either protective or detrimental effects in a ligand-dependent manner, also MIF can exert positive as well as negative effects depending on the receptor this pleiotropic protein interacts with, and the overall physiological context, making this specificity especially important. The validity of this approach, using findings from our aforementioned publication and others, was recently proven by the development of an inhibitory peptide targeting specifically the MIF/CXCR4-interface, blocking atheroproliferative and inflammatory effects of MIF *in vitro* and *in vivo* [123].

Intrigued by the – predicted – structural similarity between MIF orthologs of the model plant *A. thaliana* and their human counterpart, in Sinitski *et al.*, 2020, we characterized these proteins

3. Summary

further, after expressing them recombinantly in *E. coli*. We found that, despite their overall similarity to human MIF according to circular dichroism spectroscopy, *AtMDLs* show only a minor residual tautomerase activity compared to the human protein when tested for their ability to convert the substrates *p*-hydroxyphenylpyruvate and *L*-dopachrome methyl ester. A closer inspection of the tautomerase pocket revealed crucial changes in amino acids in the area of the enzymatic site, foremost Asn-98 in MIF, which is replaced by a basic lysine residue in the *AtMDLs*. Essentially, these differences lead to a change in shape and charge distribution at the tautomerase site, sufficient to render it unable to perform the enzymatic reaction. Despite this difference in the enzymatic site – which was proven to be also a formidable target for MIF inhibitors that block its chemokine-like functions – we found that these plant-derived MIF orthologs are able to exert a biological function in the human system. Given the similarity to human MIF, with receptor binding sites for CXCR4 and CD74 being conserved in *AtMDLs*, we tested their ability to engage human MIF receptors. Our experiments showed that *A. thaliana* MDLs do not only bind to CD74 and CXCR4, they are also able to activate and signal through the human chemokine receptor CXCR4, showing for the first time that cross-kingdom interactions of plant-derived MIF proteins and human receptors of MIF are possible. In subsequent functional studies, it was demonstrated that *AtMDLs* activate CXCR4, inducing Akt-signaling as well as monocyte and T-cell migration. T cells were also desensitized for CXCL12 or MIF mediated CXCR4 responses, showing the extent of cross-kingdom interactions between plant-derived MIF-proteins and the human chemokine system. Especially the findings on CXCR4-desensitization show that by these interactions, such plant proteins could have an modulating effect on the human immune system, making them a worthwhile target for future studies. While their function in plant physiology has been shown to related to immunity and susceptibility to pathogen infection, an aim for future studies – apart from their potential relevance for the human immune system – could also be the generation of structural data of *AtMDLs*, e.g., via X-ray crystallography, allowing for a more thorough comparison with their human counterpart [149].

In summary, this work leads to a more complete understanding of the interplay between the atypical chemokine MIF and the classical chemokine network. We were able to add valuable information to the existing knowledge of the MIF/CXCR4 interface by identification a tripeptide motif of MIF that extends site 1 binding, but also found that *AtMDLs*, plant orthologs of MIF proteins, are able to engage in signaling via human CXCR4 and CD74. This, to our knowledge, is the first description of plant proteins mimicking human chemokine activity, and this connection by which plant-derived proteins could influence the human chemokine network and modulate the immune system should be investigated further. Additionally, this study shows a separation of the enzymatic activity and the chemokine function of these MIF-family proteins, which exhibit only minimal tautomerase activity compared to human MIF.

In the course of this project, it also became apparent that human MIF-family proteins as atypical chemokines engage in direct interactions with classical chemokines, as described in section A.1.1. These interactions, exemplified by a novel heteromeric complex of MIF and CXCL4L1 which inhibits MIF-mediated effects on immune cell recruitment and thrombus formation (see manuscript in section A.1.2), point towards an additional modulatory level of interplay between MIF-family proteins and the chemokine network. While additional studies are necessary to investigate the role of this and other MIF/chemokine complexes in the context of cardiovascular diseases, these findings expand the insights gained from previous investigations which targeted MIF-family protein interactions with chemokine receptors. These MIF/chemokine complexes showcase a more extensive than previously known functional connection between MIF-family proteins and the chemokine network.

4. Zusammenfassung

Chemokine und ihre Rezeptoren vermitteln Signale für die Migration von Immun- und anderen Zellen, und stellen somit wichtige Regulatoren sowohl in entzündlichen als auch homeostatischen Prozessen dar. Während die Gruppe der klassischen Chemokine (CK) gut erforscht und klassifiziert ist, gibt es neben ihnen auch andere Proteine die zwar von der konservierten Struktur klassischer Chemokine abweichen, aber ebenfalls mit Chemokinrezeptoren interagieren können um chemotaktische Effekte zu erzielen. Diese Mediatoren mit chemokin-artiger Funktion werden daher als *atypische* Chemokine (ACKs) bezeichnet. *Macrophage migration inhibitory factor* (MIF), eines der ersten beschriebenen Zytokine und Basis der MIF-Proteinfamilie, gehört zu dieser Gruppe der ACKs. Es wurde gezeigt, dass MIF durch Signaltransduktion über die Chemokinrezeptoren CXCR2 und CXCR4 als entscheidender Faktor an Entzündungsprozessen beteiligt ist. Durch seine pro-inflammatorischen Eigenschaften spielt MIF eine bedeutende Rolle in kardiovaskulären Erkrankungen wie etwa der Atherosklerose. Weiterhin ist die Expression von MIF-Proteinen nicht auf Säugetiere beschränkt – diese Proteine existieren auch in einer Vielzahl anderer Spezies, darunter Pflanzen, wo sie häufig eine Rolle im Immunsystem und der Interaktion von Pathogenen mit ihren Wirten spielen.

Im Rahmen dieser Arbeit wurden unterschiedliche Aspekte des Zusammenspiels von MIF-Proteinen und dem humanen Chemokin-Netzwerk untersucht. Wir fokussierten uns auf die Interaktions-Schnittstelle von humanem MIF mit seinem *non-cognate* Chemokinrezeptor CXCR4 und weiteten unsere Studien auch auf MIF/Chemokinrezeptor Interaktionen von nicht aus Säugetieren stammenden MIF-Proteinen aus.

In Lacy *et al.*, 2018, beschäftigten wir uns mit der Bindung von MIF an CXCR4 und konnten das bestehende Wissen zur Interaktionsfläche durch Identifikation eines Tripeptid-Motivs (Arginin-Leucin-Arginin, RLR) von MIF erweitern, welches die *site 1* Bindungsstelle mit CXCR4 ergänzt. Ohne das Motiv verlor MIF die Fähigkeit zur Signaltransduktion und seine durch CXCR4 vermittelten chemotaktischen Eigenschaften. Alanin-scanning des Motivs sowie der angrenzenden Regionen, in Verbindung mit Peptid-basierten Bindungs-Assays, zeigte die Bedeutung des RLR-Motivs für die Interaktion zwischen dem N-Terminus von CXCR4 – Teil der *site 1* Bindungsstelle mit der *N-like loop* Region von MIF – gemäß des *two-site* Bindungsmodells von Chemokinrezeptoren und ihren Liganden. Unterstützt werden diese Funde durch *in silico* Vergleiche von MIF, CXCL12 und HBD3, welche auch die Bedeutung der positiven Nettoladung der Proteinoberfläche in dieser Region für die Bindung an den N-terminalen Teil von CXCR4 hervorheben. Unsere Daten vervollständigen damit das Bild der Interaktion von MIF als ACK mit seinem eigentlich artfremden Rezeptor CXCR4. Sie dienen auch der Differenzierung zwischen der CXCR4/MIF Interaktion und der von CXCR4 mit seinem natürlichen Liganden CXCL12, dem Antagonisten HBD3, oder der Bindung von MIF an andere Rezeptoren. Dies wiederum sind essentielle Informationen welche nötig sind um etwa Strategien zur spezifischen Inhibierung der Interaktion von MIF und CXCR4 zu entwickeln, ohne dabei die Bindung von MIF an andere Rezeptoren oder die CXCL12/CXCR4-Achse zu beeinträchtigen. Ähnlich zu CXCR4, dessen Aktivierung ligandenspezifisch entweder protektive oder schädliche Effekte bewirken kann, so kann auch der pleiotrope Mediator MIF positive wie negative Wirkung entfalten, abhängig

4. Zusammenfassung

von physiologischem Kontext und dem Rezeptor mit dem es interagiert. Dies unterstreicht die Wichtigkeit der Spezifität eines solchen Inhibitors. Validiert wurde diese Herangehensweise – aufbauend auf, unter anderem, Daten dieser Publikation, durch die kürzlich gelungene Entwicklung eines inhibierenden Peptids, welches selektiv auf die MIF/CXCR4-Interaktion abzielt und MIF-vermittelte Effekte im Entzündungsgeschehen und der Progression der Atherosklerose *in vitro* und *in vivo* blockiert [123].

Angeregt durch die Ähnlichkeit der – *in silico* modellierten – 3D-Struktur von MIF-Proteinen des pflanzlichen Modellorganismus *A. thaliana* und humanem MIF, charakterisierten wir diese Proteine, rekombinant in *E. coli* exprimiert, in Sinitski *et al.*, 2020, genauer. Wir fanden heraus, dass *AtMDLs* ungeachtet ihrer mittels Zirkulardichroismus Spektroskopie bestätigten generellen Ähnlichkeit zu humanem MIF nur einen Bruchteil der Tautomeraseaktivität ihres humanen Gegenstücks aufweisen. Getestet wurde dabei ihre Fähigkeit die Substrate *p*-Hydroxyphenylpyruvat und *L*-Dopachrommethylester umzuwandeln. Eine genauere Untersuchung des aktiven Zentrums zeigte entscheidende Unterschiede in der Aminosäurezusammensetzung, insbesondere Asn-98 in MIF ist in *AtMDLs* durch einen basisches Lysin ersetzt. Diese Unterschiede führen im Wesentlichen zu Form- und Ladungsänderungen im aktiven Zentrum des Proteins, welche es an der Katalyse von Tautomerase-Reaktionen hindern. Trotz dieser Unterschiede der katalytisch aktiven Region – welche sich als prominentes Ziel für MIF-Inhibitoren etabliert hat, um dessen Chemokin-Aktivität zu hemmen – konnten wir zeigen, dass die pflanzlichen MIF-Orthologe biologische Aktivität im humanen System aufweisen. In Anbetracht ihrer Ähnlichkeit zu humanem MIF und der in *AtMDLs* konservierten Bindestellen für CXCR4 und CD74 prüften wir ihre Fähigkeit mit humanen MIF-Rezeptoren zu interagieren. Unsere Experimente zeigten das *A. thaliana* MDLs nicht nur an CD74 und CXCR4 binden, sondern auch zur Aktivierung von CXCR4 und Signaltransduktion über diesen Rezeptor fähig sind. Dies zeigte erstmals, dass biologische Reiche übergreifende Interaktionen zwischen pflanzlichen MIF-Proteinen und humanen MIF-Rezeptoren möglich sind. In anschließenden funktionalen Studien konnte gezeigt werden, dass *AtMDLs* CXCR4 aktivieren und somit den Akt-Signalweg sowie Monozyten- und T Zell-Migration induzieren. T-Lymphozyten wurden zudem durch *AtMDLs* für CXCL12 oder MIF-vermittelte CXCR4 Funktionen desensibilisiert, was das Ausmaß dieser Interaktion von pflanzlichen Proteinen und dem humanen Chemokinsystem weiter unterstreicht. Insbesondere die Daten zur Desensibilisierung von CXCR4 zeigen, wie pflanzliche Proteine auf diesem Wege einen modulierenden Effekt auf das humane Immunsystem ausüben könnten, was *AtMDLs* zu einem lohnenden Gegenstand weiterer Untersuchungen macht.

Während Studien bereits zeigen konnten dass ihre physiologische Rolle in Pflanzen mit Immunabwehr und der Anfälligkeit für Infektionen mit Pathogenen verbunden ist, könnte weitere Forschung – abgesehen von einer potenziellen Relevanz für das humane Immunsystem – die Generierung von Strukturdaten, etwa mittels Röntgenkristallographie, zum Ziel haben um einen tiefergehenden Vergleich von *AtMDLs* mit humanen MIF-Proteinen zu erlauben [149].

Zusammenfassend führen diese Arbeiten zu einem vollständigeren Verständnis des Zusammenspiels zwischen dem atypischen Chemokin MIF und dem Netzwerk klassischer Chemokine. Es gelang uns wertvolle Informationen zum bestehenden Wissen über die Interaktion von MIF und CXCR4 zu ergänzen, indem wir ein tripeptid-Motiv von MIF identifizierten, welches die *site 1* Bindungsregion erweitert. Zudem entdeckten wir, dass *AtMDLs* – pflanzliche MIF Orthologe – in der Lage sind, Signale über die humanen Rezeptoren CXCR4 und CD74 zu vermitteln. Dies ist nach unserem Wissen die erste Beschreibung von pflanzlichen Proteinen die in der Lage sind, die Aktivität humaner Chemokine nachzuahmen. Diese Interaktion, über die es pflanzlichen Proteinen möglich sein könnte, das humane Chemokin-Netzwerk zu beeinflussen und somit auch

einen modulierenden Effekt auf das Immunsystem zu erwirken, sollte in weiterführenden Studien ausführlicher untersucht werden. Zudem zeigen diese Untersuchungen auch eine Trennung von enzymatischer Aktivität und der Rolle als Chemokin dieser pflanzlichen MIF-Proteine, welche im Vergleich zu humanem MIF nur über einen Bruchteil an Tautomeraseaktivität verfügen.

Im Zuge dieses Projekts wurde auch ersichtlich, dass humane MIF-Proteine als ACKs in der Lage sind direkte Interaktionen mit klassischen Chemokinen einzugehen, wie in Abschnitt A.1.1 beschrieben wird. Diese Interaktionen deuten auf eine zusätzliche, modulierende Ebene des Zusammenspiels von MIF-Proteinen und dem Chemokin-Netzwerk hin. Dies wird veranschaulicht durch einen neuartigen heteromeren Komplex zwischen MIF und CXCL4L1, welcher die MIF-vermittelte Immunzellrekrutierung und Thrombusbildung inhibiert (siehe Manuskript in Abschnitt A.1.2). Während weitere Studien nötig sind um die Rolle dieses und anderer MIF/Chemokin-Komplexe im Kontext kardiovaskulärer Erkrankungen zu untersuchen, so erweitern diese Ergebnisse unsere bestehenden Kenntnisse aus Arbeiten zur Interaktion von MIF mit Chemokin-Rezeptoren. Diese MIF/Chemokin-Komplexe zeigen eine funktionale Verbindung zwischen MIF-Proteinen und dem Chemokin-Netzwerk welche umfangreicher ist als bisher angenommen.

5. Publication I: Lacy *et al.*, 2018

Identification of an Arg-Leu-Arg tripeptide that contributes to the binding interface between the cytokine MIF and the chemokine receptor CXCR4

M. Lacy*, C. Kontos*, **M. Brandhofer***, K. Hille, S. Groning, D. Sinitski, P. Bourilhon, E. Rosenberg, C. Krammer, T. Thavayogarajah, G. Pantouris, M. Bakou, C. Weber, E. Lolis, J. Bernhagen and A. Kapurniotu

(*: Equally contributing, shared first authors)

Published 2018 in Scientific Reports.¹

DOI: 10.1038/s41598-018-23554-5

¹Open access publication, licensed under the CC BY 4.0 licence: <https://creativecommons.org/licenses/by/4.0/>.

SCIENTIFIC REPORTS

OPEN

Identification of an Arg-Leu-Arg tripeptide that contributes to the binding interface between the cytokine MIF and the chemokine receptor CXCR4

Received: 3 October 2017
Accepted: 15 March 2018
Published online: 26 March 2018

Michael Lacy¹, Christos Kontos², Markus Brandhofer¹, Kathleen Hille², Sabine Gröning³, Dzmitry Sinitski¹, Priscila Bourilhon¹, Eric Rosenberg⁴, Christine Krammer¹, Tharshika Thavayogarah¹, Georgios Pantouris⁴, Maria Bakou², Christian Weber^{5,6,7}, Elias Lolis⁴, Jürgen Bernhagen^{1,5,8} & Aphrodite Kapurniotu²

MIF is a chemokine-like cytokine that plays a role in the pathogenesis of inflammatory and cardiovascular disorders. It binds to the chemokine-receptors CXCR2/CXCR4 to trigger atherogenic leukocyte migration albeit lacking canonical chemokine structures. We recently characterized an N-like-loop and the Pro-2-residue of MIF as critical molecular determinants of the CXCR4/MIF binding-site and identified allosteric agonism as a mechanism that distinguishes CXCR4-binding to MIF from that to the cognate ligand CXCL12. By using peptide spot-array technology, site-directed mutagenesis, structure-activity-relationships, and molecular docking, we identified the Arg-Leu-Arg (RLR) sequence-region 87–89 that – in three-dimensional space – ‘extends’ the N-like-loop to control site-1-binding to CXCR4. Contrary to wildtype MIF, mutant R87A-L88A-R89A-MIF fails to bind to the N-terminal of CXCR4 and the contribution of RLR to the MIF/CXCR4-interaction is underpinned by an ablation of MIF/CXCR4-specific signaling and reduction in CXCR4-dependent chemotactic leukocyte migration of the RLR-mutant of MIF. Alanine-scanning, functional competition by RLR-containing peptides, and molecular docking indicate that the RLR residues directly participate in contacts between MIF and CXCR4 and highlight the importance of charge-interactions at this interface. Identification of the RLR region adds important structural information to the MIF/CXCR4 binding-site that distinguishes this interface from CXCR4/CXCL12 and will help to design MIF-specific drug-targeting approaches.

Chemokines (CKs) are a complex family of 49 small chemotactic polypeptides, which along with their 23 receptors orchestrate leukocyte migration processes in health and disease. They are structurally characterized by conserved N-terminal cysteine residues and a so-called chemokine-fold and they are sub-divided into four main classes, the CC-, CXC-, C-, and CXXC-chemokines, based on the nature of the cysteine motif. Chemokine receptors (CKRs) are typical G protein-coupled receptors (GPCRs) with seven transmembrane-spanning

¹Department of Vascular Biology, Institute for Stroke and Dementia Research, Klinikum der Universität München, Ludwig-Maximilians-University of Munich, Feodor-Lynen-Str. 17, D-81377, Munich, Germany. ²Division of Peptide Biochemistry, Technische Universität München, D-85354, Freising-Weihenstephan, Germany. ³Department of Anaesthesiology, RWTH Aachen University Hospital, D-52074, Aachen, Germany. ⁴Department of Pharmacology, Yale University School of Medicine, 333 Cedar Street, New Haven, CT, USA. ⁵Institute for Cardiovascular Prevention, Klinikum der Universität München, Ludwig-Maximilians-University of Munich, Pettenkofer Str. 8, D-80336, Munich, Germany. ⁶Munich Heart Alliance, D-80802, Munich, Germany. ⁷Cardiovascular Research Institute Maastricht, Maastricht University, 6229, Maastricht, The Netherlands. ⁸Munich Cluster for Systems Neurology, D-81377, Munich, Germany. Michael Lacy, Christos Kontos and Markus Brandhofer contributed equally to this work. Correspondence and requests for materials should be addressed to J.B. (email: juergen.bernhagen@med.uni-muenchen.de) or A.K. (email: akapurniotu@wzw.tum.de)

α -helices and a C-terminal heterotrimeric G protein-binding domain. CKRs are grouped according to the class of chemokine ligand(s) they interact with. In addition, atypical CKRs (ACKRs) that do not support G_i protein-mediated signaling have been defined. Owing to the GPCR nature of chemokine receptors and the involvement of chemokines in numerous pathophysiological processes they are attractive drug targets^{1–4}.

Recent advances in GPCR crystallography have led to the elucidation of the three-dimensional structures of the chemokine receptor CXCR4 complexed to small molecule ligands and the herpesvirus-8 chemokine vMIP-II^{5,6}, CCR5 with the FDA-approved compound maraviroc⁷ and a chemokine⁸, CX3CL1 in complex with the human cytomegalovirus GPCR US28⁹, CCR2 in complex with orthosteric and allosteric antagonists¹⁰, and an intracellular antagonist with CCR1¹¹. The structure of CXCR1 has been solved by NMR spectroscopy¹². Together with structure-activity relationship (SAR) experiments, these studies have helped to understand the activation of chemokine receptors by their cognate ligands and the elicited cellular signaling processes. Most CKs have a two-site mechanism for binding their receptors^{13,14}. Site 1 involves interactions between the chemokine N-loop, which follows the N-terminal cysteine motif, and the receptor N-domain. The interactions for site 2 are between the chemokine N-terminal residues prior to the cysteine motif and the extracellular loops (ECLs), e.g. the Glu-Leu-Arg sequence for ELR + chemokines such as CXCL8 in its engagement of CXCR1 or CXCR2¹³. Furthermore, chemokine responses may be fine-tuned by interactions with neighboring glycosaminoglycans (GAGs)^{15,16}. Agonist interactions for the homeostatic chemokine receptor CXCR4 are less well understood despite the available X-ray crystallographic information^{5,6}. For CXCR4 and its cognate ligand CXCL12 (also known as SDF-1 α), the CXCL12 N-loop is comprised of a RFFESH sequence, which interacts with the CXCR4 N-domain (site 1)¹⁷. CXCL12 lacks an ELR motif and its disordered N-terminus interacts with ECL2 of CXCR4 and penetrates into the transmembrane cavity of the receptor (site 2)^{5,13,17}.

Macrophage migration inhibitory factor (MIF) is a multi-functional chemokine-like cytokine that plays a pivotal role in the pathogenesis of numerous inflammatory and cardiovascular disorders such as sepsis, rheumatoid arthritis, systemic lupus erythematosus, inflammatory lung diseases, myocardial ischemia/reperfusion injury, and atherosclerosis^{18–22}. It is the prototypical member of an emerging family of mediators with both intra- and extracellular activities termed atypical chemokines (ACKs) or chemokine-like function (CLF) chemokines that, once secreted into the extracellular space, bind to and activate classical chemokine receptors albeit lacking the canonical structural elements^{23–25}. Other examples of ACKs are human β -defensin-1 (HBD-1) that binds to CCR6, a secreted tyrosyl tRNA synthetase fragment that is an agonist of CXCR1, or β 3-defensin that is an agonist for CXCR4. A complex between the alarmin HMGB1 and CXCL12 also binds to CXCR4^{24,26}. Thus, ACKs add significantly to the complexity and redundancy within the CK/CKR network, but also serve to fine-tune the signaling responses and to increase variability in the network. Like their classical chemokine counterparts, ACKs have been recognized as important players in inflammatory and cardiovascular disease^{25,27–29}. ACKs are a heterogeneous functional family of proteins and most members do not share structural similarity with each other^{24,25}. Accordingly, the structural basis underlying the engagement of chemokine receptors by these mediators is relatively poorly understood and is likely to differ for each member or chemokine-like function. One example of an ACK for which structural information regarding its binding interface with a cognate CKR has been obtained is HBD1, which mimics a charge cluster exposed on the outside of the three-dimensional structure of CCL20/MIP-3 α , the cognate ligand of CCR6²⁷, but mimicry elements will be different for other ACKs.

MIF exerts its chemokine activities through interactions with the CXC chemokine receptors CXCR2 and CXCR4 to elicit atherogenic leukocyte recruitment. It also binds to the type-II receptor CD74/invariant chain, driving cell-proliferative responses in inflammation and cancer, and to the chemokine scavenger receptor CXCR7/ACKR3^{24,25,30–32}. We showed that MIF binds to CXCR2 by a two-site binding mechanism involving an N-like loop and a pseudo-ELR motif within MIF, thus mimicking interactions between CXCR2 and its ELR + ligand CXCL8^{30,33,34}. In contrast, the interaction between MIF and CXCR4 remains incompletely understood. We recently characterized an extended N-like loop and the evolutionarily conserved Pro-2 residue of MIF to constitute critical molecular determinants of the CXCR4/MIF binding site and identified partial allosteric agonism as the mechanism that distinguishes CXCR4 binding to MIF from that to the cognate ligand CXCL12³⁵. Yet, due to the lack of a RFFESH motif in MIF and its conformationally constrained N-terminus³⁶, this only partly explains the affinity and specificity observed for the MIF/CXCR4 interaction^{24,25,30}.

Here, we applied peptide spot array technology, site-directed mutagenesis, structure-activity relationship studies, and molecular docking to identify a discontinuous three-amino acid stretch (Arg-Leu-Arg; RLR) that is remotely located at the C-terminal end of the second α -helix in MIF which may serve to extend the N-like loop of MIF and contribute to site 1 binding to CXCR4. The contribution of these residues to functional MIF/CXCR4 interactions was tested using a CXCR4-specific yeast-based cellular signaling system³⁷ and a MIF/CXCR4-dependent chemotactic leukocyte migration assay. We also performed alanine scanning and molecular docking techniques to understand the structural details as well as investigate if the RLR motif directly takes part in site 1 contacts between MIF and CXCR4.

Results

Identification of the RLR residues, expression and biochemical characterization of the MIF R87A-L88A-R89A triple mutant. We previously showed that an extended N-like loop sequence in MIF contributes to site 1 binding with CXCR4³⁵. The N-like loop comprises a flexible loop region followed by residues of the ensuing β -strand. Residues at the C-terminal of this region have been implied in binding to MIF receptor CD74 (amino acids 79–86)³⁸, but not in interactions between MIF and CXCR4.

Peptide spot array analysis of the C-terminal region of the extended N-like loop of MIF using immobilized 15-mer human MIF peptides with each peptide positionally shifted by three residues, was probed for binding to biotinylated CXCR4 N-terminus (CXCR4(1–27)). Analysis revealed a marked signal for MIF peptides 82–96 and 85–99, while giving a small signal for peptide 79–93 and no signal for peptides 88–102 and 91–105 (Fig. 1a).

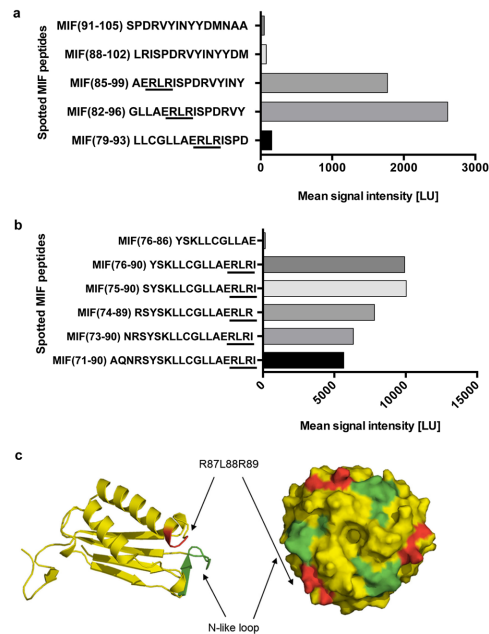


Figure 1. Identification of the RLR sequence as a potential MIF binding region to the N-terminal peptide of CXCR4. (a,b) The peptide spot microarray method suggests that the RLR tripeptide at sequence position 87–89 may contribute to MIF/CXCR4 binding. A peptide spot array containing 15-mer spotted MIF peptides positionally shifted by three amino acids were probed with biotin-CXCR4(1–27). Graphs are plots of spotted MIF peptides over the intensity of the binding signal to biotin-CXCR4(1–27) as read-out by streptavidin Cy5.5 fluorescence. (a) Of five positionally shifted 15-mer peptides of the region 79–105 only peptides containing RLR interact with CXCR4(1–27). (b) Binding of RLR-containing MIF peptides is modulated by N-terminal extension, but residues N-terminal of RLR do not exhibit binding activity *per se*. (c) Structural model of MIF (as monomer and trimer) and position of the N-like loop (green) and the RLR sequence (red). Note: in the three-dimensional conformation of the monomer, RLR is located in the vicinity of the N-like loop of MIF. The trimeric structure shows that both the N-like loop and RLR are surface-exposed on the trimer (see also Fig. 7).

Among the residues shared by the responsive peptides was the Arg-87-Leu-88-Arg-89 (RLR) sequence segment. Considering sequences comprising basic residues such as Arg or Lys have been found to contribute to the site 1 interaction surface between CXCL12 and CXCR4³⁹, we hypothesized the RLR region may contribute to MIF/CXCR4 binding. To further test the potential relevance of this sequence, the influence of N-terminal or C-terminal neighboring amino acids, and peptide length, we also analyzed peptides 71–90, 73–90, 74–89, 75–90, 76–90. Peptide 76–86 was used as an RLR-void control. Overall, this analysis confirmed a role for the RLR sequence of MIF in CXCR4(1–27) binding. While the comparison of the tested peptides in Fig. 1a also implied that a net positive charge (+1 versus 0 or –1) may foster the interaction with CXCR4(1–27), the extended comparison of probed peptides in Fig. 1b suggested that signal strength also is modulated by N-terminal extension of the RLR sequence, while N-terminally extended peptides with a net positive charge of +2 showed higher signal intensities than the shorter peptides with a net charge of +3 (Fig. 1b). A more specific role for the RLR sequence also was confirmed by a control experiment using randomized - ‘scrambled’ - peptides. Binding of biotin-CXCR4(1–27) to peptide 75–90, i.e. the strongest interacting MIF peptide tested, was compared with the binding of five randomized - ‘scrambled’ - sequences of MIF peptide 75–90, Supplementary Fig. 1 shows that binding of the scrambled peptides to CXCR4(1–27) was markedly lower than binding of the RLR-containing wildtype sequence.

When we inspected the position of RLR in the three-dimensional structure of MIF, it appeared that residues 87–89 are positioned in the vicinity of the N-like loop of MIF. RLR is located at the C-terminal end of the second α -helix, with the two arginine residues of RLR being surface-exposed and the leucine making hydrophobic contacts (see ref.³⁶). Overall, this may lead to an expansion of the surface of the N-like loop, both in the monomeric and trimeric structures of MIF (Fig. 1c). Interestingly, CXCR4(1–27) comprises seven negatively charged residues (Glu-2, Asp-10, Glu-14, Glu-15, Asp-20, Asp-22, Glu-26) that could qualify for interactions with the positive

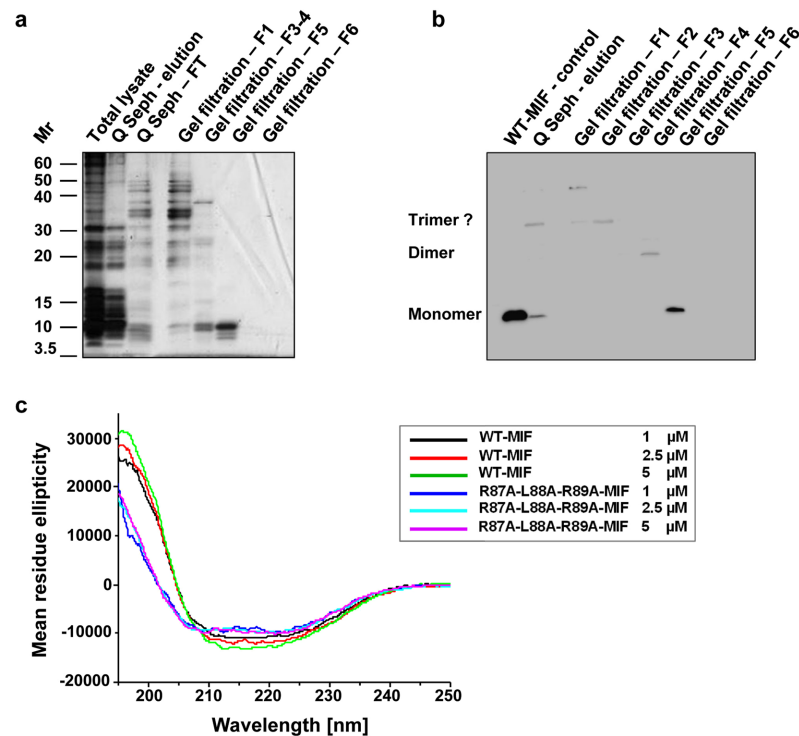


Figure 2. Expression, purification, and conformational integrity of R87A-L88A-R89A-MIF. (a) Recombinant expression and purification of R87A-L88A-R89A-MIF by anion exchange chromatography (Q Seph) and size exclusion chromatography (SEC, gel filtration) as analyzed by SDS-PAGE and silver staining. Total lysate, bacterial lysate after IPTG induction; Q Seph - elution, specific elution of protein from Q sepharose column by increasing salt gradient; Q Seph - FT, flow-through; gel filtration F1-F5, elution fractions 1-5 (see Supplementary Fig. 3). (b) Same as (a) but analysis by Western blot using a polyclonal anti-MIF antibody. (c) Circular dichroism (CD) spectropolarimetry shows that the folding and secondary structure profile of R87A-L88A-R89A-MIF is overall similar to that of WT-MIF. Spectra of R87A-L88A-R89A-MIF and WT-MIF at different concentrations are presented according to the indicated color code. Conformations in the CD spectra were measured as mean residue ellipticity versus the wavelength in the far-UV range.

charges within RLR of MIF. Therefore based on these initial data, we hypothesized that the RLR sequence stretch could contribute to the site 1 binding region between MIF and its chemokine receptor CXCR4.

A triple alanine mutant of MIF (R87A-L88A-R89A-MIF) was expressed in *E. coli* BL21/DE3. The expression efficiency of the mutant was lower than that of WT-MIF. The mutant was recovered from the cleared bacterial lysate and did not form inclusion bodies. It has a predicted lower isoelectric point than WT-MIF (pI (R87A-L88A-R89A-MIF) = 6.1) compared to 7.73 for WT-MIF and a predicted higher grand average of hydrophobicity (GRAVY) (0.090434 versus -0.001739; Supplementary Fig. 2). Accordingly, we chose a purification strategy that was different from that established for WT-MIF⁴⁰. Whereas WT-MIF does not bind to an anion exchange column at pH 7.5⁴⁰, R87A-L88A-R89A-MIF interacts with the anion exchange material under these conditions. The mutant protein was eluted from the anion exchange column via salt gradient and subjected to size exclusion chromatography (SEC) for further purification. The RLR mutant eluted at peaks with an approximate molecular size of 23 and 38 kDa, suggesting that it forms dimers and trimers under these conditions (Supplementary Fig. 3). Similar to WT-MIF^{41,42}, these oligomers constituted the major peak(s) in the size exclusion chromatogram, but the mutant additionally also showed several high molecular weight peaks (52–124 kDa), likely representing high molecular weight oligomers or aggregates. Applying this procedure, the mutant protein was obtained in appreciable yield, purity, and free of endotoxin contamination, as confirmed by SDS-PAGE silver-staining and Western blot analysis of the obtained fractions (Fig. 2a,b and Supplementary Table 1).

Next, we performed circular dichroism (CD) spectropolarimetry to address the question whether the alanine substitutions at the RLR site affect the structural integrity of MIF. Far-ultraviolet (UV) spectra were recorded between 195 and 250 nm and the spectrum of the RLR mutant compared with that of WT-MIF. CD spectroscopy provides a good estimation of the secondary structural profile of a protein and records relative changes in average secondary structural content, e.g. when a mutated protein is compared to its wildtype counterpart. Figure 2c shows that the secondary structure profile of the RLR mutant is similar to that of WT-MIF. Significant changes were limited to the spectral region below 210 nm. Dose-dependent recordings at 1, 2.5, and 5 μM did not lead to substantial spectral changes, neither for WT-MIF nor for the triple alanine mutant, indicating that neither protein showed an aggregation-tendency in this concentration range. Moreover, the quantification of the secondary structural contents following deconvolution of the CD spectra applying Dichroweb^{43,44} indicated that approximately 80% of the average ordered secondary structural content remained unaffected by the alanine substitutions (Supplementary Table 2). The deconvolution of the CD spectra also indicated that the typical α/β -structure of WT-MIF^{36,40} was preserved in the mutant, although the α -helix content, and to a lower extent, the β -strand percentage, in the mutant protein were found to be reduced by 12% and 7%, respectively, compared to the WT-MIF protein (Supplementary Table 2). In turn, random coil content was increased in the mutant by approximately 20%. Overall, the biochemical and biophysical data indicated that the alanine substitutions did not substantively interfere with the overall structural integrity of the MIF protein, although smaller changes of the average secondary structural content were observed and slight alterations on tertiary structure level cannot be excluded.

The RLR residues contribute to MIF/CXCR4 binding and the CXCR4-mediated cellular signaling activity of MIF. We previously determined the binding interaction between Alexa-488-labeled WT-MIF and CXCR4(1–27) by fluorescence spectroscopic titration. The K_d was estimated to be in the range of 10 μM ³⁵. Here, we performed fluorescence titrations with different concentrations of CXCR4(1–27) and Alexa-488-labeled R87A-L88A-R89A-MIF. The fluorescence emission of Alexa-488-labeled R87A-L88A-R89A-MIF at 522 nm did not exhibit any dose-dependent changes up to a 763-fold molar excess of CXCR4(1–27) (Supplementary Fig. 4). This suggested that R87A-L88A-R89A-MIF does not bind to CXCR4(1–27) and supports the notion that the RLR peptide contributes to MIF/CXCR4 binding.

To address the contribution of the RLR motif to MIF/CXCR4-specific cell signaling responses, we employed a genetically modified strain of *Saccharomyces cerevisiae* that replaces the yeast ste2 GPCR with human CXCR4 as previously reported³⁵. This cell system eliminates complications from mammalian cells that usually express more than one or all MIF cell surface receptors and is based on agonist-mediated activation of CXCR4 leading to a signaling cascade that results in β -galactosidase expression from the Fus1-lacZ reporter plasmid. We recently demonstrated that MIF activates CXCR4 signaling in this system. MIF agonism is similar but not identical to that of CXCL12, exhibiting partial allosteric agonism in comparison with CXCL12³⁵. Recombinant WT-MIF but not a control buffer triggered a marked CXCR4 response as previously reported³⁵ (Fig. 3a). In contrast, R87A-L88A-R89A-MIF failed to activate CXCR4 (Fig. 3a), confirming that the RLR sequence is involved in MIF/CXCR4 binding, and suggesting that it is necessary for MIF/CXCR4-mediated cell signaling.

Although the yeast cell system elegantly bypasses the problem of multiple MIF receptor expression in mammalian cells, it is somewhat artificial in that yeast features an outer cell wall in addition to the plasma membrane, necessitating the use of micromolar concentrations of agonists due to impaired access to CXCR4 in the membrane^{35,45}. We thus next wished to confirm and extend these findings in a cell system with an even higher physiological and pathophysiological relevance. One major function of the MIF/CXCR4 axis is to support the chemotactic recruitment of T and B lymphocytes^{30,32,46,47}. Here, we employed the human B cell line JVM-3, which expresses significant levels of the MIF receptors CXCR4 (Supplementary Fig. 5) and CD74, but not CXCR2 or CXCR7 (T. Thavayogarah, D. Sinitski, and J. Bernhagen, unpublished observation) and is an established cell model to monitor chemokine-mediated chemotactic migration responses⁴⁸. Figure 3b demonstrates that CXCL12 elicited a marked JVM-3 chemotaxis response ($\text{CTX}_{\text{CXCL12}} = 3.5 \pm 0.4$, $p < 0.0001$). The chemotactic effect of WT-MIF was lower than that of CXCL12 as previously seen, followed a concentration-dependence, and was similar to previously observed chemotactic effects of MIF on mouse B cells⁴⁶ (8 nM: $\text{CTX}_{\text{MIF}} = 1.58 \pm 0.4$, $p = 0.07$; 16 nM: $\text{CTX}_{\text{MIF}} = 2.43 \pm 0.06$, $p < 0.0001$). The RLR mutant did not exhibit a significant chemotactic activity on JVM-3 B cells at any of the concentrations tested (8 nM, 16 nM, 32 nM; $p = \text{ns}$; Fig. 3b). This suggested that the RLR sequence segment significantly contributes to MIF/CXCR4-mediated chemotactic cell migration responses.

Direct involvement of the RLR sequence in MIF/CXCR4 interactions. To obtain evidence that the RLR residues are directly involved in the MIF/CXCR4 interface, we combined the peptide spot array technology of the C-terminal region of the extended N-like loop of MIF with an alanine scanning approach. 15-mer human MIF peptides 75–89, 78–92, and 84–98, containing RLR in the C-terminal, middle or N-terminal part of the sequence, respectively, were synthesized as either wildtype sequence or as one of nine different alanine scan variants, with one or two alanine substitutions introduced across the entire sequence length (Fig. 4). Immobilized alanine scan variants were then probed for binding to biotinylated CXCR4(1–27). As expected from the peptide array analysis of RLR-containing MIF 15-mer peptides (Fig. 1), wild-type peptides 75–89, 78–92, and 84–98 bound CXCR4(1–27) with signal intensities between 2000 and 4000 LU. Overall, alanine scanning supported the notion that only alanine substitutions of the RLR region itself led to marked reductions in CXCR4(1–27) binding activity (Fig. 4a–c). This is most apparent in peptides 75–89 and 78–92. An exception is the alanine substitution of residues 94 and 95 in peptide 84–98. Interestingly, residue 94 in WT-MIF is an arginine, insinuating that another positively charged amino acid in the vicinity of RLR may further contribute to MIF/CXCR4 binding. One other intriguing observation was made in the alanine scanning experiment. The substitution of the glutamic acid (residue 86) immediately preceding RLR in peptides 75–89 and 84–98 led to a pronounced increase in the binding signal (Fig. 4a,c). The substitution of glutamic acid by alanine at this position eliminates a negative charge in the

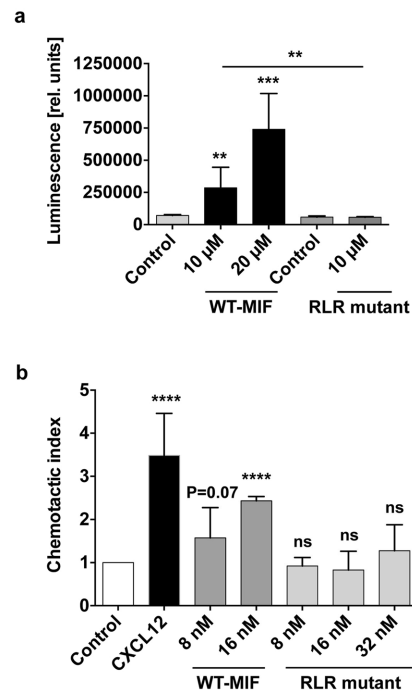


Figure 3. Mutation of the RLR residues markedly impairs CXCR4-dependent MIF cell signaling activities. (a) MIF signaling through CXCR4 in *S. cerevisiae* is abolished in R87A-L88A-R89A-MIF. CXCR4 replaces the Ste 2 receptor pheromone response pathway of *S. cerevisiae*. The pathway is further modified to enable activated human CXCR4 to elicit a robust signaling response that couples to the expression of different levels of lacZ gene dependent on the level of signaling, which is measured by enzymatic activity. Enzymatic activity is represented as relative luminescence. The concentrations of WT-MIF and RLR mutant are as indicated. Corresponding control buffers were used for WT-MIF (control 1) and the RLR mutant (control 2). Values are means \pm SD of 3–9 replicates representing three-to-four experiments. (b) Impaired chemotactic effect of R87A-L88A-R89A-MIF in CXCR4-dependent lymphocyte migration. Chemotactic migration (represented as chemotactic index) of JVM-3 lymphocytes towards R87A-L88A-R89A-MIF is compared with that elicited by WT-MIF at the indicated concentrations and CXCL12 (8 nM). PBS buffer was used as negative control to normalize for spontaneous random migration (control). The bar graph shows means \pm SD of 3–5 experiments. ** $p < 0.01$; *** $p < 0.005$; **** $p < 0.001$.

vicinity of RLR, supporting the conclusion that a net positive charge within RLR or in its immediate vicinity is important for CXCR4(1–27) binding. Altogether, these data show that only alanine substitutions within or in the vicinity of RLR lead to alterations in CXCR4(1–27) binding activity, suggesting a direct role for this MIF region in the MIF/CXCR4 binding interface.

To confirm this notion, we asked whether the RLR-spanning peptides MIF(86–100 or ERLRISPDVYINYY) and MIF(76–90 or YSKLLCGLLAERLRI), i.e. peptide sequences with strong binding signals in the peptide array experiments and a representing more N-terminal and C-terminal RLR positions, respectively, are able to interfere with MIF-mediated JVM3 B cell chemotaxis. The competition experiments adding different concentrations of the RLR-spanning peptides together with 16 nM of full-length WT-MIF into the chemotaxis chambers showed that both peptides competed with WT-MIF, leading to a reduction/ablation of the CXCR4-dependent chemotactic activity of MIF (Fig. 5). Peptide MIF(86–100) showed a concentration-dependent competition behavior with a trend towards inhibition seen at concentrations of 10 and 100 nM, and a significant and complete blockade of MIF activity at a concentration of 1 μ M. Peptide MIF(76–90) was even more potent and ablated the CXCR4-dependent chemotactic activity of MIF at concentrations of 10 and 100 nM. Together, the peptide competition experiment corroborated the notion that the RLR region directly contributes to functional MIF/CXCR4 interactions.

Finally, we tested this structural concept by molecular docking simulations. The N-terminal 22 or 26 amino acids of CXCR4, respectively, did not have interpretable density in the available CXCR4 X-ray structures^{5,6}. However, a recent nuclear magnetic resonance (NMR)-based structure of the complex between CXCR4(1–38)

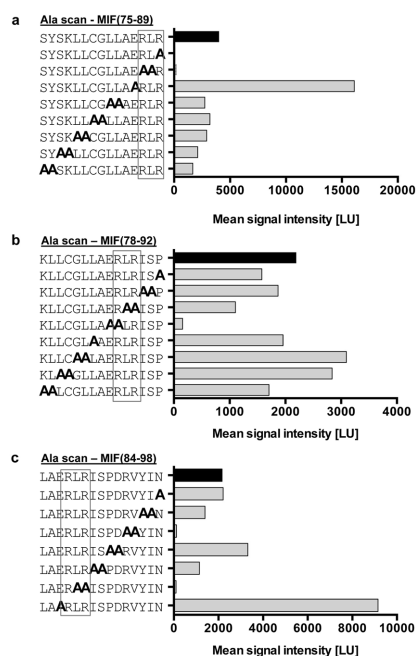


Figure 4. Alanine scanning of RLR-containing MIF peptides reveals role for RLR in binding the CXCR4 N-terminal peptide 1–27. A peptide spot array containing spotted 15-mer MIF peptides (a) 75–89, (b) 78–92, and (c) 84–98 was subjected to alanine scanning and probed with biotin-CXCR4(1–27). Sequential mono- or di-alanine substitutions were performed across the entire sequence of the peptides as indicated. Graphs are plots of spotted MIF/Ala scan peptides over the intensity of the binding signal to biotin-CXCR4(1–27) as read-out by streptavidin Cy5.5 fluorescence. Bars for wild-type peptides without alanine substitution are depicted in black; the position of the RLR sequence is framed.

and a CXCL12 monomer provides structural information about the amino terminus of human CXCR4⁴⁹. We subjected this structure of the CXCR4 N-terminus (2n55 CXCR4 Nterm.pdb) and the structure of human MIF (hmif 3djhmonomer.pdb) to the PATCHDOCK molecular docking algorithm that is based on shape complementarity principles. Both the restricted analysis, confined to residues 1–27 of the N-terminus, and the unrestricted approach, covering all 38 amino acids of the N-terminus, provided similar results in the PATCHDOCK calculation (data not shown) and were submitted to FIREDOCK for refinement and rescoring. For the highest ranked docking solution, a global energy of –43.76 kcal/mole was obtained for the MIF/CXCR4(1–38) complex. The following 10 lower ranked solutions also had global energies > 30 kcal/mole. Similar results were obtained for the complex with CXCR4(1–27). Figure 6 illustrates the structures obtained for the highest ranked docking solution of the complex between human MIF and the CXCR4 N-terminal. The molecular docking result confirms the notion that the N-terminus of CXCR4 could engage in multiple direct interactions with both the N-like loop and the RLR tripeptide area (Fig. 6a–c). Moreover, GPCRs are known to be dynamic and the N-terminal of CXCR4 is conformationally flexible^{5,6,49}, facilitating dynamic ligand contacts. A potential charge interaction between Arg-89 of the MIF RLR sequence and Asp-20 of the CXCR4 N-terminal is indicated (Fig. 6d).

Overall, these data suggest that the RLR region directly contributes to the MIF/CXCR4 binding interface to control CXCR4-mediated cellular effects of MIF. Charge interactions could play an important role in stabilizing the binding interface. In fact, the interaction between CXCR4 and its known ligands CXCL12 and human β-defensin-3 (HBD3) involves charge clusters^{39,50}. We have compared the sequence and structure of MIF with that of the CXCR4 ligands CXCL12 and HBD3 and analyzed the positions of residues, motifs, and charge clusters that have been implicated in the interaction with CXCR4 (Figs 7 and 8, and Supplementary Fig. 6). Figure 7a and Supplementary Fig. 6 highlight the residues and motifs in MIF that have previously been implicated in site 1 and 2 interactions between MIF and CXCR4 and compare them to the presumed corresponding residues in CXCL12 and HBD3. Of note, the MIF RLR sequence could represent a positive charge cluster similar to those represented by the K1-R8-R12 residues or the KHLK motif in CXCL12 as well as the K8-K32-R36 cluster in HBD3 (Fig. 7)^{39,50}. This notion is supported when comparing the surface charges in these regions between MIF, CXCL12, and HBD3 (Fig. 8).

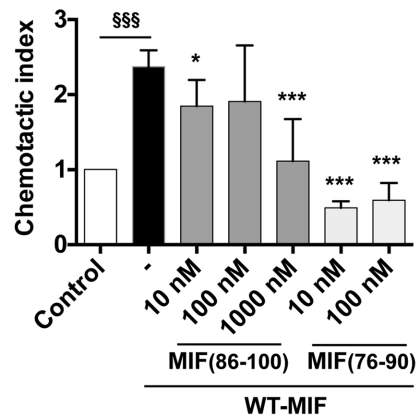


Figure 5. RLR-containing 15-mer MIF peptides block MIF/CXCR4-dependent JVM-3 lymphocyte chemotaxis. Chemotactic migration (represented as chemotactic index) of JVM-3 lymphocytes towards WT-MIF (16 nM) in the presence versus absence of different concentrations of RLR-containing peptides MIF(76–90) or YSKLLCGLLAERLRI and MIF(86–100) or ERLRISPDRVYINYY as indicated. PBS buffer was used as negative control to normalize for spontaneous random migration (control). The bar graph shows means \pm SD of 3–12 replicates and represent 2–3 experiments. Statistical comparisons were done between the MIF and MIF + peptide data sets (* $p < 0.05$; ** $p < 0.005$) and between control and MIF ($^{§§§}p < 0.005$).

Discussion

MIF is a pivotal inflammatory cytokine^{18,20,25} and prototypical atypical chemokine (ACK) that exhibits key ACK features^{24,25,30}. This study identifies residues in MIF, namely the Arg-Leu-Arg (RLR) tripeptide region, that contribute to site 1 binding of the MIF/CXCR4 interface to control CXCR4-mediated cellular effects of MIF. With an N-like loop and the Pro-2 residue previously identified to support MIF/CXCR4 binding³⁵, the current study completes the picture as to how an ACK such as MIF engages a classical chemokine receptor (CKR) such as CXCR4 and will help to mechanistically understand differences versus similarities between MIF-mediated CXCR4 signaling and that of the cognate ligand.

Chemokine receptors control numerous cellular pathways and orchestrate leukocyte trafficking under physiological and pathophysiological conditions. Hence, CKs and their receptors have been implicated as pivotal mediators in numerous diseases, e.g. inflammatory and cardiovascular diseases, autoimmune conditions, or cancer. As prototypical GPCRs of the G α i subtype, CKRs are druggable and numerous small molecule and peptide-based inhibitors are being pursued as potential therapeutic candidates, but considerable challenges remain^{31,32}. In particular, it has been difficult to devise CKR-specific approaches. The specificity problem occurs partly because the same receptor is expressed by different cell types but is activated by different chemokines expressed in various tissues and can potentially lead to adverse effects⁴. Accordingly, chemokine signaling mechanisms underlying ligand, receptor, and tissue bias are extensively studied.

The ACK activities of MIF contribute to its key role in inflammatory and cardiovascular diseases and cancer. For example, the MIF/CXCR2 axis controls atherogenic monocyte recruitment²⁹ and natural killer T (NKT) cell migration in inflammatory skin conditions³³. CXCR4-mediated MIF cell signaling activities encompass atherogenic lymphocyte recruitment^{30,32,46}, ischemia-triggered endothelial progenitor cell migration^{54,55}, eosinophil inflammation⁵⁶, promotion of inflammatory platelet survival⁵⁷, or colon cancer cell metastasis⁵⁸. It would thus be desirable to therapeutically interfere with these pathophysiological activities. However, there are multiple homeostatic and 'beneficial' functions mediated by CXCR4 following activation with its *bona fide* ligand CXCL12 such as cell homing, cardiac development, or neutrophil egress^{24,59,60}. Also, CXCR4 can form receptor complexes with CD74^{60,61}, and MIF/CD74 signaling has important cardioprotective activities in myocardial ischemia/reperfusion injury^{62,63}. In atherosclerosis, recent cell-specific knockouts of CXCR4 as well as the study of neutrophil-mediated atherogenic effects has established that the CXCR4/CXCL12 axis has cell-dependent protective or exacerbating effects^{64–66}.

Thus, to interfere with disease-promoting activities of the MIF/CXCR4 axis, specifically tailored targeting strategies need to be established that block MIF- but not CXCL12-mediated CXCR4 functions. This in turn requires a detailed structural understanding of the MIF/CXCR4 binding interface. We recently demonstrated that the unique N-terminal Pro-2 residue of MIF and its N-like loop region that MIF shares with classical chemokines are important determinants of the MIF/CXCR4 interface and that MIF activates CXCR4 by partial allosteric agonism compared with CXCL12³⁵. However, these structural features can only partially explain the high binding affinity between MIF and CXCR4, and the various functional differences to CXCL12/CXCR4^{24,30}. Although the reactivity of Pro-2 is unique and the cavity that contains it is an excellent druggable site⁶⁷, Pro-2 is involved in

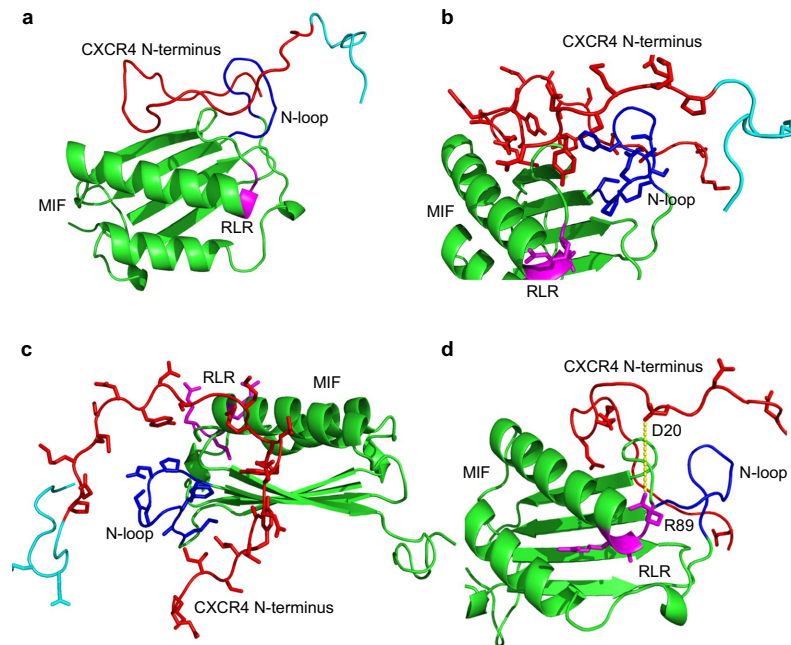


Figure 6. Structure model of the complex between human MIF and the N-terminus of CXCR4 as determined by molecular docking. Ribbon structures of the complex between full-length human MIF and human CXCR4(1–38) as determined by molecular docking are shown in different orientations with and without the representation of side chains. (a) Ribbon structure of the complex between MIF and CXCR4(1–38) without depicting any side chains. The following color code was used: MIF structure (green), CXCR4 N-terminus (red), RLR sequence of MIF (magenta), N-like loop of MIF (blue), residues 28–38 of CXCR4 (turquoise). (b) Same as (a) in slightly rotated orientation with relevant side chains of RLR, N-like loop, and CXCR4 N-terminus visualized. For clarity reasons, these residues are not labeled. (c) Side view of the structure in (b). (d) Same as (a) but with focus on the negatively charged residues in CXCR4(1–27), i.e. Glu-2, Asp-10, Glu-14, Glu-15, Asp-20, Asp-22, Glu-26, and the two positively charged arginine residues in RLR. A potential interaction between Arg-89 (R89) in RLR and Asp-20 (D20) of the CXCR4 N-terminus is indicated by a yellow dotted line.

MIF/CD74 binding as mutations of Pro-2 impair MIF signaling responses⁶⁸. Inhibition at this site could be problematic in cardiovascular diseases, as MIF/CD74 signaling conveys cardioprotection in early ischemia/reperfusion injury in the heart via activation of the tissue-protective AMP kinase pathway^{62,63}. MIF-targeting strategies should therefore ideally obviate Pro-2 and nearby residues as well as MIF region 79–85, both of which have been implicated in mediating CD74 activation^{38,68}.

In the current study, we have addressed these requirements by further characterizing the MIF/CXCR4 interface. We have identified an important additional structural element that contributes to the MIF/CXCR4 interface and is required for critical CXCR4-mediated MIF functions. Using biochemical/biophysical techniques and structure-activity studies in conjunction with peptide array technology, CXCR4-controlled cell function analysis, alanine scanning, and molecular docking, we show that an RLR tripeptide located at position 87–89 of the MIF sequence is positioned in close proximity to the N-like loop of MIF, contributes to the MIF/CXCR4 binding interface, and is functionally involved in CXCR4-mediated MIF activities. The peptide array and docking experiments suggest an important role for charge interactions by RLR arginine residues, in line with the view that electrostatic interactions are important in protein-protein interactions in general and in CXCR4/ligand interactions in particular.

Initial evidence for a role of RLR was obtained by a peptide spot array experiment, when we tested the binding of numerous RLR-spanning 15-mer peptides to the N-terminal sequence of CXCR4 using biotin-CXCR4(1–27). Although the N-terminal sequence of CXCR4 is not 'visible' in the available X-ray crystallographic structures of CXCR4, it has also been implicated in interactions with the cognate ligand CXCL12 by structure-activity studies and a recent NMR spectroscopy structure of a complex between CXCL12 and the N-terminal peptide 1–38 of CXCR4 together with NMR/X-ray structure hybrid modeling suggested a distinct role for the receptor N-terminus in chemokine recognition and receptor activation^{5,6,49}. Of note, the N-terminal region of CXCR4 had

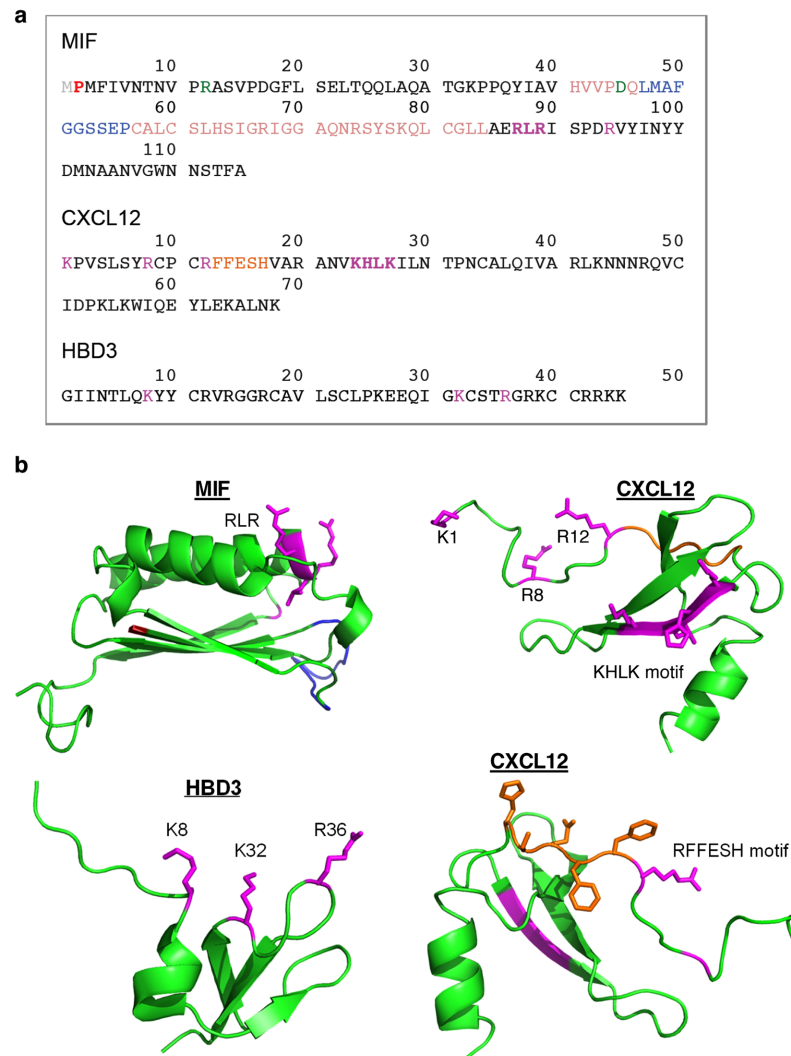


Figure 7. Structure comparison of MIF, CXCL12, and human β -defensin-3. **(a)** Comparison of the amino acid sequences, highlighting residues/motifs that have been implicated in binding to CXCR4. MIF: RLR (magenta, bold), Arg-94 (R94; magenta), N-like loop (suggested to contribute to site 1 binding³⁵; blue), Pro-2 (suggested to contribute to site 1 binding³⁵; red), extended N-like loop (suggested to contribute to site 1 binding³⁵; beige), pseudo-ELR motif (discontinuous, contributes to MIF/CXCR2 interface; green), Met-1 (cleaved upon expression; grey). CXCL12: KHLK motif (magenta, bold), Lys-1/Arg-8/Arg-12 charge cluster (magenta), RFFESH motif (orange). HBD3: Lys-8/Lys-32/Arg-36 charge cluster (magenta). **(b)** Comparison of the three-dimensional structures. Ribbon structures of the respective monomers are shown, with the backbones depicted in green. The corresponding color code and the captions for the residues/motifs that have been implicated in CXCR4 binding are as in (a); in the MIF structure, the 'extension' of the N-like loop (beige color in Fig. 7a) is not colored and the processed N-terminal methionine is not shown for clarity reasons. CXCL12 is depicted in two views (i) to highlight the KHLK motif and the charge cluster (top right) and (ii) the RFFESH motif (bottom right). Protein structures were produced/visualized with PyMOL.

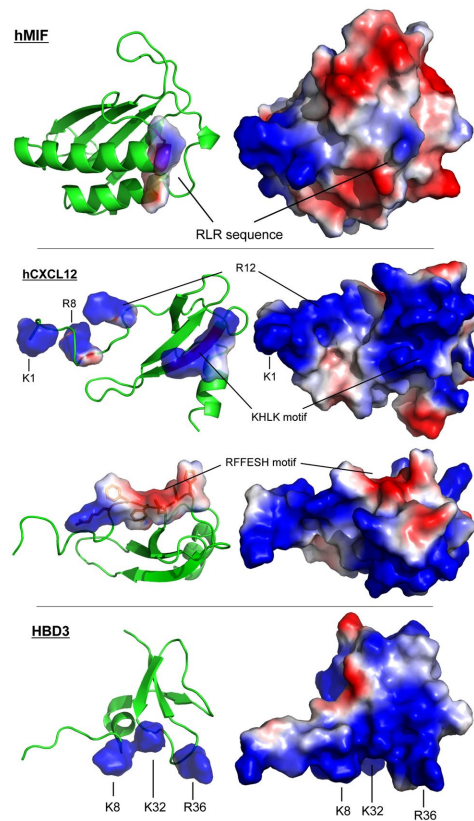


Figure 8. Comparison of the surface charges of MIF, CXCL12, and human β -defensin-3. Comparison of the three-dimensional structures of MIF, CXCL12, and human β -defensin-3 (HBD3) focusing on the surface charges. The relevant positively charged residues, the RLR, and the KHLK sequence, as well as the RFFESH motif are indicated as shown. Blue, positively charged residues arginine, lysine, or histidine; red, negatively charged residues aspartate and glutamate. Protein structures were produced/visualized with PyMOL.

previously been implicated in MIF/CXCR4 binding and peptide CXCR4(1–27) was found to bind to WT-MIF with a K_d of approximately $10\ \mu\text{M}$ ³⁵.

A fluorescence titration-based binding experiment in our current study showed that increasing concentrations of CXCR4(1–27) did not evoke conformational changes of a fluorescently labeled MIF mutant in which all three residues of the RLR sequence were substituted to alanine. Thus, we conclude that the triple mutant R87A-L88A-R89A-MIF does not bind to the CXCR4 N-terminus. This confirms the peptide array observations and suggests that the RLR sequence also is important for CXCR4(1–27) binding in the context of the three-dimensional –folded– MIF structure.

Importantly, the site-specific RLR mutant had a fully ablated CXCR4 signaling response in *S. cerevisiae* transformants specifically expressing CXCR4 and a reduced CXCR4-dependent lymphocyte migration response when compared with RLR-containing WT-MIF. The CXCR4-dependent yeast-signaling assay is a powerful functional tool³⁷, as it represents a signaling-competent cell system that does not express any of the other MIF receptors. Accordingly, a signaling response can be directly linked to interactions between MIF and CXCR4. The MIF R87A-L88A-R89A triple mutant elicited a reduced cell migratory response in CXCR4-expressing JVM-3 lymphocytes compared to WT-MIF, but contrary to CXCR4-mediated signaling in the *S. cerevisiae* system the response was not completely abolished. While the mutant failed to show any chemotactic activity at the optimal concentration of WT-MIF (16 nM), a slight increase in activity was noted at 32 nM, although this effect did not reach statistical significance. The yeast only signals through a modified G-protein to induce expression of β -galactosidase, whereas JVM-3 cells signal through both G-proteins and β -arrestin. β -arrestin is known to have roles in cellular

chemotaxis⁶⁹. Another explanation for the subtle differences in WT-MIF versus triple mutant behavior between the yeast and JVM-3 chemotaxis cell systems could be that JVM-3 cells also express the MIF receptor CD74 (unpublished observations). Overall, ablation or reduction of MIF-mediated CXCR4-dependent cell responses by R87A-L88A-R89A-MIF in the yeast and JVM-3 lymphocyte assays suggests that the RLR sequence is critically involved in the MIF/CXCR4 interface.

The RLR mutant bioactivity data together with our structure-activity studies point toward a role for RLR in CXCR4 binding and CXCR4-mediated signaling. In fact, RLR may represent a novel hot segment in the binding interface⁷⁰, but our study also has some limitations. The peptide spot array method is based on interactions of surface-immobilized 10–20-mer peptides with their binding partner. These peptides can only represent regions that are linear in nature with many different conformations. In our experiments, the RLR-containing peptides or their mutant counterparts were probed with biotinylated CXCR4(1–27). There are 7 acidic residues (Asp or Glu, including a di-Glu repeat) within the CXCR4 sequence 1–27 that could interact with the RLR motif by electrostatic/polar interactions. A role for electrostatic interactions between CXCR4(1–27) and MIF-RLR is further supported by our alanine scanning and the molecular docking results.

Alanine scanning shows that substitution of Glu-86, the acidic glutamic acid residue immediately preceding RLR, by alanine, causes a marked increase in the interaction signal between biotin-CXCR4(1–27) and the respective RLR-containing peptide. Although our alanine scanning and molecular docking data did not lend fully unanimous support to the notion that positive charges in or around the RLR sequence are the decisive factor of the binding force at the MIF/CXCR4-N-terminus interface, the E86A mutation was noticeable in that it led to an enormous increase in binding signal between MIF-RLR-containing peptide and biotin-CXCR4(1–27) in two independent MIF peptides (peptides 75–89 and 84–98), increasing the net positive charge in this region by +1. In the same vein, substitution of Arg-94 by alanine in peptide 84–98 led to a marked reduction in binding signal. The molecular docking approach between MIF and the CXCR4-N-terminus and the performed sequence and three-dimensional structure comparisons between MIF and CXCL12 as well as HBD3 confirmed the conclusion that positive charge interactions critically contribute to the site 1 interface between MIF and CXCR4. Arg-89 of MIF may engage in a binding interaction with Asp-20 of CXCR4 and numerous similarities were noted between the relevant positive charge clusters in CXCL12 (i.e. the KHLK motif) or HBD3 and the RLR area of MIF with its excess of net positive charges.

The alanine mutations of RLR do not interfere with the overall structural integrity of protein. To this end, CD spectroscopy of R87A-L88A-R89A-MIF confirmed the overall structural integrity of the folded mutant protein, although a 20% decrease in ordered secondary structural content was observed that was paralleled by a corresponding increase in unordered elements. However, CD can only determine average changes across all secondary structure elements of a protein and it is unknown whether e.g. the reduction in α -helix content affected the second α -helix of MIF, at the far C-terminal end of which RLR is located. Moreover, some of the available structures of human MIF place the RLR segment C-terminal of the α -helix³⁶. Thus, RLR might reside in a less structured part of the MIF protein. Furthermore, although MIF has been suggested to interact with its receptor CD74 as a trimer⁷¹, it is currently unknown which oligomeric form binds to CXCR4. Monomeric and dimeric species of MIF have been reported^{42,72,73} and a MIF monomer may have a higher structural flexibility than the more rigid trimeric architecture. Our molecular docking experiments were performed with monomeric MIF, yielding reasonable global binding energies regarding the interaction with the N-terminal of CXCR4 and suggesting that the MIF RLR site and/or the N-like loop could engage in numerous direct interactions with the N-terminal 27 residues of CXCR4. The experiments performed in this study cannot fully rule out the possibility that the mutation of RLR leads to slight changes in the secondary or tertiary conformation of MIF, but the data obtained strongly point toward the conclusion that the three residues play a strong role in the interaction with CXCR4. The future X-ray crystallographic elucidation of the three-dimensional structure of R87A-L88A-R89A-MIF and eventually a co-crystal structure between WT-MIF and CXCR4(1–27) or full-length CXCR4 will clarify the precise positioning of RLR at the MIF/CXCR4 interface.

All five randomized control peptides of MIF(75–90) showed an impaired binding signal to CXCR4(1–27), when compared to the wildtype sequence featuring a preserved RLR site. This experiment suggested that, in addition to the net positive charge in the RLR region, the RLR sequence itself is critical for CXCR4 binding. Comparing the MIF/CXCR4 interaction with those of the other known CXCR4 ligands confirms this notion and further supports the role of the positive charge cluster in MIF. CXCL12 is one of the most basic chemokines, with an overall charge of +8. The corresponding net charge of the extracellular regions of CXCR4 is –9. Interestingly, the post-translational sulfation of tyrosine residues Tyr-7, Tyr-12, and Tyr-21 in the N-terminus of CXCR4, introducing additional negative charges, has been suggested to further enhance CXCL12 binding^{74,75}, but the influence of post-translational CXCR4 modifications on MIF effects have not yet been studied.

With respect to the MIF RLR sequence, there is an HLK sequence (residues 25–27) in CXCL12. The strong increase in signal intensity of the ALRL mutant peptide as compared to a MIF ERLR peptide might thus correspond to the CXCL12 KHLK motif. Although in the absence of a MIF-CXCR4, nor CXCL12-CXCR4, structure it is difficult to know how MIF is oriented with respect to CXCR4, given that the MIF Glu-86 and CXCL12 Lys-24 are in the same position of the RLR and HLK residues of both proteins, respectively, gives support that this region is important for binding to CXCR4. The available vMIP-II-CXCR4 structure⁵ only is of limited usefulness in this regard. From a structural point of view, the vMIP-II residues at the position of the CXCL12 residues KHLK have no charge and are on the β -strand nearest to receptor interactions. However, it is not known what the subtle rotations of the proteins CXCL12 and CXCR4 relative to the vMIP-II-CXCR4 structure are. And it is far harder to predict what the structure of the MIF-CXCR4 complex is. Similar considerations apply to the charge cluster of HBD3⁵⁰.

It needs to be emphasized that the binding sequences and properties of MIF, CXCL12, and HBD3 do not need to be exactly the same for binding to occur. This notion is borne out by the sequence of vMIP-II bound to CXCR4⁵ versus the

sequence of CXCL12³⁹ as well as the comparison of the vMIP-II-CXCR4 and CXCL12-CXCR4(1–38) co-structures^{5,49}. Moreover, GPCRs are known to be very dynamic and are able to accommodate different types of structures.

In summary, identification of the RLR tripeptide of the atypical chemokine MIF provides important structural information to our understanding of the MIF/CXCR4 binding site and helps to further distinguish this interface from that between CXCR4 and its cognate ligand CXCL12. This should also aid in the design drug-targeting approaches that are specific to MIF while leaving homeostatic CXCR4/CXCL12 or tissue-protective MIF/CD74 responses unaffected.

Methods

Cell culture, endotoxin assay, and reagents. JVM-3 cells (ACC-18) are a chronic B cell leukemia cell line and were kindly provided by Prof. M. Hallek, University of Cologne Medical School, Cologne, Germany. JVM-3 were grown in RPMI media with 1% penicillin/streptomycin and 10% fetal bovine serum (Invitrogen-Thermo Fisher Scientific, Karlsruhe, Germany) essentially as described previously⁴⁸. Miscellaneous cell culture reagents also were bought from Invitrogen-Thermo Fisher Scientific and from PAA (Pasching, Austria). LPS content of the purified WT-MIF and RLR mutant proteins was tested by limulus amoebocyte assay (LAL, Lonza, Cologne, Germany) following the manufacturer's recommendation. All other reagents were obtained from Sigma, Merck, Roth, or Calbiochem, and were of the highest purity degree available.

Peptide synthesis. All peptides were produced by Fmoc solid phase synthesis (SPPS) and purified by high-performance liquid chromatography (HPLC) essentially as described previously⁷⁶. The quality was checked by mass spectrometry analysis. Biotinylated N-terminal peptide human CXCR4(1–27) was synthesized by Fmoc-SPPS and biotin introduced N-terminally following an amino-caproic acid (Aca) spacer. RLR-containing MIF peptides 76–90 (YSKLLCGLLAERLR) and 86–100 (ERLRISPDRVYINYY) were custom-synthesized by Peptide Specialty Laboratories (PSL, Heidelberg, Germany).

Recombinant proteins, cloning of R87A-L88A-R89A-MIF, and SDS-PAGE/Western blotting. SDF-1 α /CXCL12 was purified as previously described⁷⁷. Biologically active recombinant human MIF (rMIF) was expressed and purified essentially as described⁴⁰.

The RLR triple alanine mutant of MIF (MIF(R87A-L88A-R89A-MIF)) was cloned into the pET11b vector by site-specific mutagenesis using Quikchange II (Agilent, Waldbronn, Germany) and the cDNA of wildtype (WT) human MIF as template⁴⁰ and expressed in *E. coli* BL21/DE3. Mutagenic primers were first synthesized to create single mutations within the wild-type human MIF insert⁴⁰. Subsequent mutagenic reactions created double mutant and triple mutant plasmids. Plasmids were sequenced to verify the accuracy and location of the mutations within the vector.

The RLR mutant protein was expressed in *E. coli* B21/DE3 (Merck-Novagen, Darmstadt, Germany). Cultures of 250 mL were grown at 37 °C until an optical density of 0.6–0.8 was reached. A final concentration of 1 mM isopropyl 1-thio- β -D-galactopyranoside (IPTG) was used to induce protein expression for an additional 3.5 h. Bacteria were then harvested in aliquots of 50 mL by centrifugation, and the cell pellets were frozen at –20 °C for later use. For protein purification, cells pellets were resuspended in 2 mL Tris-based saline (25 mM Tris, 10 mM NaCl, pH 7.5). The bacteria were lysed under 75 MPa using a French Press (Emulsi-Flex C5, Avestin, Germany). Cell debris was removed by centrifugation at 38000 g for 30 min. To further reduce debris, the supernatant, referred to as the raw protein extract of the bacterial lysate, was sterile-filtered through a 0.22 μ m membrane filter. Recombinant RLR mutant protein was first purified using anion exchange chromatography (Q sepharose, GE Healthcare, Freiburg, Germany) using a fast protein liquid chromatography system (FPLC, ÄKTA Pure, GE Healthcare). The system was equilibrated with Tris-buffered saline, pH 7.5. The triple mutant protein was eluted using a buffer gradient (ending in 25 mM Tris, 1 M NaCl, pH 7.5). Mutant protein-containing fractions were pooled and stored on ice. Following Q sepharose, the protein was further purified by size exclusion chromatography (SEC, Superdex 75, GE Healthcare) in 20 mM sodium phosphate buffer, pH 7.2, i.e. buffer conditions compatible with MIF bioactivity. R87A-L88A-R89A-MIF was sterile-filtered and stored at 4 °C until further use. The RLR mutant protein was obtained free of endotoxin contamination (<20 pg LPS/ μ g protein), suitable for subsequent biochemical and cell-based tests. Fractions containing the RLR mutant protein were confirmed by SDS-PAGE and Western blotting.

SDS-PAGE was performed in 15% gels under reducing conditions. Gels were either silver-stained or processed for Western blotting. For silver staining, gels were fixed for 16 h in 50% methanol/10% acetic acid in addition to 10% fixation enhancer (161–0461, BioRad, Munich, Germany). For Western blotting, proteins were transferred to nitrocellulose membranes at 20 V for 90 min. Blots were blocked with 5% bovine serum albumin and stained for MIF or RLR mutant bands using our rabbit polyclonal anti-MIF antibody (Ka345)²³. Both gels and blots were imaged with the LiCor Odyssey Fc system (LICOR Biotechnology GmbH, Bad Homburg, Germany).

CXCR4-specific yeast-signaling assay. The *S. cerevisiae* strain (CY12946) expressing a functional CXCR4 has been previously described³⁷. Upon CXCR4 activation, MAP kinase signaling transcribes and translates β -galactosidase (lacZ), which is quantified by an enzymatic assay. To study the CXCR4 signaling by extracellular WT-MIF or R87A-L88A-R89A-MIF, CY12946 strain was transformed with CXCR4 in Cp4181 and β -gal in Cp1584. The transformed cells were grown overnight in selective medium. The cells were diluted to 0.3–0.8 OD_{600 nm} and incubated with WT-MIF or R87A-L88A-R89A-MIF. WT-MIF was tested at a final concentration of 10 and 20 μ M, showing dose-dependent activation of CXCR4 signaling. Due to solubility restrictions of the corresponding stock solution, the triple alanine mutant could only be tested at a concentration of 10 μ M. The activation of CXCR4 was quantitated by β -galactosidase activity using Beta glo kit (Promega). The data shown is the mean \pm SD of 3–9 replicates representing three-to-four experiments.

Peptide array methodology. The peptide microarray method using glass slide technology has been described previously³⁵. Briefly, following stepwise SPOT synthesis (Intavis MultiPep RSi/CelluSpot Array, Cologne, Germany, or JPT, Berlin, Germany), the peptides were dispensed on an activated glass surface using a droplet-depositing system. Target peptides were immobilized chemo-selectively and purified by reaction of the peptides with the modified glass surface resulting in the formation of a covalent bond, which allowed the removal of all truncated and acetylated sequences by subsequent washing steps. After all peptides were arrayed on the glass surface, active residues were passivated. Analysis of interactions was performed using a microarray processing station (Intavis Slide Spotting Robot). The microarrays were incubated with biotinylated CXCR4(1–27) peptide. For determination of false-positives, one microarray was incubated with fluorescently-labeled streptavidin only. After incubation with 200 μ l of biotinylated CXCR4(1–27) (10 μ g/ml) in blocking buffer for 30 min and washing with Tris-buffered saline (TBS) buffer containing 0.1% Tween 20, the array was developed with Cy5-streptavidin or horse-radish peroxidase (HRP)-streptavidin in blocking buffer. Scanning or chemiluminescence imaging at the appropriate wavelength showed the signal intensity as a single measurement for each peptide and the intensity of each fluorescent spot on the scanned or imaged microarray slide was quantified. Each spot-feature was analyzed for total intensity and background intensity and corrected for background. Data shown represent the mean values of corrected mean/median of signal intensities from two or three identical subarrays on each microarray image.

Lymphocyte chemotaxis assay. Migration assays using the CXCR4-expressing JVM-3 B cell line were performed in a transmigration well as previously described³² using the following modifications. Briefly, JVM-3 B cells were sub-cultured and transferred to media without FBS. A migration assay was performed using 24-well format Transwell membranes (Sigma-Corning; 5 μ m pore size) containing 1×10^6 JVM-3 cells in the upper chamber. 8 nM or 16 nM of WT-MIF and 8 nM, 16 nM, or 32 nM of R87A-L88A-R89A-MIF was added to the lower chamber as chemoattractant. As positive control, 8 nM CXCL12 was used. Wells without chemoattractant served as negative control and were used to normalize migration effects to 'chemotactic index' (number of migrated cells in the presence of chemoattractant divided by the number of migrated cells in the absence of the chemoattractant) – as described previously³⁰. In the inhibition assay, 10 nM, 100 nM, or 1 μ M of the RLR-containing MIF peptides 76–90 (YSKLLCGLLAERLR) or 86–100 (ERLRISPDRVYINYY) were pre-incubated with WT-MIF for 30 min prior to the migration process and also added to the upper chamber. Cells were allowed to migrate for 24 h. After migration, cells in the lower chamber were counted using CountBright absolute counting beads (Invitrogen) using a FACSVerse flow cytometer (BD Biosciences, Heidelberg, Germany).

Circular dichroism spectroscopy. Far-UV circular dichroism (CD) spectra were recorded in a Jasco 700 CD spectropolarimeter (Jasco Labor- u. Datentechnik GmbH, Groß-Umstadt, Germany). Scans were recorded at 25 °C between 195 and 250 nm as an average of three scans and smoothed to obtain the final data. Spectra were collected at 1.0 nm intervals with a bandwidth of 1 nm in a buffer containing 10 mM sodium phosphate, pH 7.2. Spectra of WT-MIF and R87A-L88A-R89A-MIF were measured at concentrations of 1, 2.5, and 5 μ M and were recorded in a 1 cm quartz cuvette. CD spectra are presented as a plot of mean residue ellipticities. Dynode voltage values generally were below 800 and did not interfere with CD measurements. Secondary structure fractions were quantitated by the DichroWeb online software webtool by deconvolutions of CD spectra using ContinLL at DichroWeb and the reference spectra set 7^{43,44}.

Fluorescence spectroscopy. Fluorescence spectroscopy titrations of R87A-L88A-R89A-MIF with the N-terminal peptide of CXCR4 were performed as previously described for WT-MIF³⁵. Briefly, titrations were recorded in quartz cuvettes in a JASCO FP-6500 fluorescence spectrophotometer. MIF-CXCR4 interactions were probed by titrating CXCR4 peptide(1–27) against Alexa Fluor-488- R87A-L88A-R89A-MIF. The triple mutant MIF was applied at a concentration of 6.5 nM in 20 mM sodium phosphate buffer, pH 7.2, and the peptide was added at ratios of 1:0.76, 1:1.52, 1:7.63, 1:76.3, and 1:763 in the same buffer. Changes in Alexa Fluor-488 emission were recorded between 500 and 600 nm wavelength.

Structural models. Three-dimensional structures of human MIF, human CXCL12, and human β -defensin-3 (HBD3) were visualized using the PyMOL Molecular Graphics System, version 1.8.2.2 (Schrödinger, LLC, New York). Surface charge distributions were calculated using PyMOL's protein contact potential function. The structures were modeled according to the Protein Data Bank (PDB) file for human MIF (PDB identifier: 3DJH), human CXCL12 (PDB identifier: 1SDF), HBD3 (3KJ6), human CXCR4 (Chain B of 2N55), or our molecular docking results. In the structure file of the N-terminus of CXCR4, there are two additional amino acids – glycine and serine – prior to the coding sequence. For clarity in the visualization, these residues were removed before producing the images.

Molecular docking. For molecular docking simulations of MIF with the N-terminus of CXCR4, we used the PatchDock + FireDock framework. The online tool PatchDock (Beta 1.3 version) for rigid body docking was used with complex type set to default and a clustering root-mean-square deviation (RMSD) of 4.0 Å⁷⁸. Monomeric MIF (chain A of the human MIF structure file 3DJH) was used as a 'ligand'; the N-terminal region (residues 1–38) of CXCR4 (chain B of the structure file 2N55) as the 'receptor'. The 1000 best solutions obtained by PatchDock were then submitted to FireDock for refinement by introducing flexibility in the docking process, and rescoring according to free energy calculations^{79,80}. Out of the calculated complexes, the highest-ranking solution was chosen for further analysis and visualization.

Statistical analysis. Data are expressed as means \pm SD. Student's t-tests (two-sided, unpaired) was performed to compare experimental groups. Differences with a value of $p < 0.05$ were considered statistically significant.

References

1. Nibbs, R. J. & Graham, G. J. Immune regulation by atypical chemokine receptors. *Nat Rev Immunol* **13**, 815–829 (2013).
2. Charo, I. F. & Ransohoff, R. M. The many roles of chemokines and chemokine receptors in inflammation. *N Engl J Med* **354**, 610–621 (2006).
3. Murphy, P. M. *et al.* International union of pharmacology. XXII. Nomenclature for chemokine receptors. *Pharmacol Rev* **52**, 145–176 (2000).
4. Bachelier, F. *et al.* International Union of Basic and Clinical Pharmacology. LXXXIX. Update on the extended family of chemokine receptors and introducing a new nomenclature for atypical chemokine receptors. *Pharmacol Rev* **66**, 1–79 (2014).
5. Qin, L. *et al.* Structural biology. Crystal structure of the chemokine receptor CXCR4 in complex with a viral chemokine. *Science* **347**, 1117–1122 (2015).
6. Wu, B. *et al.* Structures of the CXCR4 chemokine GPCR with small-molecule and cyclic peptide antagonists. *Science* **330**, 1066–1071 (2010).
7. Tan, Q. *et al.* Structure of the CCR5 chemokine receptor-HIV entry inhibitor maraviroc complex. *Science* **341**, 1387–1390 (2013).
8. Zheng, Y., *et al.* Structure of CC chemokine receptor 5 with a potent chemokine antagonist reveals mechanisms of chemokine recognition and molecular mimicry by HIV. *Immunity* **46**, 1005–1017 e1005 (2017).
9. Burg, J. S. *et al.* Structural biology. Structural basis for chemokine recognition and activation of a viral G protein-coupled receptor. *Science* **347**, 1113–1117 (2015).
10. Zheng, Y. *et al.* Structure of CC chemokine receptor 2 with orthosteric and allosteric antagonists. *Nature* **540**, 458–461 (2016).
11. Oswald, C. *et al.* Intracellular allosteric antagonism of the CCR9 receptor. *Nature* **540**, 462–465 (2016).
12. Park, S. H. *et al.* Structure of the chemokine receptor CXCR1 in phospholipid bilayers. *Nature* **491**, 779–783 (2012).
13. Kofuku, Y. *et al.* Structural basis of the interaction between chemokine stromal cell-derived factor-1/CXCL12 and its G-protein-coupled receptor CXCR4. *J Biol Chem* **284**, 35240–35250 (2009).
14. Rajagopalan, L. & Rajarathnam, K. Structural basis of chemokine receptor function—a model for binding affinity and ligand selectivity. *Biosci Rep* **26**, 325–339 (2006).
15. Dyer, D. P., Salanga, C. L., Volkman, B. F., Kawamura, T. & Handel, T. M. The dependence of chemokine-glycosaminoglycan interactions on chemokine oligomerization. *Glycobiology* **26**, 312–326 (2016).
16. Joseph, P. R., Mosier, P. D., Desai, U. R. & Rajarathnam, K. Solution NMR characterization of chemokine CXCL8/IL-8 monomer and dimer binding to glycosaminoglycans: structural plasticity mediates differential binding interactions. *Biochem J* **472**, 121–133 (2015).
17. Crump, M. P. *et al.* Solution structure and basis for functional activity of stromal cell-derived factor-1; dissociation of CXCR4 activation from binding and inhibition of HIV-1. *EMBO J* **16**, 6996–7007 (1997).
18. Morand, E. F., Leech, M. & Bernhagen, J. MIF: a new cytokine link between rheumatoid arthritis and atherosclerosis. *Nat Rev Drug Discov* **5**, 399–410 (2006).
19. Bernhagen, J. *et al.* MIF is a pituitary-derived cytokine that potentiates lethal endotoxaemia. *Nature* **365**, 756–759 (1993).
20. Calandra, T. & Roger, T. Macrophage migration inhibitory factor: a regulator of innate immunity. *Nat Rev Immunol* **3**, 791–800 (2003).
21. Tilstam, P. V., Qi, D., Leng, L., Young, L. & Bucala, R. MIF family cytokines in cardiovascular diseases and prospects for precision-based therapeutics. *Exp Opin Ther Targets* **21**, 671–683 (2017).
22. Rassaf, T., Weber, C. & Bernhagen, J. Macrophage migration inhibitory factor in myocardial ischaemia/reperfusion injury. *Cardiovasc Res* **102**, 321–328 (2014).
23. Kleemann, R. *et al.* Intracellular action of the cytokine MIF to modulate AP-1 activity and the cell cycle through Jab1. *Nature* **408**, 211–216 (2000).
24. Pawig, L., Klasen, C., Weber, C., Bernhagen, J. & Noels, H. Diversity and inter-connections in the CXCR4 chemokine receptor/ligand family: molecular perspectives. *Front Immunol* **6**, 429 (2015).
25. Tillmann, S., Bernhagen, J. & Noels, H. Arrest functions of the MIF ligand/receptor axes in atherogenesis. *Front Immunol* **4**, 115 (2013).
26. Howard, O. M. *et al.* Histidyl-tRNA synthetase and asparaginyl-tRNA synthetase, autoantigens in myositis, activate chemokine receptors on T lymphocytes and immature dendritic cells. *J Exp Med* **196**, 781–791 (2002).
27. Oppenheim, J. J., Biragyn, A., Kwak, L. W. & Yang, D. Roles of antimicrobial peptides such as defensins in innate and adaptive immunity. *Ann Rheum Dis* **62**(Suppl 2), ii17–21 (2003).
28. Yang, D. & Oppenheim, J. J. Antimicrobial proteins act as “alarmins” in joint immune defense. *Arthritis Rheum* **50**, 3401–3403 (2004).
29. Oppenheim, J. J. & Yang, D. Alarmins: chemotactic activators of immune responses. *Curr Opin Immunol* **17**, 359–365 (2005).
30. Bernhagen, J. *et al.* MIF is a noncognate ligand of CXC chemokine receptors in inflammatory and atherogenic cell recruitment. *Nat Med* **13**, 587–596 (2007).
31. Leng, L. *et al.* MIF signal transduction initiated by binding to CD74. *J Exp Med* **197**, 1467–1476 (2003).
32. Alampour-Rajabi, S. *et al.* MIF interacts with CXCR7 to promote receptor internalization, ERK1/2 and ZAP-70 signaling, and lymphocyte chemotaxis. *FASEB J* **29**, 4497–4511 (2015).
33. Kraemer, S. *et al.* MIF-chemokine receptor interactions in atherogenesis are dependent on an N-loop-based 2-site binding mechanism. *FASEB J* **25**, 894–906 (2011).
34. Weber, C. *et al.* Structural determinants of MIF functions in CXCR2-mediated inflammatory and atherogenic leukocyte recruitment. *Proc Natl Acad Sci USA* **105**, 16278–16283 (2008).
35. Rajasekaran, D. *et al.* Macrophage Migration Inhibitory Factor-CXCR4 Receptor Interactions: Evidence for partial allosteric agonism in comparison with cxcl12 chemokine. *J Biol Chem* **291**, 15881–15895 (2016).
36. Sun, H. W., Bernhagen, J., Bucala, R. & Lolis, E. Crystal structure at 2.6-Å resolution of human macrophage migration inhibitory factor. *Proc Natl Acad Sci USA* **93**, 5191–5196 (1996).
37. Sachpatzidis, A. *et al.* Identification of allosteric peptide agonists of CXCR4. *J Biol Chem* **278**, 896–907 (2003).
38. Assis, D. N. *et al.* The role of macrophage migration inhibitory factor in autoimmune liver disease. *Hepatology* **59**, 580–591 (2014).
39. Dealwis, C. *et al.* Crystal structure of chemically synthesized [N33A] stromal cell-derived factor 1alpha, a potent ligand for the HIV-1 “fusin” coreceptor. *Proc Natl Acad Sci USA* **95**, 6941–6946 (1998).
40. Bernhagen, J. *et al.* Purification, bioactivity, and secondary structure analysis of mouse and human macrophage migration inhibitory factor (MIF). *Biochemistry* **33**, 14144–14155 (1994).
41. Philo, J. S., Yang, T. H. & LaBarre, M. Re-examining the oligomerization state of macrophage migration inhibitory factor (MIF) in solution. *Biophys Chem* **108**, 77–87 (2004).
42. Mischke, R., Kleemann, R., Brunner, H. & Bernhagen, J. Cross-linking and mutational analysis of the oligomerization state of the cytokine macrophage migration inhibitory factor (MIF). *FEBS Lett.* **427**, 85–90 (1998).

43. Whitmore, L. & Wallace, B. A. DICHROWEB, an online server for protein secondary structure analyses from circular dichroism spectroscopic data. *Nucleic Acids Res* **32**, W668–673 (2004).
44. Whitmore, L. & Wallace, B. A. Protein secondary structure analyses from circular dichroism spectroscopy: methods and reference databases. *Biopolymers* **89**, 392–400 (2008).
45. De Nobel, J. G. & Barnett, J. A. Passage of molecules through yeast cell walls: a brief essay-review. *Yeast* **7**, 313–323 (1991).
46. Klasen, C. *et al.* MIF promotes B cell chemotaxis through the receptors CXCR4 and CD74 and ZAP-70 signaling. *J Immunol* **192**, 5273–5284 (2014).
47. Lue, H., Dewor, M., Leng, L., Bucala, R. & Bernhagen, J. Activation of the JNK signalling pathway by macrophage migration inhibitory factor (MIF) and dependence on CXCR4 and CD74. *Cell Signal* **23**, 135–144 (2011).
48. Malet-Engra, G. *et al.* CIP4 controls CCL19-driven cell steering and chemotaxis in chronic lymphocytic leukemia. *Cancer Res* **73**, 3412–3424 (2013).
49. Ziarek, J. J. *et al.* Structural basis for chemokine recognition by a G protein-coupled receptor and implications for receptor activation. *Sci Signal* **10** (2017).
50. Feng, Z., Dubyak, G. R., Jia, X., Lubkowski, J. T. & Weinberg, A. Human beta-defensin-3 structure motifs that are important in CXCR4 antagonism. *FEBS J* **280**, 3365–3375 (2013).
51. Proudfoot, A. E., Bonvin, P. & Power, C. A. Targeting chemokines: Pathogens can, why can't we? *Cytokine* **74**, 259–267 (2015).
52. Schall, T. J. & Proudfoot, A. E. Overcoming hurdles in developing successful drugs targeting chemokine receptors. *Nat Rev Immunol* **11**, 355–363 (2011).
53. Hsieh, C. Y. *et al.* Macrophage migration inhibitory factor triggers chemotaxis of CD74+CXCR2+NKT cells in chemically induced IFN-gamma-mediated skin inflammation. *J Immunol* **193**, 3693–3703 (2014).
54. Kanzler, I. *et al.* Differential roles of angiogenic chemokines in endothelial progenitor cell-induced angiogenesis. *Basic Res Cardiol* **108**, 310–323 (2013).
55. Simons, D. *et al.* Hypoxia-induced endothelial secretion of macrophage migration inhibitory factor and role in endothelial progenitor cell recruitment. *J Cell Mol Med* **15**, 668–678 (2011).
56. de Souza, H. S. *et al.* Macrophage migration inhibitory factor promotes eosinophil accumulation and tissue remodeling in eosinophilic esophagitis. *Mucosal Immunol* **8**, 1154–1165 (2015).
57. Chatterjee, M. *et al.* Macrophage migration inhibitory factor limits activation-induced apoptosis of platelets via CXCR7-dependent Akt signaling. *Circ Res* **115**, 939–949 (2014).
58. Dessein, A. F. *et al.* Autocrine induction of invasive and metastatic phenotypes by the MIF-CXCR4 axis in drug-resistant human colon cancer cells. *Cancer Res* **70**, 4644–4654 (2010).
59. Weber, C., Doring, Y. & Noels, H. Potential cell-specific functions of CXCR4 in atherosclerosis. *Hamostaseologie* **36**, 97–102 (2016).
60. Doring, Y., Pawig, L., Weber, C. & Noels, H. The CXCL12/CXCR4 chemokine ligand/receptor axis in cardiovascular disease. *Front Physiol* **5**, 212 (2014).
61. Schwartz, V. *et al.* A functional heteromeric MIF receptor formed by CD74 and CXCR4. *FEBS Lett* **583**, 2749–2757 (2009).
62. Miller, E. J. *et al.* Macrophage migration inhibitory factor stimulates AMP-activated protein kinase in the ischaemic heart. *Nature* **451**, 578–582 (2008).
63. Qi, D. *et al.* Cardiac macrophage migration inhibitory factor inhibits JNK pathway activation and injury during ischemia/reperfusion. *J Clin Invest* **119**, 3807–3816 (2009).
64. Doring, Y. *et al.* Vascular CXCR4 limits atherosclerosis by maintaining arterial integrity: evidence from mouse and human studies. *Circulation* **136**, 388–403 (2017).
65. Zerneck, A. *et al.* Protective role of CXC receptor 4/CXC ligand 12 unveils the importance of neutrophils in atherosclerosis. *Circ Res* **102**, 209–217 (2008).
66. Liehn, E. A. *et al.* Double-edged role of the CXCL12/CXCR4 axis in experimental myocardial infarction. *J Am Coll Cardiol* **58**, 2415–2423 (2011).
67. Lolis, E. & Bucala, R. Macrophage migration inhibitory factor. *Exp Opin Ther Targets* **7**, 153–164 (2003).
68. Pantouris, G. *et al.* An analysis of MIF structural features that control functional activation of CD74. *Chem Biol* **22**, 1197–1205 (2015).
69. DeFea, K. A. Stop that cell! Beta-arrestin-dependent chemotaxis: a tale of localized actin assembly and receptor desensitization. *Annu Rev Physiol* **69**, 535–560 (2007).
70. London, N., Ravch, B. & Schueler-Furman, O. Druggable protein-protein interactions—from hot spots to hot segments. *Curr Opin Chem Biol* **17**, 952–959 (2013).
71. Fan, C. *et al.* MIF intersubunit disulfide mutant antagonist supports activation of CD74 by endogenous MIF trimer at physiologic concentrations. *Proc Natl Acad Sci USA* **110**, 10994–10999 (2013).
72. Ouertatani-Sakouhi, H. *et al.* Identification and characterization of novel classes of macrophage migration inhibitory factor (MIF) inhibitors with distinct mechanisms of action. *J Biol Chem* **285**, 26581–26598 (2010).
73. Muhlhahn, P. *et al.* NMR characterization of structure, backbone dynamics, and glutathione binding of the human macrophage migration inhibitory factor (MIF). *Protein Sci* **5**, 2095–2103 (1996).
74. Ziarek, J. J. *et al.* Sulfopeptide probes of the CXCR4/CXCL12 interface reveal oligomer-specific contacts and chemokine allostery. *ACS Chem Biol* **8**, 1955–1963 (2013).
75. Seibert, C. *et al.* Sequential tyrosine sulfation of CXCR4 by tyrosylprotein sulfotransferases. *Biochemistry* **47**, 11251–11262 (2008).
76. Andretto, E. *et al.* A Hot-segment-based approach for the design of cross-amyloid interaction surface mimics as inhibitors of amyloid self-assembly. *Angew Chem Int Ed Engl* **54**, 13095–13100 (2015).
77. Murphy, J. W., Yuan, H., Kong, Y., Xiong, Y. & Lolis, E. J. Heterologous quaternary structure of CXCL12 and its relationship to the CC chemokine family. *Proteins* **78**, 1331–1337 (2010).
78. Schneidman-Duhovny, D., Inbar, Y., Nussinov, R. & Wolfson, H. J. PatchDock and SymmDock: servers for rigid and symmetric docking. *Nucleic Acids Res* **33**, W363–367 (2005).
79. Andrusier, N., Nussinov, R. & Wolfson, H. J. FireDock: fast interaction refinement in molecular docking. *Proteins* **69**, 139–159 (2007).
80. Mashach, E., Schneidman-Duhovny, D., Andrusier, N., Nussinov, R. & Wolfson, H. J. FireDock: a web server for fast interaction refinement in molecular docking. *Nucleic Acids Res* **36**, W229–232 (2008).

Acknowledgements

This study was supported by Deutsche Forschungsgemeinschaft (DFG) grant SFB1123/A03 to A.K. and J.B., SFB1123/A01 to C.W., DFG grant IRTG1508 to M.Ba. and J.B., and NIH AI065029 to E.L. We thank C. Amette for assistance with the protein preparations.

Author Contributions

A.K. and J.B. wrote the manuscript; E.L., G.P., C.W. and M.L. edited the manuscript; A.K., J.B., E.L., M.L. and S.G. designed the experiments. M.L., C.Ko., M.Br., S.G., D.S., P.B., C.Kr. and T.T. performed the experiments and

docking studies. E.R., E.L., G.P., C.W., K.H. and M.Ba. provided critical technical expertise and materials. S.G., J.B. and A.K. prepared Figures 1 and 4. C.Ko. and M.L. prepared Figure 2. P.B., M.L., D.S., J.B. and T.T. prepared Figure 3. D.S., A.K., P.B. and J.B. prepared Figure 5. M.B., A.K. and J.B. prepared Figures 6–8. M.L., C.Ko., C.Kr., T.T., J.B. and A.K. prepared the Supplementary Figures and Tables. All authors reviewed the manuscript.

Additional Information

Supplementary information accompanies this paper at <https://doi.org/10.1038/s41598-018-23554-5>.

Competing Interests: The authors declare no competing interests.

Publisher's note: Springer Nature remains neutral with regard to jurisdictional claims in published maps and institutional affiliations.



Open Access This article is licensed under a Creative Commons Attribution 4.0 International License, which permits use, sharing, adaptation, distribution and reproduction in any medium or format, as long as you give appropriate credit to the original author(s) and the source, provide a link to the Creative Commons license, and indicate if changes were made. The images or other third party material in this article are included in the article's Creative Commons license, unless indicated otherwise in a credit line to the material. If material is not included in the article's Creative Commons license and your intended use is not permitted by statutory regulation or exceeds the permitted use, you will need to obtain permission directly from the copyright holder. To view a copy of this license, visit <http://creativecommons.org/licenses/by/4.0/>.

© The Author(s) 2018

6. Publication II: Sinitski *et al.*, 2020

Cross-kingdom mimicry of the receptor signaling and leukocyte recruitment activity of a human cytokine by its plant orthologs

D. Sinitski, K. Gruner, **M. Brandhofer**, C. Kontos, P. Winkler, A. Reinstadler, P. Bourilhon, Z. Xiao, R. Cool, A. Kapurniotu, F. J. Dekker, R. Panstruga and J. Bernhagen

Published in printed format 2020 in the Journal of Biological Chemistry.¹

DOI: 10.1074/jbc.RA119.009716

¹Open access publication, licensed under the CC BY 4.0 licence: <https://creativecommons.org/licenses/by/4.0/>.



Cross-kingdom mimicry of the receptor signaling and leukocyte recruitment activity of a human cytokine by its plant orthologs

Received for publication, June 7, 2019, and in revised form, November 17, 2019. Published, Papers in Press, December 6, 2019. DOI 10.1074/jbc.RA119.009716

Dzmitry Sinitski[‡], Katrin Gruner[§], Markus Brandhofer[‡], Christos Kontos[¶], Pascal Winkler[§], Anja Reinstädler[§], Priscila Bourilhon[‡], Zhangping Xiao^{||}, Robbert Cool^{||}, Aphrodite Kapurniotu[¶], Frank J. Dekker^{||}, Ralph Panstruga^{§1}, and Jürgen Bernhagen^{‡**2}

From the [‡]Chair of Vascular Biology, Institute for Stroke and Dementia Research (ISD), Klinikum der Universität München (KUM), Ludwig-Maximilians-University (LMU), 81377 Munich, Germany, the [§]Unit of Plant Molecular Cell Biology, Institute for Biology I, RWTH Aachen University, 52056 Aachen, Germany, the [¶]Division of Peptide Biochemistry, Technische Universität München (TUM), 85354 Freising, Germany, the ^{||}Division of Chemical and Pharmaceutical Biology, University of Groningen, 9713 AV Groningen, The Netherlands, and the ^{**}Munich Cluster for Systems Neurology (SyNergy), 81377 Munich, Germany

Edited by Luke O'Neill

Human macrophage migration-inhibitory factor (MIF) is an evolutionarily-conserved protein that has both extracellular immune-modulating and intracellular cell-regulatory functions. MIF plays a role in various diseases, including inflammatory diseases, atherosclerosis, autoimmunity, and cancer. It serves as an inflammatory cytokine and chemokine, but also exhibits enzymatic activity. Secreted MIF binds to cell-surface immune receptors such as CD74 and CXCR4. Plants possess MIF orthologs but lack the associated receptors, suggesting functional diversification across kingdoms. Here, we characterized three MIF orthologs (termed MIF/D-dopachrome tautomerase-like proteins or MDLs) of the model plant *Arabidopsis thaliana*. Recombinant *Arabidopsis* MDLs (*AtMDLs*) share similar secondary structure characteristics with human MIF, yet only have minimal residual tautomerase activity using either *p*-hydroxyphenylpyruvate or dopachrome methyl ester as substrate. Site-specific mutagenesis suggests that this is due to a distinct amino acid difference at the catalytic cavity-defining residue Asn-98. Surprisingly, *AtMDLs* bind to the human MIF receptors CD74 and CXCR4. Moreover, they activate CXCR4-dependent signaling in a receptor-specific yeast reporter system and in CXCR4-expressing human HEK293 transfectants. Notably, plant MDLs exert dose-dependent chemotactic activity toward human monocytes and T cells. A small molecule MIF inhibitor and an allosteric CXCR4 inhibitor counteract this function, revealing

its specificity. Our results indicate cross-kingdom conservation of the receptor signaling and leukocyte recruitment capacities of human MIF by its plant orthologs. This may point toward a previously unrecognized interplay between plant proteins and the human innate immune system.

Chemokines are chemotactic cytokines that orchestrate immune cell trafficking in development, homeostasis, and disease. They are small polypeptides characterized by a distinctive chemokine fold and conserved N-terminal cysteine residues. According to the spacing of these cysteines, they are grouped into CC-, CXC-, CX₃C-, and C-type sub-classes, and correspondingly-termed chemokine receptors (CKRs)³ exist. Chemokines interact with G-protein-coupled receptor (GPCR)-type CKRs to constitute a complex network characterized by both specificity and redundancy (1–4). Due to their major role in immune cell migration, chemokines are pivotal players in the host innate and adaptive immune response in infections, but also upon tissue injury and during tumorigenesis. When dysregulated and owing to their role in controlling leukocyte infiltration, chemokines contribute to the pathogenesis of human inflammatory and autoimmune diseases, but also cardiovascular disease and cancer (5, 6). The significance of the chemokine system to host defense against pathogens is additionally highlighted by viral mimicry mechanisms that interfere with host chemokine pathways as an immune evasion strategy (7).

Macrophage migration-inhibitory factor (MIF) is an inflammatory cytokine with chemokine-like characteristics and a regulator of host innate immunity. Dysregulated MIF has been

This work was supported by the Deutsche Forschungsgemeinschaft (DFG)-Agence Nationale Recherche (ANR) co-funded project “X-KINGDOM-MIF-cross-kingdom analysis of macrophage migration inhibitory factor (MIF) functions,” DFG Grants BE1977/10-1 (to J. B.) and PA861/15-1 (to R. P.), and DFG Grant within the framework of Munich Cluster for Systems Neurology EXC 1010 SyNergy, and in part by DFG Grant SFB1123/A03 (to A. K. and J. B.). The authors declare that they have no conflicts of interest with the contents of this article.

This article contains Figs. S1–S6, Tables S1–S4, and supporting Ref. 1.

¹ To whom correspondence may be addressed: Unit of Plant Molecular Cell Biology, Institute for Biology I, RWTH Aachen University, Worringerweg 1, 52056 Aachen, Germany. Tel.: 49-241-80-26655; Fax: 49-241-80-22637; E-mail: panstruga@bio1.rwth-aachen.de.

² To whom correspondence may be addressed: Chair of Vascular Biology, Institute for Stroke and Dementia Research (ISD), Klinikum der Universität München (KUM), Ludwig-Maximilians-University (LMU) Munich, Feodor-Lynen-Strasse 17, 81377 Munich, Germany. Tel.: 49-89-4400-46151; Fax: 49-89-4400-46010; E-mail: juergen.bernhagen@med.uni-muenchen.de.

This is an Open Access article under the CC BY license.

850 J. Biol. Chem. (2020) 295(3) 850–867



© 2020 Sinitski et al. Published under exclusive license by The American Society for Biochemistry and Molecular Biology, Inc.

Mimicry of human cytokine activity by *Arabidopsis* orthologs

identified as a pivotal mediator of human diseases such as acute and chronic inflammatory diseases, autoimmunity, atherosclerosis, and cancer (8–12). MIF is a member of the emerging family of atypical chemokines (ACKs). ACKs lack the chemokine fold and the consensus cysteine residues, but behave as chemoattractants by binding to CKRs (13–15). MIF not only binds to its cognate receptor CD74 to regulate cell proliferation (16), but also engages in binding to the CKRs CXCR2 and CXCR4 (17) as well as CXCR7 (18). MIF/CXCR pathways are drivers in several human diseases. The MIF/CXCR4 signaling axis controls monocyte, T-cell, and B-cell infiltration in atherosclerosis and other inflammatory conditions (17, 19). It also contributes to cancer metastasis, cardiac fibroblast survival, and eosinophil inflammation (20, 21).

MIF is a structurally unique 12.5-kDa protein and the founding member of the MIF protein family that also comprises D-DT/MIF-2 and MIF orthologs in various species (8, 17, 22–25). MIF proteins are structurally distinct from other cytokines and classical chemokines (26), but they share high architectural homology with bacterial tautomerase (8, 13, 27–29). The coding regions of human MIF and its paralog D-DT/MIF-2 are homologous and in close proximity to each other, suggesting an ancestral duplication event (24, 30). D-DT was named for its ability to tautomerize the nonnatural D-stereoisomer of dopachrome, and this catalytic property is shared by MIF (8, 27, 30). Thus, MIF proteins are bifunctional, acting as cytokines/chemokines and enzymes, although the functional significance of the tautomerase activity in mammals has remained elusive. The three-dimensional (3D) structures of MIF and D-DT/MIF-2 are highly similar (26, 31), whereas the amino acid sequence homology is limited to 34 and 27% in humans and mice, respectively. D-DT/MIF-2 shares biological and pathological activities with MIF, but also has distinct characteristics (30).

MIF proteins exhibit a remarkable degree of evolutionary conservation across kingdoms, ranging from mammals to vertebrates, including fish and unicellular parasites (8, 25, 32, 33). Mammalian MIFs are intracellularly expressed and secreted from cytosolic pools via a nonconventional secretion pathway (13). It has been speculated that MIFs are evolutionary ancient cytosolic enzymes that have “acquired” a secondary role as regulatory proteins during evolution from unicellular to multicellular organisms. Consistent with this hypothesis, intracellular MIF has been found to interact with several cytoplasmic proteins to control cell behavior by (co-)regulating cellular redox homeostasis, transcription, and signaling (13, 34). The role as a secreted cytokine/chemokine can be regarded as a further extension of its functional properties in the vertebrate lineage.

Thus, it is not surprising that interactions between MIF/receptor networks from different species/kingdoms have been reported. However, these are so far confined to interactions between a mammalian host and parasitic microbes, with MIF proteins from pathogenic species employing molecular mimicry strategies to contribute to virulence and immune evasion mechanisms (32). For example, *Plasmodium falciparum* produces a MIF ortholog that modulates the host immune response to malaria by suppressing T-cell memory (35). Similar to viral chemokine mimics, parasite MIFs appear to “hijack”

host MIF receptors, albeit so far only interactions with CD74 have been reported (36, 37).

Based on sequence data bank information, the presence of MIF/D-DT-like proteins (MDLs) is also predicted in the plant kingdom, and we recently performed comprehensive *in silico* analyses of MDL genes/proteins across kingdoms and in the model plant *Arabidopsis thaliana* (*AtMDLs*) (33, 38). The *A. thaliana* genome harbors three MDL genes, and the predicted proteins exhibit a sequence identity of 28–33% to human MIF (*HsMIF*). A main conclusion of the *in silico* analysis has been that plant MDL proteins share residues reported to be critical for the tautomerase pocket of human MIF/D-DT and may thus have tautomerase activity (38). Interestingly, MIF orthologs from the plant-parasitic aphid *Acyrtosiphon pisum* are secreted in its saliva and mediate aphid survival and feeding on its host plant pea, representing an example of modulating plant immunity by a plant parasite. However, to date no experimental studies have been conducted with plant MDLs and their functions remain completely elusive.

Given the significant degree of sequence homology between MIFs and a predicted structural similarity across kingdoms, including a predicted conserved tautomerase site, we hypothesized that there might exist plant MIF protein-based mimicry mechanisms and that plant MDLs might interact with components of the human MIF network. To test this hypothesis, we cloned and expressed the three known *AtMDL* proteins, studied their structural features by CD spectroscopy, molecular modeling, and site-specific mutagenesis, and explored functional commonalities and potential direct interactions with the human MIF protein/receptor network.

Results

Generation and characterization of His-tagged recombinant *AtMDLs*

To initiate functional characterization of the three predicted *AtMDL* proteins *AtMDL1*, *AtMDL2*, and *AtMDL3* and to test the hypothesis that they might share similarities with mammalian MIFs, we recombinantly expressed these proteins and purified them for functional studies. The nucleotide and amino acid sequences of *AtMDL1*, *AtMDL2*, and *AtMDL3* were retrieved from UniProt and the European Nucleotide Archive (ENA) database. The *AtMDLs* share a sequence identity of 28–33% with *HsMIF*; this value is similar to the homology between human MIF and its paralog D-DT/MIF-2. For purification purposes, the *AtMDLs* as well as *HsMIF* were designed to express a C-terminal hexahistidine (6xHis) epitope tag. Table S1 summarizes key molecular parameters of the studied His-tagged proteins (*AtMDL1*–6xHis, *AtMDL2*–6xHis, *AtMDL3*–6xHis, and *HsMIF*–6xHis), *i.e.* the molecular mass and isoelectric points as predicted by ExPASy M_r/pI point calculator (https://web.expasy.org/compute_pi/).

The protein sequences, including the Leu–Glu linker residues and the C-terminal His-tags, were aligned using ClustalW algorithm (<https://www.genome.jp/tools-bin/clustalw>) (Fig. S1A). Prediction of the 3D structures of the *AtMDL* proteins using the Phyre² Protein Fold Recognition Server (<http://www.sbg.bio.ic.ac.uk/phyre2/html/page.cgi?id=index>) suggests an

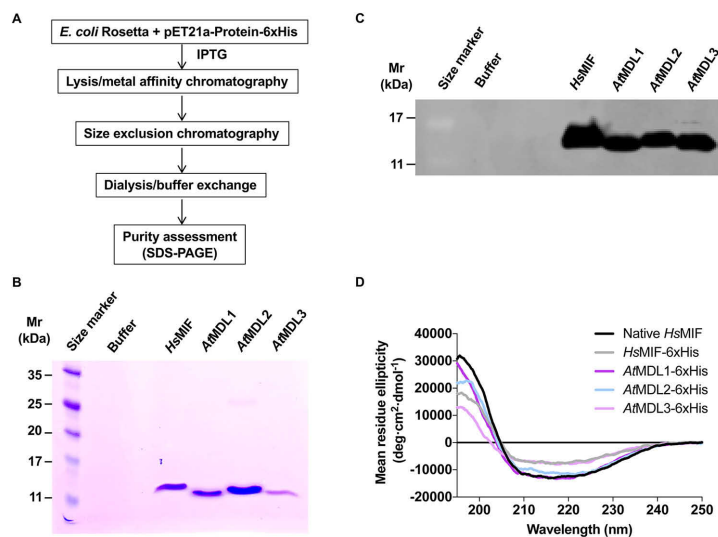
Mimicry of human cytokine activity by *Arabidopsis* orthologs

Figure 1. Expression, purification, and analysis of recombinant hexahistidine-tagged *HsMIF* and *AtMDLs*. A, schematic experimental procedure of protein expression and purification. B, Coomassie Blue staining of purified proteins after SDS-PAGE. C, protein detection by Western blotting using a monoclonal anti-His antibody. Relative molecular masses (M_r) are indicated on the left in kDa. D, CD spectropolarimetry of recombinant *HsMIF* and *AtMDLs*. Representative spectra of His-tagged *AtMDLs* and *HsMIF* as well as native (untagged) *HsMIF* are presented according to the indicated color code. Conformations in the CD spectra were measured as mean residue ellipticity as a function of the wavelength (given in nanometers) in the far-UV range.

apparent high-structural similarity between the authentic (untagged) *HsMIF*, 6xHis-tagged *HsMIF*, and its 6xHis-tagged plant orthologs (Fig. S1B). To assess potential structural similarities also experimentally, *AtMDL1*-6xHis, *AtMDL2*-6xHis, *AtMDL3*-6xHis, and *HsMIF*-6xHis were cloned and expressed in a bacterial expression system (Fig. 1A). All four C-terminally His-tagged recombinant proteins were purified by immobilized metal ion affinity (HisTrap) and subsequent size-exclusion chromatography. All four proteins were obtained in good quantities, without any detectable degradation products, and in high purity of >95% as assessed by SDS-PAGE (Fig. 1B and Table S2), although the yield for *AtMDL3* was lower compared with the other three proteins due to an observed increased aggregation tendency. Endotoxin concentrations were found to be negligible (Table S2). The identity of the enriched proteins was validated by SDS-PAGE/Western blotting detection with an anti-His antibody (Fig. 1C). We additionally conducted Western blot analysis using antibodies raised against human MIF. Both the polyclonal rabbit anti-mouse MIF antibody Ka565 and the monoclonal anti-human MIF antibody MAB289 substantially cross-reacted with *AtMDL1* and also weakly bound to *AtMDL2* (Fig. S2). This result supports the notion that the *AtMDLs* exhibit overlapping antigenic epitopes.

To further compare structural properties of the plant MDLs with those of *HsMIF*, we performed circular dichroism (CD) spectroscopy. This method is a valuable tool to compare the secondary structures of proteins of interest. CD spectra of all *AtMDLs* were recorded at concentrations of 1, 2.5, and 5 μM and compared with those of both His-tagged *HsMIF* and

nontagged (“fully native”) *HsMIF* (Fig. 1D and Fig. S3). This analysis verified that the recombinant *AtMDLs* were folded and that their secondary structure was very similar to that of His-tagged *HsMIF* and native *HsMIF*. It also suggested that the introduced His-tag has a minimal (if any) influence on the structures of the studied proteins, as the spectral features of *HsMIF* and *HsMIF*-6xHis were similar at all concentrations measured (Fig. 1D and Fig. S3). The deconvoluted spectra recorded at a concentration of 5 μM further indicated that the proportions of secondary structure elements of the recombinant *AtMDLs* differ only slightly from those of *HsMIF*. In line with previous CD data for human and mouse MIF (39), the calculated α -helical content of the *AtMDLs* was in the range of 20–37%, the β -strand contribution was between 28 and 33%, and β -turns were predicted to represent 17–22% of the secondary structural contents (Table S3). Overall, *AtMDL1*-6xHis and *AtMDL2*-6xHis showed the highest degree of similarity in experimentally determined secondary structural features to *HsMIF*-6xHis; *AtMDL3*-6xHis exhibited an elevated proportion of unordered secondary structural elements, an observation that is consistent with the reduced solubility of this MDL homolog compared with the other *AtMDLs* and *HsMIF*.

AtMDLs only exhibit minimal residual tautomerase activity

Whereas the functional role of the tautomerase activity of *HsMIF* and its natural substrate in a physiological context has remained elusive, the catalytic pocket residues have also been implicated to contribute to the receptor-binding interface between MIF and its receptors CD74 and CXCR4 (12, 13, 27, 40, 41). As the *AtMDLs* contain the consensus proline residue

Mimicry of human cytokine activity by Arabidopsis orthologs

in position 2 (Pro-2) known to be essential for tautomerase activity (Fig. S1) (38), we surmised that they may exhibit this catalytic capacity. Purified AtMDL1–6xHis, AtMDL2–6xHis, and AtMDL3–6xHis were subjected to a MIF tautomerase activity assay using *p*-hydroxyphenylpyruvate (HPP) as substrate. Using a MIF concentration of 250 nM, HsMIF and HsMIF–6xHis exhibited a similar tautomerase activity of 80–90 $\mu\text{mol min}^{-1} \text{mg}^{-1}$ (Fig. 2A). This value is in line with previous reports (42), indicating that the C-terminal His-tag does not interfere with the tautomerase activity of HsMIF, and underscoring that the epitope-tagged variant retains structural integrity, which is consistent with previous observations made for MIF orthologs from parasites (43). Surprisingly, all three AtMDLs were found to exhibit only minimal HPP tautomerase activity (Fig. 2A). Compared with buffer control conditions, the AtMDLs at a concentration of 250 nM exhibited an apparent activity of only 1–3 $\mu\text{mol min}^{-1} \text{mg}^{-1}$, which did not differ from the control at the level of statistical significance. A more detailed comparison of the enzyme kinetics of AtMDL1–6xHis with those of HsMIF–6xHis confirmed the notion that the AtMDLs only have minimal HPP tautomerase activity. Whereas the K_m value of the plant MDL was in the low millimolar range, *i.e.* similar to that of its human ortholog, the k_{cat} of AtMDL1–6xHis was substantially lower than that for HsMIF–6xHis, translating into a 300-fold higher k_{cat}/K_m value for HsMIF–6xHis compared with the plant ortholog (Table 1). To further explore the surprising difference in tautomerase activity between HsMIF and the AtMDLs, we also compared the tautomerase activities of AtMDL1–6xHis and HsMIF–6xHis in an assay using 1-dopachrome methyl ester (DCME) as substrate. At an enzyme concentration of 100 nM, HsMIF–6xHis exhibited an activity of 300 $\mu\text{mol min}^{-1} \text{mg}^{-1}$ toward DCME, whereas AtMDL1–6xHis only showed an activity $<20 \mu\text{mol min}^{-1} \text{mg}^{-1}$ (Fig. 2B). The notion that AtMDL1–6xHis only has a marginal residual activity was underscored by the kinetic parameters (K_m (HsMIF–6xHis) = 0.6 mM; K_m (AtMDL1–6xHis) = 4.1 mM; k_{cat} (HsMIF–6xHis) = 77.4 s^{-1} ; and k_{cat} (AtMDL1–6xHis) = 2.1 s^{-1}) with the k_{cat}/K_m value of HsMIF–6xHis 250-fold higher than that of AtMDL1–6xHis (Table 1). Thus, although the critical Pro-2 residue of the tautomerase activity site is conserved in all three AtMDLs, the catalytic activity itself is drastically reduced in the plant orthologs of human MIF.

To begin to explore the structural basis for this striking difference, we inspected the residues that shape the catalytic tautomerase pocket (42) in 3D space more closely. We noted that in addition to Pro-2 of human MIF, Lys-32, Ile-65, and Tyr-96 are either identical or homologous in the AtMDLs (Fig. 2C). By contrast, the basic His-63 residue of HsMIF is substituted by a hydrophobic residue (Ile or Val) in the AtMDLs, and even more strikingly, Asn-98 of human MIF is replaced by the strongly basic Lys-98 in all AtMDLs, introducing a positively-charged residue in a critical position (Fig. 2C). The predicted 3D structures shown in Fig. 2D visualize the positions of residue Asn-98 versus Lys-98 (*top panel*; ribbon structure) and indicate that the Asn \rightarrow Lys substitution may condition a conformational change of the catalytic pocket, paralleled by a different orientation of the Lys-98 side chain (*top panel*; ribbon structure, and

middle panel; surface structure). Furthermore, the electrostatic surface potential model (Fig. 2D, *bottom panel*) highlights the effects of the substitutions on charge distribution around the pocket.

To experimentally test the presumed role of residue 98 for the ablated catalytic activity of the AtMDLs, we cloned an HsMIF mutant, in which Asn-98 was replaced by Lys-98. The expression and purification characteristics of N98K–HsMIF–6xHis were similar to those of WT HsMIF–6xHis and the hexahistidine-tagged AtMDLs. However, when compared with WT HsMIF–6xHis for its HPP- and DCME-dependent tautomerase activity, N98K–HsMIF–6xHis exhibited a drastically-reduced catalytic activity (Fig. 2, E and F). Thus, the replacement of asparagine by lysine at position 98 in the AtMDLs at least partially explains the essential absence of HPP- and DCME-dependent tautomerase activity noted in the AtMDLs.

AtMDLs bind to and signal through human MIF receptors

The Pro-2 residue not only is a central component of the tautomerase cavity of human MIF, but also was identified to contribute to HsMIF binding to the MIF receptors CD74 and CXCR4 (40, 41). Furthermore, additional motifs contributing to the binding interface between HsMIF and these MIF receptors are also found in the AtMDLs (Fig. 3A). Mutations in Pro-2 of HsMIF have been found to invoke a conformational change in the MIF structure, resulting in altered binding and activation characteristics of CD74, suggesting that Pro-2 is a critical determinant of the MIF-binding site for CD74 (40). In addition, HsMIF residues 80–87 have been identified to contribute to CD74 binding (44), and this site also is well-conserved in all three AtMDLs (Fig. 3A). We therefore tested the possibility that AtMDLs may bind to CD74, although this receptor is not present in plants. We capitalized on a recently developed MIF/CD74-binding assay that employs an MBP–sCD74 fusion protein, in which maltose-binding protein (MBP) is fused to the MIF-binding CD74 ectodomain (45). Intriguingly, all three hexahistidine-tagged AtMDLs were found to bind to MBP–sCD74. AtMDL3–6xHis exhibited a binding capacity that was similar to that of HsMIF–6xHis (Fig. 3B) and bound to MBP–sCD74 with an apparent K_D of 200 nM (Fig. 3C and Fig. S4A).

For CXCR4, Pro-2 supports binding at the site 2 location of the MIF/CXCR4 interface (41, 46). Because HsMIF and the AtMDLs additionally exhibit an appreciable degree of homology in the extended N-like loop region that fosters site 1 binding of human MIF (Fig. 3A), we also tested the possibility that AtMDLs may bind to human CXCR4. As GPCR ectodomains are not amenable to *in vitro* binding studies such as those performed for CD74, we employed a genetically-modified yeast transformant stably expressing human CXCR4. These cells represent a receptor-specific cell system, in which the native yeast GPCR Ste2 was replaced by human CXCR4, which is functionally linked to the yeast Ste/MAPK signaling cascade and enables us to detect receptor-specific binding and signaling responses of CXCR4 following activation with CXCL12 or MIF by β -gal reporter activity. Moreover, the system is devoid of any other mammalian receptors that might be involved in MIF signaling, thus representing a “pure” *in vivo* receptor-binding/signaling system (41, 47). Yeast CXCR4 transformants were incubated

Mimicry of human cytokine activity by Arabidopsis orthologs

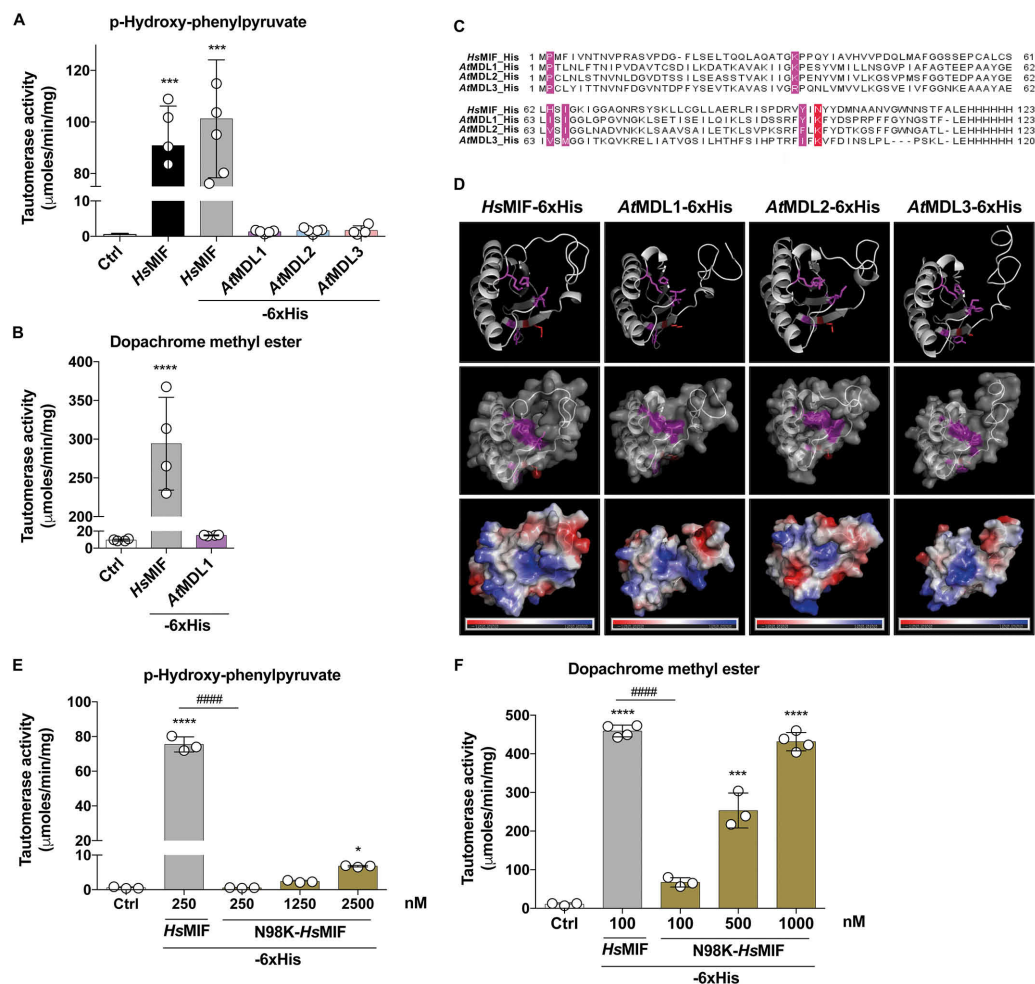


Figure 2. Recombinant AtMDLs only have residual tautomerase activity, likely due to a sterically-impeded substrate-binding pocket. *A* and *B*, tautomerase activity of recombinant HsMIF/AtMDL protein homologs measured by spectrophotometry. *A*, tautomerase activity of the three 6xHis-tagged AtMDLs was compared with that of 6xHis-tagged HsMIF using HPP as a substrate. Untagged HsMIF was measured for comparison. Data shown are from four to seven independent experiments \pm S.D., each performed in triplicate (scatter plot with white circles indicates individual data points). For statistical comparisons, one-way ANOVA between buffer control and the different samples was applied (***, $p < 0.005$). *B*, comparison of the tautomerase activity of AtMDL1-6xHis and HsMIF-6xHis using DCME as a substrate. Data shown are from four independent experiments \pm S.D., performed in triplicate each (scatter plot with white circles indicates individual data points). For statistical comparisons, one-way ANOVA between buffer control and the different samples was applied (***, $p < 0.005$). *C*, multiple sequence alignment of 6xHis-tagged variants of AtMDLs and HsMIF. Amino acid sequences of AtMDL1 (identifier Q9LU69), AtMDL2 (identifier Q9M011), AtMDL3 (identifier Q8LG92), and HsMIF (identifier P14174) were retrieved from the UniProt database and aligned by ClustalW using standard parameters in the Jalview multiple sequence alignment editor desktop application. The amino acid residues forming the tautomerase substrate-binding pocket are highlighted in magenta and red. *D*, comparative view of predicted 3D structures of 6xHis-tagged HsMIF and the three AtMDLs. Only the monomers are shown for simplicity reasons. Amino acid sequences of the AtMDL proteins were subjected to analysis via the PHYRE² Fold Recognition server and visualized with PyMOL. The predicted 3D structures (ribbon, surface, and electrostatic surface potential models) of AtMDL1-6xHis, AtMDL2-6xHis, and AtMDL3-6xHis were analyzed compared with the known X-ray-resolved 3D structure of HsMIF-6xHis. The upper and middle panels highlight the location of crucial tautomerase pocket residues in the ribbon structure and on the protein surface (magenta and red). In the lower panel, red and blue, respectively, indicate an excess of negative or positive charges near the surface, and grayish color symbolizes neutral regions. *E*, comparison of the tautomerase activity of N98K-HsMIF-6xHis and HsMIF-6xHis using HPP as a substrate. Data shown are from three to four independent experiments \pm S.D., performed in triplicate each (scatter plot with white circles indicates individual data points). For statistical comparisons, one-way ANOVA between buffer control and the different samples was applied (*, $p < 0.05$; ****, $p < 0.001$), as well as comparison between 250 nM HsMIF and 250 nM N98K-HsMIF-6xHis (####, $p < 0.001$). *F*, same as *E* except that DCME was used as a substrate, and HsMIF-6xHis was applied at a concentration of 100 nM (***, $p < 0.005$; ****, $p < 0.001$; ####, $p < 0.001$).

Mimicry of human cytokine activity by *Arabidopsis* orthologs

Table 1
Comparison of the kinetic tautomerase activity parameters between recombinant His₆-tagged *HsMIF* and *AtMDL1*

Data represent triplicate measurements ± S.D.

Enzyme assay	Protein	K_m^a	k_{cat}^b	k_{cat}/K_m
		<i>mM</i>	<i>s</i> ⁻¹	<i>mM</i> ⁻¹ <i>s</i> ⁻¹
HPP	<i>HsMIF</i> -6xHis ₆	2.31 ± 0.86	39.78 ± 0.89	17.22
	<i>AtMDL1</i> -6xHis	7.81 ± 6.63	0.44 ± 0.01	0.06
DCME	<i>HsMIF</i> -6xHis	0.59 ± 0.18	77.39 ± 1.67	131.17
	<i>AtMDL1</i> -6xHis	4.10 ± 5.19	2.11 ± 0.11	0.51

^a K_m is the Michaelis-Menten constant.

^b k_{cat} is turnover number.

with the recombinant *AtMDLs* and their potential CXCR4 binding/signaling activity compared with that of untagged and 6xHis-tagged human MIF. CXCR4 activation by *HsMIF*-6xHis was similar to that of *HsMIF*, confirming that the C-terminal hexahistidine tag neither impairs nor enhances MIF binding to CXCR4 (Fig. 3D). In line with previous data (41), CXCR4 activation by MIF was slightly less potent than that of the cognate ligand CXCL12. Strikingly, all three *AtMDLs* significantly promoted CXCR4 signaling activity. Moreover, CXCR4 activation by the plant MIF orthologs *AtMDL1*-6xHis and *AtMDL3*-6xHis was markedly stronger than that of *HsMIF*-6xHis and *HsMIF* (Fig. 3D).

These data suggested that *AtMDLs* have the capacity to interact with the human MIF receptors CD74 and CXCR4. As the yeast CXCR4-transformant experiments also implied a role in the activation of signal transduction, we focused on CXCR4 for subsequent functional studies and next asked whether *AtMDLs* would also trigger MIF-like CXCR4-facilitated signaling responses in mammalian cells. The MIF/CXCR4-induced PI3K/Akt signaling cascade is a well-studied MIF-mediated response pathway with physiological/pathophysiological relevance in human macrophages and T cells, as well as for cancer cell survival (20, 48, 49). We performed signaling studies in HEK293 cells stably overexpressing CXCR4 (HEK293-CXCR4), fostering appreciable surface expression levels of CXCR4 (Fig. S4B). In accordance with previous results (48), *HsMIF*-6xHis elevated phospho-Akt levels up to 4.5-fold within 15 min of stimulation (Fig. 4, A and B). Of note, all three *AtMDLs* stimulated Akt signaling in these cells. The most pronounced effect was seen for *AtMDL1*-6xHis, which not only shared with human MIF the capacity to trigger Akt phosphorylation, but even exhibited a more pronounced signaling effect, with its maximum shifted to an early peak at 5 min after stimulation (Fig. 4, C and D). *AtMDL2*-6xHis and *AtMDL3*-6xHis had slightly weaker effects than *HsMIF*-6xHis, and their activation maximum was delayed toward 15 min (Fig. 4, E-H). This result suggests that the *AtMDLs* are able to mimic the CXCR4-mediated Akt phosphorylation activity of human MIF in a mammalian cell system.

Plant MIF orthologs engage CXCR4 to act as chemoattractants for human monocytes

Induction of CXCR4-dependent intracellular signaling (Figs. 3 and 4) suggests that *AtMDLs* might modulate or mimic MIF's CXCR4-mediated leukocyte recruitment potential. To investigate this possibility, we tested the effect of the plant orthologs

on monocyte chemotaxis, applying Transwell migration chamber experiments that represent an established setup mirroring chemokine receptor-dependent immune cell migration responses. Recombinant hexahistidine-tagged *AtMDLs* were loaded into the lower compartment of a Transwell device, and their chemoattractant potency for THP-1 monocytes was compared with that of *HsMIF*-6xHis and the classical chemokine CXCL12. In line with prior findings obtained with untagged MIF (17), *HsMIF*-6xHis enhanced monocyte chemotaxis in a concentration-dependent manner with bell-shaped dose-response behavior and a maximal 4-fold chemotactic effect at a concentration of 16–32 nM. This compared well to the effect of the cognate CXCR4 ligand CXCL12 (chemotactic index = 4–7.5-fold compared with the untreated control at a concentration of 8 nM). Notably, all three *AtMDLs* were also able to promote THP-1 cell chemotaxis, featuring dose-dependent bell-shaped behavior, albeit at slightly lower potency compared with *HsMIF*-6xHis (Fig. 5). The maximal chemotactic effect of *AtMDL1*-6xHis and *AtMDL2*-6xHis was 2.5-fold compared with the buffer control and, like for *HsMIF*-6xHis, was observed at a concentration of 32 nM. *AtMDL3*-6xHis was also able to trigger monocyte migration, but its maximum effect was shifted toward a 5-fold higher concentration (chemotactic index = 3.5 at 80 nM) (Fig. 5).

We next sought to further confirm the specificity of this effect and to directly test for the involvement of CXCR4 in this process. ISO-1 is a well-established small molecule inhibitor of MIF that not only inhibits its tautomerase activity but also interferes with proinflammatory activities of MIF and MIF binding to CXCR4 (41, 50, 51). Similarly, AMD3100 is an allosteric inhibitor of CXCR4 that blocks the interaction with its cognate ligand CXCL12 and partially interferes with MIF-mediated CXCR4 activation (17, 41, 52–56). In line with these prior findings, co-application of AMD3100 fully abrogated the chemotactic effect of CXCL12 and also significantly inhibited *HsMIF*-6xHis-mediated monocyte migration (Fig. 6 and Fig. S5). Co-application of ISO-1 blunted the effect of *HsMIF*-6xHis, but did not interfere with CXCL12-triggered migration, confirming the specificity of MIF-driven monocyte chemotactic responses in our experimental system. Strikingly, both inhibitors completely ablated the chemotactic effect of *AtMDL1*-6xHis, which was studied as a representative of the three *AtMDLs*. Although not statistically significant, the drugs lowered the chemotactic effect even below baseline levels, and their effect on *AtMDL1*-6xHis appeared to be even more potent than that on *HsMIF*-6xHis. Together, these data suggested that the *AtMDLs*, in particular *AtMDL1*, are capable of triggering human monocyte recruitment with an efficiency similar to human MIF via interaction with the monocyte-expressed chemokine receptor CXCR4.

Plant MIF orthologs act as chemoattractants for human T cells and desensitize T-cell chemotaxis induced by human CXCL12 or MIF

THP-1 cells are monocyte-like human cells but have leukemic properties. To further test the significance of the chemotactic activity of the *AtMDLs*, we wished to study primary cells to ask whether other leukocyte cell types that express CXCR4

Mimicry of human cytokine activity by Arabidopsis orthologs

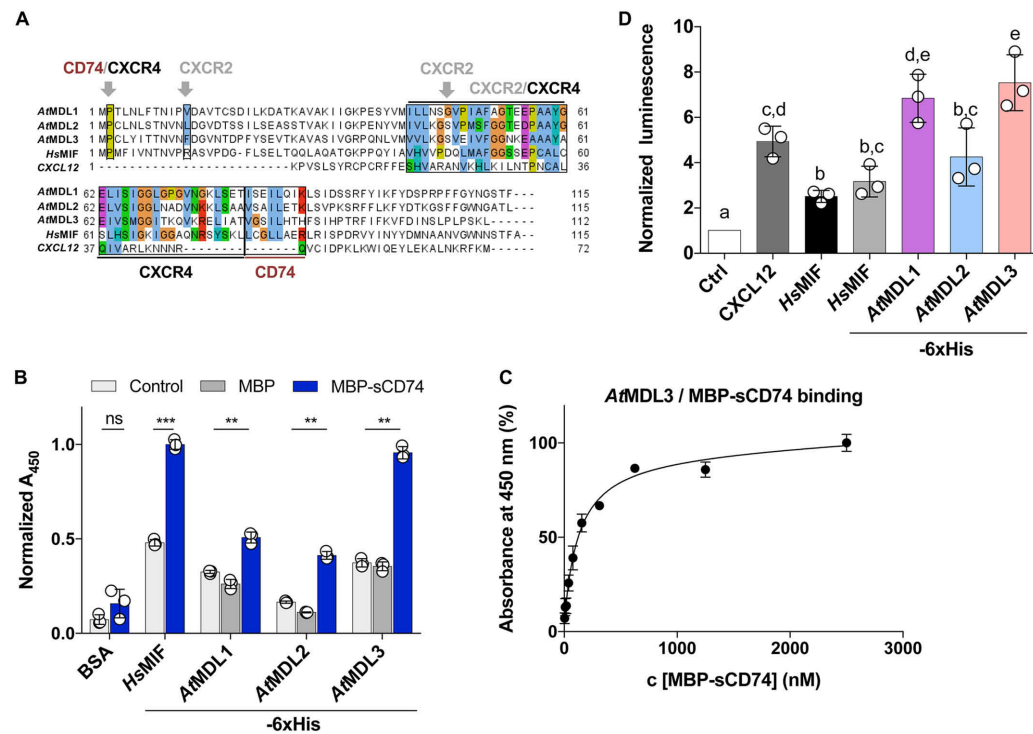


Figure 3. AtMDLs share homology with human MIF in the MIF receptor-binding sites, bind to CD74, and activate CXCR4-mediated signaling in a yeast-based reporter system. A, multiple sequence alignment of the AtMDLs, HsMIF, and human CXCL12. Amino acid sequences of AtMDL1 (identifier Q9LU69), AtMDL2 (identifier Q9M011), AtMDL3 (identifier Q8LG92), and HsMIF (identifier P14174) were retrieved from the UniProt database and aligned by ClustalW using standard parameters in the Jalview multiple sequence alignment editor desktop application. The amino acid residues contributing to the site I and II binding interface between HsMIF and CXCR4 (41) or CXCL12 and CXCR4 (90, 91), the binding sites between HsMIF and CD74, and the predicted corresponding regions in the AtMDLs are indicated. Determinants of HsMIF contributing to CXCR2 binding, although not further examined in this study, are indicated for comparison. The degree of homology/identity of the MIF, CXCL12, or AtMDL residues in these regions is highlighted by the following color score: blue, hydrophobic; red, positively charged; magenta, negatively charged; green, polar; pink, cysteine; orange, glycine; yellow, proline; cyan, aromatic; white, unconserved. B, comparison of the *in vitro* binding capacity between HsMIF-6xHis and MBP-sCD74 with that of the three His-tagged AtMDLs. Binding was measured by an ELISA-type plate-binding assay. BSA, blank PBS buffer (control), and MBP alone served as negative controls as indicated to account for nonspecific binding effects. Wells were coated with BSA (2% w/v), 500 nM HsMIF, and AtMDL1-6xHis, AtMDL2-6xHis, and AtMDL3-6xHis (500 nM), followed by binding of MBP or MBP-sCD74 (500 nM). After signal development, absorbance at 450 nm was measured, and the signals were normalized by setting the absorbance of HsMIF as 1. C, curve for binding of MBP-sCD74 and AtMDL3 using increasing concentrations of MBP-sCD74 as indicated. The data in B and C are displayed as means \pm S.D. ($n = 3$); (scatter plot with white circles indicates individual data points); ns, not significant; ***, $p < 0.001$; **, $p < 0.01$. D, CXCR4-mediated signaling in a yeast-based reporter system. In this assay, the Ste2 GPCR of the pheromone-response pathway of *S. cerevisiae* was substituted by the human CXCR4 receptor. Ligand binding to CXCR4 triggers signaling and expression of the *lacZ* gene, as assessed by β -gal activity. The concentrations of native (untagged) HsMIF, HsMIF-6xHis, and His-tagged AtMDLs were 20 μ M each. The concentration of human CXCL12 was equal to 2 μ M. Reporter activity is given as relative luminescence, normalized to the untreated control (Ctrl). Values shown represent means \pm S.D. from three independent experiments, in which the activity of each was assessed in technical duplicates (scatter plot with white circles indicates individual data points). Statistical analysis was performed using one-way ANOVA and post-hoc Tukey's HSD test with multiple comparisons. Different letters above the bars denote a statistically significant difference between groups ($p < 0.05$), and groups showing the same letters are not statistically significantly different from each other.

also chemotactically respond to the AtMDLs. Peripheral human blood-derived T cells are primary leukocytes that express substantial levels of surface CXCR4 and whose chemotactic response has been shown to be triggered by MIF (17). When examining the chemotactic migration of primary human T cells obtained from healthy donors, the dose optimum for HsMIF-6xHis was found to be between 16 and 32 nM (chemotactic index = 2.3) compared with a chemotactic index of 3.5 for 8 nM CXCL12. Of note, all AtMDLs elicited T-cell chemotaxis, and their pro-chemotactic capacity was compar-

able with their activity on monocyte migration, except that the optimum dose for AtMDL1-6xHis and AtMDL2-6xHis was at 16 nM (chemotactic index = 2–2.5) and that a significant migratory effect of AtMDL3-6xHis was only seen at a concentration 160 nM (Fig. 7A). Thus, AtMDLs also serve as chemoattractants for primary human T cells.

We employed this physiologically-relevant cell system to mechanistically explore the potential interplay between the AtMDLs and the endogenous human CXCR4 agonists CXCL12 and MIF, hypothesizing that the plant MIF orthologs might act

Mimicry of human cytokine activity by Arabidopsis orthologs

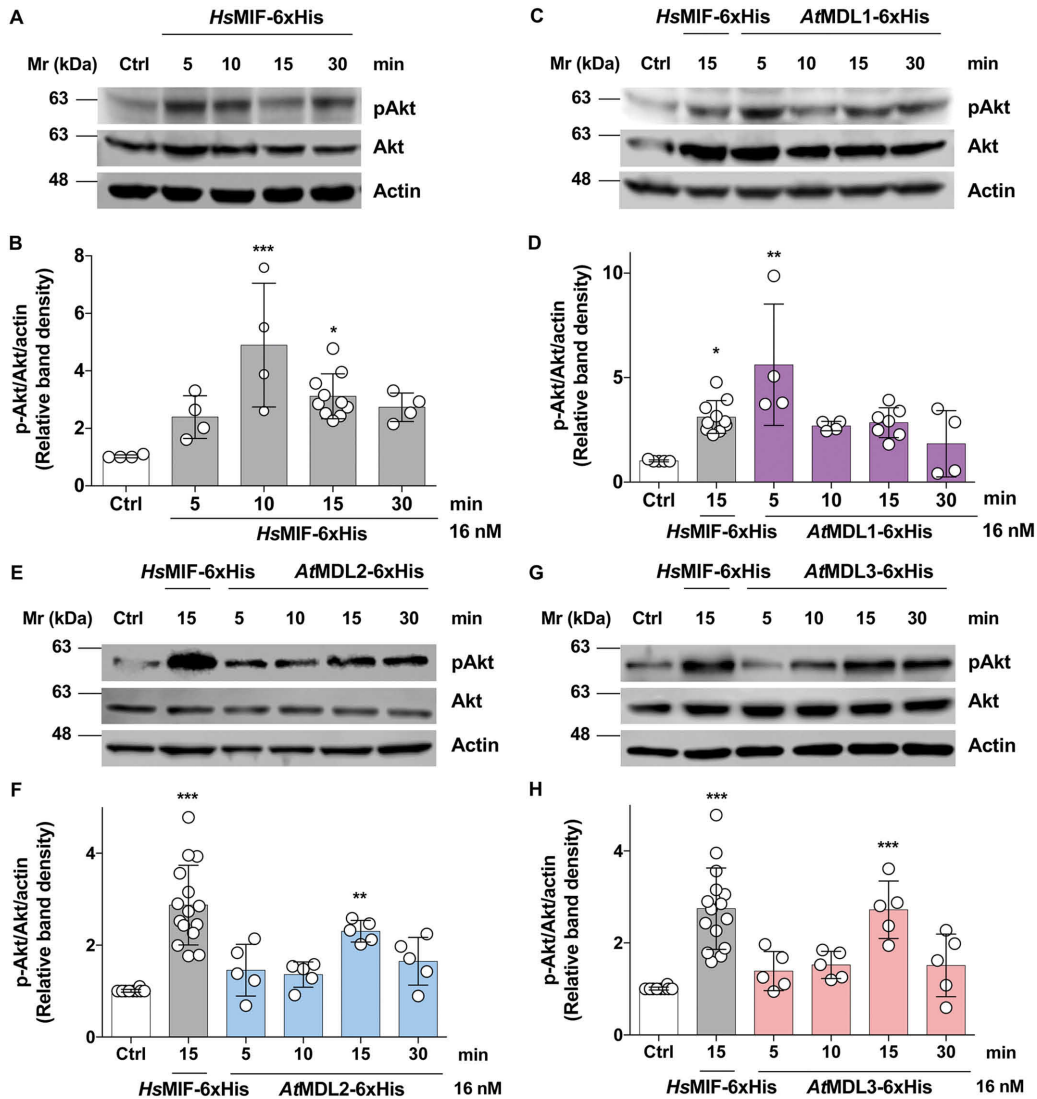


Figure 4. AtMDLs activate the CXCR4-PI3K/Akt-signaling pathway in human CXCR4-transfected HEK293 cells. *A*, representative Western blotting indicates Akt phosphorylation (pAkt) at different time intervals as indicated following stimulation with HsMIF-6xHis at a concentration of 16 nM. Ctrl, untreated control sample. Total Akt and actin were analyzed as loading control and for quantification purposes. *B*, quantification of pAkt band intensities in relation to Akt and actin band intensities according to the Western blot analysis in *A*. Bar graph represents means \pm S.D. of 5–15 experiments (scatter plot with white circles indicates individual data points). Statistical analysis was performed using one-way ANOVA between the untreated control (Ctrl) and the various time points following treatment (*, $p < 0.05$; ***, $p < 0.005$). *C*, *E*, and *G*, same as *A* except that the time-dependent phosphorylation of Akt following treatment with AtMDL1-6xHis, AtMDL2-6xHis, and AtMDL3-6xHis, respectively, was analyzed and compared with the effect of HsMIF-6xHis at 15 min. *D*, *F*, and *H*, same as *B*, except that the quantification refers to the Western blot analysis in *C*, *E*, and *G* and that data are from 5 to 10 experiments (*, $p < 0.05$; **, $p < 0.01$; ***, $p < 0.005$).

to modulate T-cell chemotactic responses induced by the human agonists. We specifically asked whether the AtMDLs would be able to enhance or desensitize T-cell chemotaxis responses triggered by the human CXCR4 chemokines. Pre-

treatment with all three hexahistidine-tagged AtMDLs added to the upper chamber of the Transwell setup fully ablated the chemoattractant activity of 16 nM HsMIF-6xHis in the lower chamber (Fig. 7B). Similarly, all three AtMDLs also attenuated

Mimicry of human cytokine activity by Arabidopsis orthologs

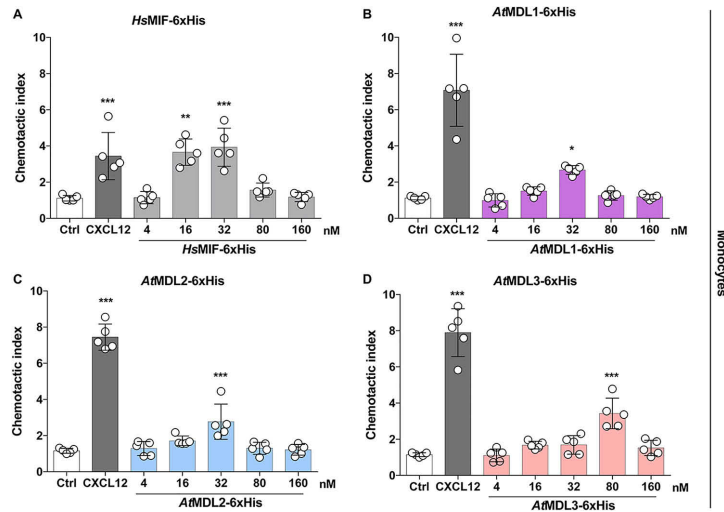


Figure 5. Recombinant 6xHis-tagged AtMDLs trigger chemotactic migration of human THP-1 monocytes in a dose-dependent manner. Chemotaxis (referred to here as chemotactic index) of THP-1 monocytes toward HsMIF-6xHis (A), AtMDL1-6xHis (B), AtMDL2-6xHis (C), or AtMDL3-6xHis (D) at the different indicated concentrations. The chemotactic potency was compared with human CXCL12 (at a concentration of 8 nM) serving as a positive control and to buffer control (Ctrl), which also served to normalize treatments to spontaneous (random) migration events. The bar graphs show means \pm S.D. of five independent experiments (scatter plot with white circles indicates individual data points). Statistical analyses were performed using one-way ANOVA between the buffer control and the treatment groups at the various doses (*, $p < 0.05$; **, $p < 0.01$; ***, $p < 0.005$).

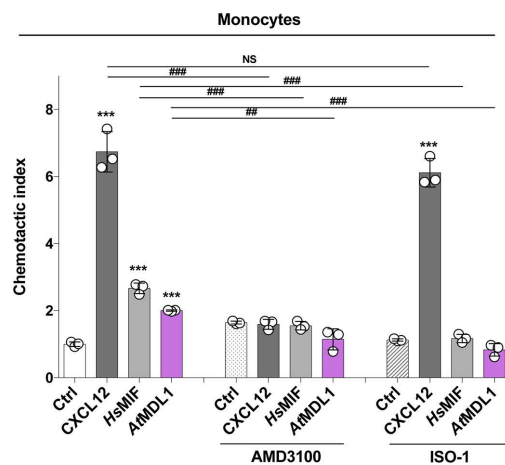


Figure 6. AtMDL1-6xHis-triggered monocyte chemotaxis is blocked by the small molecule inhibitors AMD3100 and ISO-1, indicating MIF and CXCR4 specificity. Chemotaxis experiments were performed as shown in Fig. 5 in the absence or presence of the small molecule inhibitors AMD3100 (10 μ M) or ISO-1 (100 μ M) as indicated. Concentrations of the recombinant proteins were equal to 32 nM for HsMIF-6xHis and AtMDL1-6xHis and 8 nM for CXCL12. Sodium phosphate buffer was used to normalize treatments to spontaneous random migration (control, Ctrl). Bar graph shows means \pm S.D. of one of two independently performed experiments carried out as technical triplicates each (for the other experiment see Fig. 5) (scatter plot with white circles indicates individual data points). Statistical analysis was done using one-way ANOVA for comparisons within a group (***, $p < 0.005$) and paired t test for comparisons between control and the AMD3100 and ISO-1 treatment groups (##, $p < 0.01$; ###, $p < 0.005$; NS, not significant).

the chemotactic effect of CXCL12, although full blockade was only seen for AtMDL3-6xHis (Fig. 7B). As verified by an experiment adding polymyxin B, which neutralizes endotoxin, together with the AtMDL pretreatment regimen, the desensitization effect was not due to minute endotoxin contaminants in our AtMDL-6xHis preparations (Fig. S6). These data therefore suggested that treatment of primary human T cells with AtMDLs desensitizes the cells for subsequent exposure to chemokines signaling through CXCR4. Plant MIF orthologs can thus directly modulate human immune cell behavior elicited by human chemokines.

Discussion

Chemokine-orchestrated immune cell trafficking is a central regulatory mechanism of the host immune response, but pathogens have developed intricate mimicry mechanisms to compromise the host chemokine system at both the ligand and receptor level. This capability is typically limited to viruses (7, 57). Prominent examples include the following: (i) lentiviridae such as HIV with the envelope protein gp120 binding to human CXCR4; (ii) γ -herpesviridae such as HHV8 that encode for the viral CC-chemokine mimic vMIP-II that functions as a chemoattractant and also binds to CXCR4; and (iii) β -herpesviridae such as human cytomegalovirus that encodes for the soluble CKR US28, serving to sequester host chemokines (7, 57, 58). Molecular mimicry of chemokines or their receptors by bacteria and fungi has not been observed, but indirect mechanisms to manipulate the host chemokine system have been reported, e.g. fungal mimicry of a mammalian dipeptidyl-peptidase that cleaves and inactivates CCL2 (59). Upon first view, chemokine mimicry mechanisms are counterintuitive for plants. MIF pro-

Mimicry of human cytokine activity by *Arabidopsis* orthologs

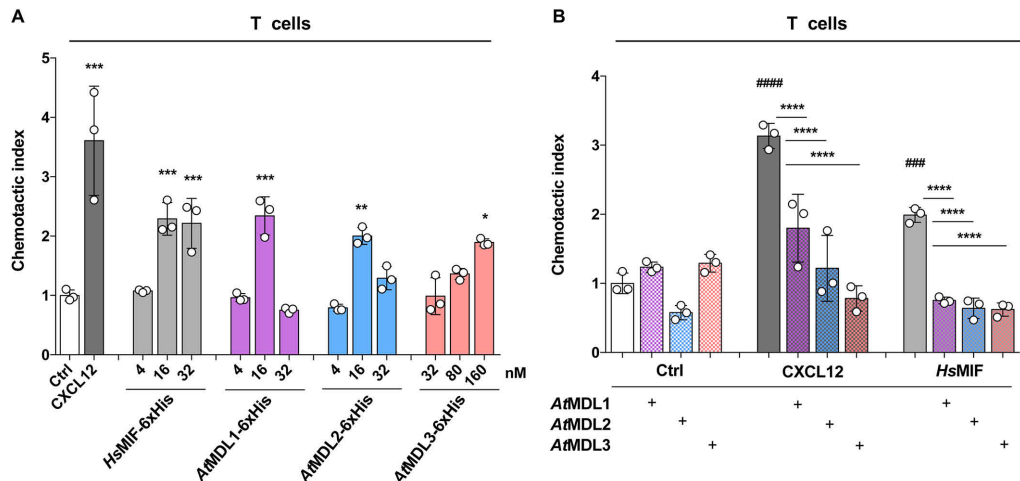


Figure 7. Recombinant 6xHis-tagged AtMDLs dose-dependently trigger chemotactic migration of primary human T cells and desensitize T cells from CXCR4 agonist-triggered chemotaxis. A, recombinant 6xHis-tagged AtMDLs trigger chemotactic migration of primary human T cells in a dose-dependent manner. The chemotactic potency was compared with HsMIF-6xHis and human CXCL12 (at a concentration of 8 nM) serving as a positive control and to buffer control (Ctrl), which also served to normalize treatments to spontaneous (random) migration events. Bar graphs show means \pm S.D. of three independent experiments (scatter plot with white circles indicates individual data points). Statistical analyses were performed using one-way ANOVA between buffer control and the treatment groups at the various doses (*, $p < 0.05$; **, $p < 0.01$; ***, $p < 0.005$). B, recombinant 6xHis-tagged AtMDLs desensitize T cells from chemotaxis elicited by CXCL12 or HsMIF-6xHis. Data are the same as in A, except that T cells in the upper chamber were preincubated with the His-tagged AtMDLs for 2 h (+), before being subjected to chemoattractant exposure (CXCL12 or HsMIF-6xHis) in the lower chamber. Control (Ctrl) incubations were performed without chemoattractant in the lower chamber (random migration). Bar graphs show means \pm S.D. of three experiments (scatter plot with white circles indicates individual data points). Statistical analyses were performed using one-way ANOVA between control and CXCL12 or HsMIF (###, $p < 0.005$; ####, $p < 0.001$) and between CXCL12 or MIF with and without pre-treatment with AtMDLs (****, $p < 0.001$).

teins are atypical chemokines that control pathogenic cell recruitment in human diseases, such as atherosclerosis and cancer through noncognate interactions with classical CKRs such as CXCR4 (8, 9, 11, 13, 17, 24, 60). CKR engagement by MIF is reminiscent of chemokine mimicry mechanisms (13). Furthermore, MIF proteins are characterized by a unique enzymatic tautomerase activity that is unprecedented in the chemokine/cytokine group of proteins and that is a notable component of the remarkable evolutionary conservation of the MIF sequence (8, 25, 61). MIF has been implicated as a player in various host-parasite interactions, and MIF orthologs have been predicted to exist even in the plant kingdom (32, 33, 38).

Here, we have cloned and experimentally characterized three MIF proteins from the model plant *A. thaliana*, i.e. *A. thaliana* MIF/D-T-like (MDL) proteins (AtMDLs), and we provide evidence that they are all structurally similar to human MIF (Fig. 1D and Figs. S1B and S3) and are able to mimic biological activities of human MIF (Figs. 3–7). Surprisingly, mimicry of human MIF by AtMDLs is not related to the conserved MIF tautomerase activity, which is almost absent in AtMDLs (Fig. 2 and Table 1), but AtMDLs were found to interact with the human MIF receptors CD74 and CXCR4. Importantly, we discovered that they activate CXCR4-mediated Akt signaling (Fig. 4) and monocyte and T-cell chemotaxis (Figs. 5–7). These activities represent cellular functionalities of MIF typically encountered in MIF-regulated inflammatory and/or host defense responses (8, 9, 12, 25). The AtMDLs desensitized human T cells from responding to gradients of the human

CXCR4-ligating chemokines CXCL12 and MIF (Fig. 7), offering one potential mechanism of how plant MIF orthologs might influence human immunity.

Our findings indicate that AtMDLs preserve a sufficient level of sequence conservation (Fig. 3A) and conformational similarity (Fig. 1D) to enable binding to the human MIF receptors CD74 and CXCR4, thereby allowing them to mimic functions of the endogenous human MIF or to influence human MIF or CXCL12 responses. Notably, although our experiments were only performed with MDLs from the model plant *A. thaliana*, this is to the best of our knowledge the first report demonstrating that plant proteins can phenocopy or “mimic” inflammatory activities of a *bona fide* human cytokine/chemokine.

Moreover, although plant MDLs were identified in data banks and their sequences and structures predicted by *in silico* methods (33, 38), our current study offers the first experimental characterization of plant MDLs. In fact, little is known about plant MDLs. The *in silico* analyses trace back MDLs several hundred million years in evolution and predict a role for them in plant stress-response pathways (33, 38), but an experimental validation of this presumption has been elusive. Also, there has only been a single experimental study in which plant MDL proteins have been “indirectly” implicated. Naessens *et al.* (62) previously showed that a MIF ortholog secreted in the saliva of a plant-parasitic insect modulates the immune response of the host plant. However, whether host plant MDLs are involved in this effect has remained unresolved.

Mimicry of human cytokine activity by *Arabidopsis* orthologs

To study experimentally the three predicted *AtMDLs*, we opted to express these proteins recombinantly in a standard *Escherichia coli* expression system and use a C-terminal hexahistidine tag for purification purposes. Importantly, comparison of the structural and functional properties of C-terminally hexahistidine-tagged *HsMIF* with those of native untagged *HsMIF* in all experiments of this study essentially excluded the possibility that the hexahistidine tag artificially influences the observed mimicry effects of *AtMDLs*. These findings suggest that mimicry of human MIF activities by *AtMDLs* is a true property of these plant proteins.

Unique among cytokines/chemokines, MIF proteins contain a conserved tautomerase cavity that they share with the tautomerase superfamily, an evolutionarily-conserved protein family, the members of which feature an invariant N-terminal proline residue and a characteristic β - α - β -fold (28, 61). In fact, the entire 3D architecture of the MIF structure is remarkably similar to members of this family, such as the bacterial enzymes 4-oxalocrotonate tautomerase (4-OT) or 5-(carboxymethyl)-2-hydroxyomuconate isomerase (CHMI), and it is similar between MIF-like proteins from different species and kingdoms, as determined by X-ray crystallographic analysis or predicted by *in silico* analyses (61). The tautomerase superfamily is characterized by catalytic promiscuity and diversity and has been suggested to be derived from a common ancestor by divergent evolution (33, 61). The known catalytic tautomerization activity of human MIF is limited to the nonnatural substrate D-dopachrome or DCME and to HPP. Whereas the keto-enol tautomerization of HPP has been generally associated with tyrosine and phenylalanine metabolism, a role for MIF in this process in mammalian cells has not been detected. Moreover, a physiological or pathophysiological relevance of the tautomerase activity of human MIF remains to be demonstrated. Nevertheless, the high degree of sequence similarity among members of the tautomerase superfamily and the conservation of the tautomerase consensus motif in plant MDLs prompted us to speculate initially that the tautomerase activity would be the basis of potential functional similarities, if any, between plant and human MIF proteins. In fact, mammalian MIF proteins have been suggested to exert dual roles with functions both in the extracellular space as cytokines/atypical chemokines and in the intracellular compartment as regulators of cell homeostasis and gene transcription (13, 34, 63). The extracellular cytokine/chemokine activities of MIF proteins are mediated by high-affinity binding to the cell-surface receptors CD74, CXCR2, and CXCR4 (and CXCR7) that are typically expressed in immune cells, and thus they represent the activities of a prototypical innate cytokine/chemokine (9, 16, 17). The molecular basis of the intracellular activities of MIF proteins is much less defined, but protein-protein-binding events and redox processes possibly also involving MIF's catalytic capacity have been implied (13, 25, 34, 63). Functional dichotomy as both the extracellular cytokine/chemokine and intracellular regulator is not unique to MIF proteins but has also been reported for proteinaceous alarmins such as the high-mobility-group box protein 1 (HMGB1) or some ribosomal tRNA transferases (13).

Given these considerations, the observed dramatic reduction in tautomerase activity of the *AtMDLs* as measured in both the

HPP and DCME enzymatic assays is surprising (Fig. 2, A and B). Both assays are widely applied to evaluate tautomerase activities of MIF and its variants, and *HsMIF*-6xHis displayed full catalytic activity comparable with native untagged human MIF (Fig. 2A). It is likely that the almost complete lack of tautomerase activity in the *AtMDLs* is a general property of these orthologs. Neither D-dopachrome nor DCME has been identified in plants, and although L-dopachrome has been implicated as a metabolite that is synthesized in some plant species and expelled via root exudates to compete out other plant species, *A. thaliana* is not a producer of this substance (64), together suggesting that dopachrome or its derivatives are unlikely to be substrates for MDLs in *Arabidopsis*. Similarly, although HPP-metabolizing enzymes have been found in plants, not much is known about the function of this metabolite, let alone its connection with MDL proteins (65). The observed marked reduction of tautomerase activity in *AtMDLs* may be explained by the following mechanism. Although the K_m values of HPP and DCME are higher than that of human MIF, they are in the same order of magnitude, with a 3.5- and 8-fold lower apparent affinity for the plant MDLs, respectively (Table 1), suggesting these substrates may be capable of binding into the tautomerase pocket of *AtMDLs*. However, the measured k_{cat} values indicate that catalytic conversion of both substrate types is highly inefficient in the *AtMDLs*. In fact, although the overall 3D consensus motif of the tautomerase site is conserved in the three *AtMDLs*, we noticed a potentially critical amino acid substitution at position 98, in which a positively-charged lysine residue in all three *AtMDLs* replaces the neutral asparagine residue of *HsMIF* (Fig. 2C). In fact, a model suggested by our *in silico*-modeling analysis predicting that this could trigger a conformational change and an altered charge distribution profile in the vicinity of the pocket (Fig. 2D) was underpinned experimentally by the generation of a site-specific mutant of human MIF, in which Asn-98 was replaced by Lys-98. N98K-*HsMIF* showed a greatly reduced catalytic activity using both HPP and DCME as substrate (Fig. 2, E and F). Thus, the replacement of Asn-98 by Lys-98 in the *AtMDLs* may be the basis for an impeded catalytic turnover in plant MDLs. Furthermore, the observed inhibitory effect of the MIF tautomerase inhibitor ISO-1, which shares structural similarities with HPP and not only fully blocked *HsMIF*- but also *AtMDL*-mediated monocyte migration (Fig. 6), further the notion that HPP (and DCME) binding still occurs, but that substrate tautomerization is not efficiently catalyzed by *AtMDLs*. The further resolution of these mechanistic questions will have to await the 3D structural characterization of *Arabidopsis* MIF orthologs by X-ray crystallography and the elucidation of *AtMDL*/inhibitor co-complexes.

In considering alternative molecular mechanisms that could give rise to functional overlaps between plant MDLs and human MIF, we explored the possibility that *AtMDLs* might interact with human MIF receptors. At first glance, this appeared to be an unlikely option. Neither CD74 nor the MIF chemokine receptors CXCR2 or CXCR4 are present in plants. In fact, the existence of *bona fide* GPCRs in the plant kingdom is still controversially discussed, and it seems that only few candidates exist, none of which has been functionally linked to signaling via heterotrimeric G-proteins (66). Plants lack a cir-

Mimicry of human cytokine activity by *Arabidopsis* orthologs

culational-based immune system and deploy nonproteinaceous phytohormones such as salicylic acid, jasmonic acid, and ethylene as pivotal players for immune signaling (67). However, intriguingly, we found that *AtMDLs* not only share with *HsMIF* some degree of sequence homology regarding Pro-2 and in the site 2 binding region of the MIF/CXCR4 interface (Fig. 3A), but they elicited CXCR4-mediated cell signaling responses in both a yeast-based model cell system (Fig. 3D) and mammalian HEK293 cells (Fig. 4), comparable with the signaling effects triggered by *HsMIF*. Moreover, the data obtained in the yeast transfectant system, which specifically expresses human CXCR4 but none of the other MIF receptors nor other mammalian proteins, argue that *AtMDLs* are able to directly bind to human CXCR4. This appears surprising at first sight, but CXCR4, which was long regarded as a highly-specific chemokine receptor that only binds to one chemokine ligand, namely its cognate ligand CXCL12, has more recently been recognized to be fairly promiscuous, binding to several non-*bona fide* chemokine ligands. These include the atypical chemokine MIF, viral macrophage inflammatory protein II (vMIP-II), viral HIV gp120, human β -defensin-3 (HBD3), and extracellular ubiquitin (9, 13, 17, 56, 57, 68–70). As it seems unlikely that there has been any evolutionary pressure on plant MDLs to develop agonistic properties for a human CKR, we speculate that the CXCR4-binding capacity of plant MDLs may have developed as an “evolutionary side-reaction” of plant interactions with pathogenic animals, such as recently described for plant–parasitic aphids feeding on *Nicotiana benthamiana* leaves (62). The latter scenario is somewhat reminiscent of vertebrate–parasite interactions that rely on cross-species utilization of MIF ligand/receptor pathways (71). Alternatively, the capacity of plant MDLs to activate human CKRs could be the indirect consequence of constraints imposed on MIF evolution to maintain one or several core functions of this protein family.

Although interactions between *AtMDLs* and the cognate human MIF receptor CD74 were only studied by *in vitro* binding experiments on a biochemical level (Fig. 3, B and C), the data insinuate that *AtMDLs* might also influence human MIF-triggered CD74 responses. On the one hand, this appears unlikely, as plants do not express a major histocompatibility (MHC) system. On the other hand, CD74 has been found to be an amenable target of parasite MIF orthologs such as leishmania, plasmodium, or hookworm (32, 35, 37, 71, 72), suggesting that it is a receptor molecule prone to be engaged during host–parasite interactions. In fact, it has been suggested that the MIF-binding functionality of CD74, which is best known as the MHC class II chaperone invariant chain II, already represents a “secondary” function of this membrane protein (16, 73).

Understanding the multiple functions of mammalian MIF proteins that are mediated by specific interactions with four cell-surface receptors and several intracellular-binding partners has been challenging. We have only begun to decipher the binding determinants that govern the molecular promiscuity of the interactions between MIF proteins and these binding partners (13, 17, 34, 40, 41, 46, 60, 74). Including the herein-described three *AtMDLs* in corresponding comprehensive structure–activity relationship studies will add important information to the sequence and 3D motifs that specify such

interactions. Accordingly, it should assist in gathering further insight for novel site-specific drug discovery approaches against human MIF that could eventually be beneficial in treating human diseases such as atherosclerosis and cancer that are at least partially mediated by MIF pathways (17, 75).

The most notable result of this study is the observation that all three *AtMDLs* were found to promote monocyte and T-cell chemotactic migration (Figs. 5 and 7A). Moreover, the measured chemotactic effect for *AtMDL1* and -2 peaked at the same concentration as that of *HsMIF*, albeit the chemotactic index was lower (2.5–3-fold versus 3.5–4-fold, respectively). Importantly, ablation of the effect by the small molecule MIF tautomerase inhibitor ISO-1 (51), which also inhibits the MIF–CXCR4 interaction (41), verified MIF specificity of the observed migration response (Fig. 6). It will be interesting to explore whether other documented small molecule MIF tautomerase inhibitors such as 4-IPP or MIF098 (25, 76) have a similar effect on *AtMDLs*. Monocytes express all four MIF receptors, but pre-incubation of the monocytes with the small molecule inhibitor AMD3100, which is an established specific CXCR4 inhibitor (53) and has already been shown to partially interfere with MIF binding to CXCR4 (41), blocked the *AtMDL*-mediated migration effect, providing evidence that *AtMDL*-triggered monocyte chemotaxis is in fact mediated by CXCR4 (Fig. 6). T cells only express CXCR4 (as well as the relatively poorly-characterized CXCR7), but not CD74 or CXCR2, suggesting that the observed chemotaxis induced by the plant MDLs as well as the desensitization effect toward subsequent human MIF or CXCL12 chemotaxis are also mediated by CXCR4 (Fig. 7, A and B, and Fig. S6).

Thus, *AtMDLs* have the surprising capacity to manipulate human immune cell motility via “hijacking” the chemokine receptor CXCR4. This raises a number of follow-up questions and hypotheses. As we already obtained biochemical-binding evidence, it could be asked whether *AtMDLs* also functionally affect MIF-driven CD74 responses. Moreover, *AtMDLs* might interact with CXCR2, the other chemokine receptor that human MIF engages to modulate immune cell migration and that is a prominent atherogenic arrest (77) and neutrophil recruitment receptor (78). Our results may also justify the hypothesis that MDLs from other plant species have a similar ability to engage human MIF receptors and to modulate mammalian immune cell responses.

Our study, which to the best of our knowledge shows for the first time that a plant protein with homology to a mammalian cytokine/chemokine can interact with two human cytokine receptors, may have broader implications. Following contact with plant MDLs, *e.g.* through the respiratory or the gastrointestinal tract during respiration or dietary ingestion, immune cells in the surrounding mammalian tissue might be modulated in their migratory activity by plant MDLs. Our T-cell migration desensitization data (Fig. 7) argue that this could be one mechanism how MDLs modulate human immunity. Although it is well-known that plant proteins, *e.g.* from pollen, can function as allergens to hyper-activate human adaptive immunity (79), our data may also suggest effects on components of the innate human immune system. Plant MDLs might enhance or suppress MIF-dependent innate immune responses, and this may

Mimicry of human cytokine activity by Arabidopsis orthologs

have a role in tissue homeostasis or in MIF-driven diseases such as acute or chronic inflammation, cardiovascular conditions, or cancer. This hypothesis will have to be tested in suitable experimental *in vivo* models in the future.

Materials and methods

Cell lines, reagents, and antibodies

The human monocytic cell line THP-1 and primary human T cells were grown in complete RPMI 1640 medium supplemented with GlutaMAXTM, 10% fetal calf serum (FCS), and 1% penicillin/streptomycin. Primary human T cells were isolated from enriched peripheral blood mononuclear cell (PBMC) fractions using the human Pan T-cell isolation kit from Miltenyi Biotec (Bergisch Gladbach, Germany). PBMC fractions were obtained by apheresis via a Leucoreduction System Chamber ("Kegel") from anonymous thrombocyte donations at the Department of Transfusion Medicine, Cell Therapeutics, and Hemostaseology of the Klinikum der University Hospital (KUM) of the Ludwig-Maximilians-University (LMU). The studies abide by the Declaration of Helsinki principles and were approved by ethics approval 18-104 of the Ethics Committee of LMU Munich entitled "The MIF Protein/Receptor Network in Atherosclerosis" and encompasses the use of anonymized tissue and blood specimens for research purposes.

The human embryonic kidney cell line HEK293 was cultured in Dulbecco's minimal essential medium (DMEM) supplemented with GlutaMAXTM, 10% FCS, and 1% penicillin/streptomycin. To obtain HEK293 transfectants stably expressing the human CXC chemokine receptor CXCR4, a high-affinity receptor for both CXCL12 and MIF, WT HEK293 cells were stably transfected with the pcDNA3.1 plasmid containing a 3xHA-HsCXCR4 insert under the control of a human cytomegalovirus immediate-early promoter by an established procedure as described previously (17, 41). THP-1 monocytes, T cells, and HEK293 cells were incubated at 37 °C in a humidified atmosphere containing 5% CO₂. All cell culture reagents were cell culture grade and were obtained from Thermo Fisher Scientific (Waltham, MA).

Other reagents, *e.g.* salts, chemicals, and miscellaneous reagents, were of the highest research grade possible and were purchased from Merck KGaA (Darmstadt, Germany) and Carl Roth GmbH (Karlsruhe, Germany). Imidazole was from Sigma GmbH (Taufkirchen, Germany), and skimmed milk was from SERVA electrophoresis GmbH (Heidelberg, Germany).

Antibodies used in this study were as follows: polyclonal rabbit anti-actin (A2066; Sigma), polyclonal rabbit anti-Akt (catalog no. 9272; Cell Signaling Technologies, Danvers, MA), and polyclonal rabbit anti-phospho-Akt (Ser-473) (catalog no. 9271; Cell Signaling Technologies).

Multiple sequence alignments

Multiple sequence alignments were performed by the ClustalW algorithm (<http://www.genome.jp/tools-bin/clustalw>) using standard parameters in the Jalview multiple sequence alignment editor desktop application (80–82). Sources of the sequences used in the alignment are given in Table S1.

Cloning of HsMIF and the three AtMDLs with C-terminal hexahistidine tags

HsMIF and the three *A. thaliana* MIF/DDT-like (MDL) genes, AtMDL1, AtMDL2, and AtMDL3, were cloned into the pET21a vector via a classical cloning strategy. The genes were N-terminally fused in-frame to a 6xHis tag present in the vector using the restriction enzymes *Nde*I and *Xho*I. For this purpose, the respective restriction sites were added to the desired cDNAs in a PCR using the corresponding primers *Nde*I-"gene"_Fwd and "gene"-*Xho*I_Rev (Table S4). The reverse primer at the same time served to remove the endogenous stop codon. For AtMDL1 and AtMDL3, an internal *Nde*I restriction site was removed using the splice overlap–extension PCR strategy (SOE-PCR) with the internal primer "gene"-mut_Fwd and "gene"-mut_Rev (Table S4) in combination with the above-mentioned restriction site-adding forward and reverse primers. Through the SOE-PCR, the cDNA sequences of AtMDL1 and AtMDL3 were modified at position 177 (GCA to GCG), introducing a silent mutation (A59A). Successfully-fused plasmid products were confirmed by sequencing, propagated in One ShotTM TOP10 chemically-competent *E. coli* (Thermo Fisher Scientific), and then transformed into RosettaTM (DE3)-competent *E. coli* (Novagen/Merck KGaA) for expression of recombinant protein. The N98K-HsMIF mutant gene was synthesized by and purchased from BaseClear (Leiden, The Netherlands). After subcloning from the pUC57 plasmid into pET21a and transformation of competent RosettaTM (DE3) *E. coli* cells, all following procedures were identical to those described above.

Expression and purification of proteins

Recombinant nontagged human CXCL12 and HsMIF proteins, used as controls in this study, were cloned, expressed, and purified as described before (46). RosettaTM (DE3)-competent *E. coli* cells were used to express the pET21-derived gene constructs to yield HsMIF-6xHis-, AtMDL1-6xHis-, AtMDL2-6xHis-, AtMDL3-6xHis-, and N98K-HsMIF-6xHis-tagged protein products. Culturing of bacteria and protein expression was carried out essentially as described before (46).

For protein purification, cells were harvested by centrifugation, and cell pellets were resuspended in 2 ml of binding buffer (20 mM sodium phosphate, 0.5 M NaCl, 20 mM imidazole, pH 7.2). After homogenizing the bacteria at 75 megapascals using an Aventin EmulsiFlex C5 high-pressure homogenizer (ATA Scientific Pty. Ltd., Lucas Heights, Australia), recombinant hexahistidine-tagged proteins were initially purified using immobilized metal ion affinity chromatography (HisTrap; GE Healthcare, Freiburg, Germany) with an FPLC system (FPLC; ÄKTA Pure, GE Healthcare). Prior to the run, the FPLC system was equilibrated with binding buffer. His-tagged proteins were eluted using elution buffer (20 mM sodium phosphate, 0.5 M NaCl, 0.5 M imidazole, pH 7.2). Resulting protein fractions were stored at 4 °C until subsequent purification steps or experimental usage. Additional purification of the proteins was performed by size-exclusion chromatography (Superdex 75, GE Healthcare) using 20 mM sodium phosphate buffer, pH 7.2, as elution buffer, *i.e.* conditions previously reported to support stability

Mimicry of human cytokine activity by *Arabidopsis* orthologs

and bioactivity of recombinant *HsMIF* (17, 39). Subsequently, purified proteins were sterile-filtered using 0.2- μm pore size filters and then stored at 4 °C until use. Proteins were used for biochemical and biological assays within 4 weeks of purification. Endotoxin content was determined in the final enriched, sterile-filtered protein solution, using the PierceTM LAL Chromogenic Endotoxin Quantitation Kit (Thermo Fisher Scientific).

Western blotting analyses of recombinant *HsMIF*-6xHis and *AtMDL*-6xHis proteins

Assessment of protein purity and integrity was performed by SDS-PAGE, using 15% acrylamide gels under reducing conditions essentially as described (39). Proteins were detected by Coomassie Blue staining and/or Western blot analysis, using nitrocellulose membranes and a Novex[®] Tris-glycine transfer buffer and Tris-buffered saline (TBS: 150 mM NaCl, 20 mM Tris, pH 7.3), supplemented with 0.01% Tween 20 and 1% BSA for blocking/staining. His-tagged proteins were detected by mouse anti-6xHis tag mAb (Ma1-135; Invitrogen) followed by incubation with horseradish peroxidase (HRP)-conjugated secondary goat anti-mouse IgG (ab6789; Abcam, Cambridge, UK). In addition, for testing the relative structural similarity between the mammalian and plant orthologs, anti-*HsMIF* antibodies (anti-human MIF mAb MAB289; R&D Systems, Minneapolis, MN; anti-mouse MIF polyclonal rabbit antibody Ka565 (34)) were used, followed by HRP-conjugated secondary antibodies (catalog no. ab6789, Abcam; catalog no. P0448, DAKO) and imaging with SuperSignalTM West Dura Extended Duration Substrate (Thermo Fisher Scientific) on an Odyssey[®] Fc Imaging System with Image StudioTM software (LICOR Biosciences, Bad Homburg, Germany).

Far-UV CD spectroscopy

Far-UV CD spectroscopy was performed with a JASCO J-715 spectropolarimeter (JASCO, Tokyo, Japan). Measurements were carried out at room temperature between 195 and 250 nm at 0.1-nm intervals with a response time of 1 s in a buffer containing 10 mM sodium phosphate, pH 7.4. CD spectra were recorded at protein concentrations of 1, 2.5, and 5 μM in a 1-, 0.5-, or 0.2-cm quartz cuvette, respectively. The background spectrum of buffer alone was subtracted from the CD spectra of the protein solutions. The final data result from an average of three CD spectra. The CD spectra of native *HsMIF* and their deconvolution were published previously (46) and were represented in this study for comparison after verifying similarity/identity with a representative current native *HsMIF* preparation. Dynode voltage values were below 850 and did not interfere with CD measurements. Deconvolutions were performed using Dichroweb online software (<http://dichroweb.cryst.bbk.ac.uk>), and estimation of the secondary protein structure was carried out with the analysis program Contin LL, using the reference spectra Set 7 (83–86).

Tautomerase activity assays

The HPP tautomerase activity assay was performed as described before (87) with the following adjustments: 500 mM boric acid, pH 6.2, was used instead of 435 mM. Enzymatic mea-

surements were conducted in a solution of 8 mM HPP and 250 nM of the respective recombinant protein. An increase in absorbance due to complex formation was recorded at 306 nm every 5 s for a duration of 300 s.

The DCME tautomerase activity assay was performed essentially as described before (50, 88). Briefly, DCME was prepared at a final concentration of 1 mM by oxidizing L-3,4-dihydroxyphenylalanine methyl ester with 1 mM sodium *m*-periodate. DCME was then dissolved in 25 mM potassium phosphate buffer, pH 6.0, containing 0.5 mM EDTA, and enzyme (recombinant *HsMIF*-6xHis or *AtMDL*-6xHis) was added at a final concentration of 100 nM. The decrease in absorbance at 475 nm was measured for 240 s in 10-s intervals.

All tautomerase activity experiments were performed using a JASCO version 650 spectrophotometer (JASCO).

MBP-sCD74/MIF-binding assay

The MBP-sCD74/MIF binding assay was performed essentially as described previously (45). Briefly, freshly thawed *HsMIF*-6xHis or *AtMDL*-6xHis aliquots were diluted into phosphate-buffered saline (PBS) to prepare a solution of 500 nM from which 100 μl was used for coating the wells of a medium-binding 96-well plate overnight at 4 °C. Wells were washed three times with 220 μl of washing buffer (PBS + Tween 0.05%) and subsequently blocked for nonspecific binding with 210 μl of a commercial blocker solution (Rockland Immunochemicals Inc., Limerick, PA) at room temperature for 30 min. During all incubation steps, the plate was shaken slowly. The blocker solution was removed, and the plate was washed three times with washing buffer. Subsequently, the wells were incubated with 100 μl of a 500 nM maltose-binding protein-soluble CD74 fusion protein (MBP-sCD74) solution in PBS for 30 min at room temperature. 100 μl of PBS were used as control at this step to exclude nonspecific binding of the anti-CD74 polyclonal antibody (pAb). After washing, wells were incubated with 100 μl of a rabbit anti-CD74 pAb solution (1:2500 dilution in PBS) (Sinobiological, Vienna, Austria) for 30 min at room temperature. After removing the anti-CD74 solution and washing, a solution of 100 μl of goat anti-rabbit horseradish peroxidase conjugate (1:2000 dilution in PBS) (Life Technologies, Inc., The Netherlands) was added and incubated for 30 min at room temperature. After washing, binding was visualized by conversion of 100 μl of aqueous tetramethylbenzidine solution (Sigma, Zwijndrecht, The Netherlands), which was quenched with an aqueous 1 N H₂SO₄ solution (100 μl). Absorbance was detected at 450 nm. A freshly-prepared solution of 2% (w/v) BSA in PBS was used as negative control for coating. An additional control was done to confirm that binding between the *AtMDL*s and MBP-sCD74 is not caused by the fused protein MBP. Toward this aim, the incubation with MBP-sCD74 was replaced by 500 nM MBP (ProSPEC Inc., Fullerton, CA) in PBS. MBP binding was detected using mouse anti-MBP mAb (1:2500 dilution in PBS) (Sigma) as primary antibody and goat anti-mouse horseradish peroxidase conjugate (1:1500 dilution in PBS) (Thermo Fisher Scientific, Landsmeer, The Netherlands). The binding curve between *AtMDL*3 with MBP-sCD74 was determined by using titrations of different concentrations of MBP-sCD74.

Mimicry of human cytokine activity by *Arabidopsis* orthologs

Yeast-signaling assay

The functional human CXCR4-expressing transformant of *S. cerevisiae* strain CY12946 was described before (46, 47). Briefly, agonist binding to the CXCR4 cell-surface receptor leads to the activation of a MAPK kinase-type signaling cascade initiating the transcription of the β -gal (*lacZ*) reporter gene. CXCR4 engagement and activation can therefore be measured and quantified by a β -gal enzymatic assay.

S. cerevisiae CY12946 cells were diluted to an OD₆₀₀ of 0.3–0.8 and incubated with the respective test proteins (*HsMIF*–6xHis, *AtMDL1*–6xHis, *AtMDL2*–6xHis, and *AtMDL3*–6xHis) or the established control agonists human CXCL12 and *HsMIF* (41, 46). All test proteins were applied at a final concentration of 20 μ M, a concentration that had previously been shown to mediate MIF-based activation of CXCR4 in this system (41). CXCL12 was used at a final concentration of 2 μ M. It should be noted that in this system, elevated MIF and CXCL12 ligand concentrations are needed for appreciable receptor activation due to the barrier properties of the yeast cell wall. β -Gal activity was detected using the Beta-Glo[®] assay system (Promega Corp., Madison, WI). Luminescence signals were recorded in a multimode plate reader (Enspire[®] 2300, PerkinElmer Life Sciences).

Monocyte and T-cell chemotaxis assay

The chemotactic potential of hexahistidine-tagged *AtMDL* proteins was assessed using the Transwell migration device essentially as described previously (18) using THP-1 monocytes or primary human T cells and an overnight transmigration interval. THP-1 and T cells were cultured in RPMI 1640 medium supplemented with 10% FCS and 1% penicillin/streptomycin. The evening before the assay, cells were transferred into standard RPMI medium without FCS. For the assay, the upper chambers of a 24-well format Transwell device (Sigma-Corning; pore size 5 μ m) were loaded with 1×10^6 THP-1 cells. Tested proteins (*HsMIF*–6xHis, *AtMDL1*–6xHis, *AtMDL2*–6xHis, or *AtMDL3*–6xHis) were studied at a concentration range of 4–160 nM, representing the chemoattractant in the lower chamber. As a positive control, 8 nM human CXCL12 was used; 20 mM sodium phosphate buffer, pH 7.2, served as negative control. For the desensitization experiment, 16 nM recombinant hexahistidine-tagged *AtMDL*s were added to the upper T-cell-containing chamber 2 h before exposure to the chemoattractants in the lower chamber. In the endotoxin control experiment, 20 μ g/ml polymyxin B was added to the upper chamber together with the *AtMDL*s.

Cells that migrated into lower chambers were quantitated and obtained values normalized to buffer control (“chemotactic index”) (17). The CXCR4 and MIF inhibitors AMD3100 (Sigma) and ISO-1 (Abcam, Cambridge, UK) were used at final concentrations of 10 and 100 μ M, respectively, and were added to the cell suspensions 30 min before the addition of the chemotactic stimulus. Following a 16-h migration interval, cells were removed from the lower chambers, mixed with CountBright[™] Absolute Counting Beads (Invitrogen/Thermo Fisher Scientific), and enumerated using a BD FACSVerse[™] flow cytometer (BD Biosciences, Heidelberg, Germany).

Akt cell-signaling assay

HEK293 transfectants stably-expressing CXCR4 or non-transfected HEK293 control cells were subjected to treatment with *HsMIF*–6xHis or *AtMDL1*–6xHis, *AtMDL2*–6xHis, or *AtMDL3*–6xHis at a concentration of 16 nM. After different stimulation intervals, treated cells were lysed in NuPAGE[®] lithium dodecyl sulfate/dithiothreitol lysis buffer containing PhosSTOP[™] reagent (Roche Applied Science, Mannheim, Germany). Lysates were boiled at 95 °C for 5 min, sonicated for 5 min, and electrophoresed in 11% SDS-polyacrylamide gels. For Western blotting detection of phosphorylated Akt, proteins were transferred to nitrocellulose membrane using Novex[®] Tris-glycine transfer buffer. Human MIF, which has been previously shown to activate Akt signaling (48), was used for comparison. Phospho-Akt band densities were determined by usage of an anti-phospho-Akt(Ser-473) antibody and an HRP-conjugated secondary antibody. Total Akt and actin were used for normalization applying polyclonal rabbit anti-Akt and -actin antibodies. Band densitometry was performed with the Odyssey[®] Fc imaging system (LICOR) using Image Studio[™] software (LICOR Biosciences).

Fluorescence-activated cell sorting (FACS)

The cell-surface expression of the human CXCR4 receptor in HEK293 cells was verified by flow cytometry. HEK293 transfectants stably-overexpressing CXCR4 were grown in standard DMEM, supplemented with GlutaMAX[™], 10% FCS, and 1% penicillin/streptomycin, until the cells reached confluence. After washing in cold phosphate-buffered saline (PBS) buffer, cells were incubated with fluorescein-isothiocyanate (FITC)-labeled mouse anti-*HsCXCR4* or FITC-labeled isotype control antibody (IgG2a) (both R&D Systems) at 4 °C for 2 h in the dark. Cells were washed in cold PBS before subjection to FACS analysis using a FACSVerse[™] flow cytometer (BD Biosciences).

Structure prediction

Prediction of the 3D protein structures of *AtMDL1*–6xHis, *AtMDL2*–6xHis, and *AtMDL3*–6xHis was performed using the Phyre² Protein Fold Recognition Server (www.sbg.bio.ic.ac.uk/phyre2) (89). Modeling was carried out in intensive mode, using the amino acid sequences obtained from public repositories (Table S1) and accounting for the His-tag–modified variants used in this study. For structure prediction and modeling, Phyre² performs template-based modeling together with *ab initio* folding simulations for sequence segments for which no appropriate model was found.

Structure visualization

The predicted 3D protein structures of monomeric *HsMIF*–6xHis and *AtMDL1*–6xHis, *AtMDL2*–6xHis, and *AtMDL3*–6xHis were visualized using the PyMOL Molecular Graphics System Version 1.8.2.2 (Schrodinger Ltd. Liability Co.). The structures shown in this work correspond to the Protein Data Bank (PDB) file for human MIF (PDB identifier 3DJH) or our structure prediction results. The 3D structures were rendered both as a cartoon model showing the secondary protein structure and as a space-filling model depicting the protein surface.

Mimicry of human cytokine activity by *Arabidopsis* orthologs

This surface model was also used to visualize the electrostatic surface potential, as calculated by PyMOL. For visualization of the three 6xHis-tagged AtMDL proteins and their comparison with HsMIF, the initial methionine residue was removed, as it has been found to be processed in all cell systems studied so far (8, 12).

Statistics

Unless otherwise indicated, statistical analyses were performed using one-way analysis of variance (ANOVA) followed by post hoc comparison with the Bonferroni test using GraphPad Prism 6 (GraphPad Prism Software Inc., San Diego, CA) with multiple comparisons. Data are presented as means \pm S.D. Considered as significant: $p < 0.05$. Asterisks indicate statistically significant differences as follows: *, $p < 0.05$; **, $p < 0.01$; ***, $p < 0.005$; ****, $p < 0.001$. Letter symbols above bars in Fig. 3 indicate statistically significant different groups (at least $p < 0.05$) according to one-way ANOVA using multiple comparisons and Student's t-test.

Author contributions—D. S., K. G., M. B., C. K., P. B., and Z. X. data curation; D. S., K. G., M. B., and Z. X. formal analysis; D. S., K. G., M. B., Z. X., and R. P. visualization; D. S., K. G., C. K., P. W., A. R., P. B., Z. X., and R. H. C. methodology; D. S., K. G., M. B., C. K., P. W., A. R., P. B., Z. X., R. H. C., A. K., F. J. D., R. P., and J. B. writing-review and editing; M. B. software; R. H. C., A. K., F. J. D., R. P., and J. B. supervision; A. K., F. J. D., R. P., and J. B. conceptualization; A. K., R. P., and J. B. funding acquisition; F. J. D., R. P., and J. B. project administration; R. P. and J. B. writing original draft.

Acknowledgments—We acknowledge Christine Coustau, Harald Keller, Karl-Heinz Kogel, Richard Bucala, and Lin Leng for constructive discussions, and we thank Ying-Tung Liu for valuable assistance with the Akt phosphorylation experiments. We are grateful to the Department of Transfusion Medicine, Cell Therapeutics, and Hemostaseology of the University Hospital (KLIM) of the Ludwig-Maximilians-University (LMU) for providing us with enriched PBMC fractions from thrombocyte donations to isolate primary human T cells.

References

- Murphy, P. M., Baggiolini, M., Charo, I. F., Hébert, C. A., Horuk, R., Matsushima, K., Miller, L. H., Oppenheim, J. J., and Power, C. A. (2000) International union of pharmacology. XXII. Nomenclature for chemokine receptors. *Pharmacol. Rev.* **52**, 145–176 [Medline](#)
- Bachelier, F., Ben-Baruch, A., Burkhardt, A. M., Combadiere, C., Farber, J. M., Graham, G. J., Horuk, R., Sparre-Ulrich, A. H., Locati, M., Luster, A. D., Mantovani, A., Matsushima, K., Murphy, P. M., Nibbs, R., Nomiyama, H., et al. (2014) International Union of Basic and Clinical Pharmacology. LXXXIX. Update on the extended family of chemokine receptors and introducing a new nomenclature for atypical chemokine receptors. *Pharmacol. Rev.* **66**, 1–79 [CrossRef Medline](#)
- Mantovani, A. (1999) The chemokine system: redundancy for robust outputs. *Immunol. Today* **20**, 254–257 [CrossRef Medline](#)
- Steen, A., Larsen, O., Thiele, S., and Rosenkilde, M. M. (2014) Biased and G protein-independent signaling of chemokine receptors. *Front. Immunol.* **5**, 277 [CrossRef Medline](#)
- Koenen, R. R., and Weber, C. (2011) Chemokines: established and novel targets in atherosclerosis. *EMBO Mol. Med.* **3**, 713–725 [CrossRef Medline](#)
- Charo, I. F., and Ransohoff, R. M. (2006) The many roles of chemokines and chemokine receptors in inflammation. *N. Engl. J. Med.* **354**, 610–621 [CrossRef Medline](#)
- Murphy, P. M. (2001) Viral exploitation and subversion of the immune system through chemokine mimicry. *Nat. Immunol.* **2**, 116–122 [CrossRef Medline](#)
- Calandra, T., and Roger, T. (2003) Macrophage migration inhibitory factor: a regulator of innate immunity. *Nat. Rev. Immunol.* **3**, 791–800 [CrossRef Medline](#)
- Tillmann, S., Bernhagen, J., and Noels, H. (2013) Arrest functions of the MIF ligand/receptor axes in atherogenesis. *Front. Immunol.* **4**, 115 [CrossRef Medline](#)
- Morand, E. F., Leech, M., and Bernhagen, J. (2006) MIF: a new cytokine link between rheumatoid arthritis and atherosclerosis. *Nat. Rev. Drug Discov.* **5**, 399–410 [CrossRef Medline](#)
- Zernecke, A., Bernhagen, J., and Weber, C. (2008) Macrophage migration inhibitory factor in cardiovascular disease. *Circulation* **117**, 1594–1602 [CrossRef Medline](#)
- Sinitski, D., Kontos, C., Krammer, C., Asare, Y., Kapurniotu, A., and Bernhagen, J. (2019) Macrophage migration inhibitory factor (MIF)-based therapeutic concepts in atherosclerosis and inflammation. *Thromb. Haemost.* **119**, 553–566 [CrossRef Medline](#)
- Kapurniotu, A., Gokce, O., and Bernhagen, J. (2019) The multitasking potential of alarmins and atypical chemokines. *Front. Med.* **6**, 3 [CrossRef Medline](#)
- Noels, H., Bernhagen, J., and Weber, C. (2009) Macrophage migration inhibitory factor: a noncanonical chemokine important in atherosclerosis. *Trends Cardiovasc. Med.* **19**, 76–86 [CrossRef Medline](#)
- Oppenheim, J. J., Tewary, P., de la Rosa, G., and Yang, D. (2007) Alarmins initiate host defense. *Adv. Exp. Med. Biol.* **601**, 185–194 [CrossRef Medline](#)
- Leng, L., Metz, C. N., Fang, Y., Xu, J., Donnelly, S., Baugh, J., Delohery, T., Chen, Y., Mitchell, R. A., and Bucala, R. (2003) MIF signal transduction initiated by binding to CD74. *J. Exp. Med.* **197**, 1467–1476 [CrossRef Medline](#)
- Bernhagen, J., Krohn, R., Lue, H., Gregory, J. L., Zernecke, A., Koenen, R. R., Dewor, M., Georgiev, I., Schober, A., Leng, L., Kooistra, T., Fingerle-Rowson, G., Ghezzi, P., Kleemann, R., McColl, S. R., et al. (2007) MIF is a noncognate ligand of CXCR2 chemokine receptors in inflammatory and atherogenic cell recruitment. *Nat. Med.* **13**, 587–596 [CrossRef Medline](#)
- Alampour-Rajabi, S., El Bounkari, O., Rot, A., Müller-Newen, G., Bachelier, F., Gawaz, M., Weber, C., Schober, A., and Bernhagen, J. (2015) MIF interacts with CXCR7 to promote receptor internalization, ERK1/2 and ZAP-70 signaling, and lymphocyte chemotaxis. *FASEB J.* **29**, 4497–4511 [CrossRef Medline](#)
- Schmitz, C., Noels, H., El Bounkari, O., Straussfeld, E., Megens, R. T. A., Sternkopf, M., Alampour-Rajabi, S., Krammer, C., Tilstam, P. V., Gerdes, N., Bürger, C., Kapurniotu, A., Bucala, R., Jankowski, J., Weber, C., and Bernhagen, J. (2018) Mif-deficiency favors an atheroprotective autoantibody phenotype in atherosclerosis. *FASEB J.* **32**, 4428–4443 [CrossRef Medline](#)
- Soppert, J., Kraemer, S., Beckers, C., Averdunk, L., Möllmann, J., Denecke, B., Goetzenich, A., Marx, G., Bernhagen, J., and Stoppe, C. (2018) Soluble CD74 reroutes MIF/CXCR4/AKT-mediated survival of cardiac myofibroblasts to necroptosis. *J. Am. Heart Assoc.* **7**, e009384 [CrossRef Medline](#)
- de Souza, H. S., Tortori, C. A., Lintomen, L., Figueiredo, R. T., Bernardazzi, C., Leng, L., Bucala, R., Madi, K., Buongusto, F., Elia, C. C., Castelo-Branco, M. T., and Bozza, M. T. (2015) Macrophage migration inhibitory factor promotes eosinophil accumulation and tissue remodeling in eosinophilic esophagitis. *Mucosal Immunol.* **8**, 1154–1165 [CrossRef Medline](#)
- David, J. R. (1966) Delayed hypersensitivity in vitro: its mediation by cell-free substances formed by lymphoid cell-antigen interaction. *Proc. Natl. Acad. Sci. U.S.A.* **56**, 72–77 [CrossRef Medline](#)
- Bernhagen, J., Calandra, T., Mitchell, R. A., Martin, S. B., Tracey, K. J., Voelter, W., Manogue, K. R., Cerami, A., and Bucala, R. (1993) MIF is a pituitary-derived cytokine that potentiates lethal endotoxaemia. *Nature* **365**, 756–759 [CrossRef Medline](#)
- Merk, M., Mitchell, R. A., Endres, S., and Bucala, R. (2012) D-Dopachrome tautomerase (D-DT or MIF-2): doubling the MIF cytokine family. *Cytokine* **59**, 10–17 [CrossRef Medline](#)

Mimicry of human cytokine activity by *Arabidopsis* orthologs

25. Bloom, J., Sun, S., and Al-Abed, Y. (2016) MIF, a controversial cytokine: a review of structural features, challenges, and opportunities for drug development. *Exp. Opin. Ther. Targets* **20**, 1463–1475 [CrossRef Medline](#)
26. Sun, H. W., Bernhagen, J., Bucala, R., and Lolis, E. (1996) Crystal structure at 2.6-Å resolution of human macrophage migration inhibitory factor. *Proc. Natl. Acad. Sci. U.S.A.* **93**, 5191–5196 [CrossRef Medline](#)
27. Lolis, E., and Bucala, R. (2003) Macrophage migration inhibitory factor. *Exp. Opin. Ther. Targets* **7**, 153–164 [CrossRef Medline](#)
28. Stamps, S. L., Fitzgerald, M. C., and Whitman, C. P. (1998) Characterization of the role of the amino-terminal proline in the enzymatic activity catalyzed by macrophage migration inhibitory factor. *Biochemistry* **37**, 10195–10202 [CrossRef Medline](#)
29. Taylor, A. B., Johnson, W. H., Jr, Czerwinski, R. M., Li, H. S., Hackert, M. L., and Whitman, C. P. (1999) Crystal structure of macrophage migration inhibitory factor complexed with (E)-2-fluoro-*p*-hydroxycinnamate at 1.8 Å resolution: implications for enzymatic catalysis and inhibition. *Biochemistry* **38**, 7444–7452 [CrossRef Medline](#)
30. Merk, M., Zierow, S., Leng, L., Das, R., Du, X., Schulte, W., Fan, J., Lue, H., Chen, Y., Xiong, H., Chagnon, F., Bernhagen, J., Lolis, E., Mor, G., Lesur, O., and Bucala, R. (2011) The D-Dopachrome tautomerase (DDT) gene product is a cytokine and functional homolog of macrophage migration inhibitory factor (MIF). *Proc. Natl. Acad. Sci. U.S.A.* **108**, E577–E585 [CrossRef Medline](#)
31. Sugimoto, H., Taniguchi, M., Nakagawa, A., Tanaka, I., Suzuki, M., and Nishihira, J. (1999) Crystal structure of human D-dopachrome tautomerase, a homologue of macrophage migration inhibitory factor, at 1.54 Å resolution. *Biochemistry* **38**, 3268–3279 [CrossRef Medline](#)
32. Sparkes, A., De Baetselier, P., Roelants, K., De Trez, C., Magez, S., Van Ginderachter, J. A., Raes, G., Bucala, R., and Stijlemans, B. (2017) The non-mammalian MIF superfamily. *Immunobiology* **222**, 473–482 [CrossRef Medline](#)
33. Michelet, C., Danchin, E. G. J., Jaouannet, M., Bernhagen, J., Panstruga, R., Kogel, K. H., Keller, H., and Coustau, C. (2019) Cross-kingdom analysis of diversity, evolutionary history, and site selection within the eukaryotic macrophage migration inhibitory factor superfamily. *Genes* **10**, E740 [CrossRef Medline](#)
34. Kleemann, R., Hausser, A., Geiger, G., Mischke, R., Burger-Kentscher, A., Flieger, O., Johannes, F. J., Roger, T., Calandra, T., Kapurniotu, A., Grell, M., Finkemeier, D., Brunner, H., and Bernhagen, J. (2000) Intracellular action of the cytokine MIF to modulate AP-1 activity and the cell cycle through Jab1. *Nature* **408**, 211–216 [CrossRef Medline](#)
35. Baeza Garcia, A., Siu, E., Sun, T., Exler, V., Brito, L., Hekele, A., Otten, G., Augustijn, K., Janse, C. J., Ulmer, J. B., Bernhagen, J., Fikrig, E., Geall, A., and Bucala, R. (2018) Neutralization of the *Plasmodium*-encoded MIF ortholog confers protective immunity against malaria infection. *Nat. Commun.* **9**, 2714 [CrossRef Medline](#)
36. Twu, O., Dessi, D., Vu, A., Mercer, F., Stevens, G. C., de Miguel, N., Rappelli, P., Cocco, A. R., Clubb, R. T., Fiori, P. L., and Johnson, P. J. (2014) *Trichomonas vaginalis* homolog of macrophage migration inhibitory factor induces prostate cell growth, invasiveness, and inflammatory responses. *Proc. Natl. Acad. Sci. U.S.A.* **111**, 8179–8184 [CrossRef Medline](#)
37. Kamir, D., Zierow, S., Leng, L., Cho, Y., Diaz, Y., Griffith, J., McDonald, C., Merk, M., Mitchell, R. A., Trent, J., Chen, Y., Kwong, Y. K., Xiong, H., Vermeire, J., Cappello, M., et al. (2008) A *Leishmania* ortholog of macrophage migration inhibitory factor modulates host macrophage responses. *J. Immunol.* **180**, 8250–8261 [CrossRef Medline](#)
38. Panstruga, R., Baumgarten, K., and Bernhagen, J. (2015) Phylogeny and evolution of plant macrophage migration inhibitory factor/D-dopachrome tautomerase-like proteins. *BMC Evol. Biol.* **15**, 64 [CrossRef Medline](#)
39. Bernhagen, J., Mitchell, R. A., Calandra, T., Voelter, W., Cerami, A., and Bucala, R. (1994) Purification, bioactivity, and secondary structure analysis of mouse and human macrophage migration inhibitory factor (MIF). *Biochemistry* **33**, 14144–14155 [CrossRef Medline](#)
40. Pantouris, G., Syed, M. A., Fan, C., Rajasekaran, D., Cho, T. Y., Rosenberg, E. M., Jr, Bucala, R., Bhandari, V., and Lolis, E. J. (2015) An analysis of MIF structural features that control functional activation of CD74. *Chem. Biol.* **22**, 1197–1205 [CrossRef Medline](#)
41. Rajasekaran, D., Gröning, S., Schmitz, C., Zierow, S., Drucker, N., Bakou, M., Kohl, K., Mertens, A., Lue, H., Weber, C., Xiao, A., Luker, G., Kapurniotu, A., Lolis, E., and Bernhagen, J. (2016) Macrophage migration inhibitory factor-CXCR4 receptor interactions: evidence for partial allosteric agonism in comparison with CXCL12 chemokine. *J. Biol. Chem.* **291**, 15881–15895 [CrossRef Medline](#)
42. Lubetsky, J. B., Swope, M., Dealwis, C., Blake, P., and Lolis, E. (1999) Pro-1 of macrophage migration inhibitory factor functions as a catalytic base in the phenylpyruvate tautomerase activity. *Biochemistry* **38**, 7346–7354 [CrossRef Medline](#)
43. Sommerville, C., Richardson, J. M., Williams, R. A., Mottram, J. C., Roberts, C. W., Alexander, J., and Henriquez, F. L. (2013) Biochemical and immunological characterization of *Toxoplasma gondii* macrophage migration inhibitory factor. *J. Biol. Chem.* **288**, 12733–12741 [CrossRef Medline](#)
44. Assis, D. N., Leng, L., Du, X., Zhang, C. K., Grieb, G., Merk, M., Garcia, A. B., McCrann, C., Chapiro, J., Meinhardt, A., Mizue, Y., Nikolic-Pateron, D. J., Bernhagen, J., Kaplan, M. M., Zhao, H., et al. (2014) The role of macrophage migration inhibitory factor in autoimmune liver disease. *Hepatology* **59**, 580–591 [CrossRef Medline](#)
45. Kok, T., Wasiel, A. A., Dekker, F. J., Poelarends, G. J., and Cool, R. H. (2018) High yield production of human invariant chain CD74 constructs fused to solubility-enhancing peptides and characterization of their MIF-binding capacities. *Protein Expr. Purif.* **148**, 46–53 [CrossRef Medline](#)
46. Lacy, M., Kontos, C., Brandhofer, M., Hille, K., Gröning, S., Sinitski, D., Bourilhon, P., Rosenberg, E., Krammer, C., Thavayogarah, T., Pantouris, G., Bakou, M., Weber, C., Lolis, E., Bernhagen, J., and Kapurniotu, A. (2018) Identification of an Arg-Leu-Arg tripeptide that contributes to the binding interface between the cytokine MIF and the chemokine receptor CXCR4. *Sci. Rep.* **8**, 5171 [CrossRef Medline](#)
47. Sachpatzidis, A., Benton, B. K., Manfredi, J. P., Wang, H., Hamilton, A., Dohlman, H. G., and Lolis, E. (2003) Identification of allosteric peptide agonists of CXCR4. *J. Biol. Chem.* **278**, 896–907 [CrossRef Medline](#)
48. Lue, H., Thiele, M., Franz, J., Dahl, E., Speckgens, S., Leng, L., Fingerle-Rowson, G., Bucala, R., Lüscher, B., and Bernhagen, J. (2007) Macrophage migration inhibitory factor (MIF) promotes cell survival by activation of the Akt pathway and role for CSN5/JAB1 in the control of autocrine MIF activity. *Oncogene* **26**, 5046–5059 [CrossRef Medline](#)
49. Schwartz, V., Lue, H., Kraemer, S., Korbil, J., Krohn, R., Ohl, K., Bucala, R., Weber, C., and Bernhagen, J. (2009) A functional heteromeric MIF receptor formed by CD74 and CXCR4. *FEBS Lett.* **583**, 2749–2757 [CrossRef Medline](#)
50. Lubetsky, J. B., Dios, A., Han, J., Aljabari, B., Ruzsicska, B., Mitchell, R., Lolis, E., and Al-Abed, Y. (2002) The tautomerase active site of macrophage migration inhibitory factor is a potential target for discovery of novel anti-inflammatory agents. *J. Biol. Chem.* **277**, 24976–24982 [CrossRef Medline](#)
51. Al-Abed, Y., Dabideen, D., Aljabari, B., Valster, A., Messmer, D., Ochani, M., Tanovic, M., Ochani, K., Bacher, M., Nicoletti, F., Metz, C., Pavlov, V. A., Miller, E. J., and Tracey, K. J. (2005) ISO-1 binding to the tautomerase active site of MIF inhibits its pro-inflammatory activity and increases survival in severe sepsis. *J. Biol. Chem.* **280**, 36541–36544 [CrossRef Medline](#)
52. De Clercq, E. (2003) The bicyclam AMD3100 story. *Nat. Rev. Drug Discov.* **2**, 581–587 [CrossRef Medline](#)
53. Burger, J. A., and Stewart, D. J. (2009) CXCR4 chemokine receptor antagonists: perspectives in SCLC. *Exp. Opin. Investig. Drugs* **18**, 481–490 [CrossRef Medline](#)
54. Kessans, M. R., Gatesman, M. L., and Kockler, D. R. (2010) Plexixafor: a peripheral blood stem cell mobilizer. *Pharmacotherapy* **30**, 485–492 [CrossRef Medline](#)
55. De Clercq, E. (2015) AMD3100/CXCR4 inhibitor. *Front. Immunol.* **6**, 276 [CrossRef Medline](#)
56. Pawig, L., Klasek, C., Weber, C., Bernhagen, J., and Noels, H. (2015) Diversity and inter-connections in the CXCR4 chemokine receptor/ligand family: molecular perspectives. *Front. Immunol.* **6**, 429 [CrossRef Medline](#)
57. Qin, L., Kufareva, I., Holden, L. G., Wang, C., Zheng, Y., Zhao, C., Fenalti, G., Wu, H., Han, G. W., Cherezov, V., Abagyan, R., Stevens, R. C., and

Mimicry of human cytokine activity by *Arabidopsis* orthologs

- Handel, T. M. (2015) Structural biology: Crystal structure of the chemokine receptor CXCR4 in complex with a viral chemokine. *Science* **347**, 1117–1122 [CrossRef Medline](#)
58. Szpakowska, M., and Chevigné, A. (2016) vCCL2/vMIP-II, the viral master KEYmokine. *J. Leukoc. Biol.* **99**, 893–900 [CrossRef Medline](#)
59. Sterkel, A. K., Lorenzini, J. L., Fites, J. S., Subramanian Vignesh, K., Sullivan, T. D., Wuthrich, M., Brandhorst, T., Hernandez-Santos, N., Deepe, G. S., Jr., and Klein, B. S. (2016) Fungal mimicry of a mammalian aminopeptidase disables innate immunity and promotes pathogenicity. *Cell Host Microbe* **19**, 361–374 [CrossRef Medline](#)
60. Weber, C., Kraemer, S., Drechsler, M., Lue, H., Koenen, R. R., Kapurniotu, A., Zernecke, A., and Bernhagen, J. (2008) Structural determinants of MIF functions in CXCR2-mediated inflammatory and atherogenic leukocyte recruitment. *Proc. Natl. Acad. Sci. U.S.A.* **105**, 16278–16283 [CrossRef Medline](#)
61. Poelarends, G. J., Veetil, V. P., and Whitman, C. P. (2008) The chemical versatility of the β - α - β fold: catalytic promiscuity and divergent evolution in the tautomerase superfamily. *Cell. Mol. Life Sci.* **65**, 3606–3618 [CrossRef Medline](#)
62. Naessens, E., Dubreuil, G., Giordanengo, P., Baron, O. L., Minet-Kebdani, N., Keller, H., and Coustau, C. (2015) A secreted MIF cytokine enables aphid feeding and represses plant immune responses. *Curr. Biol.* **25**, 1898–1903 [CrossRef Medline](#)
63. Koga, K., Kenessey, A., Powell, S. R., Sison, C. P., Miller, E. J., and Ojamaa, K. (2011) Macrophage migration inhibitory factor provides cardioprotection during ischemia/reperfusion by reducing oxidative stress. *Antiox. Redox Signal.* **14**, 1191–1202 [CrossRef Medline](#)
64. Soares, A. R., Marchiosi, R., Siqueira-Soares Rde, C., Barbosa de Lima, R., Dantas dos Santos, W., and Ferrarese-Filho, O. (2014) The role of L-DOPA in plants. *Plant Signal. Behav.* **9**, e28275 [CrossRef Medline](#)
65. Norris, S. R., Shen, X., and DellaPenna, D. (1998) Complementation of the *Arabidopsis pds1* mutation with the gene encoding *p*-hydroxyphenylpyruvate dioxygenase. *Plant Physiol.* **117**, 1317–1323 [CrossRef Medline](#)
66. Taddese, B., Upton, G. J., Bailey, G. R., Jordan, S. R., Abdulla, N. Y., Reeves, P. J., and Reynolds, C. A. (2014) Do plants contain G protein-coupled receptors? *Plant Physiol.* **164**, 287–307 [CrossRef Medline](#)
67. Pieterse, C. M., Van der Does, D., Zamioudis, C., Leon-Reyes, A., and Van Wees, S. C. (2012) Hormonal modulation of plant immunity. *Annu. Rev. Cell Dev. Biol.* **28**, 489–521 [CrossRef Medline](#)
68. Feng, Z., Dubyak, G. R., Jia, X., Lubkowski, J. T., and Weinberg, A. (2013) Human β -defensin-3 structure motifs that are important in CXCR4 antagonism. *FEBS J.* **280**, 3365–3375 [CrossRef Medline](#)
69. Saini, V., Marchese, A., and Majetschak, M. (2010) CXC chemokine receptor 4 is a cell surface receptor for extracellular ubiquitin. *J. Biol. Chem.* **285**, 15566–15576 [CrossRef Medline](#)
70. Saini, V., Marchese, A., Tang, W. J., and Majetschak, M. (2011) Structural determinants of ubiquitin-CXC chemokine receptor 4 interaction. *J. Biol. Chem.* **286**, 44145–44152 [CrossRef Medline](#)
71. Cho, Y., Jones, B. F., Vermeire, J. J., Leng, L., DiFedele, L., Harrison, L. M., Xiong, H., Kwong, Y. K., Chen, Y., Bucala, R., Lolis, E., and Cappello, M. (2007) Structural and functional characterization of a secreted hookworm macrophage migration inhibitory factor (MIF) that interacts with the human MIF receptor CD74. *J. Biol. Chem.* **282**, 23447–23456 [CrossRef Medline](#)
72. Pantouris, G., Rajasekaran, D., Garcia, A. B., Ruiz, V. G., Leng, L., Jorgensen, W. L., Bucala, R., and Lolis, E. J. (2014) Crystallographic and receptor binding characterization of *Plasmodium falciparum* macrophage migration inhibitory factor complexed to two potent inhibitors. *J. Med. Chem.* **57**, 8652–8656 [CrossRef Medline](#)
73. Borghese, F., and Clanchy, F. I. (2011) CD74: an emerging opportunity as a therapeutic target in cancer and autoimmune disease. *Exp. Opin. Ther. Targets* **15**, 237–251 [CrossRef Medline](#)
74. Kraemer, S., Lue, H., Zernecke, A., Kapurniotu, A., Andreetto, E., Frank, R., Lennartz, B., Weber, C., and Bernhagen, J. (2011) MIF-chemokine receptor interactions in atherogenesis are dependent on an N-loop-based 2-site binding mechanism. *FASEB J.* **25**, 894–906 [CrossRef Medline](#)
75. Desein, A. F., Stechly, L., Jonckheere, N., Dumont, P., Monté, D., Le-teurtre, E., Truant, S., Pruvot, F. R., Figeac, M., Hebbar, M., Lecellier, C. H., Lesuffleur, T., Desein, R., Grard, G., Dejonghe, M. J., et al. (2010) Auto-crine induction of invasive and metastatic phenotypes by the MIF-CXCR4 axis in drug-resistant human colon cancer cells. *Cancer Res.* **70**, 4644–4654 [CrossRef Medline](#)
76. Cournia, Z., Leng, L., Gandavadi, S., Du, X., Bucala, R., and Jorgensen, W. L. (2009) Discovery of human macrophage migration inhibitory factor (MIF)-CD74 antagonists via virtual screening. *J. Med. Chem.* **52**, 416–424 [CrossRef Medline](#)
77. Boisvert, W. A., Rose, D. M., Johnson, K. A., Fuentes, M. E., Lira, S. A., Curtiss, L. K., and Terkeltaub, R. A. (2006) Up-regulated expression of the CXCR2 ligand KC/GRO- α in atherosclerotic lesions plays a central role in macrophage accumulation and lesion progression. *Am. J. Pathol.* **168**, 1385–1395 [CrossRef Medline](#)
78. Soehnlein, O., Steffens, S., Hidalgo, A., and Weber, C. (2017) Neutrophils as protagonists and targets in chronic inflammation. *Nat. Rev. Immunol.* **17**, 248–261 [CrossRef Medline](#)
79. Murphy, K., and Weaver, C. (2016) *Janeway's Immunobiology*, 9th revised Ed., pp. 602–627, W. W. Norton and Co., New York
80. Larkin, M. A., Blackshields, G., Brown, N. P., Chenna, R., McGettigan, P. A., McWilliam, H., Valentin, F., Wallace, I. M., Wilm, A., Lopez, R., Thompson, J. D., Gibson, T. J., and Higgins, D. G. (2007) Clustal W and Clustal X version 2.0. *Bioinformatics* **23**, 2947–2948 [CrossRef Medline](#)
81. Waterhouse, A. M., Procter, J. B., Martin, D. M., Clamp, M., and Barton, G. J. (2009) Jalview Version 2—a multiple sequence alignment editor and analysis workbench. *Bioinformatics* **25**, 1189–1191 [CrossRef Medline](#)
82. Troshin, P. V., Procter, J. B., and Barton, G. J. (2011) Java bioinformatics analysis web services for multiple sequence alignment—JABAWS:MSA. *Bioinformatics* **27**, 2001–2002 [CrossRef Medline](#)
83. Whitmore, L., and Wallace, B. A. (2004) DICHROWEB, an online server for protein secondary structure analyses from circular dichroism spectroscopic data. *Nucleic Acids Res.* **32**, W668–W673 [CrossRef Medline](#)
84. Whitmore, L., and Wallace, B. A. (2008) Protein secondary structure analyses from circular dichroism spectroscopy: methods and reference databases. *Biopolymers* **89**, 392–400 [CrossRef Medline](#)
85. Sreerama, N., and Woody, R. W. (2000) Estimation of protein secondary structure from circular dichroism spectra: comparison of CONTIN, SELCON, and CDSSTR methods with an expanded reference set. *Anal. Biochem.* **287**, 252–260 [CrossRef Medline](#)
86. Greenfield, N. J. (2006) Using circular dichroism spectra to estimate protein secondary structure. *Nat. Protoc.* **1**, 2876–2890 [CrossRef Medline](#)
87. Rajasekaran, D., Zierow, S., Syed, M., Bucala, R., Bhandari, V., and Lolis, E. J. (2014) Targeting distinct tautomerase sites of D-DT and MIF with a single molecule for inhibition of neutrophil lung recruitment. *FASEB J.* **28**, 4961–4971 [CrossRef Medline](#)
88. Dios, A., Mitchell, R. A., Aljabari, B., Lubetsky, J., O'Connor, K., Liao, H., Senter, P. D., Manogue, K. R., Lolis, E., Metz, C., Bucala, R., Callaway, D. J., and Al-Abed, Y. (2002) Inhibition of MIF bioactivity by rational design of pharmacological inhibitors of MIF tautomerase activity. *J. Med. Chem.* **45**, 2410–2416 [CrossRef Medline](#)
89. Kelley, L. A., Mezulis, S., Yates, C. M., Wass, M. N., and Sternberg, M. J. (2015) The Phyre2 web portal for protein modeling, prediction and analysis. *Nat. Protoc.* **10**, 845–858 [CrossRef Medline](#)
90. Wu, B., Chien, E. Y., Mol, C. D., Fenalti, G., Liu, W., Katritch, V., Abagyan, R., Brooun, A., Wells, P., Bi, F. C., Hamel, D. J., Kuhn, P., Handel, T. M., Cherezov, V., and Stevens, R. C. (2010) Structures of the CXCR4 chemokine GPCR with small-molecule and cyclic peptide antagonists. *Science* **330**, 1066–1071 [CrossRef Medline](#)
91. Crump, M. P., Gong, J. H., Loetscher, P., Rajarathnam, K., Amara, A., Arenzana-Seisdedos, F., Virelizier, J. L., Baggiolini, M., Sykes, B. D., and Clark-Lewis, I. (1997) Solution structure and basis for functional activity of stromal cell-derived factor-1; dissociation of CXCR4 activation from binding and inhibition of HIV-1. *EMBO J.* **16**, 6996–7007 [CrossRef Medline](#)

A. Appendix

A.1. Additional findings on MIF's interaction with the chemokine network

This section contains additional work related to the main content of this thesis, mainly addressing the possibility of MIF – as an atypical chemokine – to interact directly with classical chemokines in a similar manner as it is known from other ACK/CK interactions. Such direct interactions, if possible, could modulate the function of the involved proteins and would further expand the interplay between MIF-family proteins and the chemokine network beyond receptor/ligand interactions.

As a first step of this investigation, potential interaction candidates of MIF as well as MIF-2 could be identified by an unbiased solid-phase array approach, with immobilized classical as well as atypical chemokines. Potential interaction candidates would then have to be verified, and the protein-protein interaction more thoroughly investigated by various biophysical as well as *in silico* approaches. Further studies of such an MIF/CK-complex would then be mainly focused on structural aspects like the binding site of the proteins, as well as on the role and physiological relevance of such an ACK/CK heteromer. Accordingly, this part aims at identifying CKs interacting with MIF and verifying their interaction – if one was identified – followed by the detection of these complexes in a physiological relevant context, e.g. in human tissue samples. Functional studies of identified MIF/CK-complexes would have to focus mostly on modulating known MIF-mediated effects. Additionally, the interaction site of these proteins were to be studied. For initial screenings this would have to be done by peptide-array based assays, while a more thorough picture could be obtained via NMR spectroscopy studies.

Listed here are experiments and studies along with their results, either conducted by me or in collaboration with others as indicated, that are either not fully published yet or only partially incorporated in publications or manuscripts. This includes initial investigations regarding possible MIF/CK interactions in section A.1.1 as well as a more detailed study on the newly identified MIF/CXCL4L1 heterocomplex in section A.1.2, which led to a paper manuscript – under revision at the time this doctoral thesis was submitted for evaluation – at *Cellular and Molecular Life Sciences* and is available as a preprint on bioRxiv [150].¹ This preprint, accompanied by a description of my contributions to it, is included in this chapter, while other studies are presented in a shortened, manuscript-like format.

A.1.1. Screening for MIF and MIF-2 interactors and the discovery of the ACK/CK interactome

M. Brandhofer¹, X. Blanchet², C. Weber^{2,4,5}, P. von Hundelshausen^{2,3}, J. Bernhagen^{1,4,5}

Affiliations: ¹: Institute for Stroke and Dementia Research (ISD), Klinikum der Universität München, Ludwig-Maximilians-Universität (LMU) München, Munich, Germany. ²: Institute for Cardiovascular Prevention (IPEK), Ludwig-Maximilians-Universität München, Munich, Germany. ³: German Center for Cardiovascular Research (DZHK), Partner Site Munich Heart Alliance, Munich, Germany. ⁴: Munich Cluster for Systems Neurology (SyNergy), Munich, Germany. ⁵: Munich Heart Alliance, Munich, Germany

¹Published in revised form at *Cellular and Molecular Life Sciences* in September 2022
(DOI: 10.1007/s00018-022-04539-0).

A. Appendix

Contributions: Design of study: PvH, JB, CW; Solid phase assay: XB, Data analysis: MB, XB; biotin-labeling of proteins: MB.

Parts of this study that are relevant for the interaction of MIF with CXCL4L1 or CXCL4 are included in the manuscript by Brandhofer *et al.*, 2022, incorporated in section A.1.2 [150].

Introduction

Formation of heteromeric complexes among classical chemokines is well described in the literature and identified as a regulatory mechanism of the chemokine network, aptly referred to as the “chemokine interactome” [26, 65, 69]. Similar complexes are reported for certain atypical chemokines like e.g. HMGB1 and some galectins [75, 76, 78]. As MIF-family proteins are also emerging as ACKs, we wanted to investigate whether also MIF and MIF-2 could interfere in this complex regulatory network by formation of heterocomplexes with CKs or other ACKs. Such heteromeric complexes could have a modulating effect on chemokine function, possibly allowing MIF to indirectly target others than its already known chemokine receptors. Vice versa, also MIF effects could be influenced, for example under inflammatory conditions, by the local chemokine profile. Such an expansion of the known chemokine network would therefore greatly aid in our understanding of this complex regulatory network and the multi-faceted roles of MIF-family proteins.

Accordingly, this screening approach aims to identify potential interactions between MIF as well as MIF-2 and classical chemokines. MIF/CK-complexes identified within this study are then to be investigated further regarding their role and physiological relevance in additional experiments.

Results

Classical chemokines and peroxiredoxins as potential interaction candidates for MIF and MIF-2 To screen for interactions of ACKs MIF and MIF-2 with human CKs and selected ACKs, we performed initial solid phase arrays at pH 6.0 and pH 8.0. Here, CKs and selected ACKs were immobilized on a surface and probed for interaction with biotinylated MIF or MIF-2 respectively. Bound MIF or MIF-2 was then developed chemoluminescently using a streptavidin-HRP conjugate. By using this setup, we were able to identify numerous novel interaction candidates for both MIF and MIF-2, as depicted in figures A.1 and A.2. Among these candidate interactors were various CC- and CXC-type chemokines as well as peroxiredoxin-1 and -6. These assays were performed both at pH 8.0 and 6.0 to account for variations in surface charges around a physiological pH level. While some of the interaction candidates were detected at both pH levels, a number of interactions were only observed under one of the two tested conditions. This was more prominently the case for MIF, with most interactions detected at pH 6.0, while in the case of MIF-2 results were more balanced with only slightly more hits at pH 8.0 (see also table A.1). This indicates, especially for MIF, a certain pH-sensitivity for potential MIF/(A)CK interactions.

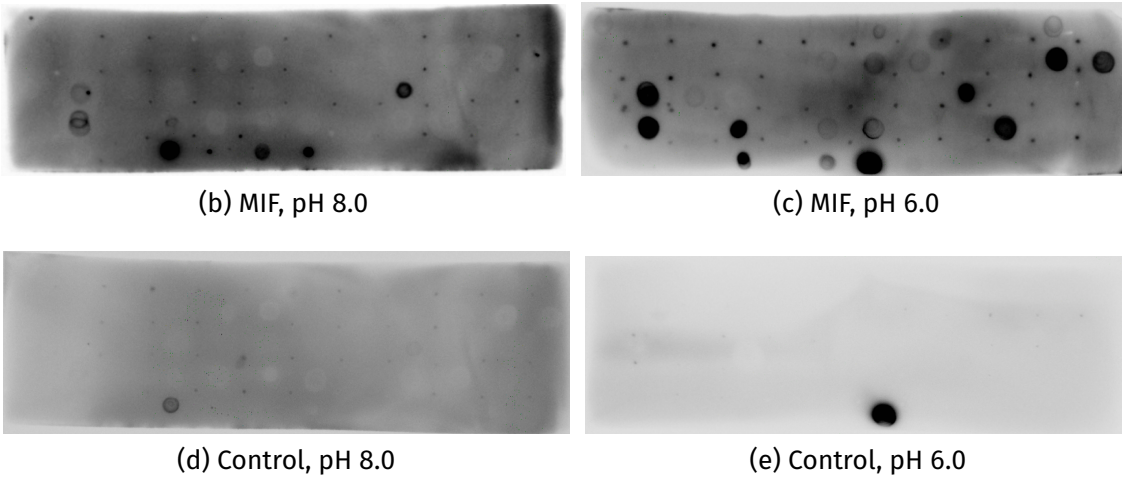
Discussion

The setup of this solid phase assay allowed for the screening of MIF-family protein interactions with classical chemokines and also selected atypical chemokines. By this approach, a variety of novel interaction candidates for both MIF and MIF-2 were identified, as listed in table A.1.

A.1. Additional findings on MIF's interaction with the chemokine network

CCL1	CCL2	CCL3	CCL3L1	CCL4	CCL4L1	CCL5	CCL7	CCL8	CCL11	CCL13	CCL14
CCL15	CCL16	CCL17	CCL18	CCL19	CCL20	CCL21	CCL22	CCL23	CCL24	CCL25	CCL26
CCL27	CCL28	XCL1	XCL2	CXCL1	CXCL2	CXCL3	CXCL4	CXCL4L1	CXCL5	CXCL6	CXCL7
CXCL8	CXCL9	CXCL10	CXCL11	CXCL12a	CXCL12b	CXCL13	CXCL14	CXCL16	CXCL17	CX ₃ CL1	
HMGB1	BD1	BD2	Prx1		Prx6	MIF	MIF-2				

(a) Membrane layout



(b) MIF, pH 8.0

(c) MIF, pH 6.0

(d) Control, pH 8.0

(e) Control, pH 6.0

Figure A.1.: Identification of classical and atypical chemokines interacting with MIF in an initial screening via solid phase assay. Dark spots indicate MIF bound to immobilized protein. (a): Layout of immobilized CKs and ACKs on surface. (b): Result for incubation with MIF at pH 8.0. (c): Result for incubation with MIF at pH 6.0. (d): Negative control membrane, incubated and developed without MIF at pH 8.0. (e): Negative control membrane, incubated and developed without MIF at pH 6.0. Used abbreviations: BD: β -defensin; Prx: peroxiredoxin.

Notably, this assay detected an interaction of MIF with peroxiredoxin-1, which has previously been found in a yeast two-hybrid screening by Jung *et al.* in 2001, indicating a general validity of this screening approach [151]. The screening was performed at both pH 6.0 and pH 8.0 to account for pH-dependent charge changes around a physiological pH-range. For MIF, the pH indeed affected the number of identified candidate interactors. Here, more candidates were identified at pH 6.0, where MIF – with an isoelectric point of pH 8.24² can be expected to have a more positive net charge compared to the situation at pH of 8.0.

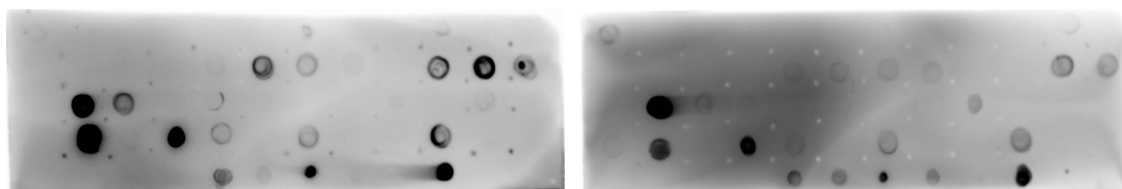
Taking the results of these other assays into account, the characterization of interactions between MIF-family proteins and CKs as well as ACKs can be schematically summarized as in figure A.3. This schematic overview also incorporates unpublished data from the Bernhagen lab, including findings from functional assays as well as various methods to analyze protein-protein-interactions. Here, for example, the interaction of MIF with CXCL4L1 and CXCL11 as well as MIF-2/CCL20 heterocomplexes were investigated and characterized further. A detailed study on

²Theoretical IEP calculated with the Expasy “Compute pI/Mw tool”, based on the amino acid residues 2 to 115 of UniProtKB entry of human MIF (P14174) [152].

A. Appendix

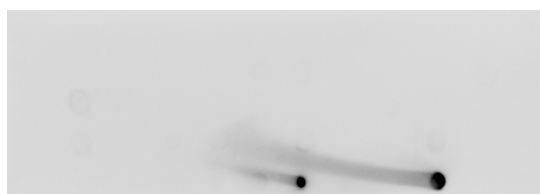
CCL1	CCL2	CCL3	CCL3L1	CCL4	CCL4L1	CCL5	CCL7	CCL8	CCL11	CCL13	CCL14
CCL15	CCL16	CCL17	CCL18	CCL19	CCL20	CCL21	CCL22	CCL23	CCL24	CCL25	CCL26
CCL27	CCL28	XCL1	XCL2	CXCL1	CXCL2	CXCL3	CXCL4	CXCL4L1	CXCL5	CXCL6	CXCL7
CXCL8	CXCL9	CXCL10	CXCL11	CXCL12a	CXCL12b	CXCL13	CXCL14	CXCL16	CXCL17	CX ₃ CL1	
HMGB1	Disulfide - HMGB1	BD1	BD2	Prx1	Prx6	Biot. MIF	MIF	MIF-2	Biot. MIF-2		

(a) Membrane Layout



(b) MIF-2, pH 8.0

(c) MIF-2, pH 6.0



(d) Control

Figure A.2.: Identification of classical and atypical chemokines interacting with MIF-2 in an initial screening via solid phase assay. Dark spots indicate MIF-2 bound to immobilized protein. (a): Layout of immobilized CKs and ACKs on surface. (b): Result for incubation with MIF-2 at pH 8.0. (c): Result for incubation with MIF at pH 6.0. (b): Result for incubation with MIF-2 at pH 8.0. (d): Negative control membrane, washed and re-used for assays at both pH levels. Used abbreviations: BD: β -defensin; Prx: peroxiredoxin. Biot.: Biotinylated.

the identified MIF/CXCL4L1 complex, for example, can be found in section A.1.2. Figure A.3 thus gives a summary on the newly discovered ACK/CK interactome.

Methodology

Proteins and Reagents: Recombinant human MIF as well as MIF-2, endotoxin-free and biologically active, was prepared as previously described with a typical purity of $\approx 98\%$ as determined by analysis via SDS-PAGE and silver staining [84, 113, 153]. Biotinylated human MIF and MIF-2 were produced using 90% to 95% pure recombinant proteins in a reaction with a D-Biotinoyl- ϵ -aminocaproic acid-N-hydroxy-succinimide ester (Biotin-7-NHS) using the “Biotin Protein Labeling Kit” manufactured by Roche Diagnostics GmbH (Mannheim, Germany). Additional biotinylation reagent suitable for the same labeling chemistry (Biotinamidohexanoic acid N-hydroxysuccinimide ester) was purchased from Sigma-Aldrich (Taufkirchen, Germany). Recombinant human CXCL4L1 (PF4var1) was purchased from ChromaTec GmbH (Greifswald, Germany). Recombinant human peroxiredoxins 1 and 6 were purchased from abcam (Abcam

A. Appendix

water and developed using streptavidin conjugated with HRP (horseradish peroxidase) (Bio-Techne GmbH, Wiesbaden-Nordenstadt, Germany), diluted 1:200 in 1× ROTI®Block, for 2 h. Bound biotin-MIF after washing was detected by chemiluminescence using SuperSignal™ West Pico Chemiluminescent Substrate purchased from Thermo Fisher Scientific using a LAS-3000 Imaging System (Fuji Photo Film Co., LTD., Japan).

A.1.2. Investigation of the novel MIF/CXCL4L1 heterocomplex

After previously screening for potential chemokine interaction partners of MIF and MIF-2, as described in section A.1.1, we selected CXCL4L1 for further investigations. As the solid phase assay showed, CXCL4L1 appeared as the strongest candidate interactor for MIF while CXCL4 – a classical chemokine highly similar in amino acid sequence – showed no sign of complex formation. Intrigued by these findings, we chose the MIF/CXCL4L1 complex as the main target for more detailed investigations. These investigations, conducted together with various collaboration partners as indicated below, led to the paper manuscript enclosed in this section.

The manuscript below reflects the state of our investigation on the MIF/CXCL4L1 heterocomplex at the time this thesis was submitted for evaluation. In September 2022, after the evaluation of this thesis, a revised version of the paper manuscript has been published in *Cellular and Molecular Life Sciences* (DOI: 10.1007/s00018-022-04539-0), as indicated in the publication list on page xiii.

Manuscript by Brandhofer *et al.*, 2022 and my contributions

Heterocomplexes between the Atypical Chemokine MIF and the CXC-Motif Chemokine CXCL4L1 Regulate Inflammation and Thrombus Formation

M. Brandhofer*, A. Hoffmann*, X. Blanchet, E. Siminkovitch, A-K. Rohlfig, O. El Bounkari, J. Nestele, A. Bild, C. Kontos, K. Hille, V. Rohde, A. Fröhlich, J. Golemi, O. Gokce, C. Krammer, P. Scheiermann, N. Tsilimparis, W. Kempf, L. Mägdefessel, R. Megens, H. Ippel, R. Koenen, K. Mayo, M. Gawaz, A. Kapurniotu, C. Weber, P. von Hundelshausen and J. Bernhagen

(*: Equally contributing, shared first authors)

DOI: 10.1101/2021.11.26.470090 (preprint on bioRxiv)

In this manuscript, we hypothesized that the cytokine and atypical chemokine MIF could engage in direct interaction with classical chemokines, as both interactions among classical chemokines as well as between classical chemokines and certain atypical ones have already been reported. We performed an unbiased interaction screening (a solid phase assay, performed with biotinylated human MIF, documented also in section A.1.1) in which MIF was shown to interact with CXCL4L1 – a variant of the platelet chemokine CXCL4 with an almost identical amino acid sequence – but strikingly not with CXCL4 itself. Subsequently we investigated this novel interaction further, employing various biophysical methods and tested the functional relevance of the assay in numerous cell-based assays. We were able to show that MIF forms a complex with CXCL4L1 *in vitro* and *in vivo*, identifying MIF/CXCL4L1 complexes both in platelets as well as in patient derived thrombus material, and that this complex formation abrogates MIF's effects on immune cell recruitment and thrombus formation as well as on the morphological changes of adhering platelets.

A.1. Additional findings on MIF's interaction with the chemokine network

As shared first author, I contributed significantly to the preparation of the manuscript, including creation of figures and analysis of data. I was involved in the conceptualization of the study, coordination and transfer of materials with cooperation partners from multiple labs and the design of the experiments. This includes, together with the shared first author A. Hoffmann, the training and supervision of students that performed experiments – with and without my direct assistance – for this publication in our lab as part of their Bachelor or Master theses. These involve chemotaxis assays, thrombocyte isolations, immunofluorescent stainings and proximity ligation assays (results depicted in figures 3, 5 and 6).

In regard of materials used in this study, the fluorescently labeled or biotinylated recombinant MIF for the experiments was labeled by me, and I produced the CXCL4L1 used for the fluorescence polarisation assay (see panel A and B in figure 4) by recombinant expression in *E. coli* and subsequent purification of the raw protein via IMAC and SEC. I performed the microscale thermophoresis experiments (figure 2D and E) together with A. Hoffmann and I analyzed the obtained data. To investigate potential interaction sites of MIF and CXCL4L1 as well as the structure of the resulting protein complex, including the plausibility of its formation, I was involved in the design and analysis of the peptide array experiments and designed, performed and analyzed the *in silico* studies shown in supplementary figure 2. These results, together with MST and SPR data from figure 2, further indicate that complex formation of MIF with CXCL4L1 is preferred over a MIF/CXCL4 complex, which in turn might be due to the different 3D structure of CXCL4L1 when compared to its close relative CXCL4. The label-free dynamic mass redistribution assay depicted in figure 4 was also performed and analyzed by me. In combination with the aforementioned fluorescence polarization experiments, this suggested that the inhibitory effect of CXCL4L1 on MIF is due to an interference with MIF/CXCR4 interactions. The effect of this interference was visible by the inhibitory effect of complex formation on MIF's functions, as seen in the chemotaxis assays. Imaging data obtained from thrombocytes, shown in figure 5, is based partially on thrombocytes isolated by me. This imaging data led us to investigate the complex formation also in clinical thrombus specimens (see figure 6), in which the occurrence of MIF/CXCL4L1 interactions could also be shown via proximity ligation assay.

bioRxiv preprint doi: <https://doi.org/10.1101/2021.11.26.470090>; this version posted February 24, 2022. The copyright holder for this preprint (which was not certified by peer review) is the author/funder, who has granted bioRxiv a license to display the preprint in perpetuity. It is made available under aCC-BY-NC-ND 4.0 International license.

1 **Heterocomplexes between the Atypical Chemokine MIF and the**
2 **CXC-Motif Chemokine CXCL4L1 Regulate Inflammation and**
3 **Thrombus Formation**

4 Markus Brandhofer^{1,#}, Adrian Hoffmann^{1,2,#}, Xavier Blanchet³, Elena Siminkovitch¹, Anne-
5 Katrin Rohlfing⁴, Omar El Bounkari¹, Jeremy A. Nестele⁴, Alexander Bild⁴, Christos Kontos⁵,
6 Kathleen Hille⁵, Vanessa Rohde¹, Adrian Fröhlich¹, Jona Golemi⁶, Ozgun Gokce^{6,7}, Christine
7 Krammer¹, Patrick Scheiermann², Nikolaos Tsilimparis⁸, Wolfgang E. Kempf⁹, Lars
8 Maegdefessel⁹, Remco T.A. Megens³, Hans Ippel¹⁰, Rory R. Koenen¹⁰, Kevin H. Mayo^{10,11},
9 Meinrad Gawaz⁴, Aphrodite Kapurniotu⁵, Christian Weber^{3,7,10,12}, Philipp von Hundels-
10 hausen^{3,*}, Jürgen Bernhagen^{1,7,12*}

11

12 ¹Division of Vascular Biology, Institute for Stroke and Dementia Research (ISD), LMU
13 University Hospital, Ludwig-Maximilians-Universität (LMU) München, 81377 Munich,
14 Germany; ²Department of Anesthesiology, LMU University Hospital, Ludwig-Maximilians-
15 Universität (LMU) München, 81377 Munich, Germany; ³Institute for Cardiovascular Pre-
16 vention, LMU University Hospital, Ludwig-Maximilians-Universität (LMU) München, 80336
17 Munich, Germany; ⁴Department of Cardiology and Angiology, University Hospital Tübingen,
18 Eberhard Karls University Tübingen, Tübingen, Germany; ⁵Division of Peptide Biochemistry,
19 TUM School of Life Sciences, Technische Universität München (TUM); ⁶Systems
20 Neuroscience Group, Institute for Stroke and Dementia Research (ISD), LMU University
21 Hospital, Ludwig-Maximilians-Universität (LMU) München, 81377 Munich, Germany; ⁷Munich
22 Cluster for Systems Neurology (SyNergy), 81377 Munich, Germany; ⁸Department of Vascular
23 Surgery, LMU University Hospital, Ludwig-Maximilians-Universität (LMU) München, 81377
24 Munich, Germany; ⁹Department for Vascular and Endovascular Surgery, Klinikum rechts der
25 Isar, Technische Universität München (TUM), 81675 Munich, Germany; ¹⁰Cardiovascular
26 Research Institute Maastricht (CARIM), Maastricht University, 6229 ER Maastricht, The
27 Netherlands; ¹¹ Department of Biochemistry, Molecular Biology and Biophysics, Health

1

A.1. Additional findings on MIF's interaction with the chemokine network

bioRxiv preprint doi: <https://doi.org/10.1101/2021.11.26.470090>; this version posted February 24, 2022. The copyright holder for this preprint (which was not certified by peer review) is the author/funder, who has granted bioRxiv a license to display the preprint in perpetuity. It is made available under aCC-BY-NC-ND 4.0 International license.

28 Sciences Center, University of Minnesota, Minneapolis, MN, USA; ¹²Munich Heart Alliance,

29 80802 Munich, Germany.

30

31

Correspondence:

Jürgen Bernhagen, PhD

Professor and Chair of Vascular Biology

Institute for Stroke and Dementia Research (ISD)

LMU University Hospital (LMU Klinikum)

Ludwig-Maximilians-Universität (LMU) München

Feodor-Lynen-Straße 17, 81377 Munich, Germany

Tel.: 0049-89 4400 - 46151

E-Mail: juergen.bernhagen@med.uni-muenchen.de

32

33

Philipp von Hundelshausen, MD

Institute for Cardiovascular Prevention (IPEK)

LMU University Hospital (LMU Klinikum)

Ludwig-Maximilians-Universität (LMU) München

Pettenkofer Straße 8a/9, 80336 Munich, Germany

Tel.: 0049-89 4400 - 54359

E-Mail: Philipp.von_Hundelshausen@med.uni-muenchen.de

34

bioRxiv preprint doi: <https://doi.org/10.1101/2021.11.26.470090>; this version posted February 24, 2022. The copyright holder for this preprint (which was not certified by peer review) is the author/funder, who has granted bioRxiv a license to display the preprint in perpetuity. It is made available under aCC-BY-NC-ND 4.0 International license.

35 **Abstract**

36 To fulfil their orchestrating function in immune cell trafficking in homeostasis and disease, a
37 network of 49 chemokines and 23 receptors capitalizes on features of specificity,
38 redundancy, and functional selectivity such as biased agonism. The discovery of the
39 chemokine interactome, i.e. heteromeric chemokine-chemokine interactions, even across
40 CC- and CXC-class borders, has further expanded the complexity within the network.
41 Moreover, some inflammatory mediators, which are not structurally linked to classical CC-,
42 CXC-, CX₃C-, or C-chemokines, can bind to chemokine receptors and behave as atypical
43 chemokines (ACKs). We identified the cytokine macrophage migration inhibitory factor (MIF)
44 as an ACK that binds to the chemokine receptors CXCR2 and CXCR4 to promote
45 atherogenic leukocyte recruitment. Here, we hypothesized that chemokine-chemokine
46 interactions extend to ACKs and that MIF may form heterocomplexes with classical
47 chemokines. We tested this hypothesis, applying an unbiased chemokine protein binding
48 array. The platelet chemokine CXCL4L1, but not its variant CXCL4 or the CXCR2/CXCR4
49 ligands CXCL8 or CXCL12, was identified as a candidate interactor. MIF/CXCL4L1
50 complexation was verified by co-immunoprecipitation, surface plasmon-resonance analysis,
51 and microscale thermophoresis, which also established high-affinity binding ($K_D \approx 100$ -150
52 nM). The binding interface was predicted by peptide array-based mapping and molecular
53 docking. We next determined whether heterocomplex formation modulates inflammatory and
54 atherogenic activities of MIF. MIF-elicited T-cell chemotaxis as assessed in a 3D-matrix-
55 based live cell-imaging set-up was abrogated, when cells were co-incubated with MIF and
56 CXCL4L1. Heterocomplexation also blocked MIF-triggered migration of Egfp⁺ microglia in
57 cortical cultures *in situ*. Of note, CXCL4L1 blocked the binding of Alexa-MIF to a soluble
58 ectodomain mimic of CXCR4 and co-incubation with CXCL4L1 attenuated MIF-triggered
59 dynamic mass redistribution in HEK293-CXCR4 transfectants, indicating that complex
60 formation interferes with MIF/CXCR4 pathways. As MIF and CXCL4L1 are abundant platelet
61 products, we finally tested their role in platelet activation. Multi-photon microscopy, FLIM-
62 FRET, and proximity ligation assay visualized heterocomplexes in platelet aggregates and

A.1. Additional findings on MIF's interaction with the chemokine network

bioRxiv preprint doi: <https://doi.org/10.1101/2021.11.26.470090>; this version posted February 24, 2022. The copyright holder for this preprint (which was not certified by peer review) is the author/funder, who has granted bioRxiv a license to display the preprint in perpetuity. It is made available under aCC-BY-NC-ND 4.0 International license.

63 clinical human thrombus sections. Moreover, heterocomplex formation inhibited MIF-
64 stimulated thrombus formation under flow and skewed the morphology of adhering platelets
65 from a large to a small lamellipodia phenotype. Together, our study establishes a novel
66 molecular interaction, adding to the complexity of the chemokine interactome and
67 chemokine/receptor network. MIF/CXCL4L1, or more generally, ACK/CXC-motif chemokine
68 heterocomplexes may be promising target structures to modulate inflammation and
69 thrombosis.

70

71

bioRxiv preprint doi: <https://doi.org/10.1101/2021.11.26.470090>; this version posted February 24, 2022. The copyright holder for this preprint (which was not certified by peer review) is the author/funder, who has granted bioRxiv a license to display the preprint in perpetuity. It is made available under aCC-BY-NC-ND 4.0 International license.

72 Introduction

73 Chemokines orchestrate immune cell trafficking in health and disease (Charo & Ransohoff,
74 2006; Noels *et al*, 2019; Weber & Noels, 2011). Chemokine-directed targeting strategies are
75 pursued in acute and chronic inflammatory conditions, autoimmunity, cancer, and athero-
76 sclerosis (Hutchings *et al*, 2017; Noels *et al.*, 2019; Zlotnik *et al*, 2011). The chemokine
77 network encompasses 49 classical chemokines (CKs) and 18 classical chemokine receptors
78 (CKRs), which belong to the class of G α protein-coupled receptors (GPCRs) (Bachelerie *et*
79 *al*, 2014a; Bachelerie *et al*, 2014b; Murphy *et al*, 2000). Depending on the particular
80 chemokine ligand/receptor pair and various disease and microenvironmental factors,
81 chemokine signaling through CKRs overall capitalizes on the principles of specificity,
82 promiscuity, and biased agonism. Accordingly, multiple chemokines can bind to a certain
83 chemokine receptor and *vice versa*, while 'biased agonism' can occur on a ligand, receptor,
84 or tissue basis (Eiger *et al*, 2021; Kleist *et al*, 2016; Steen *et al*, 2014). Fine-tuning of
85 chemokine responses within this network is further expanded by five atypical chemokine
86 receptors (ACKRs) that serve as decoy receptors and promiscuously bind many chemokines
87 to shape their gradients, but also elicit specific signaling responses (Nibbs & Graham, 2013).

88 Chemokines are well-known to form homodimers, but the discovery of the chemokine
89 interactome additionally suggested a multitude of heteromeric chemokine-chemokine inter-
90 actions even across CC- and CXC-chemokine class borders (Koenen *et al*, 2009; von
91 Hundelshausen *et al*, 2017). CC-type heterodimers between CCL5 and CCL17 or CCL5 and
92 CXCL4 (also termed platelet factor 4, PF4) were found to lead to functional synergism by
93 receptor retention or auxiliary proteoglycan binding and enhancement of chemotactic
94 responses, respectively, while CXC-type heterodimers between CXCL12 and CCL5 or
95 CXCL12 and CXCL4 led to signaling inhibition. This has demonstrated yet another level of
96 complexity within the chemokine network and offers novel intervention strategies in
97 inflammatory and cardiovascular diseases (von Hundelshausen *et al.*, 2017).

98 Moreover, some alarmin-like inflammatory mediators such as human β -defensins
99 (HBDs) and secreted fragments of amino acyl tRNA-synthetases (AARs), which do not

A.1. Additional findings on MIF's interaction with the chemokine network

bioRxiv preprint doi: <https://doi.org/10.1101/2021.11.26.470090>; this version posted February 24, 2022. The copyright holder for this preprint (which was not certified by peer review) is the author/funder, who has granted bioRxiv a license to display the preprint in perpetuity. It is made available under aCC-BY-NC-ND 4.0 International license.

100 belong to one of the four structural classes of CC-, CXC-, CX₃C-, or C-chemokines, can bind
101 to chemokine receptors by molecular mimicry and exhibit chemokine-like activities (Rohrl *et*
102 *al*, 2010; Wakasugi & Schimmel, 1999). These proteins are also referred to as atypical
103 chemokines (ACKs) (Degryse & de Virgilio, 2003; Kapurniotu *et al*, 2019; Oppenheim &
104 Yang, 2005).

105 Macrophage migration inhibitory factor (MIF) is an evolutionarily conserved pleiotropic
106 inflammatory cytokine (David, 1966; Michelet *et al*, 2019). MIF is an upstream regulator of
107 the host innate immune response and, when dysregulated, is a pivotal mediator of
108 inflammatory diseases, autoimmunity, cancer, and cardiovascular diseases (Calandra &
109 Roger, 2003; Tilstam *et al*, 2017). MIF is a structurally unique cytokine (Sun *et al*, 1996) and,
110 contrary to its eponymous name, has chemokine-like activities and functions as a
111 prototypical ACK (Bernhagen *et al*, 2007; Kapurniotu *et al.*, 2019). Accordingly, MIF not only
112 signals through its cognate receptor CD74/invariant chain, but engages in high-affinity
113 interactions with the CXC chemokine receptors CXCR2 and CXCR4 to promote atherogenic
114 monocyte and T-/B-cell recruitment, cancer metastasis, and inflammation (Bernhagen *et al.*,
115 2007; Kapurniotu *et al.*, 2019; Klasen *et al*, 2014; Leng *et al*, 2003; Pawig *et al*, 2015; Sinitski
116 *et al*, 2019; Tillmann *et al*, 2013). We elucidated the structural determinants of the binding
117 interface between MIF and its CXC-motif chemokine receptors and found that MIF mimics
118 chemokine receptor binding regions such as the ELR motif and the N-loop (Kraemer *et al*,
119 2011b; Krammer *et al*, 2021; Lacy *et al*, 2018; Rajasekaran *et al*, 2016; Weber *et al*, 2008).
120 Interestingly, CXCL12/SDF-1 α (stromal-derived factor-1 α), the cognate ligand of CXCR4,
121 was recently found to bind to the non-chemokine proteins galectin-3 (Eckardt *et al*, 2020) and
122 high-mobility group box-1 (HMGB1) (De Leo *et al*, 2019; Schiraldi *et al*, 2012), but potential
123 interactions between MIF and CXCL12 or CXCL8, the cognate ligand of its chemokine
124 receptors CXCR2, have remained unclear.

125 Here, we hypothesized that chemokine-chemokine interactions are not only possible
126 between different types of classical chemokines, as demonstrated by chemokine interactome
127 mapping (von Hundelshausen *et al.*, 2017), but might extend to ACKs. Choosing MIF as a

A. Appendix

bioRxiv preprint doi: <https://doi.org/10.1101/2021.11.26.470090>; this version posted February 24, 2022. The copyright holder for this preprint (which was not certified by peer review) is the author/funder, who has granted bioRxiv a license to display the preprint in perpetuity. It is made available under a [CC-BY-NC-ND 4.0 International license](#).

128 prototypical ACK, we thus asked whether this mediator would form heterocomplexes with
129 classical chemokines. We tested this hypothesis applying an unbiased chemokine protein
130 array and validated candidate interactors by a battery of biochemical and biophysical
131 methods. We identified the platelet chemokine CXCL4L1 (also termed PF4var1), but not its
132 variant CXCL4, nor the CXCR2 ligand CXCL8 or the CXCR4 ligand CXCL12, as a high
133 affinity interactor of MIF and tested the potential functional role of CXCL4L1/MIF
134 heterocomplex formation for MIF binding to its receptor CXCR4, and in cell systems that are
135 relevant for the inflammatory, atherogenic, and thrombogenic activities of MIF. Finally, we
136 also asked whether such heterocomplexes can be detected in clinical thrombus specimens.
137 Our study extends the chemokine interactome to ACK/CK interactions and demonstrates a
138 functional role for the MIF/CXCL4L1 heterocomplex in disease-relevant activities.

139

140

bioRxiv preprint doi: <https://doi.org/10.1101/2021.11.26.470090>; this version posted February 24, 2022. The copyright holder for this preprint (which was not certified by peer review) is the author/funder, who has granted bioRxiv a license to display the preprint in perpetuity. It is made available under aCC-BY-NC-ND 4.0 International license.

141 **Materials and Methods**

142

143 **Proteins and reagents**

144 Biologically active and endotoxin-free recombinant human MIF was prepared as previously
145 described and was obtained at a purity of ~98% as confirmed by SDS-PAGE analysis in
146 combination with silver staining (Bernhagen *et al*, 1994; Kontos *et al*, 2020). For the
147 preparation of Alexa Fluor-488- and MST-Red-labeled MIF, a 90-95% pure MIF fraction was
148 used. Alexa Fluor-488-labeled MIF was generated using the Microscale Protein Labeling Kit
149 from Invitrogen-Molecular Probes (Karlsruhe, Germany) and MST-Red-MIF was prepared
150 using the Monolith Protein Labeling Kit RED-NHS 2nd Generation from NanoTemper (Munich,
151 Germany), following the manufacturers' instructions. Biotinylated human MIF was produced
152 using D-biotinoyl- ϵ -aminocaproic acid-N-hydroxy-succinimide ester (Biotin-7-NHS) with the
153 Biotin Protein Labeling Kit from Roche (Mannheim, Germany). Alternatively, biotin-
154 amidohexanoic acid N-hydroxysuccinimide ester from Sigma-Aldrich (Taufkirchen, Germany)
155 was used.

156 For the fluorescence polarization assay, a hexahistidine-tagged variant of CXCL4L1
157 was used. Briefly, the coding sequence of human CXCL4L1 with a methionine-flanked N-
158 terminal His₆-tag was cloned into the pET21a vector for recombinant bacterial expression
159 using *Xho*I and *Nde*I restriction sites. This construct was then used to transform Rosetta-
160 gami™ 2 (DE3) competent *E. coli* (Novagen, Merck KGaA, Darmstadt, Germany) for
161 subsequent recombinant protein production following induction with 1 mM IPTG (Carl Roth,
162 Karlsruhe, Germany) according to a standard protocol. For purification, bacteria pellets were
163 resuspended in lysis buffer (20 mM Tris-HCl, pH 8.0, 0.5 M NaCl, 5 mM EDTA, 0.1% Triton
164 X-100, with added protease inhibitor tablets according to manufacturer's instructions) and
165 cells disrupted in a EmlsiFlex-C5 high pressure homogenizer (Avestin Europe GmbH,
166 Mannheim, Germany), the raw extract cleared via centrifugation at 20.000 × g and the
167 resulting pellet, containing recombinant His-CXCL4L1 in inclusion bodies, was washed in
168 lysis buffer with and without detergent. Inclusion bodies were solubilized by gentle shaking

bioRxiv preprint doi: <https://doi.org/10.1101/2021.11.26.470090>; this version posted February 24, 2022. The copyright holder for this preprint (which was not certified by peer review) is the author/funder, who has granted bioRxiv a license to display the preprint in perpetuity. It is made available under aCC-BY-NC-ND 4.0 International license.

169 overnight in 50 mM Tris-HCl, pH 8.0, 6 M guanidine-HCl, 0.5 M NaCl, 10 mM DTT and His-
170 CXCL4L1 purified from the solubilized pellet via IMAC on a HisTrap HP column on an ÄKTA
171 Pure 25 M FPLC system (Cytiva Europe GmbH, Freiburg, Germany). The obtained protein
172 was subjected to two dialysis steps in refolding buffer (50 mM Tris-HCl, pH 8.0, 0.5 M NaCl,
173 5 mM methionine, 5 mM cysteine) with and subsequently without 0.9 M guanidine-HCl,
174 followed by a final purification step by size exclusion chromatography in 20 mM sodium
175 phosphate buffer, pH 7.4, using a Superdex 75 10/300 GL column (Cytiva Europe GmbH) on
176 an ÄKTA Pure 25 M FPLC system. A purity degree of 90-95% was verified by SDS-PAGE
177 followed by Coomassie staining and Western Blot according to standard protocols.

178 Recombinant human peroxiredoxins 1 and 6 (PRX1, PRX6) were purchased from
179 Abcam (Abcam PLC, Cambridge, UK), while recombinant human β -defensin-1 and 2 (HBD-1,
180 HBD-2) were obtained from ProSpec (ProSpec-Tany TechnoGene Ltd., Ness Ziona, Israel).
181 Recombinant human HMGB1 was purchased from Novus (Novus Biologicals Europe,
182 Abingdon, UK). Recombinant human CXCL4L1 (PF4var1) as well as the CXCL4 (PF4) were
183 purchased from ChromaTec (Greifswald, Germany). The other recombinant human
184 chemokines were obtained from Peprotech (Hamburg, Germany). All other reagents and
185 chemicals were purchased from Merck KGaA (Darmstadt, Germany), Carl Roth GmbH
186 (Karslsruhe, Germany), or Sigma-Aldrich and were of the highest purity degree available.

187

188 **Cell culture and cultivation of mammalian cell lines**

189 Jurkat T cells were cultured in RPMI1640 medium (Gibco) supplemented with 10% fetal calf
190 serum (FCS), 1% penicillin/streptomycin, and 1x non-essential amino acids (NEAAs, Gibco).
191 The human monocytic cell line MonoMac6 (Ziegler-Heitbrock *et al*, 1988) was cultured in
192 RPMI1640 medium + GlutaMAX (1x), supplemented with 1x NEAAs, 10% FCS, and 1%
193 penicillin/streptomycin. HEK293 cells stably transfected with human CXCR4 (HEK293-
194 CXCR4) were used at passage 5 and were cultivated in DMEM medium (Gibco),
195 supplemented with 10% FCS and 1% penicillin/streptomycin (Gibco), and used for the
196 experiment between passage 6 and 8.

9

A.1. Additional findings on MIF's interaction with the chemokine network

bioRxiv preprint doi: <https://doi.org/10.1101/2021.11.26.470090>; this version posted February 24, 2022. The copyright holder for this preprint (which was not certified by peer review) is the author/funder, who has granted bioRxiv a license to display the preprint in perpetuity. It is made available under aCC-BY-NC-ND 4.0 International license.

197 Unless stated otherwise, cells were cultivated in a temperature- and humidity-
198 controlled incubator at a temperature of 37°C and 5% CO₂. FCS from an EU-approved origin
199 was obtained from Invitrogen-Thermo Fisher Scientific and heat-inactivated prior to usage.
200 Other cell culture reagents, media and supplements were bought from Invitrogen-Thermo
201 Fisher Scientific, unless stated otherwise. Cell lines were originally obtained from the
202 German Society for Microorganisms and Cell Cultures (DSMZ, Braunschweig, Germany) or
203 from the American Type Culture Collections (ATCC).

204

205 **Isolation of primary human CD4⁺ T cells**

206 Primary human CD4-positive T cells were isolated from enriched peripheral blood
207 mononuclear cell (PBMC) fractions using the human CD4⁺ T cell isolation kit from Miltenyi
208 Biotec (Bergisch Gladbach, Germany) according to the manufacturer's instructions. Cells
209 were cultivated in RPMI1640 medium, supplemented with 10% FCS, 1% penicillin-
210 /streptomycin, and 1x NEAAs in a cell culture incubator at 37°C and 5% CO₂ and used for
211 functional assays on the next day. PBMC fractions were obtained by apheresis from conical
212 chambers of a Leucoreduction System Chamber sourced from anonymous platelet donations
213 at the Department of Transfusion Medicine, Cell Therapeutics and Hemostaseology of LMU
214 University Hospital. Studies abide by the Declaration of Helsinki principles and were
215 approved by ethics approval 18-104 of the Ethics Committee of LMU Munich, which
216 encompasses the use of anonymized tissue and blood specimens for research purposes.

217

218 **Isolation of human platelets**

219 ***For immunofluorescent stainings***

220 Human platelets were isolated from blood, freshly drawn from healthy donors, using a
221 syringe containing 1/10 volume of CTAD-buffer (0.105 M tri-sodium citrate, 10 mM
222 theophylline, 3.7 mM adenosine, 0.198 mM dipyridamole) (Polack *et al*, 2001). To prevent
223 platelet activation, the blood was supplemented with prostaglandine E1 (Merck KGaA),
224 Apyrase (New England Biolabs GmbH, Frankfurt am Main, Germany), and EGTA (Sigma-

bioRxiv preprint doi: <https://doi.org/10.1101/2021.11.26.470090>; this version posted February 24, 2022. The copyright holder for this preprint (which was not certified by peer review) is the author/funder, who has granted bioRxiv a license to display the preprint in perpetuity. It is made available under aCC-BY-NC-ND 4.0 International license.

225 Aldrich). Briefly, platelets were isolated by sequential centrifugation steps, performed at room
226 temperature (RT) with reduced brake settings. Platelet-rich plasma (PRP) was separated
227 from whole blood by centrifugation for 5 min at 300 × g, diluted with an equal volume of
228 phosphate-buffered saline (PBS), pH 7.4, and centrifuged again for 10 min at 200 × g to
229 remove remaining leukocytes. Finally, platelets were sedimented by centrifugation for 10 min
230 at 400 × g.

231 **For functional studies**

232 Washed human platelets were isolated as previously described (Borst *et al*, 2012) and
233 subsequently used for functional flow chamber or platelet spreading assays.

234

235 **Mice and preparation and cultivation of primary mixed cortical cultures for the**
236 **microglia motility assay**

237 CX3CR1^{GFP/+} mice, which were originally obtained from the Jackson Laboratories (strain
238 005582; (Niess *et al*, 2005)), were established on a pure C57BL/6 background and housed
239 under standardized light-dark cycles in a temperature-controlled air-conditioned environment
240 under specific pathogen-free conditions at the Center for Stroke and Dementia Research
241 (CSD), Munich, Germany, with free access to food and water. Animals were sacrificed under
242 anaesthesia with a mixture of midazolam (5 mg/mL), medetomidine and fentanyl (MMF).
243 Mouse maintenance and experiments were reviewed and overseen by the institutional
244 animal use and care committee of the local authorities (Regierung von Oberbayern, ROB,
245 Germany) and performed in accordance with the procedures provided by the animal
246 protection representative of CSD.

247 Primary mixed cortical cultures containing CX3CR1^{GFP/+} microglia were prepared in
248 96-well imaging plates based on a previously established protocol (Gokce & Sudhof, 2013)
249 from the cortices of 5 newborn pups of the CX3CR1^{GFP/+} mouse line (postnatal day 0) in
250 plating medium, consisting of modified Minimum Essential Medium (MEM without glutamine
251 and phenol red) (Gibco), supplemented with 0.5% glucose, 0.02% sodium bicarbonate, 1x
252 ITS-supplement (Sigma-Aldrich), 2 mM L-glutamine (Gibco), 1% penicillin/streptomycin, and

A.1. Additional findings on MIF's interaction with the chemokine network

bioRxiv preprint doi: <https://doi.org/10.1101/2021.11.26.470090>; this version posted February 24, 2022. The copyright holder for this preprint (which was not certified by peer review) is the author/funder, who has granted bioRxiv a license to display the preprint in perpetuity. It is made available under aCC-BY-NC-ND 4.0 International license.

253 10% FCS. Cultures were incubated in a humidified atmosphere at 37 °C and 5% CO₂ for 10
254 d. One day after plating, 80% of the plating medium was replaced with growth medium,
255 prepared from MEM (without glutamine and phenol red) supplemented with 0.5% glucose,
256 0.02% sodium bicarbonate, 5% FCS, 0.5 mM L-glutamine, and serum-free B-27™
257 supplement (Gibco). On the fourth day after dissection, 50% of the medium was replaced
258 with growth medium additionally supplemented with 4 μM cytosine-1-β-D-arabinofuranoside
259 (Sigma-Aldrich).

260

261 **Chemokine protein array**

262 Human chemokines and selected atypical chemokines were spotted on a nitrocellulose
263 membrane at 100 ng per spot and left to dry at RT. Membranes were blocked with 1x
264 ROTI®Block (Carl Roth) for 2 h at RT and then probed overnight with biotinylated human
265 MIF (biotin-MIF) at a concentration of 1 μg/mL in either 10 mM Tris-HCl pH, 8.0 or 10 mM
266 MES, pH 6.0. Subsequently, membranes were washed three times with 0.01% Tween®20 in
267 water and developed with horseradish-peroxidase (HRP)-conjugated streptavidin (Bio-
268 Techne GmbH, Wiesbaden-Nordenstadt, Germany), diluted 1:200 in 1x ROTI®Block, for 2 h.
269 After another washing step, bound biotin-MIF was revealed via chemiluminescence using
270 SuperSignal™ West Pico Chemiluminescent Substrate (Thermo Fisher Scientific) on a LAS-
271 3000 Imaging System (Fuji Photo Film Co., LTD., Japan).

272

273 **Pull-down of CXCL4L1 from cell lysates**

274 MonoMac-6 cells were first washed with PBS and then lysed on ice for 30 min with
275 immunoprecipitation (IP) lysis buffer (1x cell lysis buffer, Cell Signaling, cat#9803), 100 mM
276 PMSF, and 1x protease and phosphatase inhibitors (ThermoFisher). The purified cell lysates
277 were then incubated with pre-washed streptavidin-conjugated paramagnetic beads
278 (DYNAL™ Dynabeads™ M-280 Streptavidin; Invitrogen, cat#11205D) for 2 h at 4 °C
279 (preclearing step). After centrifugation, the supernatant was incubated with biotinylated
280 human MIF by gentle, constant shaking on a rotary shaker overnight at 4 °C. To capture

12

bioRxiv preprint doi: <https://doi.org/10.1101/2021.11.26.470090>; this version posted February 24, 2022. The copyright holder for this preprint (which was not certified by peer review) is the author/funder, who has granted bioRxiv a license to display the preprint in perpetuity. It is made available under aCC-BY-NC-ND 4.0 International license.

281 MIF/CXCL4L1 complexes, prewashed streptavidin-conjugated beads were added to the
282 precleared lysates, and the mixture was incubated for 2 h at 4 °C on a rotary shaker. Beads
283 were separated from the lysate using a magnetic stand (Dyna™ MCP-S) and washed three
284 times with lysis buffer. The supernatant was removed and the beads were resuspended in
285 LDS sample buffer (Invitrogen) and boiled at 95 °C for 15 min. Samples were subjected to
286 SDS-PAGE and analyzed by Western blotting. For this purpose, equal amounts of protein
287 were loaded onto 11% SDS-polyacrylamide gels (NuPAGE, ThermoFisher) and transferred to
288 polyvinylidene difluoride (PVDF) membranes (Carl Roth, Karlsruhe, Germany). Membranes
289 were blocked in PBS-Tween-20 containing 5% BSA for 1 h and incubated overnight at 4 °C
290 with rabbit polyclonal anti-MIF antibody Ka565 (Bernhagen *et al.*, 2007) or rabbit polyclonal
291 anti-PF4V1 IgG PA5-21944 (Invitrogen) diluted in blocking buffer. Proteins were revealed
292 using anti-rabbit HRP as a secondary antibody. Signals were detected by chemilumi-
293 nescence on an Odyssey® Fc Imager (LI-COR Biosciences GmbH, Bad Homburg,
294 Germany) using SuperSignal™ West Dura ECL substrate from ThermoFisher Scientific and
295 specific primary antibodies as indicated.

296

297 **CelluSpot peptide array**

298 The CelluSpot peptide array method has been described previously (Lacy *et al.*, 2018).
299 Briefly, 15-meric peptides, positionally frame-shifted by three residues and spanning the
300 entire sequence of CXCL4 and CXCL4L1, were synthesized on modified cellulose disks
301 (Intavis MultiPep RSi/CelluSpot Array, Cologne, Germany). Peptides were then further
302 processed by dissolving the cellulose, and spotted on coated glass slides using a slide
303 spotting robot from Intavis. Slides were incubated in blocking buffer (50 mM Tris-buffered
304 saline, pH 7.4, 1% BSA, 0.1% Tween® 20), washed (50 mM Tris-buffered saline, pH 7.4,
305 0.1% Tween® 20) and probed with biotinylated human MIF (3 µM in blocking buffer). After
306 washing, slides were developed with a dilution of streptavidin-conjugated horseradish
307 peroxidase (Roche) in blocking buffer. Bound MIF was revealed by chemiluminescence on
308 an Odyssey® Fc imager using the SuperSignal™ West Dura ECL substrate

13

A.1. Additional findings on MIF's interaction with the chemokine network

bioRxiv preprint doi: <https://doi.org/10.1101/2021.11.26.470090>; this version posted February 24, 2022. The copyright holder for this preprint (which was not certified by peer review) is the author/funder, who has granted bioRxiv a license to display the preprint in perpetuity. It is made available under aCC-BY-NC-ND 4.0 International license.

309 **Microscale thermophoresis (MST)**

310 Protein-protein interactions were analyzed via microscale thermophoresis on a Monolith
311 NT.115 instrument equipped with green/red filters (NanoTemper Technologies, Munich,
312 Germany). Measurements were performed at 25°C at both 40% and 80% MST power. LED
313 excitation power was adjusted to 90 or 95% in order to obtain an initial fluorescence count of
314 700 to 800. MST traces were recorded for 40 s (-5 s to +35 s), according to default settings
315 with the sample being heated from 0 to 30 s. All measurements were performed in assay
316 buffer (10 mM Tris-HCl, pH 8.0, 0.01% BSA). MST-Red-MIF was used at a fixed
317 concentration, mixed 1:1 with serial dilutions of either CXCL4 (Peprotech, Hamburg,
318 Germany) or CXCL4L1 (ChromaTec, Greifswald, Germany) (final MIF concentrations: 456
319 nM or 312 nM, respectively). Prior to measurement, the prepared samples were incubated
320 for at least 30 min on ice. MST traces of multiple experiments were analyzed according to
321 the K_D model using the default T-jump settings, focusing on the temperature related intensity
322 change (TRIC) of the fluorescent label ("cold region" from -1 to 0 s, "hot region" from 0.5 to
323 1.5 s) using the MO.AffinityAnalysis V2.3 software (NanoTemper Technologies). Curve fitting
324 for data presentation was performed by GraphPad Prism Version 6.07 ('one site – total
325 binding').

326

327 **Analysis of protein-protein interactions by surface plasmon resonance (SPR)**

328 Surface plasmon resonance measurements were performed using a Biacore X100
329 instrument (GE Healthcare Europe GmbH) and neutravidin-modified C1 sensor chips. Biotin-
330 MIF was immobilized on flow cells to 1064.8 RU. CXCL4 (Peprotech, Hamburg, Germany)
331 and CXCL4L1 (ChromaTec, Greifswald, Germany), used at concentrations in the range of
332 0.125 to 20 µg/mL in running buffer (HBS-EP+ Buffer: 0.01 M HEPES, 0.15 M NaCl, 0.003 M
333 EDTA and 0.05% v/v surfactant P20) were injected at a flow rate of 60 µL/min. The complex
334 was allowed to associate and dissociate for 90 s and 240 s, respectively. Surfaces were
335 regenerated with 2 pulses (60 s) of 30 mM NaOH and 2 M NaCl. Responses from analyte

bioRxiv preprint doi: <https://doi.org/10.1101/2021.11.26.470090>; this version posted February 24, 2022. The copyright holder for this preprint (which was not certified by peer review) is the author/funder, who has granted bioRxiv a license to display the preprint in perpetuity. It is made available under aCC-BY-NC-ND 4.0 International license.

336 injections were fitted to a 1:1 Langmuir interaction profile using Biacore X100 evaluation
337 2.0.1 Plus package software.

338

339 **Transwell migration assay**

340 Transwell migration experiments to study the influence of CXCL4L1 on MIF-mediated
341 chemotaxis responses were performed with Jurkat T cells. Briefly, Jurkat cells were diluted in
342 RPMI1640 medium at a density of 1×10^7 cells/mL. Cells were placed in the upper chamber
343 of a 24-well Transwell insert with 5 μ m pore size (Corning, Kaiserslautern, Germany). 16 nM
344 MIF, either alone or pre-incubated (30 min on ice to allow for complex formation) with 32 nM
345 of CXCL4L1, as well as 32 nM CXCL4L1 alone were added to the lower chamber as a
346 chemoattractant. After a 12 h migration interval at 37 °C and 5% CO₂, migrated cells were
347 recovered from the lower chamber and counted via flow cytometry by using CountBright™
348 absolute counting beads (Molecular Probes-Invitrogen). In a similar experimental setup, the
349 influence of CXCL4 on MIF-mediated chemotaxis was tested as well. MIF was used at a
350 concentration of 16 nM and CXCL4 (ChromaTec, Greifswald, Germany) at 32 nM.

351

352 **3D migration of human CD4⁺ T cells**

353 The migratory behavior of primary human T cells was assessed by three-dimensional (3D)
354 migration methodology using time-lapse microscopy and single cell tracking using the 3D
355 chemotaxis μ -Slide system from Ibidi GmbH (Munich, Germany). The method was performed
356 following a slight modification of the established Ibidi dendritic cell protocol for human
357 monocytes, as described previously (Kontos *et al.*, 2020). Briefly, isolated CD4⁺ human T
358 cells (3.5×10^6) were seeded in a rat tail collagen type-I gel (Ibidi, Munich, Germany) in
359 DMEM and subjected to a gradient of human MIF, CXCL4L1, or a pre-incubated combination
360 of both. Cell motility was monitored performing time-lapse imaging every 0.5 or 2 min at 37
361 °C for a period of 120 min to cover either a short or extended migration period, using a Leica
362 DMI8 inverted microscope (Leica Microsystems, Wetzlar, Germany) and Leica live cell-
363 imaging software (LAS X version 3.7.4). Images were imported as stacks to ImageJ version

15

A.1. Additional findings on MIF's interaction with the chemokine network

bioRxiv preprint doi: <https://doi.org/10.1101/2021.11.26.470090>; this version posted February 24, 2022. The copyright holder for this preprint (which was not certified by peer review) is the author/funder, who has granted bioRxiv a license to display the preprint in perpetuity. It is made available under aCC-BY-NC-ND 4.0 International license.

364 1.51n and analyzed with the manual tracking and Chemotaxis and Migration tool (Ibidi
365 GmbH) plugin for ImageJ.

366

367 **Motility measurement of primary murine microglia**

368 The motility of mouse microglia was determined using mixed cortical cultures, established
369 and cultivated as stated above. A day prior to imaging, the medium was changed to
370 Hibernate A medium (Gibco) in order to maintain a physiological pH value during imaging.
371 Prior to imaging, different wells of cells from each individual pup were treated with either 8
372 nM MIF, 1.6 nM CXCL4L1, or both (pre-incubated for 30 min on ice to allow for complex
373 formation). A control group was treated with 20 mM sodium phosphate buffer, pH 7.4. Cell
374 motility was monitored by time-lapse imaging for 15 h at 37 °C with recordings every 5 min,
375 using a Leica DMI8 inverted Life Cell Imaging System using the FITC channel for visualizing
376 the GFP-positive cells. Images were imported as stacks to ImageJ software version 1.51n
377 and analyzed with the manual tracking and Chemotaxis and Migration tool Plugin for ImageJ
378 from Ibidi. In order to quantify microglial motility from the time-lapse videos, 20-25 GFP-
379 positive microglia per treatment group were randomly selected and manually tracked
380 throughout all frames. Cells that died or moved out of the frame were excluded from the
381 analysis. Accumulated distance of each tracked microglia was calculated with Chemotaxis
382 and Migration Tool (Ibidi).

383

384 **Fluorescence polarization spectroscopy**

385 Fluorescence polarization was measured using a JASCO FP-6500 fluorescence
386 spectrophotometer equipped with FDP-223 and FDP-243 manual polarizers (JASCO
387 Deutschland GmbH, Pfungstadt, Germany). Preparation of stock solutions, measurements
388 and analysis were performed essentially following a previously published protocol (Kontos *et*
389 *al.*, 2020). For binding/inhibition experiments, mixtures of Alexa 488-labeled MIF (10 nM) in
390 the absence/presence of CXCL4L1 (1.6 µM) (or 20 mM sodium phosphate buffer, pH 7.2),
391 and non-labeled msR4M-L1 peptide (concentration between 1 nM to 10 µM) were prepared

16

bioRxiv preprint doi: <https://doi.org/10.1101/2021.11.26.470090>; this version posted February 24, 2022. The copyright holder for this preprint (which was not certified by peer review) is the author/funder, who has granted bioRxiv a license to display the preprint in perpetuity. It is made available under aCC-BY-NC-ND 4.0 International license.

392 in 10 mM sodium phosphate, pH 7.2, containing 2% hexafluoro-isopropanol (HFIP). Where
393 CXCL4L1 was added as a putative inhibitor, Alexa488-MIF and CXCL4L1 were mixed and
394 incubated for 30 min prior to measurements. Bandwidth for excitation and emission was set
395 at 5 nm and time response at 0.5 s. The excitation wavelength was 492 nm and emission
396 was recorded at 519 nm. Measurements were taken at RT within 2 to 3 min upon preparation
397 of the solutions. Polarization P was calculated according to the equation $P = (I_{\parallel} - G \cdot I_{\perp}) / (I_{\parallel} +$
398 $G \cdot I_{\perp})$, with I_{\parallel} as the intensity of emitted light polarized parallel to the excitation light and I_{\perp} as
399 the intensity of emitted light polarized perpendicular to the excitation light. The G factor was
400 calculated based on the instrumental documentation (Moerke, 2009). Apparent K_D values
401 were calculated assuming a 1:1 binding model (Yan *et al*, 2006), using sigmoidal curve fitting
402 with OriginPro 2016 (OriginLab Corporation, Northampton, MA, USA).

403

404 **Label-free dynamic mass redistribution (DMR) assay**

405 Analysis of dynamic mass redistribution of adherent cells was performed on an EnSpire
406 Multimode plate reader equipped with an Epic® label-free measurement module
407 (PerkinElmer Inc., Waltham MA, USA) according to the manufacturer's instructions for cell-
408 based label-free DMR measurements (Schroder *et al*, 2010). The assay protocol was
409 adapted according to a previous publication to be performed in EnSpire label-free 96-well
410 fibronectin-coated cell assay microplates (Corning GmbH, Amsterdam, The Netherlands)
411 with HEK293 cells stably expressing human CXCR4 (Krammer *et al*, 2021). Briefly, 40.000
412 cells were seeded into each well and cultivated overnight (37°C, 5% CO₂) to achieve a
413 confluency of >70%. Prior to the assay, the medium was exchanged with DMR assay buffer
414 (20 mM HEPES and 1% DMSO in HBSS, pH 7.4) and the assay plate left for 6 h to
415 equilibrate to ambient temperature. Baseline measurements for each well were recorded for
416 10 min every 30 s prior to treatment of the cells with chemokines, inhibitors, or the
417 corresponding buffers as control. Treatments were applied to each well as a 5x concentrated
418 stock, prepared in assay buffer. For treatment with MIF/CXCL4L1 complexes, both proteins
419 were mixed in assay buffer and incubated for 5 h at RT. Directly after addition of the stimuli,

17

A.1. Additional findings on MIF's interaction with the chemokine network

bioRxiv preprint doi: <https://doi.org/10.1101/2021.11.26.470090>; this version posted February 24, 2022. The copyright holder for this preprint (which was not certified by peer review) is the author/funder, who has granted bioRxiv a license to display the preprint in perpetuity. It is made available under aCC-BY-NC-ND 4.0 International license.

420 the DMR response was recorded for the indicated duration. The DMR response resembles
421 the wavelength shift of the light reflected from the sensor integrated in the assay microplates
422 and serves as a cumulative cellular response signal. Measurements were performed on two
423 replicates per treatment and results are presented as their mean value.

424

425 **Staining of human thrombus specimens**

426 Human thrombus tissue specimens, obtained as disposable material from vascular surgery
427 procedures (ethics allowance LMU Munich 18-104 and TUM-MRI project # 2799/10), were
428 embedded in Tissue Tek O.C.T. Compound (Sakura Finetek Germany GmbH, Staufen,
429 Germany), frozen, and cut into 5 µm sections using a CM 1950 Cryostat (Leica Biosystems).
430 The cryosections were transferred to microscopy slides and stored at -80°C until use.

431 **Hematoxylin & eosin (HE) staining of thrombus sections**

432 Cryosections of human thrombus tissue were stained with Mayer's hematoxylin and eosin
433 (HE) according to standard protocols. Briefly, after thawing and brief air drying and
434 rehydration, sections were incubated in Mayer's hematoxylin solution (Sigma-Aldrich) for 15
435 min. After thorough rinsing of the samples, 0.5% eosin Y solution (Sigma-Aldrich) was
436 applied as a counterstain for 30 s. After dehydration of the tissue in 95 % ethanol, 100 %
437 ethanol (Merck KGaA) and xylene (VWR International GmbH), the sample was covered with
438 resinous mounting medium (Eukitt, Sigma-Aldrich), covered with a glass coverslip and
439 examined by light microscopy (Leica Dmi8 inverted microscope using a DMC2900 digital
440 camera (Leica Microsystems; 10x objective).

441

442 **Staining of platelets**

443 Freshly isolated platelets were fixed with 4% paraformaldehyde (PFA) in PBS (Morphisto
444 GmbH, Frankfurt a. M., Germany) for 10 min and subsequently permeabilized using 1x Perm
445 buffer (Invitrogen) for 15 min. After washing, platelets were blocked in ROTI@Block (Carl
446 Roth) for 1 h. Immunofluorescent staining was performed as described above for the human
447 thrombus specimens, except that the anti-human MIF antibody was used at a dilution of 1:20

18

bioRxiv preprint doi: <https://doi.org/10.1101/2021.11.26.470090>; this version posted February 24, 2022. The copyright holder for this preprint (which was not certified by peer review) is the author/funder, who has granted bioRxiv a license to display the preprint in perpetuity. It is made available under aCC-BY-NC-ND 4.0 International license.

448 and the anti-human CXCL4L1 antibody at a dilution of 1:50. Stained platelets were then
449 washed in blocking buffer and mounted on poly-L-ornithine-coated glass slides using
450 ProLong™ Glass Antifade mountant (Invitrogen), covered with coverslips and stored at 4 °C
451 until imaging by multiphoton microscopy.

452

453 **Multiphoton laser-scanning microscopy (MPM) and FLIM-FRET**

454 Imaging was conducted using a multispectral TCS SP8 DIVE FALCON LIGHTNING
455 microscope (Leica, Germany) equipped with filter-free 4TUNE NDD detection module, an
456 extended IR spectrum tunable laser (New InSight® X3™, Spectra-Physics) (680-1300 nm)
457 and fixed IR laser (1045 nm), advanced Vario Beam Expander (VBE), Ultra-high-speed
458 resonance scanner (8kHz), HC PL IRAPO 25x/1.0 WATER objective, and FLIM-FRET
459 modality. Images were collected in a sequential scanning mode using hybrid diode detectors
460 Reflected Light Hybrid Detectors (HyD-RLD) (Alexa Fluor-488: excitation 965 nm / emission
461 479-568 nm; Cy3: excitation 1095 nm / emission 538-650 nm) and were handled using the
462 LAS-X software package. Deconvolution microscopy was performed using the Leica
463 LIGHTNING (adaptive deconvolution) application.

464 For fluorescence lifetime imaging (FLIM) and FLIM-FRET measurements, up to 1000
465 photons per pixel were captured in a time-correlated single photon counting (TCSPC) mode.
466 Fluorescence lifetime decay data were fitted using Leica FALCON (FAstLifetime CONtrast)
467 software. The fitting was assessed by randomly distributed residuals and by low Chi-square
468 (χ^2) values. The number of components used for the fittings was manually fixed to a value
469 ($n=2-3$) to minimize χ^2 values. The fluorescence lifetime of the donor was acquired similarly
470 in the absence of the acceptor.

471

472

A.1. Additional findings on MIF's interaction with the chemokine network

bioRxiv preprint doi: <https://doi.org/10.1101/2021.11.26.470090>; this version posted February 24, 2022. The copyright holder for this preprint (which was not certified by peer review) is the author/funder, who has granted bioRxiv a license to display the preprint in perpetuity. It is made available under aCC-BY-NC-ND 4.0 International license.

473 Proximity ligation assay (PLA)

474 For detection of protein complexes by proximity ligation assay (PLA), the Duolink™ InSitu
475 Orange Starter Kit Mouse/Rabbit (DUO92102) from Sigma Aldrich was used. Following
476 scouting experiments to establish the PLA methodology in thrombus material, cryosections of
477 the thrombi were prepared by treatment with cold acetone for 6 min at 4 °C and for 30 min at
478 RT. Samples were rehydrated in PBS for 10 min and hydrophobic barriers were applied to
479 the microscopy slide using an ImmoEdge™ Pen (Vector Laboratories Inc. Burlingame,
480 USA).

481 For PLA detection, the Duolink® PLA Fluorescence protocol provided by the manufacturer
482 was essentially followed, using primary antibodies against human MIF (mouse anti-MIF D2,
483 sc-271631, Santa Cruz Biotechnology Inc., Dallas, USA; 1:20) and against human CXCL4L1
484 (rabbit anti-CXCL4L1, PA5-21944, Invitrogen; 1:50). Samples were then prepared for
485 microscopy using Duolink® mounting medium with DAPI, and coverslips sealed with
486 commercially available nail polish and stored at 4 °C until imaging by confocal microscopy
487 using a Zeiss LSM880 AiryScan microscope was performed.

488

489 Flow chamber assay with platelets

490 Chemokines were diluted in calcium-free PBS, pH 7.4, at their final concentrations (MIF: 16
491 nM; CXCL4L1: 32 nM) and allocated into separate reaction tubes. 200 µL of each solution
492 were distributed onto separate collagen-coated cover slips (100 µg/mL) and incubated for 2
493 h. Cover slips were blocked with PBS, pH 7.4, containing 1% BSA for 1 h. Next, human
494 whole-blood was diluted at a 5:1 ratio with PBS, pH 7.4, containing calcium. Before
495 perfusion, the blood was incubated with fluorochrome 3,3'-dihexyloxycarbocyanine iodide
496 (DiOC₆, 1 mM; Sigma Aldrich) for 10 min at RT. Thereafter, the blood was allocated into 1
497 mL syringes and perfused over the different cover slips, through a transparent flow chamber
498 with high shear rate (1000 s⁻¹) for 5 min. Per run, one 2-minute video clip was recorded (200
499 ms/frame, Nikon Eclipse Ti2-A, 20x objective). Afterwards, the chamber was rinsed and
500 pictures were taken of five representative areas using the same objective. The covered area

20

bioRxiv preprint doi: <https://doi.org/10.1101/2021.11.26.470090>; this version posted February 24, 2022. The copyright holder for this preprint (which was not certified by peer review) is the author/funder, who has granted bioRxiv a license to display the preprint in perpetuity. It is made available under aCC-BY-NC-ND 4.0 International license.

501 was analyzed using the NIS-Elements AR software (Nikon) and the mean percentage of the
502 covered area, the mean thrombus area as well as the mean thrombus count were
503 determined.

504

505 **Platelet spreading analysis**

506 Fibrinogen-coated (100 µg/mL, Sigma Aldrich) coverslips were preincubated with MIF (16
507 nM), CXCL4L1 (32 nM), or MIF (16 nM) and CXCL4L1 (32 nM) together, for 2 h. Afterwards,
508 isolated human platelets were diluted in Tyrodes buffer (pH 7.4) to match a concentration of
509 15.000 cells/µL. Platelets were supplemented with 1 mM CaCl₂, activated with 1 µg/mL CRP-
510 XL (CambCol, Cambridge, UK), and incubated on the previously prepared fibrinogen-coated
511 coverslips for 30 or 60 min at RT. Thereafter, platelets were fixed with 4% formaldehyde
512 (Sigma Aldrich) for 10 min, and washed three times with PBS, pH 7.4. The coverslips were
513 mounted onto slides and five images from randomly selected areas were taken using a Nikon
514 Eclipse Ti2-A microscope with a 100x DIC objective. Subsequently a quarter of each image
515 with at least 20 cells was analyzed.

516

517 **Protein structure visualization**

518 Three-dimensional structures as well as the surface charge distribution of human MIF,
519 CXCL4 and CXCL4L1 were visualized using the PyMOL Molecular Graphics System
520 software, version 1.8.2.2 (Schrödinger, LLC). The structures represent the Protein Data Bank
521 (PDB) files for MIF (PDB ID: 3DJH), CXCL4 (PDB ID: 1F9Q), and CXCL4L1 (PDB ID: 4HSV),
522 or our molecular docking results.

523

524 **Protein-protein docking**

525 To simulate the interaction of monomeric MIF with CXCL4 and CXCL4L1 in their monomeric
526 forms, rigid protein-protein docking, followed by clustering of the 1000 lowest energy
527 structures and removal of steric clashes was performed using the ClusPro 2.0 webserver,

A.1. Additional findings on MIF's interaction with the chemokine network

bioRxiv preprint doi: <https://doi.org/10.1101/2021.11.26.470090>; this version posted February 24, 2022. The copyright holder for this preprint (which was not certified by peer review) is the author/funder, who has granted bioRxiv a license to display the preprint in perpetuity. It is made available under a [CC-BY-NC-ND 4.0 International license](#).

528 with single chains of MIF and CXCL4L1 defined as 'receptor' and 'ligand', respectively
529 (Kozakov *et al*, 2017; Vajda *et al*, 2017).

530

531 **Statistical analysis**

532 Statistical analysis was performed using GraphPad Prism Version 6.07 software. Unless
533 stated otherwise, data are represented as means \pm standard deviation (SD). After testing for
534 normality, data were analyzed either by two-tailed Student's T-test, Mann-Whitney U test, or
535 Kruskal-Wallis test as appropriate. Differences with $P < 0.05$ were considered to be
536 statistically significant.

537

bioRxiv preprint doi: <https://doi.org/10.1101/2021.11.26.470090>; this version posted February 24, 2022. The copyright holder for this preprint (which was not certified by peer review) is the author/funder, who has granted bioRxiv a license to display the preprint in perpetuity. It is made available under aCC-BY-NC-ND 4.0 International license.

1 **Results**

2

3 **High affinity binding between the atypical chemokine MIF and the platelet CXC**
4 **chemokine CXCL4L1**

5 To begin to test the hypothesis that chemokine-chemokine interactions may extend to ACKs
6 and that MIF may form heterocomplexes with classical chemokines, we applied unbiased
7 chemokine protein array technology (*Figure 1A-B*), as previously successfully used to map
8 formation of heterocomplexes between different classical chemokines (von Hundelshausen
9 *et al.*, 2017). In addition to 47 human chemokines covering all four sub-classes (CXC-, CC-,
10 CX3C- and C-type CKs) we also included structurally related and positively charged protein
11 mediators including ACKs/DAMPs such as HMGB1, HBDs, and peroxiredoxins (Prxs)
12 (Shichita *et al.*, 2012; He *et al.*, 2019), as well as MIF itself and the MIF homolog D-
13 dopachrome tautomerase (D-DT)/MIF-2 as spotted proteins in the protein array. Probing of
14 the array with biotin-conjugated MIF and streptavidin-POD (StrAv-POD) revealed high-
15 intensity spots indicative of a tight interaction of MIF with CXCL4L1 and Prx1 (*Figure 1B-C*).
16 Weaker spots were detected for CCL28, CXCL9, Prx6, and MIF itself. No spot intensity
17 whatsoever was observed for any of the other immobilized proteins, indicating that none of
18 the other 44 chemokines interacts with MIF. This also included CXCL8 and CXCL12, which
19 share their receptors CXCR2 and CXCR4, respectively, with MIF (Bernhagen *et al.*, 2007).

20 Similarly, no binding signal of biotin-MIF was detected with HMGB1, a DAMP which
21 has been demonstrated to form heterodimers with CXCL12 and for which a functional
22 interaction with MIF has been suggested (Ma *et al.*, 2017; Schiraldi *et al.*, 2012), nor for the
23 human β -defensins HBD1 or HBD2 (*Figure 1B-C*). Importantly, when testing a control
24 chemokine array developed with StrAv-POD without a biotin MIF incubation step, only one
25 signal was not fully specific. This was the signal for Prx1 so that its interpretation was not
26 possible (*Supplementary Figure 1A*). Biotin-MIF also bound to MIF itself, but not to MIF-2
27 (*Figure 1B-C*). As MIF is known to form homo-oligomers (Sun *et al.*, 1996) and has been

A.1. Additional findings on MIF's interaction with the chemokine network

bioRxiv preprint doi: <https://doi.org/10.1101/2021.11.26.470090>; this version posted February 24, 2022. The copyright holder for this preprint (which was not certified by peer review) is the author/funder, who has granted bioRxiv a license to display the preprint in perpetuity. It is made available under aCC-BY-NC-ND 4.0 International license.

1 reported to form higher-order hexameric complexes (Bai *et al.*, 2012), this result further
2 verified the validity of the chemokine array approach for MIF.

3 A striking observation was that biotin-MIF specifically interacted with the immobilized
4 platelet chemokine CXCL4L1, but not with CXCL4 (*Figure 1C and Supplementary Figure*
5 *1B*). CXCL4 and CXCL4L1 are highly homologous chemokines, their sequences only differ
6 by three amino acids, and CXCL4L1 has also been suggested to be a decoy chemokine
7 paralog of CXCL4. Given this remarkable specificity of the interaction with MIF and that the
8 spot corresponding to biotin-MIF and CXCL4L1 was the strongest interaction detected on the
9 array, we focused on CXCL4L1 as a novel candidate interactor of MIF.

10 We first verified the interaction by co-immunoprecipitation using whole cell lysates of
11 MonoMac6 cells, which we found to express substantial amounts of CXCL4L1. Semi-
12 endogenous pulldown of proteins from MonoMac6 lysates by biotin-MIF and StrAv magnetic
13 beads and Western blot using an anti-human CXCL4L1 antibody revealed a specific band for
14 CXCL4L1, which was absent when the pulldown was performed without biotin-MIF
15 preincubation (*Figure 2A*). Pulldown specificity was further confirmed by Western blot against
16 MIF. We next applied surface plasmon resonance ('Biacore') methodology, which was
17 previously successfully used to characterize interactions within the classical chemokine
18 interactome (von Hundelshausen *et al.*, 2017). To study the MIF/CXCL4L1 interaction, MIF
19 chips were exposed to increasing concentrations of CXCL4L1 in the soluble phase. The
20 obtained surface plasmon resonance response curves indicated that MIF specifically binds to
21 CXCL4L1 (*Figure 2B-C*). Quantitative analysis determined a K_D value of 116 ± 16 nM (mean
22 \pm SD) indicating high-affinity binding between MIF and CXCL4L1. By contrast, no
23 appreciable signal was detectable for the incubation with increasing concentrations of
24 CXCL4 and no K_D could be derived, verifying the specificity of the MIF/CXCL4L1 interaction
25 in this set-up. To further confirm the MIF/CXCL4L1 interaction, we next applied microscale
26 thermophoresis (MST), which relied on the interaction between MST-Red-labeled MIF and its
27 binding partner, with both partners in the soluble phase. This methodology was recently
28 established for MIF (Kontos *et al.*, 2020). MST titrations of MST-Red-MIF with increasing

A. Appendix

bioRxiv preprint doi: <https://doi.org/10.1101/2021.11.26.470090>; this version posted February 24, 2022. The copyright holder for this preprint (which was not certified by peer review) is the author/funder, who has granted bioRxiv a license to display the preprint in perpetuity. It is made available under aCC-BY-NC-ND 4.0 International license.

1 concentrations of CXCL4L1 revealed a typical sigmoidal binding curve with a derived binding
2 constant ($K_D = 159.8 \pm 16.8$ nM) that was similar to that obtained by surface plasmon
3 resonance (*Figure 2D-E*). In contrast, binding was much weaker when CXCL4 was titrated
4 and accordingly a low affinity K_D in the micromolar range was determined ($K_D = 2.0 \pm 0.8$
5 μ M).

6 Heterodimer formation between classical chemokines relies on CC-type or CXC-type
7 interactions. To determine which residues in CXCL4L1 are critical for the interaction with
8 MIF, we employed peptide array technology. A set of 15-meric peptides derived from the
9 CXCL4L1 sequence, positionally frame-shifted by three amino acids to cover the entire
10 sequence of the processed chemokine, were synthesized and immobilized on glass slides
11 and arrays, and probed with biotin-MIF. The most pronounced binding signal was observed
12 for peptides representing the sequence region, which corresponds to the β 2-strand motif
13 IKAGPHCPTAQLIAT of CXCL4L1 (*Supplementary Figure 2A-B*). A second peak
14 encompasses the N-terminal sequence QCLCVKTTSQVRPRH. The difference in the 3D
15 structures of CXCL4 and CXCL4L1 is characterized by a significant conformational
16 rearrangement of the α -helix (Kuo *et al*, 2013), although the sequence of CXCL4 differs from
17 that of CXCL4L1 in only three α -helical residues (L58P, K66E, L67H with the conformational
18 difference being mainly governed by the L67H exchange). In this respect, CXCL4 showed an
19 essentially identical peptide binding profile as that of CXCL4L1 at the N-terminus as
20 expected, but a slightly different pattern at the β 2 strand region GPHCPTAQLIATLKN, that is
21 packed onto the C-terminal α -helix (*Supplementary Figure 2A-B*). Peptide array-based
22 mapping of the CXCL4L1 residues involved in MIF binding was confirmed by molecular
23 docking simulations. Docking applying the ClusPro software predicted that the β -sheet region
24 including the IKAGPHCPTAQLIAT motif is located near the MIF contact site, facing the 4-
25 stranded β -sheet of a single MIF monomer chain. This interaction could be promoted by an
26 energetically favorable complementary electrostatic interaction between the two surfaces
27 (*Supplementary Figure 2C*).

A.1. Additional findings on MIF's interaction with the chemokine network

bioRxiv preprint doi: <https://doi.org/10.1101/2021.11.26.470090>; this version posted February 24, 2022. The copyright holder for this preprint (which was not certified by peer review) is the author/funder, who has granted bioRxiv a license to display the preprint in perpetuity. It is made available under aCC-BY-NC-ND 4.0 International license.

1 Together, the co-immunoprecipitation, Biacore, and MST studies confirmed specific
2 binding between MIF and CXCL4L1 and determined a high-affinity binding constant in the
3 100-150 nM range for the interaction. Analysis of the binding interface by peptide array-
4 based mapping and molecular docking provides an initial prediction of the residues involved
5 in the CXCL4L1/MIF binding site.

6

7 **MIF/CXCL4L1 heterocomplex formation attenuates MIF-mediated inflammatory/athero-** 8 **genic activities**

9 We next wished to determine a potential functional role of MIF/CXCL4L1 heterocomplex
10 formation. CXCL4L1 is a potent angiostatic chemokine acting through CXCR3 (Struyf *et al.*,
11 2011), but its role in inflammatory responses and atherogenesis is not well understood. Pro-
12 atherogenic activities of MIF have been extensively characterized and are mainly mediated
13 through non-cognate interaction of MIF with CXCR2 and CXCR4 (Bernhagen *et al.*, 2007;
14 Sinitski *et al.*, 2019). Here, we hypothesized that MIF/CXCL4L1 complex formation could
15 predominantly influence CXCR4-mediated pathways of MIF.

16 We first asked whether MIF-elicited T-cell chemotaxis, a well-characterized
17 atherogenic MIF effect mediated via T-cell-expressed CXCR4 (Bernhagen *et al.*, 2007), is
18 affected by CXCL4L1. Scouting experiments using Jurkat T-cells confirmed that, when added
19 to the lower chamber of a Transwell migration device as a chemottractant, MIF elicited
20 chemotaxis with a chemotactic index (CTX) of approximately 2. Moreover, when CXCL4L1
21 was preincubated with MIF to allow for complex formation, no upregulation of Jurkat T-cell
22 chemotaxis was observed, while CXCL4L1 alone exhibited neither a chemotactic nor
23 inhibitory effect (*Supplementary Figure 3A*). In line with the observed lack of binding between
24 MIF and CXCL4, MIF-mediated Jurkat T-cell chemotaxis was not attenuated by co-
25 incubation with CXCL4, which by itself did not significantly enhance Jurkat T-cell chemotaxis
26 (*Supplementary Figure 3B*). To test the physiological relevance of this finding, we next
27 studied primary CD4⁺ T-cell chemotaxis and also applied a three-dimensional migration set-
28 up, following individual cell migration trajectories by live cell imaging. MIF potentially triggered

26

bioRxiv preprint doi: <https://doi.org/10.1101/2021.11.26.470090>; this version posted February 24, 2022. The copyright holder for this preprint (which was not certified by peer review) is the author/funder, who has granted bioRxiv a license to display the preprint in perpetuity. It is made available under aCC-BY-NC-ND 4.0 International license.

1 T-cell migration as evidenced by a significant increase in forward migration index (FMI)
2 (*Figure 3A-B*), confirming previous data showing CXCR4-dependent stimulation of monocyte
3 migration by MIF (Kontos *et al.*, 2020). This effect was abrogated when MIF was coincubated
4 with CXCL4L1, while CXCL4L1 alone had no effect on 3D T-cell motility. This suggested that
5 MIF/CXCL4L1 heterocomplex formation interferes with MIF/CXCR4-stimulated chemotaxis of
6 T cells.

7 To study the potential relevance of these findings for other inflammatory/immune cell
8 types, we next evaluated the effect of MIF/CXCL4L1 complex formation on microglial motility
9 in the physiological setting of cortical brain cultures. MIF promotes the motility of Egfp⁺
10 microglia in murine cortical brain cultures *ex vivo* in a Cxcr4-dependent manner, as read out
11 by live microscopy and as indicated by blockade of the MIF effect by the soluble CXCR4
12 mimicking peptide msR4M-L1 (*Supplementary Figure 3C*). Importantly, MIF-triggered
13 microglia migration in this setting was fully ablated when CXCL4L1 was added together with
14 MIF following preincubation, while CXCL4L1 alone had no effect on microglia motility (*Figure*
15 *3C-D*). This indicated that CXCL4L1/MIF heterocomplex formation attenuates MIF's CXCR4-
16 dependent effect on microglia migration.

17

18 **MIF/CXCL4L1 heterocomplex formation inhibits MIF binding to CXCR4**

19 The cell migration experiments implied, but did not directly test, the notion that MIF/CXCL4L1
20 complex formation affects MIF signaling through the CXCR4 pathway. To test the
21 involvement of CXCR4 directly, we performed a binding competition experiment that
22 capitalized on our recent identification of a MIF-binding CXCR4 ectodomain-mimicking
23 peptide msR4M-L1 (Kontos *et al.*, 2020). Employing fluorescence polarization spectroscopy
24 (FP), titration of increasing concentrations of msR4M-L1 with Alexa 488-MIF led to a
25 pronounced sigmoidal change in the FP signal (*Figure 4A*), in line with previous data
26 showing high affinity binding between MIF and msR4M-L1 (Kontos *et al.*, 2020). By contrast,
27 when Alexa 488-MIF was preincubated with CXCL4L1 before the titration, the FP signal was

27

A.1. Additional findings on MIF's interaction with the chemokine network

bioRxiv preprint doi: <https://doi.org/10.1101/2021.11.26.470090>; this version posted February 24, 2022. The copyright holder for this preprint (which was not certified by peer review) is the author/funder, who has granted bioRxiv a license to display the preprint in perpetuity. It is made available under aCC-BY-NC-ND 4.0 International license.

1 ablated (*Figure 4A*), suggesting that MIF/CXCL4L1 heterocomplex formation interfered with
2 MIF binding to the CXCR4 mimic.

3 To further confirm an interference of heterocomplex formation with the MIF/CXCR4
4 pathway, we next studied dynamic mass redistribution (DMR) responses in HEK293 cells
5 stably transfected with human CXCR4. Incubation of HEK293-CXCR4 transfectants with MIF
6 but not control buffer led to a pronounced time-dependent increase in the DMR signal as a
7 real-time readout of an integrated cellular response of living HEK293 cell activation through
8 the MIF/CXCR4 receptor signaling pathway (*Figure 4C*). This signal was markedly
9 attenuated by the small molecule CXCR4 inhibitor AMD3100, whereas the DMR curve of
10 AMD3100 alone was similar to the control buffer curve, confirming CXCR4-dependency of
11 the MIF-induced signal. Of note, preincubation of MIF with CXCL4L1 led to an appreciable
12 reduction in the DMR response curve as well, when compared to cell stimulation with MIF
13 alone, while CXCL4L1 alone and buffer control showed no effect (*Figure 4C*).

14 Together, the competition binding study and the DMR experiment confirmed the
15 notion that complexation by CXCL4L1 interferes with binding of MIF to CXCR4 and its ability
16 to activate CXCR4-mediated cell responses.

17

18 **MIF and CXCL4L1 colocalize and form complexes in human platelet aggregates and** 19 **clinical thrombus specimens**

20 CXCL4L1 is an abundant platelet chemokine (Karshovska *et al*, 2013; von Hundelshausen *et*
21 *al*, 2007) and we previously found that platelets also are a rich source of MIF (Strüßmann *et*
22 *al*, 2013). The colocalization of MIF and CXCL4L1 in sub-cellular platelet compartments has
23 not yet been studied, but a cell biological characterization of CXCL4 suggested that this
24 paralog may be localized in a different intracellular platelet compartment than MIF
25 (Strüßmann *et al.*, 2013). Notwithstanding, we surmised that colocalization and complex
26 formation between MIF and CXCL4L1 may occur extracellularly after secretion from
27 activated platelets.

bioRxiv preprint doi: <https://doi.org/10.1101/2021.11.26.470090>; this version posted February 24, 2022. The copyright holder for this preprint (which was not certified by peer review) is the author/funder, who has granted bioRxiv a license to display the preprint in perpetuity. It is made available under aCC-BY-NC-ND 4.0 International license.

1 Initial evidence for a colocalization of CXCL4L1 and MIF following co-secretion from
2 activated platelets came from human platelet preparations that aggregated due to handling
3 stress. Examination of these aggregates by multi-photon microscopy (MPM) using an Alexa
4 488 signal to label MIF and Cy3 immunofluorescence for CXCL4L1 revealed several areas
5 with an apparent colocalization of MIF and CXCL4L1 (*Figure 5A*). Colocalization was also
6 detectable in areas with more isolated non-aggregated platelets (*Figure 5B*). These areas
7 were then subjected to an in-depth analysis by fluorescence lifetime imaging-Förster
8 resonance energy transfer (FLIM-FRET) capitalizing on the Alexa 488/Cy3 FRET donor-
9 /acceptor pair. For molecule-molecule interactions within a distance range of 1-10 nm, FLIM-
10 FRET monitors the change in fluorescence lifetime of the donor via FRET and directly
11 visualizes the proximity of the donor (*here*: Alexa 488-labeled anti-mouse IgG secondary
12 antibody in combination with mouse anti-MIF) and the acceptor molecule (*here*: Cy3-labelled
13 anti-rabbit secondary antibody in combination with rabbit anti-CXCL4L1). We detected
14 significant donor lifetime shortening (from 2.019 ± 0.069 ns to 1.496 ± 0.033 ns) and FRET
15 events (FRET efficiency peak at 20-25%), when Alexa 488/Cy3 FLIM-FRET was recorded in
16 appropriate regions-of-interest (ROIs) (*Figure 5C-D*), an observation that is consistent with
17 the notion that MIF and CXCL4L1 not only colocalize in activated platelet preparations but
18 form true heterocomplexes.

19 To further investigate the physiological relevance of these findings, we next examined
20 clinical thrombus specimens derived from vascular surgery procedures. To determine
21 whether colocalized MIF and CXCL4L1 formed heterocomplexes in thrombus tissue, a
22 proximity ligation assay (PLA) was performed which detects inter-molecular interactions
23 within a distance of <10 nm. Specific PLA signals were detected in an atherosclerotic
24 thrombus specimen (*Figure 6A-B*), suggesting the abundant occurrence of MIF/CXCL4L1
25 heterocomplexes in the context of clinical thrombus tissue and confirming the FLIM-FRET
26 data obtained in platelet preparations from healthy blood samples. Thus, both FLIM-FRET
27 and PLA demonstrated that MIF and CXCL4L1 form heteromeric complexes upon release
28 from activated platelets.

29

29

bioRxiv preprint doi: <https://doi.org/10.1101/2021.11.26.470090>; this version posted February 24, 2022. The copyright holder for this preprint (which was not certified by peer review) is the author/funder, who has granted bioRxiv a license to display the preprint in perpetuity. It is made available under aCC-BY-NC-ND 4.0 International license.

1 **Heterocomplex formation inhibits MIF-stimulated thrombus formation and alters the**
2 **effect of MIF on platelet morphology**

3 Thrombus formation and clot retraction are relevant processes upon vessel injury and in
4 advanced atherosclerotic vessels. MIF was found to modulate these processes (Wirtz *et al*,
5 2015). As our data showed that MIF/CXCL4L1 heterocomplexes form in the micro-
6 environment of a thrombus, we next determined whether heterocomplex formation affects
7 thrombus characteristics. Thrombus formation under flow perfusing diluted human blood over
8 a collagen-coated surface harboring combinations of MIF and CXCL4L1 was studied as
9 established (Chatterjee *et al*, 2014) and was found to double following exposure to MIF when
10 applying a shear rate of 1000 s^{-1} (Figure 7). CXCL4L1 alone did not affect thrombus
11 characteristics, but when added together with MIF following preincubation, MIF-elicited
12 thrombus formation was blocked. These effects were mainly related to thrombus
13 size/coverage (Figure 7B, Supplementary Figure 5) rather than thrombus numbers (Figure
14 7C). These data indicated that heterocomplex formation inhibited MIF-stimulated thrombus
15 formation.

16 The role of platelet morphology and lamellipodia in stable thrombus formation has
17 been controversial, but platelet lamellipodia formation is critical for thrombus formation under
18 flow (Fotinos *et al*, 2015; Kraemer *et al*, 2011a; Schurr *et al*, 2019). To further study the
19 above observed effect of heterocomplex formation on thrombus behavior, we examined the
20 morphology of flow-stressed adhered platelets exposed to MIF or heterocomplexes in detail.
21 Platelet flow stress responses were recorded after 30 and 60 min, with significant changes
22 observed for the 30 min time point. Morphological changes encompassed increased platelet
23 numbers with filopodia, small lamellipodia, large lamellipodia, as well as fully spread
24 platelets. Interestingly, the strong increase in large lamellipodia under control buffer
25 conditions was significantly reduced by MIF and a further significant reduction was observed
26 for platelets cocubated with MIF and CXCL4L1. Inversely, the incubation with the
27 heterocomplex resulted in a significant increase in platelets with small lamellipodia compared
28 to stimulation with MIF alone (Figure 7D). Figure 7E further illustrates the inverse effect of

A. Appendix

bioRxiv preprint doi: <https://doi.org/10.1101/2021.11.26.470090>; this version posted February 24, 2022. The copyright holder for this preprint (which was not certified by peer review) is the author/funder, who has granted bioRxiv a license to display the preprint in perpetuity. It is made available under a [CC-BY-NC-ND 4.0 International license](#).

- 1 MIF/CXCL4L1 on large *versus* small lamellipodia formation. Together, these experiments
- 2 indicated MIF/CXCL4L1 heterocomplex formation skewed the morphology of adhering flow-
- 3 stressed platelets from a large to a small lamellipodia phenotype compared to treatment with
- 4 MIF alone.
- 5
- 6

bioRxiv preprint doi: <https://doi.org/10.1101/2021.11.26.470090>; this version posted February 24, 2022. The copyright holder for this preprint (which was not certified by peer review) is the author/funder, who has granted bioRxiv a license to display the preprint in perpetuity. It is made available under aCC-BY-NC-ND 4.0 International license.

1 **Discussion**

2

3 Chemokines control numerous pathogenic pathways contributing to inflammation and
4 atherogenesis. The recent systematic characterization of the chemokine interactome
5 revealed that heteromeric interactions between classical CC- and/or CXC-type chemokines
6 represent an important molecular adjustment screw that serves to amplify, inhibit, or
7 modulate chemokine activity (von Hundelshausen *et al.*, 2017). Here, we have identified a
8 heteromeric interaction between MIF, a pleiotropic inflammatory cytokine and ACK, and the
9 classical platelet chemokine CXCL4L1. We also show that CXCL4L1/MIF complex formation
10 affects inflammatory/atherogenic and thrombogenic activities of MIF. The scheme in *Figure 8*
11 summarizes the main findings of this study. This suggests that disease-relevant activities of
12 MIF may be fine-tuned by heterocomplexation with CXCL4L1 and that the chemokine
13 interactome extends to heteromeric interactions between classical and atypical chemokines.

14 In fact, binding of classical chemokines to non-CC- or CXC-chemokine mediators is
15 not unprecedented. Three examples have been documented: i) the CXC-chemokine
16 CXCL12 binds to the alarmin HMGB1 and HMGB1/CXCL12 complex formation promotes
17 chemotactic activity through CXCR4 (De Leo *et al.*, 2019; Schiraldi *et al.*, 2012); ii) the anti-
18 microbial peptide and α -defensin HNP1 binds to CCL5 and enhances monocyte adhesion
19 through CCR5 (Alard *et al.*, 2015); iii) macrophage-expressed galectins such as galectin-3
20 (Gal-3) bind to CXCL12 and attenuate CXCL12-stimulated signaling via CXCR4 (Eckardt *et*
21 *al.*, 2020). However, while these studies underscore that classical chemokine activity may be
22 modulated by interaction with various soluble mediators, HMGB1 and Gal-3 have no
23 chemotactic activity on their own; HNP1 has been reported to exhibit chemoattractive
24 properties, but the mediating chemoattractant receptor has remained elusive. In contrast,
25 despite lacking the signature structural elements of classical chemokines such as the
26 chemokine-fold and the N-terminal cysteine motif, MIF is a chemoattractant and depending
27 on the microenvironmental context, can signal through the CXC chemokine receptors
28 CXCR2, CXCR4, and/or ACKR3 to promote atherogenic and inflammatory leukocyte
29 recruitment. Its CXC receptor binding capacity is based on the presence of a pseudo-ELR

32

bioRxiv preprint doi: <https://doi.org/10.1101/2021.11.26.470090>; this version posted February 24, 2022. The copyright holder for this preprint (which was not certified by peer review) is the author/funder, who has granted bioRxiv a license to display the preprint in perpetuity. It is made available under aCC-BY-NC-ND 4.0 International license.

1 motif and an extended N-like loop, structurally mimicking the site 1 and 2 receptor binding
2 motifs of the corresponding cognate ligands CXCL1/8 and CXCL12, respectively. Together
3 with the β -defensins HDB1/2 and HBD3, which bind to CCR6 and CXCR4, respectively, and
4 secreted fragments of certain AARs, which bind to CXCR1 and CXCR2, MIF has therefore
5 been designated an ACK (Degryse & de Virgilio, 2003; Kapurniotu *et al.*, 2019; Oppenheim &
6 Yang, 2005; Rohrl *et al.*, 2010; Sinitski *et al.*, 2019; Wakasugi & Schimmel, 1999). Our
7 current identification of MIF/CXCL4L1 heterocomplexes thus also shows that the chemokine
8 interactome is not strictly limited to interactions between classical CC- and/or CXC-type
9 chemokines, but also encompasses heteromeric interactions between classical and atypical
10 chemokines, with potential functional modulation of the chemokine receptor pathway of both
11 the classical or atypical chemokine. Although not further validated and pursued in our current
12 study, the detection of additional candidate interactors of MIF in our performed unbiased
13 chemokine array, i.e. CCL28, CXCL9, as well as Prx6 leads us to hypothesize that
14 interactions between classical and atypical chemokines could represent a broader principal
15 of an “expanded ACK/CK interactome”.

16 The validity of the solid phase chemokine array as an unbiased screening approach
17 for candidate chemokine interactors has been previously established (von Hundelshausen *et al.*,
18 2017). The general utility and specificity of this methodology was further confirmed in the
19 current study. Out of 47 immobilized classical chemokines, in addition to CXCL4L1, only two
20 other classical chemokines, i.e. CCL28 and CXCL9, were revealed to have positivity. While a
21 functional link between MIF and CCL28 has yet to be unveiled, it is interesting to note that
22 the other detected CXC chemokine was CXCL9, a CXCR3 agonist like CXCL4L1.
23 Intriguingly, biotin-MIF neither bound to CXCL12 nor to CXCL8, indicating that implicated
24 functional interactions between MIF and the cognate CXCR4 and CXCR2 ligands,
25 respectively, are independent of heterocomplex formation.

26 Furthermore, the specificity of the performed array is underscored by the notion that
27 CXCL4, the highly homologous sister variant of CXCL4L1, did not bind to MIF, both at pH 8
28 and also when we tested for this interaction at pH 6 (data not shown) to account for pH-

A.1. Additional findings on MIF's interaction with the chemokine network

bioRxiv preprint doi: <https://doi.org/10.1101/2021.11.26.470090>; this version posted February 24, 2022. The copyright holder for this preprint (which was not certified by peer review) is the author/funder, who has granted bioRxiv a license to display the preprint in perpetuity. It is made available under aCC-BY-NC-ND 4.0 International license.

1 dependent charge differences. We hypothesize that the striking difference between
2 CXCL4L1 and CXCL4 in binding to MIF might be due to the suggested different conformation
3 of these two chemokines, e.g. the more exposed and flexible α -helix of monomeric CXCL4L1
4 (Kuo *et al.*, 2013). While CXCL4 has been amply characterized by us and others as a pro-
5 atherogenic platelet chemokine, in part also via its intriguing capacity to hetero-oligomerize
6 with CCL5 (Koenen *et al.*, 2009; von Hundelshausen *et al.*, 2007), very little is known about
7 the role of CXCL4L1 in chronic inflammatory diseases and atherosclerosis. Like its sister
8 molecule, CXCL4L1 is also abundantly expressed in platelets; however, it apparently is not
9 localized in α -granules but resides in a different sub-cellular compartment, from where it is
10 constitutively secreted (Lasagni *et al.*, 2007). It is also found in other cell types including
11 mononuclear cells and smooth muscle cells (Lasagni *et al.*, 2007). CXCL4L1 serves as an
12 inhibitor of angiogenesis and has pro-inflammatory effects by inducing the release of CCL2
13 and CXCL8 from monocytes, while – contrary to CXCL4 – it does not promote monocyte
14 survival (Domschke & Gleissner, 2019; Gouwy *et al.*, 2016; Sarabi *et al.*, 2011). There is only
15 one *in vivo* study, in which CXCL4L1 was investigated as prognostic marker in
16 cardiovascular disease. Interestingly, below-median levels of CXCL4L1 were found to
17 correlate with a worse outcome in stable coronary artery disease patients, as indicated by a
18 higher rate of cardiac death, stroke, or myocardial infarction (De Sutter *et al.*, 2012). This
19 finding might argue for a beneficial role of this chemokine in cardiovascular disease, even
20 though the mechanisms behind this remain unclear, but certainly more studies are required.
21 Of note, there is no equivalent of CXCL4L1 in mice (Eisman *et al.*, 1990), limiting functional *in*
22 *vivo* studies of this chemokine and its complex with MIF, as predicted from our study.

23 Importantly, we validated the binding between MIF and CXCL4L1 by semi-endo-
24 genous pulldown from monocytes, as well as two different biophysical *in vitro* methods, i.e.
25 SPR and MST. The combination of both methods also addresses potential disadvantages of
26 having one interaction partner immobilized (Zhou *et al.*, 2016). The binding affinity constants
27 derived from the SPR and MST experiments (116 and 160 nM, respectively) are in
28 reasonable agreement with each other. The observed (small) difference could be due to a

A. Appendix

bioRxiv preprint doi: <https://doi.org/10.1101/2021.11.26.470090>; this version posted February 24, 2022. The copyright holder for this preprint (which was not certified by peer review) is the author/funder, who has granted bioRxiv a license to display the preprint in perpetuity. It is made available under aCC-BY-NC-ND 4.0 International license.

1 number of factors, including surface immobilization effects, fluorescence *versus* biotin
2 labeling, or buffers employed. Together, the results are suggestive of a relatively high binding
3 affinity between MIF and CXCL4L1. Moreover, the obtained nanomolar K_D is consistent with
4 the reported concentrations of both proteins in inflammatory disease settings (Sinitski *et al.*,
5 2019). Flanking evidence for MIF/CXCL4L1 complex formation was obtained by our peptide
6 array mapping and molecular docking results. As expected given their high sequence
7 identity, the peptide array predicted identical binding sites for CXCL4 and CXCL4L1. Also,
8 the peptide array methodology interrogates linear binding epitopes but cannot delineate
9 conformational differences. In fact, Kuo *et al.* suggested that the three-amino acid difference
10 between CXCL4 and CXCL4L1, although marginal, leads to a slight tilting of the C-terminal
11 α -helix (Kuo *et al.*, 2013). We hypothesize that this moderate conformational change could
12 be the basis for the observed preferred binding of MIF to CXCL4L1 compared to CXCL4.
13 Differences in their binding affinity to CCL5 have already been reported for CXCL4 and
14 CXCL4L1 and also the availability of their monomers, regulated by the stability of their
15 tetrameric complexes, differs between these two chemokines (Sarabi *et al.*, 2011). Future
16 structural studies, e.g. by nuclear magnetic resonance (NMR) spectroscopy, may help to
17 further address these and other conformational questions.

18 To investigate the functional consequences of MIF/CXCL4L1 heterocomplex
19 formation, we focused on inflammatory and atherosclerosis-relevant activities of MIF. T-cell
20 migration is one such activity that is regulated by the MIF/CXCR4 pathway (Bernhagen *et al.*,
21 2007). In line with previous results, MIF promoted T-cell migration in a physiologically
22 relevant 3D migration setting. Although T cells generally express the CXCL4L1 receptor
23 CXCR3, CXCL4L1 alone had no effect on the chemotaxis of human PBMC-derived T cells.
24 Lack of CXCL4L1 activity in this assay is likely due to the fact that CXCL4L1 is not a *bona*
25 *fide* T-cell chemoattractant (Gouwy *et al.*, 2016) and that the preferential CXCL4L1 receptor
26 variant CXCR3B is poorly expressed on T cells (Korniejewska *et al.*, 2011). The 3D T-cell
27 migration data are supported by the result that MIF, but not the combination of MIF and
28 CXCL4L1, promoted Jurkat T-cell migration in a 2D Transwell assay. Confirming the

35

A.1. Additional findings on MIF's interaction with the chemokine network

bioRxiv preprint doi: <https://doi.org/10.1101/2021.11.26.470090>; this version posted February 24, 2022. The copyright holder for this preprint (which was not certified by peer review) is the author/funder, who has granted bioRxiv a license to display the preprint in perpetuity. It is made available under a [CC-BY-NC-ND 4.0 International license](#).

1 remarkable specificity of MIF binding to CXCL4L1 versus CXCL4, cocubation of MIF with
2 CXCL4 did not result in reduced Jurkat T-cell migration. Of note, heterocomplex formation
3 with MIF led to a complete blockade of MIF's pro-migratory effect on primary T cells in the 3D
4 migration setting. While *in vivo* T-cell recruitment studies were beyond the scope of our
5 study, inhibition of MIF-mediated T-cell migration by CXCL4L1 complexation could potentially
6 be relevant in atherosclerosis, where it might represent a feedback mechanism that could
7 serve to dampen the atherogenic response. In fact, abundant CXCL4L1 levels may be
8 released by activated platelets in an atherogenic microenvironment, where they could
9 colocalize with endothelial-immobilized or monocyte-secreted MIF and infiltrating T cells.
10 That complexation of MIF by CXCL4L1 can interfere with MIF's chemoattractant activities
11 was confirmed in a microglia assay, in which the motility of Egfp⁺ microglia in murine cortical
12 brain cultures *ex vivo* was studied. In addition to representing an independent cell migration
13 system, the data obtained from the microglia-containing cortical cultures further confirmed
14 that complex formation interferes with MIF signaling through the CXCR4 pathway and
15 underscored that the mechanism could be relevant in *in vivo*-like physiological tissue
16 settings. That MIF/CXCL4L1 heterocomplex formation interferes with MIF signaling through
17 CXCR4 was independently validated by biochemical experiments using FP spectroscopy and
18 DMR analysis of HEK293-CXCR4 transfectants.

19 This identified interaction of MIF with CXCL4L1, supposedly resulting in local
20 inhibition of MIF's pro-inflammatory effects was especially interesting to us in the context of
21 previous studies, in which we identified human and mouse platelets as an abundant source
22 of MIF (Strüßmann *et al.*, 2013; Wirtz *et al.*, 2015). Here, we verified expression and
23 localization of MIF in human platelets as well as in platelet-rich clinical thrombus tissue by
24 confocal (CLSM) and multiphoton microscopy (MPM). As expected, these experiments also
25 showed the abundant presence of CXCL4L1 in platelets and thrombi, and suggested the
26 colocalization and/or complex formation of MIF and CXCL4L1 in the vicinity of platelets. Due
27 to the optical resolution limits of the CLSM and MPM methods, true colocalization and the
28 specific subcellular compartment could not be determined. Evidence for the presence of

bioRxiv preprint doi: <https://doi.org/10.1101/2021.11.26.470090>; this version posted February 24, 2022. The copyright holder for this preprint (which was not certified by peer review) is the author/funder, who has granted bioRxiv a license to display the preprint in perpetuity. It is made available under aCC-BY-NC-ND 4.0 International license.

1 MIF/CXCL4L1 heteromers is suggested by PLA performed on cryosections of a human
2 thrombus. In fact, PLA is an established method to detect CK heteromers as shown
3 previously for HNP1/CCL5 complexes (Alard *et al.*, 2015).

4 Having confirmed the occurrence of this novel complex in platelet preparations and
5 thrombus tissue, lastly the effect of MIF, CXCL4L1 and their complex on platelet function and
6 thrombus formation was assessed. MIF promoted thrombus formation leading to a larger
7 thrombus-covered area in an *in vitro* setting under flow conditions. Confirming our previous
8 results, this effect was abrogated upon co-incubation with CXCL4L1. It is interesting to note
9 that in the settings used in our experiment applying a shear rate of 1000 s^{-1} for 5 min, MIF
10 acted to enhance thrombus formation. Instead, in a previous study employing a shear rate of
11 1700 s^{-1} MIF was found to reduce thrombus size, confirming that MIF is a modulator of
12 thrombus formation, but also indicating that the directionality of the effect may depend on the
13 specific microenvironmental context.

14 Moreover, studying the morphology change of isolated platelets during adhesion and
15 activation on a fibrinogen-coated surface revealed that both MIF and CXCL4L1 favored a
16 switch from large to small lamellipodia at an early time point. Interestingly, in this setting no
17 inhibition by the complex on MIF-mediated effects was observed, but a synergistic behavior
18 of MIF and CXCL4L1 was observed, suggesting that this effect may occur independently of
19 CXCR4.

20 In addition to their classical role in wound closure and haemostasis, thrombus formation
21 and platelet activation are processes that are closely linked to inflammatory processes
22 driving atherosclerosis (Gawaz, 2006; Lippi *et al.*, 2011; Nording *et al.*, 2020; von
23 Hundelshausen & Weber, 2007). MIF has been amply linked to atherosclerotic pathogenesis
24 both clinically and experimentally, with evidence for a number of contributing mechanisms
25 including leukocyte recruitment and platelet activation (Bernhagen *et al.*, 2007; Chatterjee *et al.*,
26 2014; Muller *et al.*, 2013; Sinitski *et al.*, 2019; Zernecke *et al.*, 2008) The identified
27 heteromerization of MIF and CXCL4L1 in our current study and the observed effect of
28 MIF/CXCL4L1 complex formation on immune cell migration as well as thrombus size and

A.1. Additional findings on MIF's interaction with the chemokine network

bioRxiv preprint doi: <https://doi.org/10.1101/2021.11.26.470090>; this version posted February 24, 2022. The copyright holder for this preprint (which was not certified by peer review) is the author/funder, who has granted bioRxiv a license to display the preprint in perpetuity. It is made available under a [CC-BY-NC-ND 4.0 International license](#).

1 platelet morphology might imply that CXCL4L1 could have a protective role in atherosclerosis
2 by mitigating the pro-atherosclerotic effects of MIF via complex formation. This hypothesis
3 would warrant future studies in corresponding experimental *in vivo* models, albeit the lack of
4 CXCL4L1 expression in rodents will impose a particular challenge here.

5 In summary, we provide evidence that MIF does not only behave as a chemokine-like
6 mediator by way of engaging classical chemokine receptors but also by direct binding to
7 classical chemokines. Interestingly, the identified chemokine interactor of MIF is not one of
8 the cognate ligands of the MIF receptors CXCR2 or CXCR4, but CXCL4L1, a prominent
9 platelet chemokine not previously implicated in MIF biology or MIF-mediated pathologies.
10 While evidence from experimental *in vivo* disease models will have to be obtained in future
11 studies, our data suggest that MIF/CXCL4L1 complex formation could serve to attenuate
12 inflammatory/atherogenic activities of MIF through the CXCR4 receptor axis. Our study also
13 gives insight into the growing "chemokine interactome" with a particular focus on ACKs.
14 While modulatory effects on the interactome by mediators not belonging to the class of
15 chemokines have already been exemplified by intriguing studies involving HMGB1, HNP1,
16 and the galectins (Alard *et al.*, 2015; Eckardt *et al.*, 2020; Schiraldi *et al.*, 2012), the current
17 study is first in demonstrating a role for MIF family proteins in particular, and *bona fide* ACKs
18 in general, as defined by their chemotactic activity mediated through engagement of classical
19 chemokine receptors. While not yet validated by follow up analyses, the identification of
20 additional potential interactors in our array indicates that this could represent a broader
21 principle of an ACK/CK interactome.

22

23

24

bioRxiv preprint doi: <https://doi.org/10.1101/2021.11.26.470090>; this version posted February 24, 2022. The copyright holder for this preprint (which was not certified by peer review) is the author/funder, who has granted bioRxiv a license to display the preprint in perpetuity. It is made available under a [CC-BY-NC-ND 4.0 International license](#).

1 **Acknowledgements**

2 This work was supported by Deutsche Forschungsgemeinschaft (DFG) grant SFB1123-A3 to
3 J.B. and A.K., DFG INST 409/209-1 FUGG to J.B., SFB1123-A2 to P.v.H., SFB1123-A1 to
4 C.W., SFB1123-B5 to L.M., SFB240-B01 (374031971 – TRR 240) to M.G., and by DFG
5 under Germany's Excellence Strategy within the framework of the Munich Cluster for
6 Systems Neurology (EXC 2145 SyNergy—ID 390857198) to J.B., C.W., and O.G. A.H. was
7 supported by a Metiphs scholarship of LMU Munich and by the Friedrich-Baur-Foundation
8 e.V. at LMU University Hospital. E.S. and J.B. received funding from the LMU-FöFoLe
9 program under project 52114016. C.W. is Van de Laar Professor of Atherosclerosis. We
10 thank Simona Gerra, Priscila Bourilhon, and Lusine Saroyan for technical support, and
11 Christine Krammer for help with the DMR assay. We are grateful to the mouse core facility of
12 the Center for Stroke and Dementia Research (CSD) for their support. We also thank the
13 Biophysics Core Facility at the School of Biology of LMU Munich and Dr. Sophie Brameyer
14 for usage of the MST instrument.
15

A.1. Additional findings on MIF's interaction with the chemokine network

bioRxiv preprint doi: <https://doi.org/10.1101/2021.11.26.470090>; this version posted February 24, 2022. The copyright holder for this preprint (which was not certified by peer review) is the author/funder, who has granted bioRxiv a license to display the preprint in perpetuity. It is made available under aCC-BY-NC-ND 4.0 International license.

1 **Figure legends**

2

3 **Figure 1:** Unbiased chemokine protein array identifies CXCL4L1, but not CXCL4, as a novel
4 interaction candidate of MIF. (A) Schematic illustrating binding of biotinylated MIF to the
5 chemokine protein array. (B) Layout of the immobilized chemokines, atypical chemokines
6 and alarmins (*top*) and membrane of chemokine solid phase assay performed at pH 8.0,
7 developed against bound biotin-MIF (*bottom*). (C) Close-up of the membrane with a focus on
8 CXCL4 and CXCL4L1 with the corresponding negative control membrane, incubated without
9 biotin-MIF.

10

11 **Figure 2:** Validation of MIF/CXCL4L1 complex formation by a variety of protein-protein
12 interaction assays and verification of the specificity of MIF complexation with CXCL4L1 over
13 CXCL4. (A) Semi-endogenous pull-down assay, in which endogenous CXCL4L1 from
14 MonoMac6 lysates was captured with recombinant biotinylated MIF and pulled down by
15 streptavidin-coated paramagnetic beads. Blots, developed against MIF (*left*) and CXCL4L1
16 (*right*), show representative results of three independent experiments. Input corresponds to
17 5% cell lysate without pull-down and control (Ctrl) refers to pull-downs performed in the
18 absence of biotin-MIF. Molecular weight markers were lelectrophoresed in the same gel and
19 relevant marker sizes are indicated. (B) Interrogation of MIF/CXCL4L1 complex formation by
20 surface plasmon resonance (SPR) spectroscopy using chip-immobilized biotin-MIF titred
21 against increasing concentrations of CXCL4L1. Measurements indicate an interaction
22 between MIF and CXCL4L1 with an estimated K_D of 116 ± 16 nM. The SPR response signal
23 is given in relative units (RU). (C) Same as (B), except that titration was performed with
24 CXCL4. Corresponding SPR spectroscopy data for MIF and CXCL4. No detectable binding
25 signal was obtained and no K_D could be derived. (D) Interrogation of MIF/CXCL4L1 complex
26 formation by microscale thermophoresis (MST) utilizing fluorescently labeled MIF and
27 CXCL4L1 in solution. MST analysis revealed a K_D of 159.8 ± 16.8 nM for the interaction of

40

A. Appendix

bioRxiv preprint doi: <https://doi.org/10.1101/2021.11.26.470090>; this version posted February 24, 2022. The copyright holder for this preprint (which was not certified by peer review) is the author/funder, who has granted bioRxiv a license to display the preprint in perpetuity. It is made available under aCC-BY-NC-ND 4.0 International license.

1 MIF and CXCL4L1. (E) Same as (D), except that CXCL4 was tested. The derived apparent
2 K_D of $2.0 \pm 0.8 \mu\text{M}$ was ten-fold higher compared to MIF/CXCL4L1.

3

4 **Figure 3.** Co-incubation with CXCL4L1 inhibits MIF-mediated immune cell chemotaxis. (A)
5 Migration of human CD4^+ T-cells embedded in a gel matrix, subjected to gradients of MIF,
6 CXCL4L1 or both. Movement of cells was followed by live cell imaging and individual tracks
7 reconstructed from acquired images. Tracks of cells migrating towards the indicated stimuli
8 are marked in the corresponding color. Starting point was centered to $x = y = 0$. The black
9 crosshair indicates the cell population's center of mass after migration. (B) Quantification of
10 the 3D chemotaxis experiment in (A), indicating that complexation of MIF by CXCL4L1
11 attenuates MIF-mediated directed migration of human CD4^+ T-cells. Plotted is the calculated
12 forward migration index (FMI), based on manual tracking of at least 30 individual cells per
13 treatment. (C) Migration trajectories of murine microglia, obtained by live cell imaging for 15
14 h, treated with MIF, CXCL4L1, or both. Used concentrations: MIF: 8 nM, CXCL4L1: 1.6 nM;
15 $n=5$ independent experiments; horizontal bar: 100 μm . (D) Analysis of microglia motility,
16 based on each tracked cell accumulated distance, shown in (C). Data is presented as mean
17 \pm SD. Statistical significance is indicated as described: *, $P < 0.05$; **, $P < 0.01$; ***, $P <$
18 0.001.

19

20 **Figure 4.** MIF/CXCL4L1 complex formation inhibits binding of MIF to CXCR4 and signaling
21 of MIF through the CXCR4 signaling axis. (A) Fluorescence polarization (FP) spectroscopy
22 shows the interaction of Alexa488-labeled MIF with the soluble CXCR4 receptor mimic
23 msR4M-L1 with an apparent K_D of 237.2 ± 24.2 nM. Data is presented as mean of 3
24 independent experiments; error bars represent the SD. (B) Pre-incubation of MIF with
25 CXCL4L1 (160-fold molar excess) prevents the interaction of MIF with msR4M-L1 (app. $K_D >$
26 10 μM). Mean of 3 experiments \pm SD. (C) Dynamic mass redistribution (DMR)
27 measurements with HEK293 cells stably expressing CXCR4 indicate that the cellular
28 response to MIF is reduced, when MIF is pre-incubated with CXCL4L1. The DMR response

41

A.1. Additional findings on MIF's interaction with the chemokine network

bioRxiv preprint doi: <https://doi.org/10.1101/2021.11.26.470090>; this version posted February 24, 2022. The copyright holder for this preprint (which was not certified by peer review) is the author/funder, who has granted bioRxiv a license to display the preprint in perpetuity. It is made available under aCC-BY-NC-ND 4.0 International license.

1 of CXCR4-expressing HEK293 cells to MIF in the presence or absence of the CXCR4-
2 antagonist AMD3100 is also shown, confirming the CXCR4-dependency of the cellular
3 response to MIF.

4

5 **Figure 5.** Co-localization and interaction of MIF and CXCL4L1 in human platelet
6 preparations, detected in multiphoton microscopy (MPM). (A): MPM images of isolated
7 platelets, forming small aggregates, stained for MIF and CXCL4L1. White arrowheads
8 indicate areas of colocalization. Size bar: 5 μm . (B) MPM images of isolated, more separated
9 platelets, stained as in (A), showing colocalization of MIF and CXCL4L1. Size bar: 5 μm . (C)
10 Fluorescence lifetime imaging (FLIM) of platelets isolation as shown in (B). Color-code
11 corresponds to lifetime of the donor, Alexa 488, the dye used for the antibody-based staining
12 of MIF. (D) Histogram of the Förster Resonance Energy Transfer (FRET) efficiency in (C).
13 (E) Donor lifetime shortening, presented as the mean lifetime (τ), average weighted, of the
14 donor (Alexa 488, MIF staining) alone, and in combination with the acceptor fluorophore
15 (Cy3, CXCL4L1 staining), where FRET occurred.

16

17 **Figure 6.** Proximity ligation assay (PLA) indicates that MIF/CXCL4L1 heterocomplexes are
18 present in human thrombus tissue. (A) MIF/CXCL4L1 complex formation in thrombus
19 specimen revealed by PLA. PLA-positive signals are depicted in yellow; tissue was
20 counterstained with fluorescent-labeled phalloidin (cyan). Stained tissue samples were
21 imaged by CLSM; size bar: 50 μm . (B) HE staining of thrombus tissue specimen; size bar: 75
22 μm .

23

24 **Figure 7.** (A) Thrombus formation in human blood under flow stress is enhanced by MIF,
25 and this effect is diminished by pre-incubation of MIF with CXCL4L1. Fluorescent staining
26 with DiOC₆. Shown are representative images of one experiment, performed at a shear rate
27 of 1000 s^{-1} ; size bar: 100 μm . (B) Quantification of thrombi sizes from flow chamber
28 experiments, as depicted exemplarily in (A). MIF-mediated increase in thrombus-covered

42

A. Appendix

bioRxiv preprint doi: <https://doi.org/10.1101/2021.11.26.470090>; this version posted February 24, 2022. The copyright holder for this preprint (which was not certified by peer review) is the author/funder, who has granted bioRxiv a license to display the preprint in perpetuity. It is made available under aCC-BY-NC-ND 4.0 International license.

1 area is diminished, when MIF is pre-incubated with CXCL4L1. n = 6 experiments and
2 platelets coming from 4 donors. (C) Quantification of total thrombi numbers per treatment
3 group. As thrombus numbers remain unchanged, effects on thrombus-covered area originate
4 from the size of the formed thrombi (see also Supplementary Figure 5); n = 6 experiments.
5 (D) Analysis and quantification of platelet morphology upon adhesion on fibrinogen-coated
6 coverslips. Activated platelets were allowed to adhere on fibrinogen-coated coverslips that
7 were pre-treated with MIF, CXCL4L1 or a mixture of both for the indicated times. After fixing
8 with PFA, images of randomly selected areas were taken and platelet morphology analyzed.
9 Treatment with a combination of MIF and CXCL4L1 led to a reduction in the large
10 lamellopodia phenotype, favoring small lamellopodia, with the MIF/CXCL4L1 complex
11 showing a stronger effect than the individual proteins; n = 6 experiments. (E) Platelet
12 morphology distribution after 30 min for each treatment group according to panel (D).

13

14 **Figure 8:** Summary scheme and suggested model of CXCL4L1/MIF complex formation and
15 functions. The atypical chemokine MIF and the classical chemokine CXCL4L1, e.g. present
16 in an inflammatory or atherogenic microenvironment after release from platelets, form
17 heteromeric complexes. Complexes inhibit inflammatory effects of MIF on leukocyte
18 recruitment as well as its pro-thrombotic effects through impairing MIF interactions with its
19 non-cognate receptor CXCR4.

20

21

A.1. Additional findings on MIF's interaction with the chemokine network

bioRxiv preprint doi: <https://doi.org/10.1101/2021.11.26.470090>; this version posted February 24, 2022. The copyright holder for this preprint (which was not certified by peer review) is the author/funder, who has granted bioRxiv a license to display the preprint in perpetuity. It is made available under aCC-BY-NC-ND 4.0 International license.

1 **Supplementary figure legends**

2

3 **Supplementary Figure 1.** Additional data for chemokine protein array. (A) Negative control
4 membrane related to the experiment in **Figure 1**, incubated in buffer at pH 8.0 without biotin-
5 MIF. (B) Close-up of membrane from a chemokine protein array experiment with a focus on
6 CXCL4 and CXCL4L1. The membrane was incubated with biotin-MIF and the incubation was
7 performed at pH 6.0.

8

9 **Supplementary Figure 2.** Investigation of the MIF/CXCL4L1 interaction interface and *in*
10 *silico* studies. (A) CelluSpot peptide array experiments, where overlapping peptides of
11 CXCL4 (*left*) and CXCL4L1 (*right*) were spotted on an array and probed with biotin-MIF.
12 Chemiluminescence signal intensity indicates binding of biotin-MIF to the respective peptide.
13 Arrows indicate peptides of interest that are most likely to be involved in the interaction with
14 MIF. (B) Sequences of peptides identified in **A** are highlighted in the 3D structure of
15 monomeric CXCL4 and CXCL4L1, showing their localization in the folded proteins. For both
16 chemokines, these peptides of interest represent almost identical amino acid sequences,
17 corresponding to highly similar regions of the protein. This indicates that not only the
18 sequence but also the three-dimensional conformation of the chemokines might play a role in
19 the interaction with MIF. Amino acid residues, in which CXCL4L1 differs from CXCL4 are in
20 italics. PyMOL was used to visualize a CXCL4 (PDB ID: 1F9Q Chain A) and CXCL4L1
21 monomer (PDB ID: 4HSV Chain A). (C) To visualize the proposed MIF/CXCL4L1 complex,
22 an unbiased *in silico* protein-protein docking approach was taken. The ClusPro 2.0
23 webserver was used to simulate a complex consisting of both a MIF and CXCL4L1
24 monomer. Depicted here is the highest-ranking docking result, with peptides identified in **A** to
25 be potentially part of the interaction interface highlighted in CXCL4L1. According to this *in*
26 *silico* prediction, they are partially directed towards MIF, allowing parts of their sequences
27 being involved in complex formation. PyMOL was used to calculate the surface charge
28 distribution of these proteins (red: negatively charged; blue: positively charged), revealing an

44

bioRxiv preprint doi: <https://doi.org/10.1101/2021.11.26.470090>; this version posted February 24, 2022. The copyright holder for this preprint (which was not certified by peer review) is the author/funder, who has granted bioRxiv a license to display the preprint in perpetuity. It is made available under aCC-BY-NC-ND 4.0 International license.

1 area of opposite charges in the proposed contact region of MIF and CXCL4L1 that partially
2 matches the peptide array results.

3

4 **Supplementary Figure 3.** Effects on cell migration in Jurkat T cells and microglia. (A) Effect
5 of CXCL4L1 on MIF-mediated chemotaxis of Jurkat T cells as analyzed in a Transwell
6 migration assay. Used concentrations: MIF: 16 nM, CXCL4L1: 32 nM; Data is presented as
7 mean \pm SD. n = 2-4 independent experiments. (B) Same as (A), except that co-incubation
8 with CXCL4 was analyzed. Data is presented as mean \pm SD. n = 4 independent experiments
9 with duplicates each. (C) Quantification of murine microglia motility, based on the
10 accumulated distance of GFP-positive microglia tracked during live cell imaging (n = 5). MIF
11 was used at a concentration of 8 nM, the soluble CXCR4-mimicking peptide msR4M-L1 at 40
12 nM and the cognate ligand of CXCR4, CXCL12, at 16 nM. Data presented as mean \pm SD.
13 Statistical significance: *, P < 0.05; **, P < 0.01; ***, P < 0.005; ****, P < 0.0001.

14

15 **Supplementary Figure 4.** Quantification of mean thrombus sizes from **Figure 5A**, showing a
16 trend for CXCL4L1 inhibiting the MIF-mediated increase in thrombus size in samples, in
17 which MIF and CXCL4L1 were pre-incubated together.

18

A.1. Additional findings on MIF's interaction with the chemokine network

bioRxiv preprint doi: <https://doi.org/10.1101/2021.11.26.470090>; this version posted February 24, 2022. The copyright holder for this preprint (which was not certified by peer review) is the author/funder, who has granted bioRxiv a license to display the preprint in perpetuity. It is made available under aCC-BY-NC-ND 4.0 International license.

1 **References**

2

3 Alard JE, Ortega-Gomez A, Wichapong K, Bongiovanni D, Horckmans M, Megens RT, Leoni
4 G, Ferraro B, Rossaint J, Paulin N *et al* (2015) Recruitment of classical monocytes can be
5 inhibited by disturbing heteromers of neutrophil HNP1 and platelet CCL5. *Sci Transl Med* 7:
6 317ra196

7 Bachelerie F, Ben-Baruch A, Burkhardt AM, Combadiere C, Farber JM, Graham GJ, Horuk
8 R, Sparre-Ulrich AH, Locati M, Luster AD *et al* (2014a) International Union of Basic and
9 Clinical Pharmacology. LXXXIX. Update on the extended family of chemokine receptors and
10 introducing a new nomenclature for atypical chemokine receptors. *Pharmacol Rev* 66: 1-79

11 Bachelerie F, Graham GJ, Locati M, Mantovani A, Murphy PM, Nibbs R, Rot A, Sozzani S,
12 Thelen M (2014b) New nomenclature for atypical chemokine receptors. *Nat Immunol* 15:
13 207-208

14 Bai F, Asojo OA, Cirillo P, Ciustea M, Ledizet M, Aristoff PA, Leng L, Koski RA, Powell TJ,
15 Bucala R *et al* (2012) A novel allosteric inhibitor of macrophage migration inhibitory factor
16 (MIF). *J Biol Chem* 287: 30653-30663

17 Bernhagen J, Krohn R, Lue H, Gregory JL, Zerneck A, Koenen RR, Dewor M, Georgiev I,
18 Schober A, Leng L *et al* (2007) MIF is a noncognate ligand of CXC chemokine receptors in
19 inflammatory and atherogenic cell recruitment. *Nat Med* 13: 587-596

20 Bernhagen J, Mitchell RA, Calandra T, Voelter W, Cerami A, Bucala R (1994) Purification,
21 bioactivity, and secondary structure analysis of mouse and human macrophage migration
22 Inhibitory factor (MIF). *Biochemistry* 33: 14144-14155

23 Borst O, Schmidt EM, Munzer P, Schonberger T, Towhid ST, Elvers M, Leibrock C, Schmid
24 E, Eylonstein A, Kuhl D *et al* (2012) The serum- and glucocorticoid-inducible kinase 1
25 (SGK1) influences platelet calcium signaling and function by regulation of Orai1 expression
26 in megakaryocytes. *Blood* 119: 251-261

46

A. Appendix

bioRxiv preprint doi: <https://doi.org/10.1101/2021.11.26.470090>; this version posted February 24, 2022. The copyright holder for this preprint (which was not certified by peer review) is the author/funder, who has granted bioRxiv a license to display the preprint in perpetuity. It is made available under aCC-BY-NC-ND 4.0 International license.

- 1 Calandra T, Roger T (2003) Macrophage migration inhibitory factor: a regulator of innate
- 2 immunity. *Nat Rev Immunol* 3: 791-800

- 3 Charo IF, Ransohoff RM (2006) The many roles of chemokines and chemokine receptors in
- 4 inflammation. *N Engl J Med* 354: 610-621

- 5 Chatterjee M, Borst O, Walker B, Fotinos A, Vogel S, Seizer P, Mack A, Alampour-Rajabi S,
- 6 Rath D, Geisler T *et al* (2014) Macrophage migration inhibitory factor limits activation-
- 7 induced apoptosis of platelets via CXCR7-dependent Akt signaling. *Circ Res* 115: 939-949

- 8 David JR (1966) Delayed hypersensitivity in vitro: its mediation by cell-free substances
- 9 formed by lymphoid cell-antigen interaction. *Proc Natl Acad Sci U S A* 56: 72-77

- 10 De Leo F, Quilici G, Tirone M, De Marchis F, Mannella V, Zucchelli C, Preti A, Gori A,
- 11 Casalgrandi M, Mezzapelle R *et al* (2019) Diflunisal targets the HMGB1/CXCL12
- 12 heterocomplex and blocks immune cell recruitment. *EMBO Rep* 20: e47788

- 13 De Sutter J, Van de Veire NR, Struyf S, Philippe J, De Buyzere M, Van Damme J (2012) PF-
- 14 4var/CXCL4L1 predicts outcome in stable coronary artery disease patients with preserved
- 15 left ventricular function. *PLoS One* 7: e31343

- 16 Degryse B, de Virgilio M (2003) The nuclear protein HMGB1, a new kind of chemokine?
- 17 *FEBS Lett* 553: 11-17

- 18 Domschke G, Gleissner CA (2019) CXCL4-induced macrophages in human atherosclerosis.
- 19 *Cytokine* 122: 154141

- 20 Eckardt V, Miller MC, Blanchet X, Duan R, Leberzammer J, Duchene J, Soehnlein O,
- 21 Megens RT, Ludwig AK, Dregni A *et al* (2020) Chemokines and galectins form heterodimers
- 22 to modulate inflammation. *EMBO Rep* 21: e47852

- 23 Eiger DS, Boldizsar N, Honeycutt CC, Gardner J, Rajagopal S (2021) Biased agonism at
- 24 chemokine receptors. *Cell Signal* 78: 109862

A.1. Additional findings on MIF's interaction with the chemokine network

bioRxiv preprint doi: <https://doi.org/10.1101/2021.11.26.470090>; this version posted February 24, 2022. The copyright holder for this preprint (which was not certified by peer review) is the author/funder, who has granted bioRxiv a license to display the preprint in perpetuity. It is made available under aCC-BY-NC-ND 4.0 International license.

- 1 Eisman R, Surrey S, Ramachandran B, Schwartz E, Poncz M (1990) Structural and
- 2 functional comparison of the genes for human platelet factor 4 and PF4alt. *Blood* 76: 336-
- 3 344
- 4 Fotinos A, Klier M, Gowert NS, Munzer P, Klatt C, Beck S, Borst O, Billuart P, Schaller M,
- 5 Lang F *et al* (2015) Loss of oligophrenin1 leads to uncontrolled Rho activation and increased
- 6 thrombus formation in mice. *J Thromb Haemost* 13: 619-630
- 7 Gawaz M (2006) Platelets in the onset of atherosclerosis. *Blood Cells Mol Dis* 36: 206-210
- 8 Gokce O, Sudhof TC (2013) Membrane-tethered monomeric neurexin LNS-domain triggers
- 9 synapse formation. *J Neurosci* 33: 14617-14628
- 10 Gouwy M, Ruytinx P, Radice E, Claudi F, Van Raemdonck K, Bonecchi R, Locati M, Struyf S
- 11 (2016) CXCL4 and CXCL4L1 Differentially affect monocyte survival and dendritic cell
- 12 differentiation and phagocytosis. *PLoS One* 11: e0166006
- 13 Hutchings CJ, Koglin M, Olson WC, Marshall FH (2017) Opportunities for therapeutic
- 14 antibodies directed at G-protein-coupled receptors. *Nat Rev Drug Discov* 16: 787-810
- 15 Kapurniotu A, Gokce O, Bernhagen J (2019) The multitasking potential of alarmins and
- 16 atypical chemokines. *Front Med (Lausanne)* 6: 3
- 17 Karshovska E, Weber C, von Hundelshausen P (2013) Platelet chemokines in health and
- 18 disease. *Thromb Haemost* 110: 894-902
- 19 Klasen C, Ohl K, Sternkopf M, Shachar I, Schmitz C, Heussen N, Hobeika E, Levit-Zerdoun
- 20 E, Tenbrock K, Reth M *et al* (2014) MIF promotes B cell chemotaxis through the receptors
- 21 CXCR4 and CD74 and ZAP-70 signaling. *J Immunol* 192: 5273-5284
- 22 Kleist AB, Getschman AE, Ziarek JJ, Nevins AM, Gauthier PA, Chevigne A, Szpakowska M,
- 23 Volkman BF (2016) New paradigms in chemokine receptor signal transduction: Moving
- 24 beyond the two-site model. *Biochem Pharmacol* 114: 53-68

A. Appendix

bioRxiv preprint doi: <https://doi.org/10.1101/2021.11.26.470090>; this version posted February 24, 2022. The copyright holder for this preprint (which was not certified by peer review) is the author/funder, who has granted bioRxiv a license to display the preprint in perpetuity. It is made available under aCC-BY-NC-ND 4.0 International license.

- 1 Koenen RR, von Hundelshausen P, Nesmelova IV, Zernecke A, Liehn EA, Sarabi A, Kramp
- 2 BK, Piccinini AM, Paludan SR, Kowalska MA *et al* (2009) Disrupting functional interactions
- 3 between platelet chemokines inhibits atherosclerosis in hyperlipidemic mice. *Nat Med* 15: 97-
- 4 103
- 5 Kontos C, El Bounkari O, Krammer C, Sinitski D, Hille K, Zan C, Yan G, Wang S, Gao Y,
- 6 Brandhofer M *et al* (2020) Designed CXCR4 mimic acts as a soluble chemokine receptor that
- 7 blocks atherogenic inflammation by agonist-specific targeting. *Nat Commun* 11: 5981
- 8 Korniejewska A, McKnight AJ, Johnson Z, Watson ML, Ward SG (2011) Expression and
- 9 agonist responsiveness of CXCR3 variants in human T lymphocytes. *Immunology* 132: 503-
- 10 515
- 11 Kozakov D, Hall DR, Xia B, Porter KA, Padhorny D, Yueh C, Beglov D, Vajda S (2017) The
- 12 ClusPro web server for protein-protein docking. *Nat Protoc* 12: 255-278
- 13 Kraemer BF, Schmidt C, Urban B, Bigalke B, Schwanitz L, Koch M, Seizer P, Schaller M,
- 14 Gawaz M, Lindemann S (2011a) High shear flow induces migration of adherent human
- 15 platelets. *Platelets* 22: 415-421
- 16 Kraemer S, Lue H, Zernecke A, Kapurniotu A, Andreetto E, Frank R, Lennartz B, Weber C,
- 17 Bernhagen J (2011b) MIF-chemokine receptor interactions in atherogenesis are dependent
- 18 on an N-loop-based 2-site binding mechanism. *FASEB J* 25: 894-906
- 19 Krammer C, Kontos C, Dewor M, Hille K, Dalla Volta B, El Bounkari O, Tas K, Sinitski D,
- 20 Brandhofer M, Megens RTA *et al* (2021) A MIF-Derived Cyclopeptide that Inhibits MIF
- 21 Binding and Atherogenic Signaling via the Chemokine Receptor CXCR2. *Chembiochem* 22:
- 22 1012-1019
- 23 Kuo JH, Chen YP, Liu JS, Dubrac A, Quemener C, Prats H, Bikfalvi A, Wu WG, Sue SC
- 24 (2013) Alternative C-terminal helix orientation alters chemokine function: structure of the anti-
- 25 angiogenic chemokine, CXCL4L1. *J Biol Chem* 288: 13522-13533

A.1. Additional findings on MIF's interaction with the chemokine network

bioRxiv preprint doi: <https://doi.org/10.1101/2021.11.26.470090>; this version posted February 24, 2022. The copyright holder for this preprint (which was not certified by peer review) is the author/funder, who has granted bioRxiv a license to display the preprint in perpetuity. It is made available under aCC-BY-NC-ND 4.0 International license.

- 1 Lacy M, Kontos C, Brandhofer M, Hille K, Groning S, Sinitski D, Bourilhon P, Rosenberg E,
- 2 Krammer C, Thavayogarah T *et al* (2018) Identification of an Arg-Leu-Arg tripeptide that
- 3 contributes to the binding interface between the cytokine MIF and the chemokine receptor
- 4 CXCR4. *Sci Rep* 8: 5171

- 5 Lasagni L, Grepin R, Mazzinghi B, Lazzeri E, Meini C, Sagrinati C, Liotta F, Frosali F,
- 6 Ronconi E, Alain-Courtois N *et al* (2007) PF-4/CXCL4 and CXCL4L1 exhibit distinct
- 7 subcellular localization and a differentially regulated mechanism of secretion. *Blood* 109:
- 8 4127-4134

- 9 Leng L, Metz CN, Fang Y, Xu J, Donnelly S, Baugh J, Delohery T, Chen Y, Mitchell RA,
- 10 Bucala R (2003) MIF signal transduction initiated by binding to CD74. *J Exp Med* 197: 1467-
- 11 1476

- 12 Lippi G, Franchini M, Targher G (2011) Arterial thrombus formation in cardiovascular
- 13 disease. *Nat Rev Cardiol* 8: 502-512

- 14 Ma F, Kouzoukas DE, Meyer-Siegler KL, Hunt DE, Leng L, Bucala R, Vera PL (2017)
- 15 Macrophage migration inhibitory factor mediates protease-activated receptor 4-induced
- 16 bladder pain through urothelial high mobility group box 1. *Physiol Rep* 5: e13549.

- 17 Michelet C, Danchin EGJ, Jaouannet M, Bernhagen J, Panstruga R, Kogel KH, Keller H,
- 18 Coustau C (2019) Cross-Kingdom Analysis of Diversity, Evolutionary History, and Site
- 19 Selection within the Eukaryotic Macrophage Migration Inhibitory Factor Superfamily. *Genes*
- 20 *(Basel)* 10: 740

- 21 Moerke NJ (2009) Fluorescence Polarization (FP) Assays for Monitoring Peptide-Protein or
- 22 Nucleic Acid-Protein Binding. *Curr Protoc Chem Biol* 1: 1-15

- 23 Muller I, Schonberger T, Schneider M, Borst O, Ziegler M, Seizer P, Leder C, Muller K, Lang
- 24 M, Appenzeller F *et al* (2013) Gremlin-1 Is an inhibitor of macrophage migration inhibitory

A. Appendix

bioRxiv preprint doi: <https://doi.org/10.1101/2021.11.26.470090>; this version posted February 24, 2022. The copyright holder for this preprint (which was not certified by peer review) is the author/funder, who has granted bioRxiv a license to display the preprint in perpetuity. It is made available under aCC-BY-NC-ND 4.0 International license.

- 1 factor and attenuates atherosclerotic plaque growth in ApoE^{-/-} Mice. *J Biol Chem* 288:
- 2 31635-31645

- 3 Murphy PM, Baggiolini M, Charo IF, Hebert CA, Horuk R, Matsushima K, Miller LH,
- 4 Oppenheim JJ, Power CA (2000) International union of pharmacology. XXII. Nomenclature
- 5 for chemokine receptors. *Pharmacol Rev* 52: 145-176

- 6 Nibbs RJ, Graham GJ (2013) Immune regulation by atypical chemokine receptors. *Nat Rev*
- 7 *Immunol* 13: 815-829

- 8 Niess JH, Brand S, Gu X, Landsman L, Jung S, McCormick BA, Vyas JM, Boes M, Ploegh
- 9 HL, Fox JG *et al* (2005) CX3CR1-mediated dendritic cell access to the intestinal lumen and
- 10 bacterial clearance. *Science* 307: 254-258

- 11 Noels H, Weber C, Koenen RR (2019) Chemokines as therapeutic targets in cardiovascular
- 12 disease. *Arterioscler Thromb Vasc Biol* 39: 583-592

- 13 Nording H, Baron L, Langer HF (2020) Platelets as therapeutic targets to prevent
- 14 atherosclerosis. *Atherosclerosis* 307: 97-108

- 15 Oppenheim JJ, Yang D (2005) Alarmins: chemotactic activators of immune responses. *Curr*
- 16 *Opin Immunol* 17: 359-365

- 17 Pawig L, Klasen C, Weber C, Bernhagen J, Noels H (2015) Diversity and Inter-Connections
- 18 in the CXCR4 Chemokine Receptor/Ligand Family: Molecular Perspectives. *Front Immunol*
- 19 6: 429

- 20 Polack B, Schved JF, Boneu B, Groupe d'Etude sur l'Hemostase et la T (2001) Preanalytical
- 21 recommendations of the 'Groupe d'Etude sur l'Hemostase et la Thrombose' (GEHT) for
- 22 venous blood testing in hemostasis laboratories. *Haemostasis* 31: 61-68

- 23 Rajasekaran D, Groning S, Schmitz C, Zierow S, Drucker N, Bakou M, Kohl K, Mertens A,
- 24 Lue H, Weber C *et al* (2016) Macrophage Migration Inhibitory Factor-CXCR4 Receptor

A.1. Additional findings on MIF's interaction with the chemokine network

bioRxiv preprint doi: <https://doi.org/10.1101/2021.11.26.470090>; this version posted February 24, 2022. The copyright holder for this preprint (which was not certified by peer review) is the author/funder, who has granted bioRxiv a license to display the preprint in perpetuity. It is made available under aCC-BY-NC-ND 4.0 International license.

- 1 Interactions: evidence for partial allosteric agonism in comparison with CXCL12 chemokine.
- 2 *J Biol Chem* 291: 15881-15895

- 3 Rohrl J, Yang D, Oppenheim JJ, Hehlgans T (2010) Specific binding and chemotactic activity
- 4 of mBD4 and its functional orthologue hBD2 to CCR6-expressing cells. *J Biol Chem* 285:
- 5 7028-7034

- 6 Sarabi A, Kramp BK, Drechsler M, Hackeng TM, Soehnlein O, Weber C, Koenen RR, Von
- 7 Hundelshausen P (2011) CXCL4L1 inhibits angiogenesis and induces undirected endothelial
- 8 cell migration without affecting endothelial cell proliferation and monocyte recruitment. *J*
- 9 *Thromb Haemost* 9: 209-219

- 10 Schiraldi M, Raucci A, Munoz LM, Livoti E, Celona B, Venereau E, Apuzzo T, De Marchis F,
- 11 Pedotti M, Bachi A *et al* (2012) HMGB1 promotes recruitment of inflammatory cells to
- 12 damaged tissues by forming a complex with CXCL12 and signaling via CXCR4. *J Exp Med*
- 13 209: 551-563

- 14 Schroder R, Janssen N, Schmidt J, Kebig A, Merten N, Hennen S, Muller A, Blattermann S,
- 15 Mohr-Andra M, Zahn S *et al* (2010) Deconvolution of complex G protein-coupled receptor
- 16 signaling in live cells using dynamic mass redistribution measurements. *Nat Biotechnol* 28:
- 17 943-949

- 18 Schurr Y, Sperr A, Volz J, Beck S, Reil L, Kusch C, Eiring P, Bryson S, Sauer M, Nieswandt
- 19 B *et al* (2019) Platelet lamellipodium formation is not required for thrombus formation and
- 20 stability. *Blood* 134: 2318-2329

- 21 Sinitski D, Kontos C, Krammer C, Asare Y, Kapurniotu A, Bernhagen J (2019) Macrophage
- 22 Migration Inhibitory Factor (MIF)-Based Therapeutic Concepts in Atherosclerosis and
- 23 Inflammation. *Thromb Haemost* 119: 553-566

- 24 Steen A, Larsen O, Thiele S, Rosenkilde MM (2014) Biased and G protein-independent
- 25 signaling of chemokine receptors. *Front Immunol* 5: 277

A. Appendix

bioRxiv preprint doi: <https://doi.org/10.1101/2021.11.26.470090>; this version posted February 24, 2022. The copyright holder for this preprint (which was not certified by peer review) is the author/funder, who has granted bioRxiv a license to display the preprint in perpetuity. It is made available under aCC-BY-NC-ND 4.0 International license.

- 1 Strüßmann T, Tillmann S, Wirtz T, Bucala R, von Hundelshausen P, Bernhagen J (2013)
- 2 Platelets are a previously unrecognised source of MIF. *Thromb Haemost* 110: 1004-1013
- 3 Struyf S, Salogni L, Burdick MD, Vandercappellen J, Gouwy M, Noppen S, Proost P,
- 4 Opdenakker G, Parmentier M, Gerard C *et al* (2011) Angiostatic and chemotactic activities of
- 5 the CXC chemokine CXCL4L1 (platelet factor-4 variant) are mediated by CXCR3. *Blood* 117:
- 6 480-488
- 7 Sun HW, Bernhagen J, Bucala R, Lolis E (1996) Crystal structure at 2.6-Å resolution of
- 8 human macrophage migration inhibitory factor. *Proc Natl Acad Sci U S A* 93: 5191-5196
- 9 Tillmann S, Bernhagen J, Noels H (2013) Arrest functions of the MIF ligand/receptor axes in
- 10 atherogenesis. *Front Immunol* 4: 115
- 11 Tilstam PV, Qi D, Leng L, Young L, Bucala R (2017) MIF family cytokines in cardiovascular
- 12 diseases and prospects for precision-based therapeutics. *Exp Opin Ther Targ* 21: 671-683
- 13 Vajda S, Yueh C, Beglov D, Bohnuud T, Mottarella SE, Xia B, Hall DR, Kozakov D (2017)
- 14 New additions to the ClusPro server motivated by CAPRI. *Proteins* 85: 435-444
- 15 von Hundelshausen P, Agten SM, Eckardt V, Blanchet X, Schmitt MM, Ippel H, Neideck C,
- 16 Bidzhekov K, Leberzammer J, Wichapong K *et al* (2017) Chemokine interactome mapping
- 17 enables tailored intervention in acute and chronic inflammation. *Sci Transl Med* 9
- 18 von Hundelshausen P, Petersen F, Brandt E (2007) Platelet-derived chemokines in vascular
- 19 biology. *Thromb Haemost* 97: 704-713
- 20 von Hundelshausen P, Weber C (2007) Platelets as immune cells: bridging inflammation and
- 21 cardiovascular disease. *Circ Res* 100: 27-40
- 22 Wakasugi K, Schimmel P (1999) Two distinct cytokines released from a human aminoacyl-
- 23 tRNA synthetase. *Science* 284: 147-151

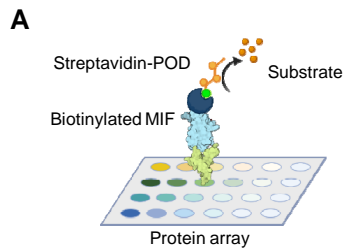
A.1. Additional findings on MIF's interaction with the chemokine network

bioRxiv preprint doi: <https://doi.org/10.1101/2021.11.26.470090>; this version posted February 24, 2022. The copyright holder for this preprint (which was not certified by peer review) is the author/funder, who has granted bioRxiv a license to display the preprint in perpetuity. It is made available under aCC-BY-NC-ND 4.0 International license.

- 1 Weber C, Kraemer S, Drechsler M, Lue H, Koenen RR, Kapurniotu A, Zernecke A,
- 2 Bernhagen J (2008) Structural determinants of MIF functions in CXCR2-mediated
- 3 inflammatory and atherogenic leukocyte recruitment. *Proc Natl Acad Sci U S A* 105: 16278-
- 4 16283
- 5 Weber C, Noels H (2011) Atherosclerosis: current pathogenesis and therapeutic options. *Nat*
- 6 *Med* 17: 1410-1422
- 7 Wirtz TH, Tillmann S, Strussmann T, Kraemer S, Heemskerk JW, Grottko O, Gawaz M, von
- 8 Hundelshausen P, Bernhagen J (2015) Platelet-derived MIF: a novel platelet chemokine with
- 9 distinct recruitment properties. *Atherosclerosis* 239: 1-10
- 10 Yan LM, Tatarek-Nossol M, Velkova A, Kazantzis A, Kapurniotu A (2006) Design of a mimic
- 11 of nonamyloidogenic and bioactive human islet amyloid polypeptide (IAPP) as nanomolar
- 12 affinity inhibitor of IAPP cytotoxic fibrillogenesis. *Proc Natl Acad Sci U S A* 103: 2046-2051
- 13 Zernecke A, Bernhagen J, Weber C (2008) Macrophage migration inhibitory factor in
- 14 cardiovascular disease. *Circulation* 117: 1594-1602
- 15 Zhou M, Li Q, Wang R (2016) Current Experimental Methods for Characterizing Protein-
- 16 Protein Interactions. *ChemMedChem* 11: 738-756
- 17 Ziegler-Heitbrock HW, Thiel E, Futterer A, Herzog V, Wirtz A, Riethmuller G (1988)
- 18 Establishment of a human cell line (Mono Mac 6) with characteristics of mature monocytes.
- 19 *Int J Cancer* 41: 456-461
- 20 Zlotnik A, Burkhardt AM, Homey B (2011) Homeostatic chemokine receptors and organ-
- 21 specific metastasis. *Nat Rev Immunol* 11: 597-606
- 22

A. Appendix

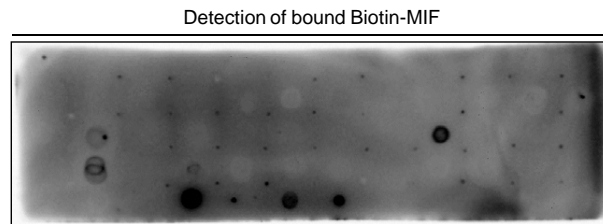
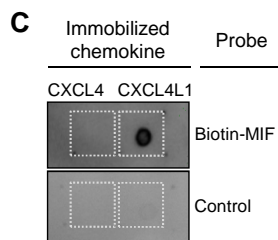
bioRxiv preprint doi: <https://doi.org/10.1101/2021.11.26.470090>; this version posted February 24, 2022. The copyright holder for this preprint (which was not certified by peer review) is the author/funder, who has granted bioRxiv a license to display the preprint in perpetuity. It is made available under aCC-BY-NC-ND 4.0 International license.



B

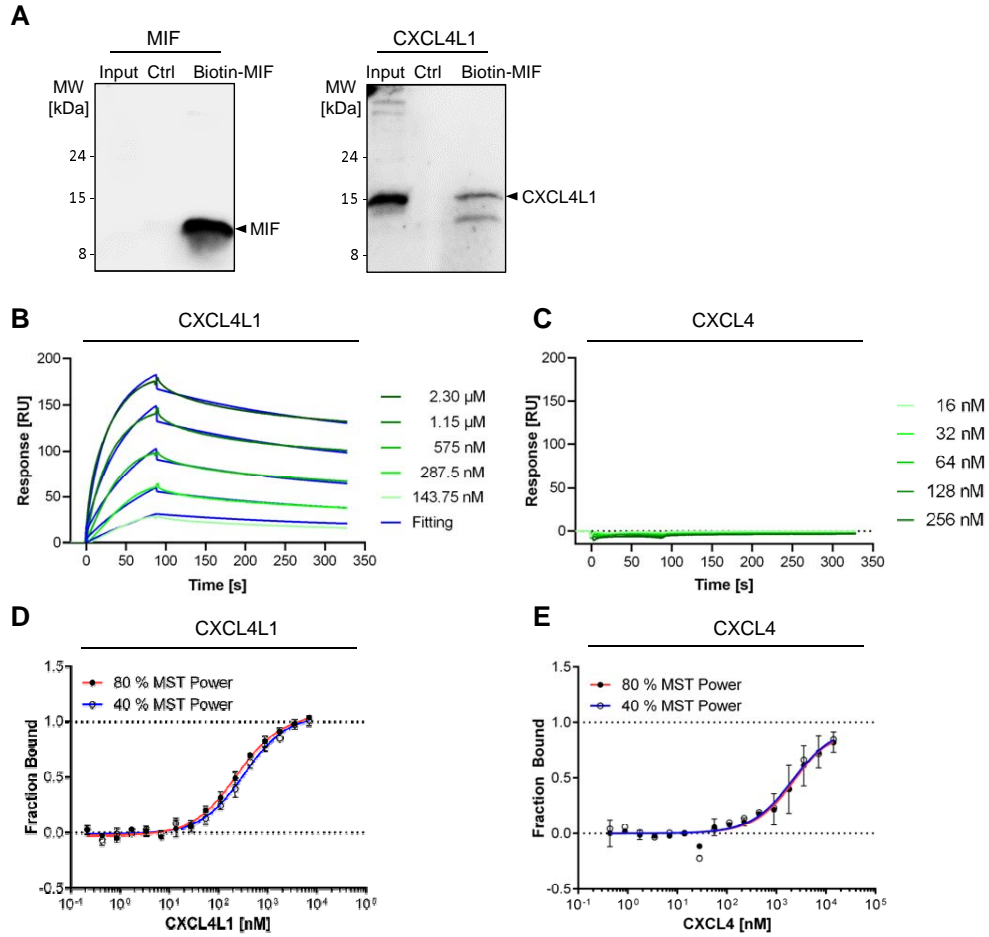
Immobilized chemokines

CCL1	CCL2	CCL3	CCL3L1	CCL4	CCL4L1	CCL5	CCL7	CCL8	CCL11	CCL12	CCL14
CCL15	CCL16	CCL17	CCL18	CCL19	CCL20	CCL21	CCL22	CCL23	CCL24	CCL25	CCL26
CCL27	CCL28	CCL1	CCL3	CXCL1	CXCL2	CXCL3	CXCL4	CXCL4L1	CXCL6	CXCL8	CXCL7
CXCL8	CXCL9	CXCL10	CXCL11	CXCL12a	CXCL12b	CXCL13	CXCL14	CXCL15	CXCL17	CXCL19	
MIP1E	MIP1	MIP2	IP10		IP10	MIP	MIP-2				



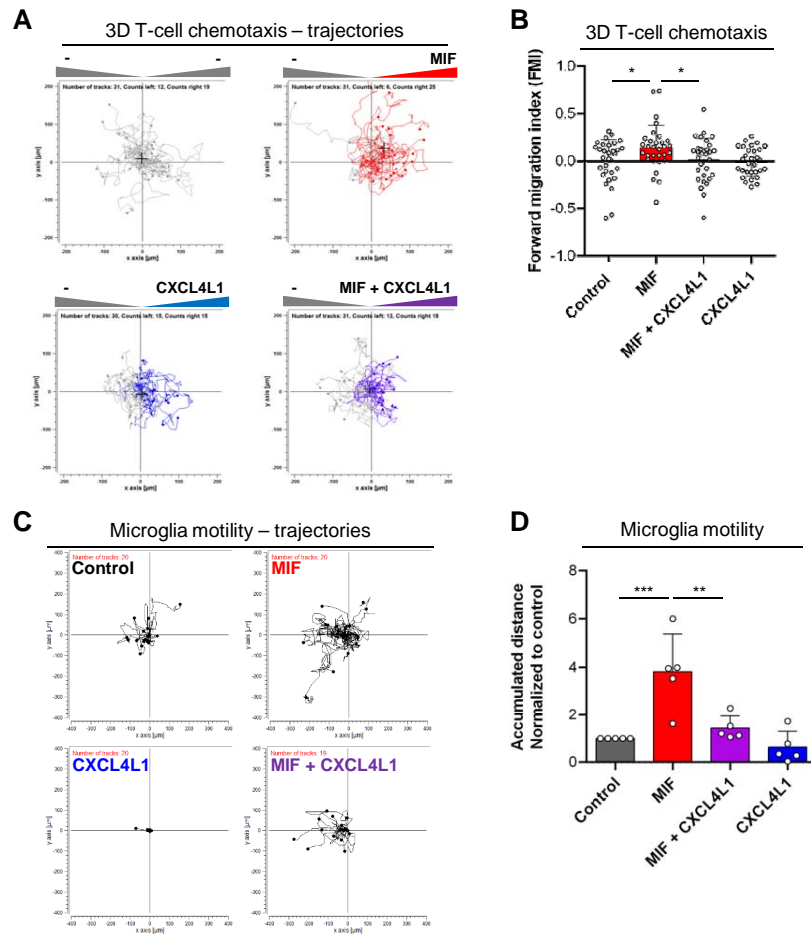
A.1. Additional findings on MIF's interaction with the chemokine network

bioRxiv preprint doi: <https://doi.org/10.1101/2021.11.26.470090>; this version posted February 24, 2022. The copyright holder for this preprint (which was not certified by peer review) is the author/funder, who has granted bioRxiv a license to display the preprint in perpetuity. It is made available under aCC-BY-NC-ND 4.0 International license.



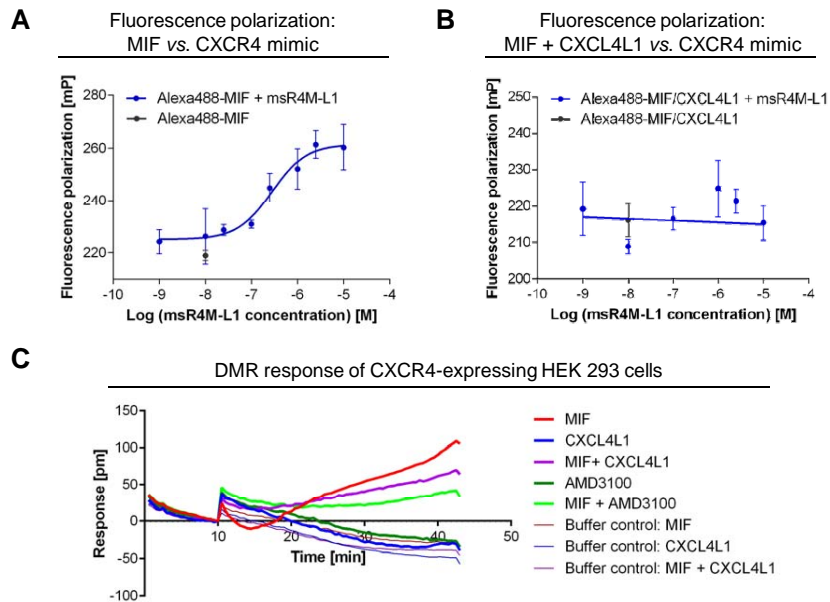
A. Appendix

bioRxiv preprint doi: <https://doi.org/10.1101/2021.11.26.470090>; this version posted February 24, 2022. The copyright holder for this preprint (which was not certified by peer review) is the author/funder, who has granted bioRxiv a license to display the preprint in perpetuity. It is made available under aCC-BY-NC-ND 4.0 International license.

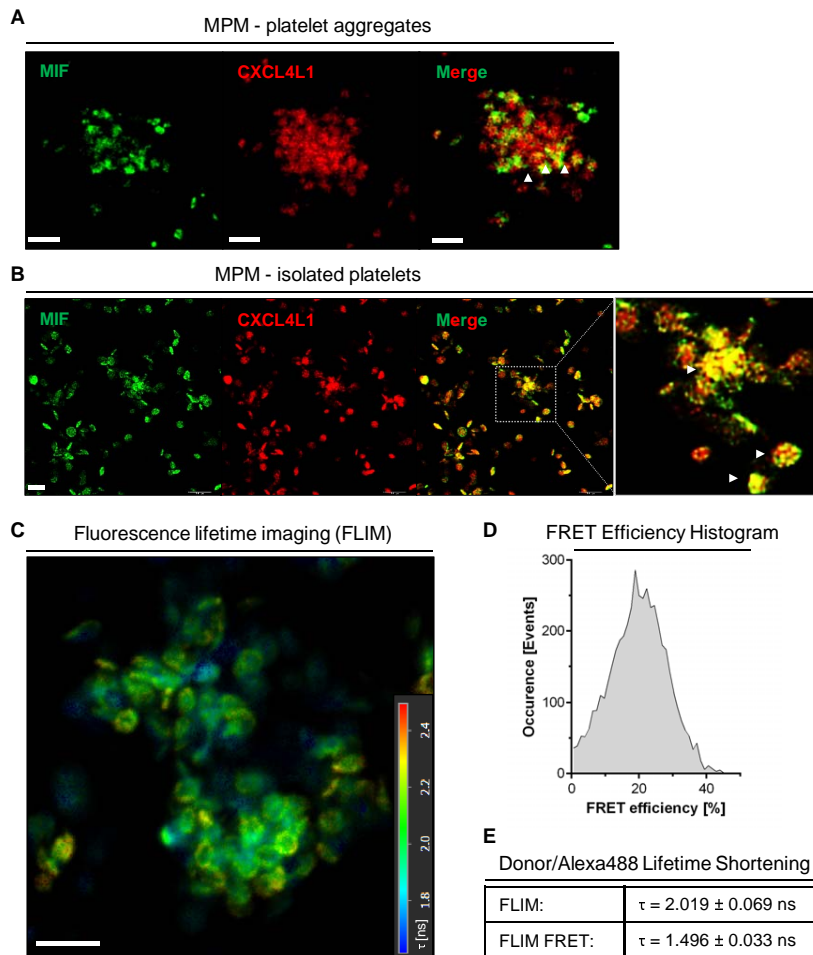


A.1. Additional findings on MIF's interaction with the chemokine network

bioRxiv preprint doi: <https://doi.org/10.1101/2021.11.26.470090>; this version posted February 24, 2022. The copyright holder for this preprint (which was not certified by peer review) is the author/funder, who has granted bioRxiv a license to display the preprint in perpetuity. It is made available under aCC-BY-NC-ND 4.0 International license.

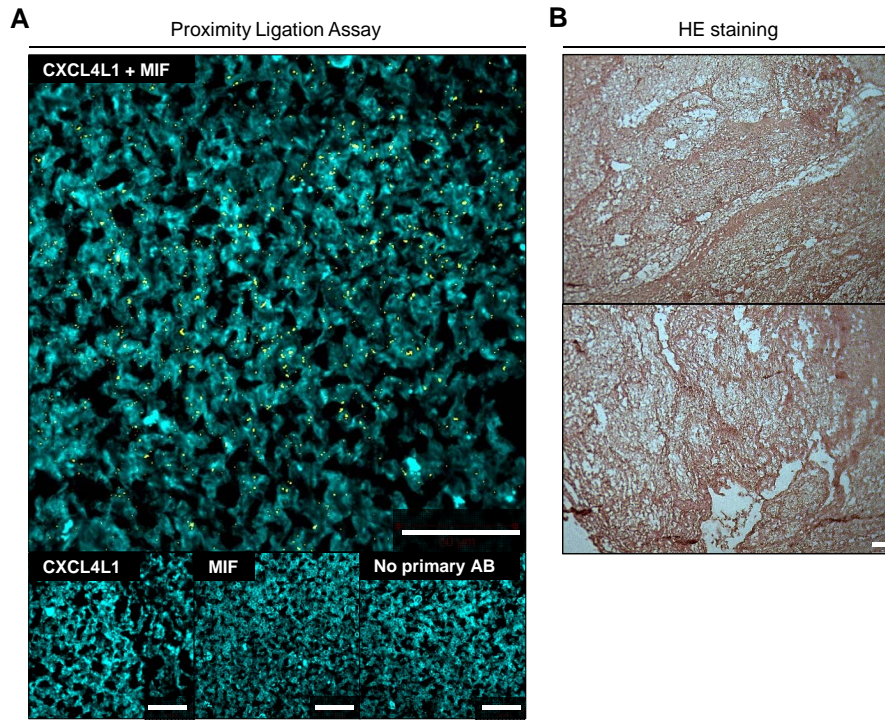


bioRxiv preprint doi: <https://doi.org/10.1101/2021.11.26.470090>; this version posted February 24, 2022. The copyright holder for this preprint (which was not certified by peer review) is the author/funder, who has granted bioRxiv a license to display the preprint in perpetuity. It is made available under aCC-BY-NC-ND 4.0 International license.

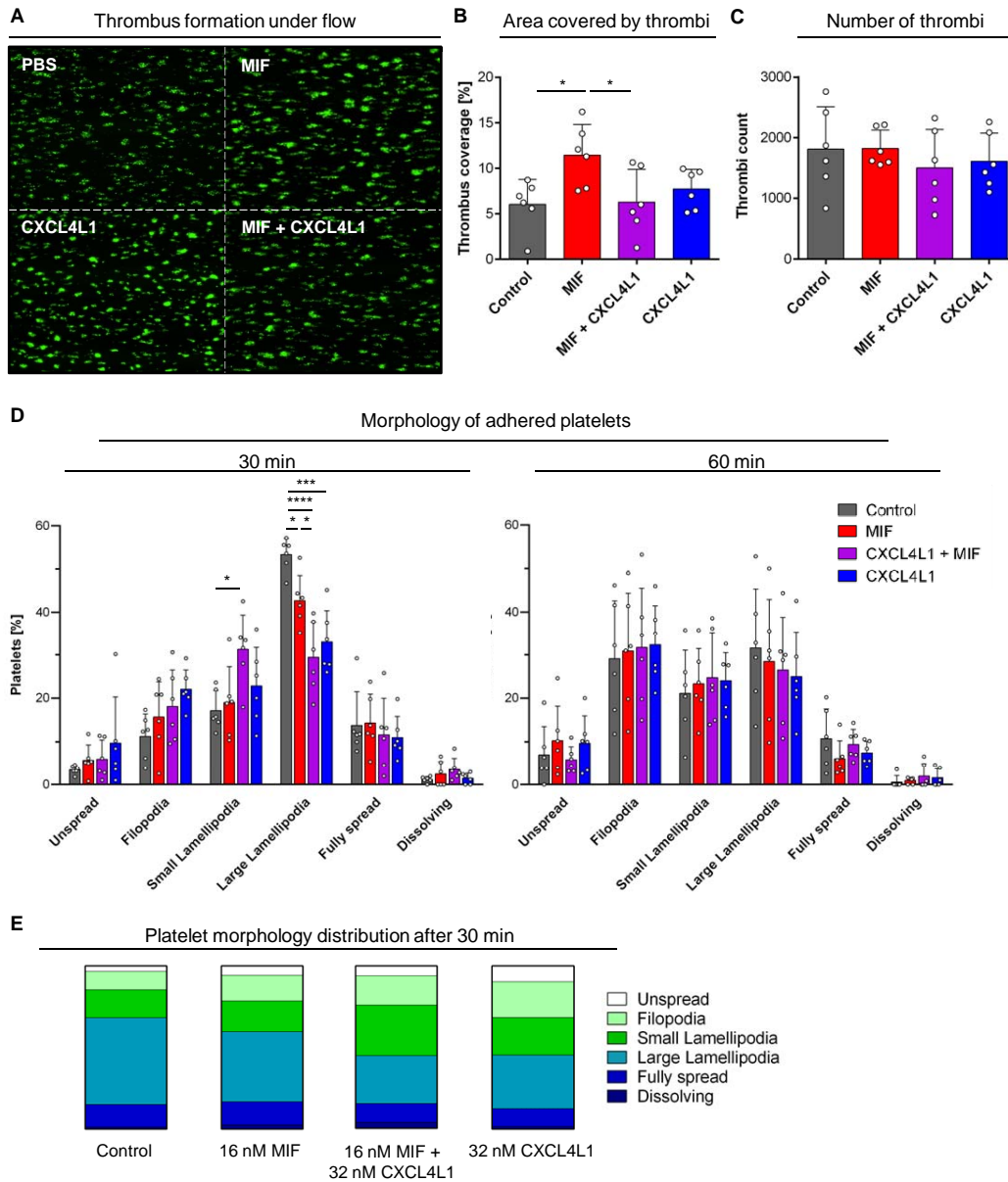


A.1. Additional findings on MIF's interaction with the chemokine network

bioRxiv preprint doi: <https://doi.org/10.1101/2021.11.26.470090>; this version posted February 24, 2022. The copyright holder for this preprint (which was not certified by peer review) is the author/funder, who has granted bioRxiv a license to display the preprint in perpetuity. It is made available under aCC-BY-NC-ND 4.0 International license.

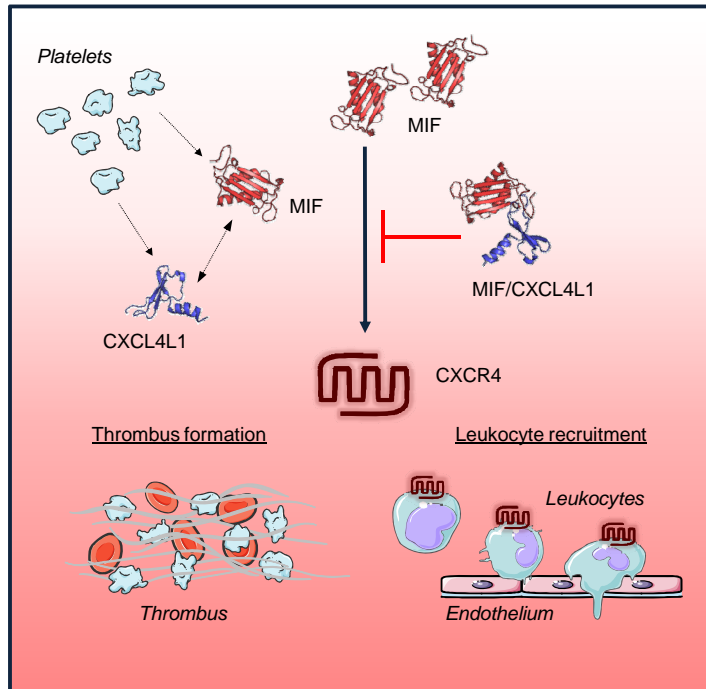


bioRxiv preprint doi: <https://doi.org/10.1101/2021.11.26.470090>; this version posted February 24, 2022. The copyright holder for this preprint (which was not certified by peer review) is the author/funder, who has granted bioRxiv a license to display the preprint in perpetuity. It is made available under aCC-BY-NC-ND 4.0 International license.



A.1. Additional findings on MIF's interaction with the chemokine network

bioRxiv preprint doi: <https://doi.org/10.1101/2021.11.26.470090>; this version posted February 24, 2022. The copyright holder for this preprint (which was not certified by peer review) is the author/funder, who has granted bioRxiv a license to display the preprint in perpetuity. It is made available under aCC-BY-NC-ND 4.0 International license.



A.1.3. Expression and purification of CXCL4L1 and isotope-labeled MIF for NMR spectroscopy studies

M. Brandhofer¹, H. Ippel², R. Koenen³, K. Mayo^{3,4}, C. Weber^{2,3,5}, J. Bernhagen^{1,5}

Affiliations: ¹: Institute for Stroke and Dementia Research (ISD), Klinikum der Universität München, Ludwig-Maximilians-Universität (LMU) München, Munich, Germany. ²: Cardiovascular Research Institute Maastricht (CARIM), Maastricht University, Maastricht, The Netherlands; ³: Institute for Cardiovascular Prevention (IPEK), Ludwig-Maximilians-Universität München, Munich, Germany. ⁴: Department of Biochemistry, Molecular Biology and Biophysics, Health Sciences Center, University of Minnesota, Minneapolis, MN, USA ⁵: German Center for Cardiovascular Research (DZHK), Partner Site Munich Heart Alliance, Munich, Germany.

Contributions: Design of study and technical expertise: RK, JB, KM, CW; Data analysis: HI, MB; protein purification: MB, NMR spectroscopy: HI.

Introduction

The identification of a possible heteromeric complex between the atypical chemokine MIF and the classical chemokine CXCL4L1 sparked not only questions of the functional relevance of such a complex, but also of its structure. The interaction interface of MIF and CXCL4L1 is of our special interest, as such information would not only provide insights into the conformation and structure of this complex, but could also lead to the development of peptides inhibiting the complex formation. Such inhibitors could be useful tools for a further investigation of the physiological relevance of this novel ACK/CK complex. While first information on the potential interaction interface was obtained by a peptide array approach and some initial molecular docking data (see section A.2.3), we planned to get a more detailed insight into complex formation by NMR spectroscopy. Here, we set out to recombinantly produce isotope-labeled human MIF – ¹⁵N-MIF as well as ¹³C-¹⁵N-MIF – to be mixed with recombinant human CXCL4L1 in varying concentrations to identify residues of MIF that are involved in the interaction with CXCL4L1.

Results

Expression and purification of CXCL4L1 Human CXCL4L1 was successfully expressed recombinantly in *E. coli* upon induction by IPTG, as evident by SDS-PAGE and Western Blot analysis of bacteria suspension samples taken before and after induction (data not shown). Bacteria pellets were harvested from multiple cultures and pooled for cell lysis and subsequent purification via FPLC using the His-Tag fused to the protein. After purification, analyzed via SDS-PAGE, CXCL4L1 presented itself in form of a double-band of around 10 kDa in size.

Chemical cleavage of the methionine-flanked histidine-tag by treatment with cyanogen bromide naturally led to a mixture of proteins with the tag either cleaved or still attached, making another purification step after cleavage necessary. This was done via FPLC, by removing the remaining tagged proteins using a HisTrap HP column to obtain untagged CXCL4L1 which was refolded by dialysis prior to a final purification step via size exclusion chromatography (SEC). A representative chromatogram of the final purification is shown in figure A.4. Here,

A.1. Additional findings on MIF's interaction with the chemokine network

fractions corresponding to three individual peaks A to C were collected and pooled accordingly. For comparison, also a protein sample that was not subjected to SEC was added to the SDS-PAGE / Western blot analysis, showing three distinct bands – two major bands in the range of 10 to 20 kDa, and a minor band of 8 kDa. From three collected peaks, only peak A and B showed a signal on Western Blots probed for either CXCL4L1 or the His-tag. While peak B consisted of three protein species and contained both tagged and untagged CXCL4L1, peak A only contained a minor amount of CXCL4L1 with the tag still present, and no further protein contaminants as apparent also by Coomassie staining of the polyacrylamide gel.

The amount of protein obtained after SEC is presented in table A.2. Based on these results, the protein fraction corresponding to peak A was chosen to be used in NMR spectroscopy studies, concentrated to 1.4 mg/ml.

Table A.2.: Yield of recombinant CXCL4L1 after final purification by size exclusion chromatography for each peak, as determined via Bradford assay.

Pooled Fractions	A ₅₉₅	c [µg/ml]	V [ml]	Protein amount [mg]
Peak A	0.475	336	26.0	8.75
Peak B	0.612	434	12.9	5.60
Peak C	0.226	160	3.5	0.75

Expression and purification of ¹⁵N-MIF Human Macrophage migration inhibitory factor (MIF) was successfully expressed recombinantly in *E. coli* upon induction by IPTG, as evident by routine SDS-PAGE and Western Blot analysis of bacteria suspension samples taken before and after induction (data not shown). Bacteria pellets were harvested from multiple cultures and pooled for cell lysis and subsequent purification via FPLC. Figure A.5 shows a representative chromatogram of the purification of MIF from bacteria raw extract, corresponding to roughly 800 ml of bacteria suspension, via anion exchange chromatography, together with SDS-PAGE and Western blot analysis of the obtained, pooled fractions from multiple chromatographic separations. The volume and protein concentration of the obtained fractions are listed in table A.3.

Table A.3.: Yield of recombinant ¹⁵N-MIF after initial purification by anion exchange chromatography, based on roughly 800 ml bacteria culture, as determined via Bradford assay. As the pooled fractions corresponding to peak 1 contained only faint amounts of protein and were not expected to contain MIF, based on prior experience, further analysis of these fractions was omitted. For diluted samples (peaks 2A, 2B and 3), absorbance measurements are given for the diluted sample, while subsequent information is presented for the undiluted sample.

Pooled Fractions	A ₅₉₅	c [µg/ml]	V [ml]	Protein amount [mg]
Peak 1	–	–	–	–
Peak 2A 1:2	0.704	998	6.0	5.9
Peak 2B 1:2	1.47	2085	6.5	13.5
Peak 3 1:2	0.795	1127	4.0	4.5
Peak 4	0.839	595	5.0	2.9
Peak 5	0.665	471	6.5	3.0

Out of the collected fractions during the anion exchange chromatography, those corresponding to peaks 2A and 2B were selected to be purified further via SEC, as they are the main MIF containing fractions. Since peak 2A shows a lower protein amount but higher purity of MIF

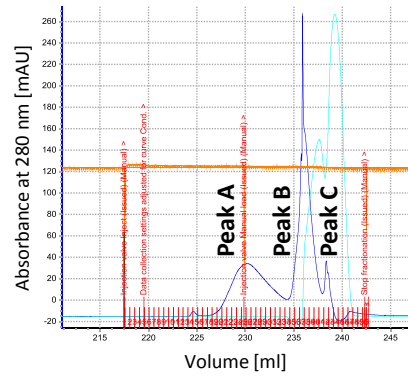
A. Appendix

compared to peak 2B, both samples were purified separately in order to obtain a high yield of MIF at a purity suitable for the planned NMR spectroscopy studies. Figure A.6 shows the corresponding chromatograms as well as the subsequent analysis of the pooled fractions of the observed peaks via SDS-PAGE followed by Coomassie staining and Western blot probed for human MIF. In the Coomassie staining, MIF presented itself as clear bands with a slightly lower molecular weight than the expected theoretical 12.5 kDa, the identity could however be confirmed by probing with an anti-MIF antibody in a Western blot. The amounts of protein obtained by size exclusion chromatography, as determined by Bradford assay of the pooled fractions corresponding to the indicated peaks (either from anion exchange chromatography peaks 2A or 2B) are given in table A.4. Out of the collected and analyzed samples, two – P2A-peak 3 and P2B-peak 2 – were selected for NMR spectroscopy studies and concentrated to 3.8 mg/ml and 11.6 mg/ml respectively.

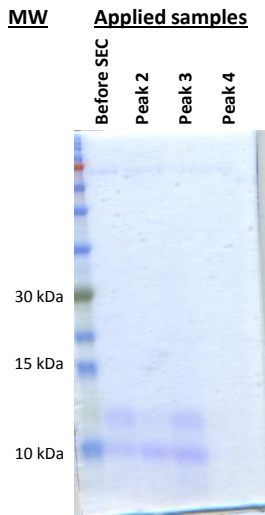
Table A.4.: Yield of recombinant ^{15}N -MIF after purification of previously collected fractions by SEC as determined via Bradford assay. For diluted samples, absorbance measurements are given for the diluted sample, while subsequent information is presented for the undiluted sample.

Pooled Fractions	A_{595}	c [$\mu\text{g}/\text{ml}$]	V [ml]	Protein amount [mg]
P2A-Peak 1	0.013	9	2.5	0.02
P2A-Peak 2	0.09	63	2.5	0.16
P2A-Peak 3	0.743	526	6.0	3.16
P2A-Peak 4	–	–	–	–
P2A-Peak 5	–	–	–	–
P2B-Peak 1	0.423	300	2.6	0.78
P2B-Peak 2 1:10	0.327	2319	3.7	8.58
P2B-Peak 3	0.01	7	1.0	0.01
P2B-Peak 4	–	–	–	–
P2B-Peak 5	–	–	–	–

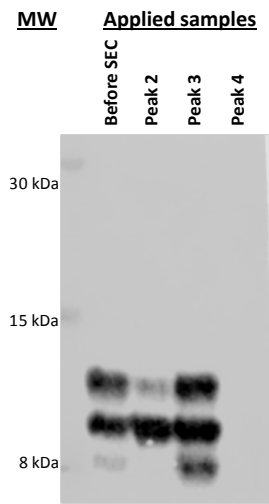
A.1. Additional findings on MIF's interaction with the chemokine network



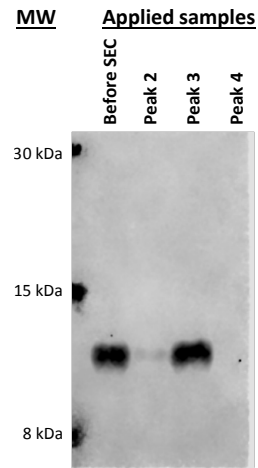
(a) Chromatogram: SEC of CXCL4L1



(b) Coomassie staining



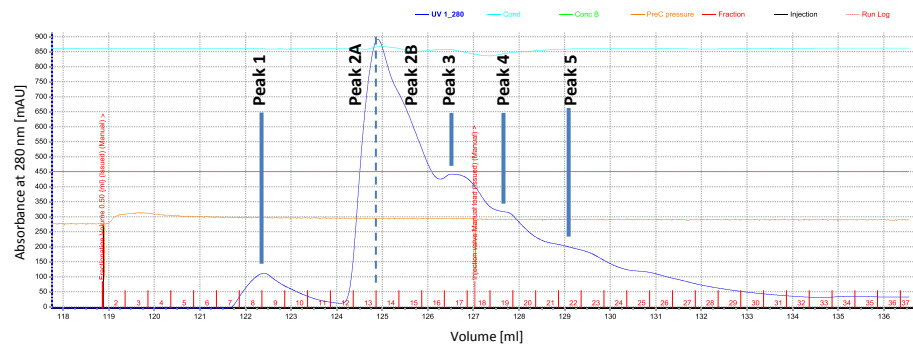
(c) Western blot against CXCL4L1



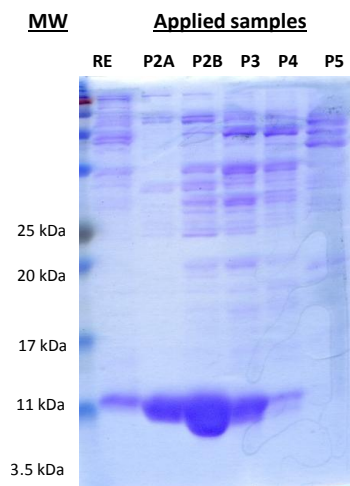
(d) Western blot against His-tag

Figure A.4.: Final purification of recombinant CXCL4L1 via size exclusion chromatography (SEC). Fractions corresponding to peaks A to C were pooled over multiple injections and subjected to SDS-PAGE and Western blot analysis. (a): Chromatogram (representative example) of CXCL4L1 after CNBr-cleavage, subjected to SEC. Blue: absorbance at 280 nm. Cyan: conductivity. Orange: pre-column pressure. Red: technical annotations. (b): Coomassie staining of pooled SEC fractions corresponding to peaks A to C, separated via SDS-PAGE. (c): Western blot of pooled SEC fractions, probed against CXCL4L1. (d): Western blot of pooled SEC fractions, probed against the Histidine-tag.

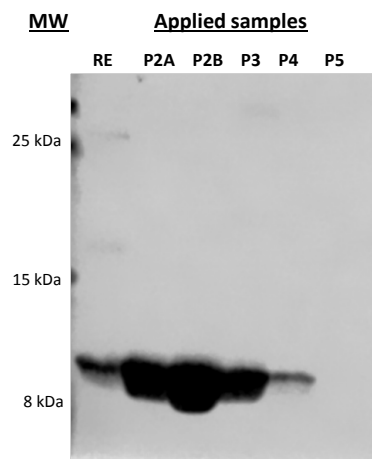
A. Appendix



(a) Chromatogram: Anion exchange chromatography of MIF



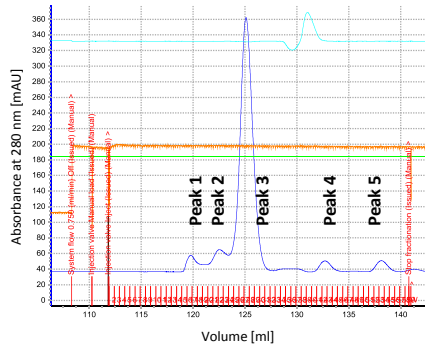
(b) Coomassie staining



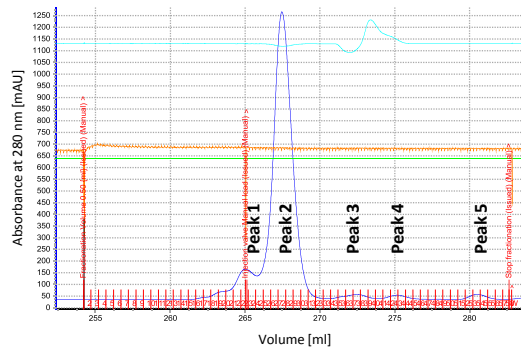
(c) Western blot against MIF

Figure A.5.: Anion exchange chromatography as first step to purify recombinant ^{15}N -MIF from bacteria lysates. Fractions corresponding to peaks 1 to 5 were pooled over multiple injections and subjected to SDS-PAGE and Western blot analysis. Left and right shoulder of peak 2 were collected separately. (a): Chromatogram (representative example) of ^{15}N -MIF, subjected to anion exchange chromatography. Blue: absorbance at 280 nm. Cyan: conductivity. Orange: pre-column pressure. Red: technical annotations. (b): Coomassie staining of pooled fractions corresponding to peaks 2A (P2A) to 5 (P5), compared to the raw bacteria extract (RE) prior to purification, separated via SDS-PAGE. Analysis of peak 1 was omitted due to a negligible protein content. (c): Western Blot of pooled fractions and the lysate before purification (RE), probed against MIF.

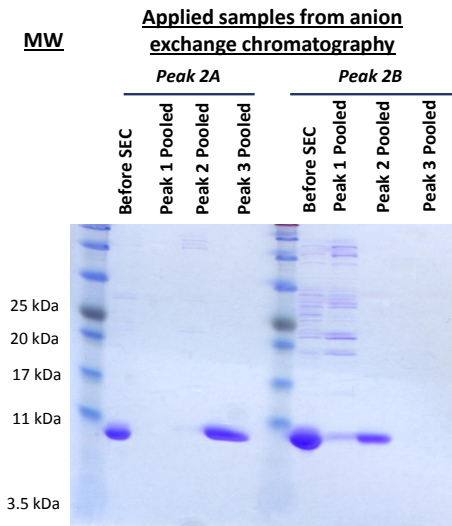
A.1. Additional findings on MIF's interaction with the chemokine network



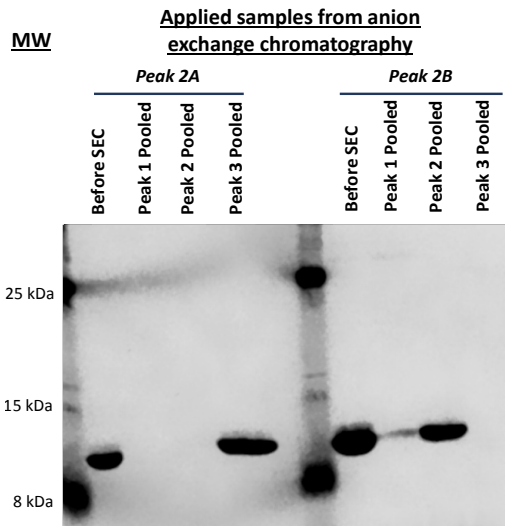
(a) Chromatogram:
SEC of MIF (Peak 2A from anion exchange chromatography)



(b) Chromatogram: SEC of MIF (Peak 2B from anion exchange chromatography)



(c) Coomassie staining



(d) Western blot against MIF

Figure A.6.: Size exclusion chromatography as second step to purify recombinant ^{15}N -MIF, after anion exchange chromatography. Fractions corresponding to peaks 1 to 5 were pooled over multiple injections and subjected to SDS-PAGE and Western Blot analysis. (a): Chromatogram (representative example of one sample injection) of ^{15}N -MIF-peak 2A, subjected to SEC. Blue: absorbance at 280 nm. Cyan: conductivity. Orange: pre-column pressure. Red: technical annotations. (b): Chromatogram (representative example of one sample injection) of ^{15}N -MIF-peak 2B, subjected to size exclusion chromatography. (c): Coomassie staining of pooled SEC fractions corresponding to peaks 1 to 3, compared to the sample prior to SEC, separated via SDS-PAGE. (d): Western blot, probed against MIF, of pooled SEC fractions corresponding to peaks 1 to 3, compared to the sample prior to SEC. Due to the negligible protein content, the fractions corresponding to peaks 4 and 5 were omitted.

Expression and purification of ^{15}N - ^{13}C -MIF To produce double-labeled ^{15}N - ^{13}C -MIF, *E. coli* expressing human MIF were first grown in LB medium according to standard protocol. After reaching a suitable amount of biomass, the cultivation medium was switched to M9 medium with isotope labeled ammonium chloride and glucose as the sole nitrogen and carbon source, respectively. To minimize the carryover of nutrients from complex LB to minimal M9 medium, the cells were washed with M9 salt solution in between and deprived of glucose prior to induction of MIF expression by IPTG. This cultivation scheme as well as *E. coli* growth and glucose concentration in the media is depicted in figure A.7.

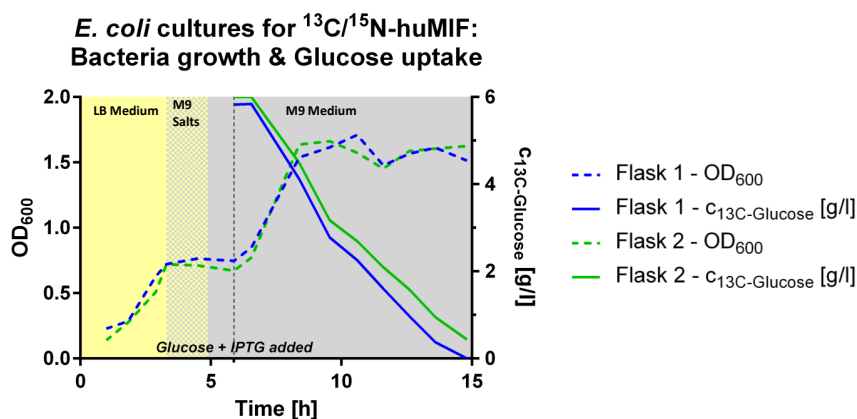


Figure A.7.: Overview of the bacteria cultivation procedure to obtain double isotope labeled ^{15}N - ^{13}C -MIF. In two flasks, *E. coli* expressing human MIF under the control of an IPTG inducible promoter were first cultivated in LB medium. Bacteria were washed in M9 salt solution to remove the nutrient rich LB medium and subsequently cultured in M9 medium with $^{15}\text{NH}_4\text{Cl}$ as their sole nitrogen source. After a starvation period to deplete intracellular carbon sources, isotope labeled glucose was added to the medium, MIF expression induced and the bacteria were cultivated until depletion of the added glucose.

The subsequent purification of ^{15}N - ^{13}C -MIF was performed by initial anion exchange chromatography followed by a second purification step via size exclusion chromatography, as for ^{15}N -MIF. Figure A.8 shows SDS-PAGE and Western blot analysis of the fractions obtained during anion exchange chromatography, as well as a representative chromatogram of one sample injection. The obtained protein amount for each peak is presented in table A.5. As evident by Coomassie staining and the Western blot probed against MIF, the pooled fractions corresponding to peak 2 contain the desired protein, together with some impurities, while the larger peak 3 consists predominantly of other proteins with a higher molecular weight. Accordingly, the pooled peak 2 fractions were chosen for subsequent purification by size exclusion chromatography to separate MIF from higher molecular weight contaminants.

Table A.5.: Yield of recombinant ^{15}N - ^{13}C -MIF after initial purification by anion exchange chromatography, as determined via Bradford assay.

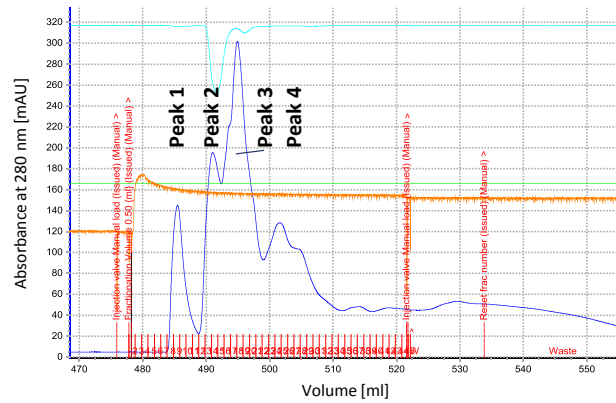
Pooled Fractions	A_{595}	c [$\mu\text{g}/\text{ml}$]	V [ml]	Protein amount [mg]
Peak 1	0.049	36.5	5.0	0.2
Peak 2	0.631	618.9	4.0	2.5
Peak 3	0.603	591.3	7.5	4.4
Peak 4	0.285	267.5	9.5	2.5

A.1. Additional findings on MIF's interaction with the chemokine network

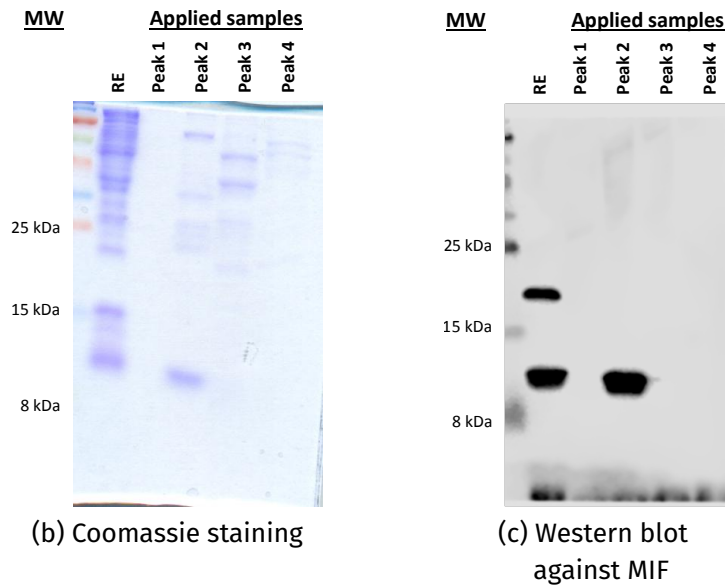
The results of this final purification step – a representative SEC chromatogram together with SDS-PAGE / Coomassie staining and Western blot analysis of the obtained, pooled fractions – is shown in figure A.9, while table A.6 shows the amount of protein obtained from each peaks collected and pooled fractions. These results indicate that higher molecular weight contaminants of MIF from the previous purification step could be separated from MIF and form the majority of peak 2, while peak 3 contains recombinant MIF at a high purity. Therefore, the pooled fractions of this peak were selected for NMR spectroscopy studies and concentrated to 1.95 mg/ml.

Table A.6.: Yield of recombinant ^{15}N - ^{13}C -MIF after additional purification by size exclusion chromatography, as determined via Bradford assay.

Pooled Fractions	A_{595}	c [$\mu\text{g}/\text{ml}$]	V [ml]	Protein amount [mg]
Peak 1	0.049	39	2.0	0.08
Peak 2	0.196	189	3.5	0.66
Peak 3	0.240	239	4.5	1.08
Peak 4	–	–	–	–
Peak 5	–	–	–	–



(a) Chromatogram:
Anion exchange chromatography of ^{15}N - ^{13}C -MIF

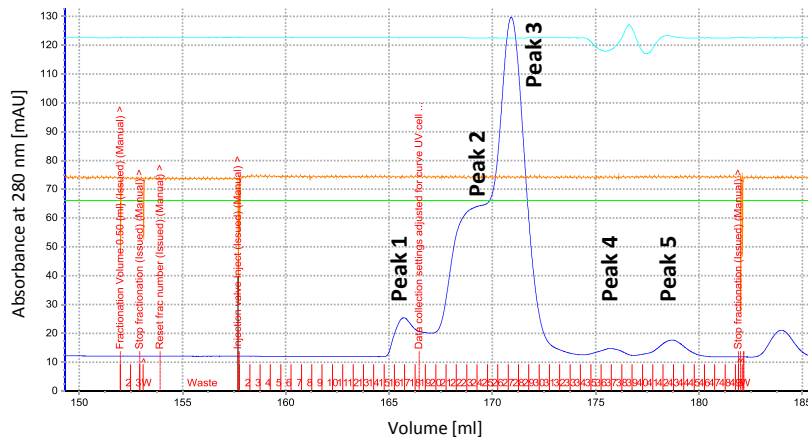


(b) Coomassie staining

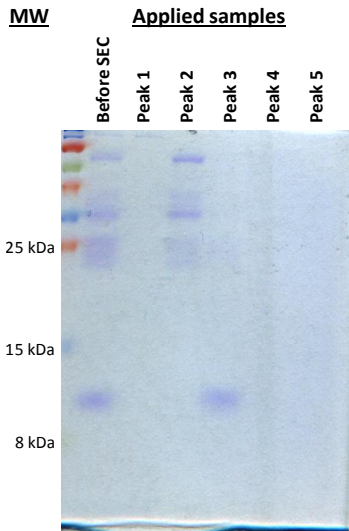
(c) Western blot
against MIF

Figure A.8.: Anion exchange chromatography as first step to purify recombinant ^{15}N - ^{13}C -MIF-MIF from bacteria lysates. Fractions corresponding to peaks 1 to 4 were pooled over multiple injections and subjected to SDS-PAGE and Western blot analysis. (a): Chromatogram (representative example) of ^{15}N - ^{13}C -MIF, subjected to anion exchange chromatography. Blue: absorbance at 280 nm. Cyan: conductivity. Orange: pre-column pressure. Red: technical annotations. (b): Coomassie staining of pooled fractions corresponding to peaks 1 to 4, compared to the raw bacteria extract (RE) prior to purification, separated via SDS-PAGE. (c): Western blot of pooled fractions and the lysate before purification (RE), probed against MIF.

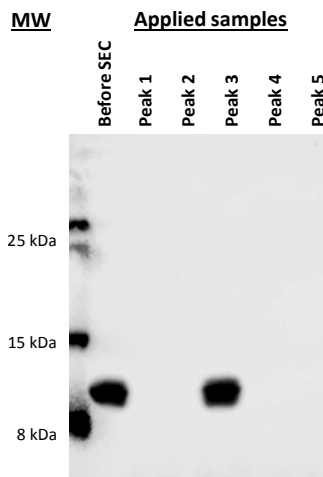
A.1. Additional findings on MIF's interaction with the chemokine network



(a) Chromatogram: Size exclusion chromatography of ^{15}N - ^{13}C -MIF



(b) Coomassie staining



(c) Western blot against MIF

Figure A.9.: Size exclusion chromatography as second step to purify recombinant ^{15}N - ^{13}C -MIF-MIF after anion exchange chromatography. Fractions corresponding to peaks 1 to 5 were pooled over two injections and subjected to SDS-PAGE and Western blot analysis. (a): Chromatogram (representative example of one sample injection) of ^{15}N - ^{13}C -MIF, subjected to SEC. Blue: absorbance at 280 nm. Cyan: conductivity. Orange: pre-column pressure. Red: technical annotations. (b): Coomassie staining of pooled fractions corresponding to peaks 1 to 5, compared to sample prior to SEC, separated via SDS-PAGE. (c): Western blot of pooled fractions and the sample before SEC, probed against MIF.

Discussion

The recombinant expression of histidine-tagged human CXCL4L1 in *E. coli*, as well as the initial purification from bacteria lysates by immobilized metal affinity chromatography (IMAC) was performed successfully. However, as the chemokine CXCL4L1 was deposited in inclusion bodies and the tag was to be removed prior to NMR spectroscopy, some additional processing and purification steps had to be performed. As evident by the existence of three protein bands after SDS-PAGE separation of the crude CXCL4L1 after removing of the tag and refolding, and prior to the final SEC purification, two aspects of the purification protocol could be optimized further to enhance yield and purity of the obtained protein. First, the presence of His-tagged CXCL4L1 before and to a minor amount also after the final size exclusion chromatography indicates that both the cleavage of the tag by CNBr as well as the removal of remaining tagged protein by IMAC were not 100% efficient. Second, the presence of multiple bands after CNBr treatment, differing in apparent molecular weight (MW) by more than what would correspond to the presence or absence of the roughly 1 kDa tag – as well as the molecular weight of the final CXCL4L1 appearing at a higher MW on the polyacrylamide gel than expected from its theoretical MW – can be seen as an indication for protein degradation and/or modification during the CNBr treatment. The chemical cleavage reaction was performed for a prolonged time at a low pH at room temperature, which was necessary for the reaction but adverse effects on the integrity of the protein cannot be ruled out. To avoid such harsh conditions, an expression construct that facilitates enzymatic cleavage of the tag could be constructed, or one could opt to purify recombinantly expressed CXCL4L1 by capitalizing on CXCL4L1's physicochemical properties, i.e. by HPLC, or a FPLC system equipped with heparin or cation exchange columns instead of an approach using an affinity tag [36, 154].

Production of isotope labeled human MIF was successful following standard protocols, with a yield and purity in the expected range based on routine purifications of (unlabeled) MIF in the lab. However, during these purifications the importance of the precise pH of the buffer used for anion exchange chromatography was demonstrated. According to standard protocol, MIF is subjected to anion exchange chromatography at pH 7.5. Under this condition, the charge of MIF allows it to pass the column while most other proteins are retained. In an attempt to optimize this protocol, an initial batch of MIF was purified at a lower pH (pH 7.2) to minimize interactions of MIF with the stationary phase. As became evident later on in the obtained NMR spectroscopy data recorded for peak assignment and was further verified by mass spectrometry, the MIF sample contained two species of MIF protein, one of which showed a higher molecular weight corresponding to an additional methionine residue. Additional experiments and data from previous studies indicate that in bacteria, removal of the initial methionine of recombinantly expressed MIF might not happen completely, leading to the existence of two MIF variants (data not shown). According to calculations³, the theoretical isoelectric point (IEP) of “methionine-MIF”⁴ is 7.73 as opposed to 8.24 for MIF⁵. As a consequence, purification at a lower pH might reduce interactions of “methionine-MIF” with the column enough so that it gets co-purified together with the desired MIF without the initial methionine. When changing the pH of the buffer back to 7.5, a sufficiently pure preparation of human MIF was again obtained, as evident by mass spectrometry.

³Theoretical IEP calculated with the Expasy “Compute pI/Mw tool”, based on the amino acid residues 2 to 115 or 1 to 115 of UniProtKB entry of human MIF (P14174) [152].

⁴Sequence MPMFI . . . ; MW 12 476.3 Da

⁵Sequence PMFI . . . ; MW 12 345.1 Da

A.1. Additional findings on MIF's interaction with the chemokine network

NMR spectroscopy studies with the supplied proteins, performed in our collaborator's lab, are currently ongoing. The peak-assignments for isotope labeled MIF were largely successful and the recorded spectra from both ^{15}N -MIF and ^{15}N - ^{13}C -MIF indicate correct folding of the protein in comparison with previous findings [92]. The titration experiments where MIF is analyzed together with CXCL4L1, in which we planned to detect backbone perturbations of isotope labeled MIF upon complex formation need to be optimized further. Preliminary data shows MIF to be present as a stable trimer at concentrations and pH levels suitable for NMR spectroscopy, which could potentially hinder complex formation with CXCL4L1, assuming the presence of monomeric MIF is needed for interaction with CXCL4L1. CXCL4L1, in turn, shows a propensity to form aggregates at higher concentrations. In first experiments, slight perturbations of some residues corresponding to central beta-strand regions of MIF could be observed upon addition of CXCL4L1, however at this point these results could not be reproduced with a second batch of purified proteins. Taken together, further optimization of the experimental setup is necessary to gain robust NMR data on the MIF/CXCL4L1 complex. Apart from NMR spectroscopy, the structure and stoichiometry of the MIF/CXCL4L1 complex could also be elucidated by other methods such as, e.g., cross-linking experiments *in vitro*, analytical size exclusion chromatography of formed complexes or, ultimately, x-ray crystallography.

Methodology

Reagents: All reagents and chemicals, unless stated otherwise, were purchased from Merck, Carl Roth, VWR, Thermo Fisher Scientific, Bio-Rad Laboratories or Sigma-Aldrich in an appropriate purity.

Recombinant expression and purification of human CXCL4L1 in *E. coli*: Recombinant CXCL4L1 was either provided by the lab of R. Koenen (to be used for NMR spectroscopy together with ^{15}N - ^{13}C -MIF) or produced in the lab of J. Bernhagen according to a protocol kindly provided by P. von Hundelshausen and X. Blanchet as described here. Briefly, *E. coli* (Rosetta-Gami 2), transformed with a pET21a plasmid to recombinantly express human CXCL4L1 with a N-terminal 6×histidine-tag flanked with methionine residues, were cultivated over night in LB-medium with added ampicillin, tetracycline and chloramphenicol at 37 °C under gentle agitation. From these overnight cultures, new cultures were inoculated at a ratio of 1:400. When an absorbance at 600 nm of 0.8 was reached, CXCL4L1 expression was induced by adding solid isopropyl β -D-1-thiogalactopyranoside (IPTG) to a final concentration of 1 mM. After an additional incubation for 4 to 5 hours, bacteria were harvested by centrifugation and bacteria pellets were stored at $-20\text{ }^{\circ}\text{C}$ until purification. To purify histidine-tagged CXCL4L1, bacteria pellets were resuspended in lysis buffer (20 mM Tris, pH 8.0, 0.5 M NaCl, 5 mM ethylenediaminetetraacetic acid (EDTA), 0.1 % Triton X-100) and mechanically lysed using a French Press type homogenizer (Emulsiflex C5, Avestin Europe GmbH, Mannheim, Germany). Inclusion bodies, containing CXCL4L1, were separated from the lysate by centrifugation, washed with lysis buffer with and without detergent and denatured by stirring over night in 6 M guanidine hydrochloride, 50 mM Tris-HCl pH 8.0, 0.5 M NaCl and 10 mM dithiothreitol (DTT). Histidine-tagged CXCL4L1 was purified from the solubilized inclusion bodies via FPLC using a His-Trap HP column (Cytiva Europe GmbH, Freiburg, Germany) (binding buffer: 6 M guanidine hydrochloride, 50 mM Tris-HCl pH 8.0; Elution buffer: 6 M guanidine hydrochloride, 50 mM Tris-HCl pH 8.0, 0.5 M imidazole. The obtained protein was dialyzed against 0.1 % trifluoroacetic acid (TFA) and lyophilized. The methionine-flanked histidine-tag was removed by chemical cleavage with cyanogen bromide in a 400-fold molar

A. Appendix

excess in 1 M HCl and 6 M guanidine hydrochloride, while stirring gently for at least 24 h. Cleaved, untagged CXCL4L1 was separated from uncleaved protein via FPLC on a His-Trap HP column as stated above. Absence of the tag was verified by SDS-PAGE and Western blotting according to standard protocols. CXCL4L1 devoid of residual His-tag was refolded by dialysis against refolding buffer (50 mM Tris-HCl pH 8.0, 0.5 M NaCl, 0.9 M guanidin hydrochloride, 5 mM cysteine, 5 mM methionine). Refolded CXCL4L1 was subjected to a final purification and buffer exchange to 20 mM KCl, pH 6.9, by size exclusion chromatography (SEC) on a Superdex 75 10/300 GL column (Cytiva Europe GmbH) at a flow rate of 0.75 ml/min.

Recombinant expression of isotope labeled human MIF in *E. coli*: To produce isotope-labeled human MIF, M9 minimal medium was inoculated at a ratio of 1:500 with over-night cultures of *E. coli* BL21(DE3), transfected with a pET11b vector designed to recombinantly express human MIF under the control of an IPTG-inducible promotor, as published previously [92]. To produce ¹⁵N-MIF, ¹⁵N ammonium chloride was used at 1 g/l as the only nitrogen source. Bacteria were cultured at 37 °C while shaking to an absorbance at 600 nm of 0.7 to 0.8 was reached. MIF expression was then induced by adding solid IPTG to a concentration of 1 mM and the bacteria were incubated for 4 h until harvested by centrifugation. Bacteria pellets were stored at –20 °C until purification. For ¹⁵N-¹³C-MIF, bacteria were grown under the conditions stated above in LB medium until an absorbance at 600 nm of 0.7 to 0.8. Then, cells were centrifuged, washed with M9 salt solution, resuspended and further cultivated in M9 minimal medium without glucose and with ¹⁵N ammonium chloride as the sole nitrogen source. After an 1 h starvation period to deplete intracellular carbon sources, ¹³C6-D-glucose (Cambridge Isotope Laboratories, Inc., Andover, MA, USA) was added to the medium to a final concentration of 5 g/l and MIF expression was induced by IPTG as stated above. After induction, the glucose concentration in the medium was monitored in regular intervals using a commercial blood glucose meter (Contour[®] XT device and Contour[®] Next sensor strips, Ascensia Diabetes Care Deutschland GmbH, Leverkusen, Germany). When all glucose in the medium was taken up, cultivation was stopped and bacteria were harvested by centrifugation.

Purification of isotope labeled MIF by FPLC: Recombinant human MIF, both ¹⁵N-labeled and ¹⁵N-¹³C-labeled, was purified via FPLC, essentially as described previously, to a typical purity of ≈90 % as confirmed by analysis via SDS-PAGE and Coomassie-staining [113, 153]. After purification of MIF from bacteria lysates via FPLC on an anion exchange chromatography column (Mono Q 10/100 GL, Cytiva Europe GmbH) at pH 7.5 and a flow rate of 0.5 ml/min, MIF-containing fractions were pooled and subjected to SEC (Superdex 75 10/300 GL, Cytiva Europe GmbH) in 20 mM sodium phosphate buffer, pH 7.2, with 150 mM NaCl at a flow rate of 0.75 ml/min for further purification. MIF-containing fractions were pooled and the buffer was exchanged to 20 mM KCl, pH 6.9. For ¹⁵N-¹³C-labeled huMIF, the buffer exchange was performed during SEC.

SDS-PAGE and Western blot analysis of proteins: Protein samples collected during various protein purification steps were analyzed by SDS-PAGE followed by Coomassie staining and Western blot analysis following standard protocols and manufacturer instructions. Briefly, protein samples were mixed with Invitrogen[™] NuPAGE[™] LDS sample buffer (Thermo Fisher Scientific GmbH, Dreieich, Germany) and heated to 95 °C for at least 10 min prior to loading on a 15 % or 20 % polyacrylamide gel, depending on the size of the protein to be analyzed.

A.1. Additional findings on MIF's interaction with the chemokine network

Electrophoresis was performed using the Invitrogen™ Mini Gel Tank system according to the user manual. For Coomassie staining, the gel was incubated over night in Coomassie Brilliant Blue R-250 staining solution (Bio-Rad Laboratories GmbH, Feldkirchen, Germany), destained by shaking in 40 % methanol and 10 % acetic acid in aqueous solution at room temperature and imaged on a commercial flatbed document scanner (HP Scanjet G3110, HP Deutschland GmbH, Böblingen, Germany). For Western blot transfer of proteins onto a Amersham™ Protran™ 0.2 µm nitrocellulose membrane (Cytiva Europe GmbH), Invitrogen™ Mini Blot modules were used. After transfer, membranes were blocked for 1 h in blocking buffer (1 % BSA in TBS-T: 20 mM Tris, 150 mM NaCl, pH 7.3, with 0.1 % Tween-20) and incubated over night at 4 °C with either a rabbit-derived polyclonal antibody against human MIF (Ka565 [113]), a rabbit-derived polyclonal antibody against human CXCL4L1 (PA5-21944, Thermo Fisher Scientific) or a mouse-derived monoclonal anti-6×His tag antibody (Clone 4E3D10H2/E3, Thermo Fisher Scientific), diluted in blocking buffer according to manufacturer instructions. Proteins were revealed using fluorescently labeled secondary antibodies raised against the species of the primary antibody (IRDye® 800CW Secondary Antibodies, LI-COR Biosciences GmbH, Bad Homburg, Germany) and the Western blot membranes were imaged on a LI-COR Odyssey Fc imaging system at the appropriate NIR channel.

Protein content measurement: The protein content of different fractions obtained during protein purifications via FPLC techniques was determined by a colorimetric assay based on the Bradford method [155]. This was done using the Bio-Rad Protein Assay Dye Reagent Concentrate (Bio-Rad Laboratories GmbH, Feldkirchen, Germany) according to manufacturer instructions. The absorbance at 595 nm was measured in polystyrene semi-micro cuvettes (BRAND GmbH + CO KG, Wertheim, Germany) on a JASCO V-650 spectrophotometer (JASCO Deutschland GmbH, Pfungstadt, Germany).

Acknowledgements

E. coli, recombinantly expressing human His-tagged CXCL4L1, were kindly provided by P. von Hundelshausen. We thank the lab of A. Kapurniotu for providing LC-MS and MALDI-TOF analyses of various batches of purified isotope labeled MIF.

A.2. Supplementary data

This section contains supplementary data files, which are part of the publications listed under chapter 2 as well as the manuscript found in section A.1.2.

A.2.1. Supplementary data for Lacy *et al.*, 2018

Supplemental information; Lacy et al., 2018

Identification of an Arg-Leu-Arg tripeptide that contributes to the binding interface between the cytokine MIF and the chemokine receptor CXCR4

Michael Lacy^{1,§}, Christos Kontos^{2,§}, Markus Brandhofer^{1,§}, Kathleen Hille², Sabine Gröning³, Dzimtry Sinitski¹, Priscila Bourilhon¹, Eric Rosenberg⁴, Christine Krammer¹, Tharshika Thavayogarajah¹, Georgios Pantouris⁴, Maria Bakou², Christian Weber^{5,6,7}, Elias Lolis⁴, Jürgen Bernhagen^{1,6,8,*}, Aphrodite Kapurniotu^{2,*}

¹Department of Vascular Biology, Institute for Stroke and Dementia Research, Klinikum der Universität München, Ludwig-Maximilians-University of Munich, Feodor-Lynen-Str. 17, D-81377 Munich, Germany; ²Division of Peptide Biochemistry, Technische Universität München, D-85354 Freising-Weihenstephan, Germany; ³Department of Anaesthesiology, RWTH Aachen University Hospital, D-52074 Aachen, Germany; ⁴Department of Pharmacology, Yale University School of Medicine, 333 Cedar Street, New Haven, CT, USA; ⁵Institute for Cardiovascular Prevention, Klinikum der Universität München, Ludwig-Maximilians-University of Munich, Pettenkofer Str. 8, D-80336 Munich, Germany; ⁶Munich Heart Alliance, D-80802 Munich, Germany; ⁷Cardiovascular Research Institute Maastricht, Maastricht University, 6229 Maastricht, The Netherlands; ⁸Munich Cluster for Systems Neurology, D-81377 Munich, Germany.

[§]Equally contributing first authors

*Corresponding authors:

Professor Dr. Aphrodite Kapurniotu, Tel.: +49 8161 713542; Fax: +49 8161 713298; *E-mail address:* akapurniotu@wzw.tum.de

Professor Dr. Jürgen Bernhagen, Tel.: +49 89 4400 46151; Fax: +49 89 4400 46148; *E-mail address:* juergen.bernhagen@med.uni-muenchen.de

Supplemental information; Lacy et al., 2018

Table of contents

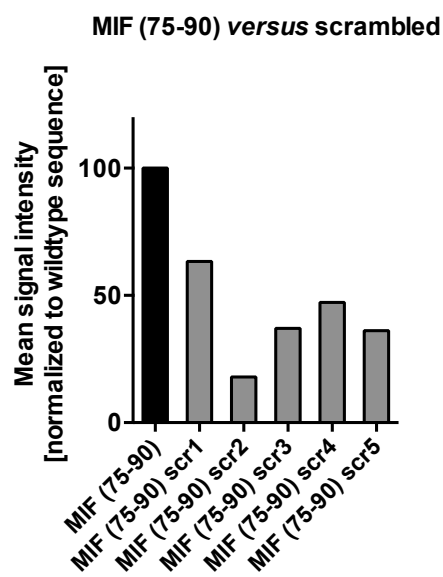
- Supplemental figures
- Supplemental tables
- Full-length gels/blots

Supplementary Figure 1; Lacy et al., 2018

a

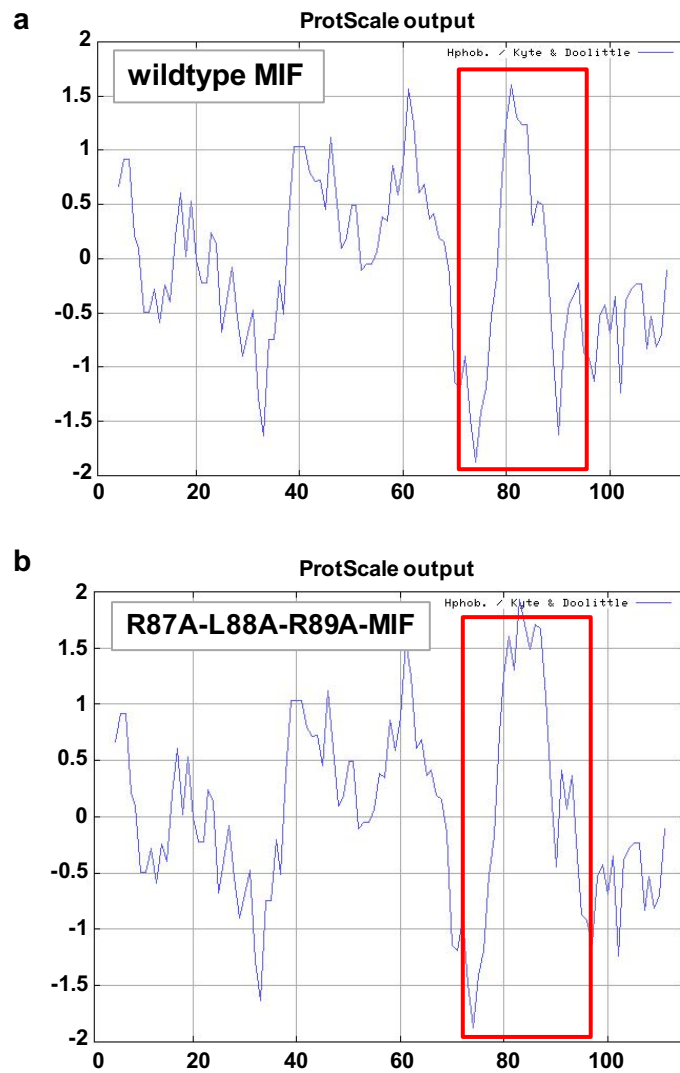
75-90	SYSKLLCGLLAER RL RI
scr1	SLALKLEYISRLGRLC
scr2	SLCSIRLALKYRLGLE
scr3	SRRGLLLL SAEYL LCKI
scr4	SLAYSRLGIEKLLLR C
scr5	SRLCLALKLEYISRL G

b



Supplementary Figure 1: Randomization of RLR-containing MIF sequence 75-90 leads to reduction in binding to CXCR4(1-27). Binding of peptide sequences to biotin-CXCR4(1-27) was analyzed by the micro slide-based peptide array technology (Intavis). Sequence 75-90 was randomized by the 'shuffle protein' method (www.bioinformatics.org) to generate the randomized peptides scrambled 1 (scr1), scr2, scr3, scr4, and scr5. Bars represent mean signal values of duplicate slides (mean signal intensity) relative to the binding signal of the wildtype peptide MIF(75-90).

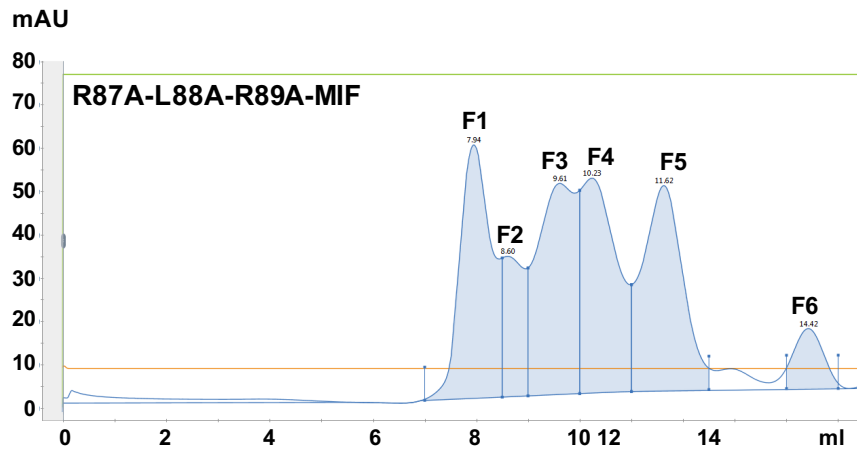
Supplementary Figure 2; Lacy et al., revised 2018



Supplementary Figure 2: Comparison of the hydrophobicity of R87A-L88A-R89A-MIF and wild-type MIF (WT-MIF) using GRAVY. The grand average of hydropathy (GRAVY) index is based on the Kyte & Doolittle algorithm and involved plotting the relative hydrophobicity (y-axis) versus the MIF or RLR mutant sequence (x-axis). The sequence region around RLR(87-89) is framed in red.

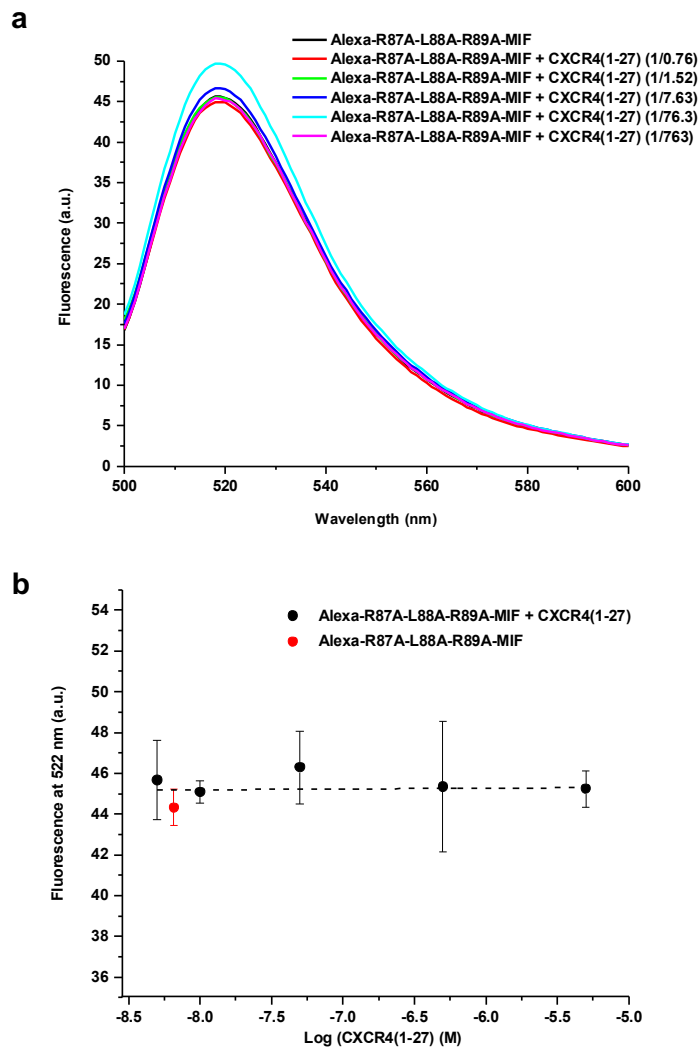
Supplementary Figure 3; Lacy et al., revised 2018

a



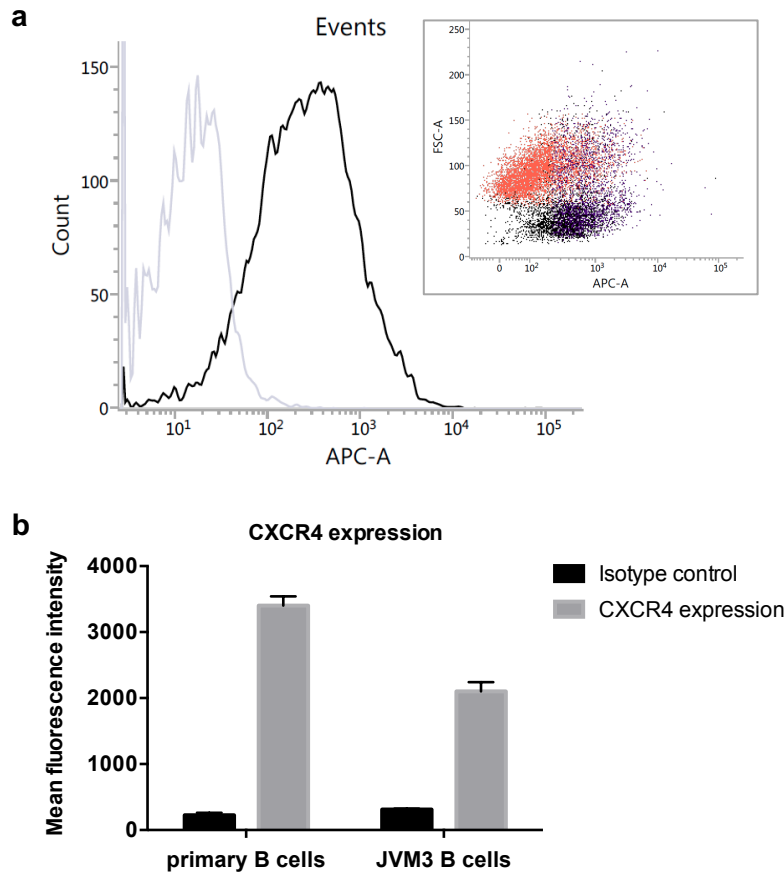
Supplementary Figure 3: Purification of R87A-L88A-R89A-MIF by size exclusion chromatography. Representative chromatogram of a Superdex 75 gel filtration run of the RLR mutant. Fractions F1 through F6 were collected and analyzed for RLR mutant content (see Fig. 2a-b for SDS-PAGE and Western blot analysis). Fractions F5 contained most of the enriched mutant protein. F3 and 4 contained minor portions of RLR mutant, which tended to form high-molecular weight oligomers. The chromatogram shown is plotted as UV absorption at 280 nm (in [mAU]; blue line) over the elution volume in [ml]. The column was run at 0.75 ml/min. The green line indicates that elution was done with one buffer (100% B; no gradient); orange line indicates conductivity, which was read for control. Small font numbers next to the fraction captions F1-F6 indicate the exact elution volumes of the peaks.

Supplementary Figure 4; Lacy et al., revised 2018



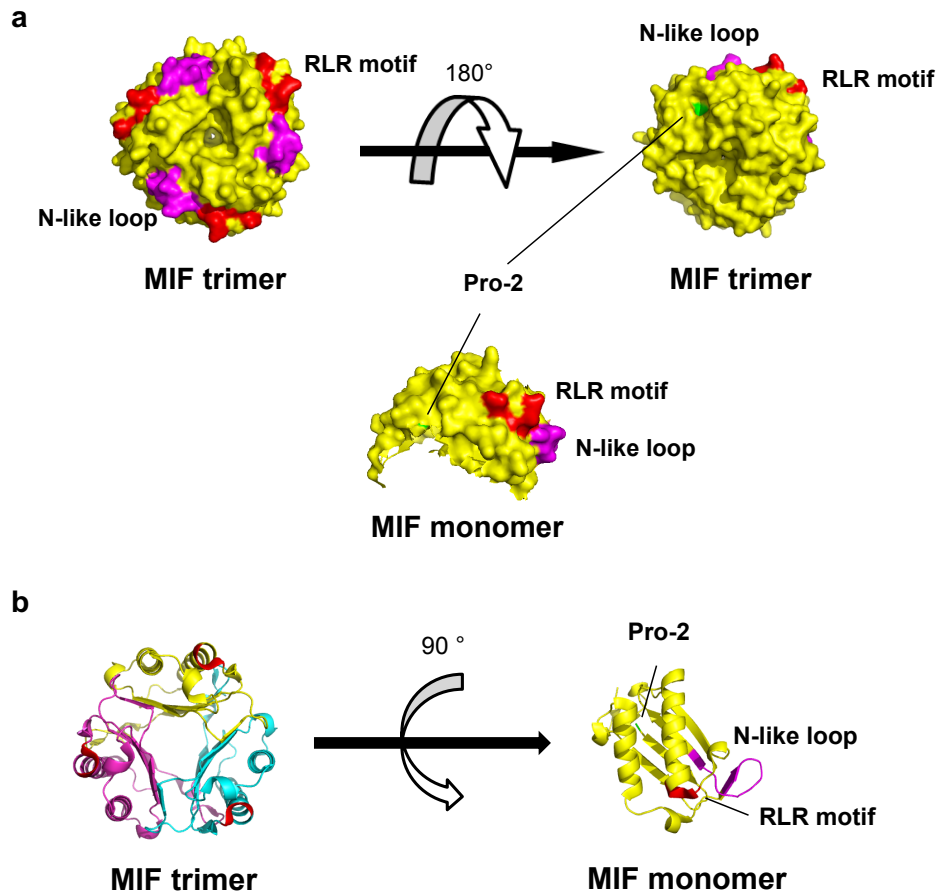
Supplementary Figure 4: The RLR triple alanine mutant does not bind to CXCR4(1-27). **(a)** Fluorescence spectroscopic titration of Alexa-488-R87A-L88A-R89A-MIF with increasing ratios of CXCR4(1-27). The solution mixture of CXCR4(1-27) peptide with Alexa-488-R87A-L88A-R89A-MIF does not evoke a conformational change in the mutant protein as indicated by a lack of change in fluorescence. Peptide was added at molar ratios of 1:0.76, 1:1.52, 1:7.63, 1:76.3, 1:763 and spectra were recorded between wavelengths 500 and 600 nm (arbitrary units, a.u.). **(b)** Concentration dependence of the CXCR4 peptide plotted against the fluorescence change at 522 nm. The horizontal dashed line is a fit through the data points and indicates no conformational change in the mutant protein.

Supplementary Figure 5; Lacy et al., revised 2018



Supplementary Figure 5: JVM-3 B lymphocytes express marked levels of CXCR4. Flow cytometry analysis of JVM-3 cells. **(a)** FACS histogram showing cell counts against staining for surface CXCR4 in JVM-3 by allophycocyanin (APC)-A label (black curve). Grey curves indicates the non-specific signal using isotype IgG control instead of anti-CXCR4-antibody. Inset, dot-plot of forward scatter (FSC-A) versus APC-A signal. **(b)** Comparison of CXCR4 expression (plotted as mean fluorescence intensity (MFI)) in JVM-3 B cells and primary human B cells isolated via MACS selection from peripheral blood mononuclear cells (PBMCs) of healthy volunteers. Specific signals using anti-CXCR4 antibody versus controls applying isotype immunoglobulin (IgG2a). Triplicate measurements \pm SD.

Supplementary Figure 6; Lacy et al., revised 2018



Supplementary Figure 6: Structure models of the human MIF monomer and trimer, highlighting the interaction motifs implicated in CXCR4 binding. **(a)** Surface structure model. The MIF motifs implicated in CXCR4 binding, i.e. N-like loop (pink), RLR motif (red), and Pro-2- residue (green) are highlighted. **(b)** Ribbon structures. Same color code and captions as in (a). Protein structures were produced/visualized with PyMOL.

Supplementary Table 1; Lacy et al., 2018

Supplementary Table 1: Purification and enrichment of R87A-L88A-R89A-MIF compared to wildtype MIF. Overview of the purification scheme.

	Total protein in bacterial lysate [mg] / % purity	Purification by anion exchange column [mg] / % purity	Secondary purification step (C8 or SEC*) [mg] / % purity
WT-MIF	96.9 / 10-20%	20.5 / 80-85%	3.2 / 95-98%
R87A-L88A-R89A-MIF	87.7 / 10-20%	4.2 / 50-60%	1.4 / >90%

For each step, total protein in [mg] (left number) and enrichment factor in % purity of total protein (right number) is given. C8, last step of the WT-MIF purification scheme via C8 reverse phase column that has been established previously to result in 95-98% pure MIF protein in endotoxin-free form (see ref. 29); SEC, size exclusion chromatography, last step of the R87A-L88A-R89A-MIF purification procedure (see Methods).

Supplementary Table 2; Lacy et al., 2018

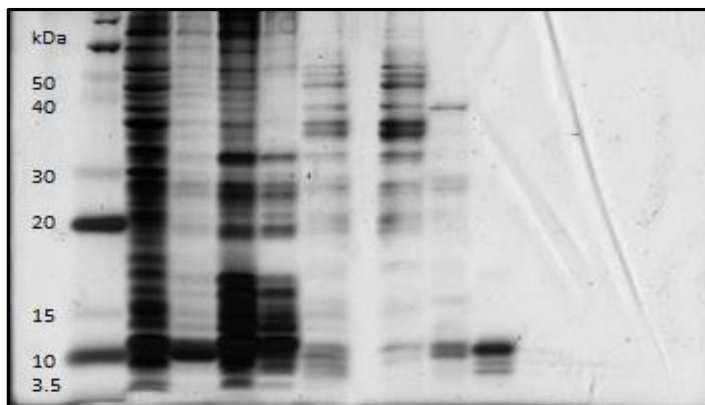
Supplementary Table 2: Circular dichroism (CD) spectropolarimetry shows that the folding and secondary structure profile of R87A-L88A-R89A-MIF is similar to that of WT-MIF. Quantification of the secondary structure contents of the CD spectra shown in **Fig. 2b**.

	α -helix	β -strand	β -strand / β -turn	Unordered	NRMSD
WT-MIF	44.7	27.8	48.6	6.8	0.090
R87A-L88A-R89A-MIF	32.3	21.0	39.8	28.7	0.044

Conformations in the CD spectra were measured as mean residue ellipticity versus the wavelength in the far-UV range. Quantification of the secondary structure fractions of WT-MIF and R87A-L88A-R89A-MIF as analyzed by the Dichroweb online software webtool. Secondary structure contents (%) were calculated by deconvolutions of CD spectra which was performed using ContinLL at DichroWeb and the reference spectra set 7. NRMSD (normalized root mean square deviation) of fits.

Supplementary full-length gels/blots 1; Lacy et al., 2018

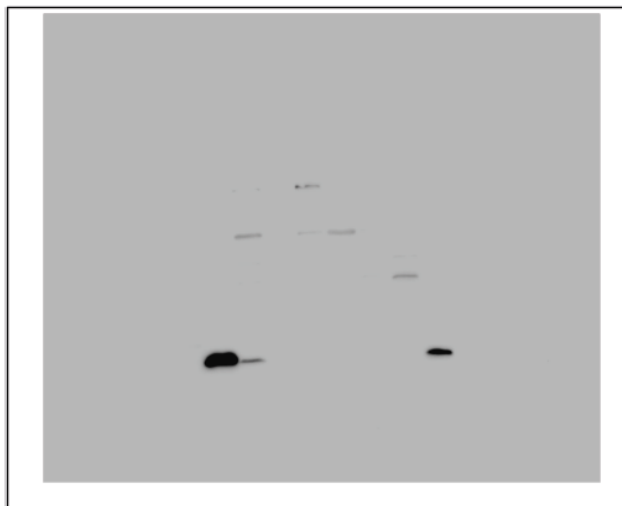
Full-length gel of Figure 2a



The original full gel underlying Figure 2 is shown above. To produce Figure 2a, the following 3 lanes on the left hand side of the gel were not shown: i) molecular weight markers (lane 1); ii) non-induced bacteria (not concentration-adjusted); iii) induced bacteria (not concentration-adjusted). Lane 4 equals the first lane in Figure 2a, i.e. the total lysate lane. The right-hand side of the gel also was cropped (empty lanes).

Supplementary full-length gels/blots 2; Lacy et al., 2018

Full-length blot of Figure 2b



To produce Figure 2b, the blot image was cropped on the left and right side (empty space).

A. Appendix

A.2.2. Supplementary data for Sinitski et al. 2020

Supplementary Information

Sinitski et al.

Content:

- Supplementary Figures
- Supplementary Tables

Cross-kingdom mimicry of the receptor signaling and leukocyte recruitment activity of a human cytokine by its plant orthologs

Dzmitry Sinitski¹; Katrin Gruner²; Markus Brandhofer¹; Christos Kontos³; Pascal Winkler²,
Anja Reinstädler², Priscila Bourilhon¹, Zhangping Xiao⁴, Robbert Cool⁴, Aphrodite
Kapurniotu³; Frank J. Dekker⁴, Ralph Panstruga^{2,#}, Jürgen Bernhagen^{1,5,#}

¹Chair of Vascular Biology, Institute for Stroke and Dementia Research (ISD), Klinikum der Universität München (KUM), Ludwig-Maximilians-University (LMU), 81377 Munich, Germany; ²Unit of Plant Molecular Cell Biology, Institute for Biology I, RWTH Aachen University, 52056 Aachen, Germany; ³Division of Peptide Biochemistry, Technische Universität München (TUM), 85354 Freising, Germany; ⁴Division of Chemical and Pharmaceutical Biology, University of Groningen, 9713 AV Groningen, The Netherlands; ⁵Munich Cluster for Systems Neurology (SyNergy), 81377 Munich, Germany.

Running head: Mimicry of human cytokine activity by Arabidopsis ortholog

#Shared last authorship and correspondence:

Professor Jürgen Bernhagen, PhD
Chair of Vascular Biology
Institute for Stroke and Dementia Research (ISD)
Klinikum der Universität München (KUM)
Ludwig-Maximilians-University (LMU) Munich
Feodor-Lynen-Straße 17, 81377 Munich, Germany
Tel.: 0049-89 4400 - 46151
Fax: 0049-89 4400 - 46010
E-Mail: juergen.bernhagen@med.uni-muenchen.de

Professor Ralph Panstruga, PhD
Unit of Plant Molecular Cell Biology
Institute for Biology I
RWTH Aachen University
Worringerweg 1, 52056 Aachen, Germany
Tel.: 0049-241 80 26655
Fax: 0049-241 80 22637
E-mail: panstruga@bio1.rwth-aachen.de

SUPPLEMENTARY FIGURE LEGENDS

Supplementary Figure 1. Similarity between hexahistidine-tagged *HsMIF* and *AtMDLs* at the level of primary amino acid sequence and predicted 3D structures. **A)** Multiple sequence alignment of 6xHis-tagged *AtMDLs* and *HsMIF*-6xHis was performed as described in **Figure 2B**. The grade of blue color represents sequence identity, with dark blue highlighting identical amino acids among all four sequences (100% identity), medium blue indicating amino acids that are identical in three of the sequences (75% identity), and light blue showing amino acids that are identical in two of the sequences (50% identity). **B)** 3D structures of 6xHis-tagged *AtMDLs* and *HsMIF*-6xHis were modeled as mentioned in **Figure 2C**. The predicted 3D structures (ribbon models) of 6xHis-tagged *AtMDL1*, *AtMDL2* and *AtMDL3* and *HsMIF*-6xHis are shown in comparison to the known X-ray-resolved 3D structure of native *HsMIF* (representation from the side of the *HsMIF* tautomerase substrate binding pocket; only the monomers are depicted).

Supplementary Figure 2. *AtMDL1*-6xHis and *AtMDL2*-6xHis partly cross-react with *HsMIF*-specific antibodies. Western blot analysis using polyclonal (Ka565) and monoclonal (MAB289) anti-*HsMIF* antibodies. Amount of loaded recombinant proteins is 1 µg per lane. Relative molecular masses (*Mr*) are indicated on the left in kDa.

Supplementary Figure 3. Detailed CD spectra of recombinant *HsMIF*, *HsMIF*-6xHis and the *AtMDL*-6xHis proteins. **A-B)** Results of comparative CD spectropolarimetric analysis of the indicated recombinant proteins in identical concentrations (1 and 2.5 µM) for the various proteins (for the 5 µM spectra see **Figure 1D**). **C-G)** Results of CD spectropolarimetric analysis of the indicated recombinant proteins in different concentrations (1, 2.5 and 5 µM) for the same protein. Conformations in the CD spectra in **A-G** were measured as mean residue ellipticity (MRE) as a function of the wavelength (given in nm) in the far-UV range.

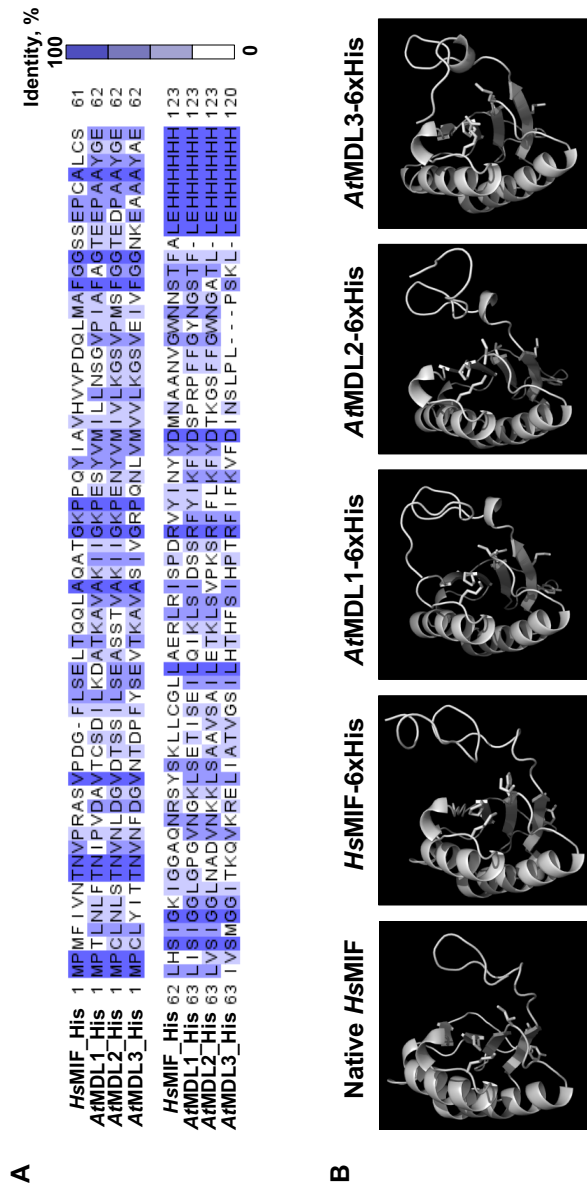
Supplementary Figure 4. Log-scale binding curve of AtMDL3 and MBP-sCD74 and CXCR4 cell surface expression in HEK293 cells stably transfected with human CXCR4.

A) Curve for binding of MBP-sCD74 and AtMDL3 on a log scale using increasing concentrations of MBP-sCD74 as indicated. The curve is derived from the saturation binding curve in **Figure 3C**. Binding was measured by an ELISA-type plate binding assay. Bovine serum albumin (BSA), blank PBS buffer (control), and MBP alone served as negative controls (not shown; see **Figure 3**). Wells were coated with BSA (2 % w/v), 500 nM AtMDL3-6xHis followed by binding of MBP-sCD74 (500 nM). After signal development, absorbance at 450 nm was measured. The data are displayed as means \pm SD (n = 3). **B)** CXCR4 cell surface expression in HEK293 cells stably transfected with human CXCR4 (HEK293-CXCR4) as determined by flow cytometry. The histogram represents the mean fluorescence intensity (MFI) on the x-axis and the number of fluorescent events on the y-axis. Blue: specific staining with FITC-conjugated mouse anti-CXCR4 antibody (anti-CXCR4); red: staining with FITC-conjugated mouse IgG1 isotype control (IgG control).

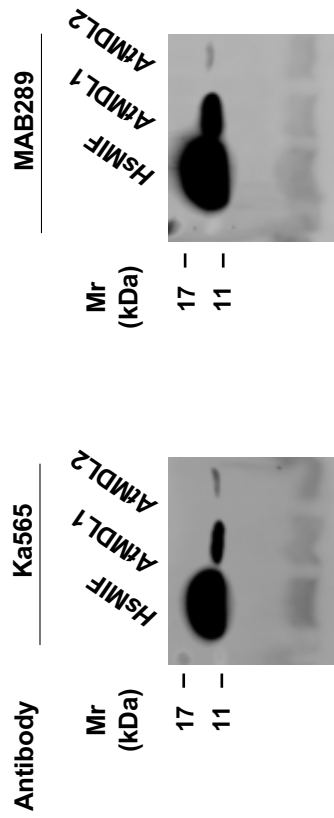
Supplementary Figure 5. AtMDL1-6xHis-triggered monocyte chemotaxis is blocked by the small molecule inhibitors AMD3100 and ISO-1, indicating MIF and CXCR4 specificity (data of an additional independent replicate of the inhibitor experiment shown in Figure 6). Chemotaxis experiments were performed as shown in **Figure 5** in the absence or presence of the small molecule inhibitors AMD3100 (10 μ M) or ISO-1 (100 μ M) as indicated. Concentrations of the recombinant proteins were equal to 32 nM for HsMIF-6xHis and AtMDL1-6xHis and 8 nM for CXCL12. Sodium phosphate buffer was used to normalize treatments to spontaneous random migration (control, Ctrl). The bar graph shows means \pm SD of one of two independently performed experiments performed as technical triplicate each (for the other experiment see **Figure 6**) (scatter plot with white circles indicating individual data points). Statistical analysis was done using one-way ANOVA for comparisons within a group (*P<0.05; **P<0.01; ***P<0.005) and paired t-test for comparisons between control and the AMD3100 and ISO-1 treatment groups (##P<0.01; ###P<0.005; NS, not significant).

Supplementary Figure 6. Desensitization of *HsMIF*- or *CXCL12*-triggered T-cell chemotaxis by *A β MDL1* is not affected by residual endotoxin content. Recombinant 6xHis-tagged *A β MDL1* desensitizes T cells from chemotaxis elicited by *CXCL12* or *HsMIF*-6xHis and this activity is unaffected by addition of polymyxin B. The experimental setup was as in **Figure 7B** with T cells migrating towards a gradient of *CXCL12* or *HsMIF*-6xHis versus buffer control (Ctrl), but preincubation of T cells in the upper chamber with *A β MDL1*-6xHis for two hours (+) in the presence of polymyxin B to neutralize potential residual traces of endotoxin in the *A β MDL1*-6xHis preparation. *CXCL12*-triggered T-cell chemotaxis without addition of polymyxin B into the upper chamber was examined as another positive control. The bar graphs show means \pm SD of three experiments (scatter plot with white circles indicating individual data points). Statistical analyses were performed using one-way ANOVA between control and *CXCL12* or *HsMIF* (# P <0.05; ### P <0.005) and between *CXCL12* or *HsMIF* with and without pre-treatment with *A β MDL1*-6xHis (* P <0.05; ** P <0.01), as well as between the *CXCL12*-stimulated groups with and without polymyxin B (ns = not significant).

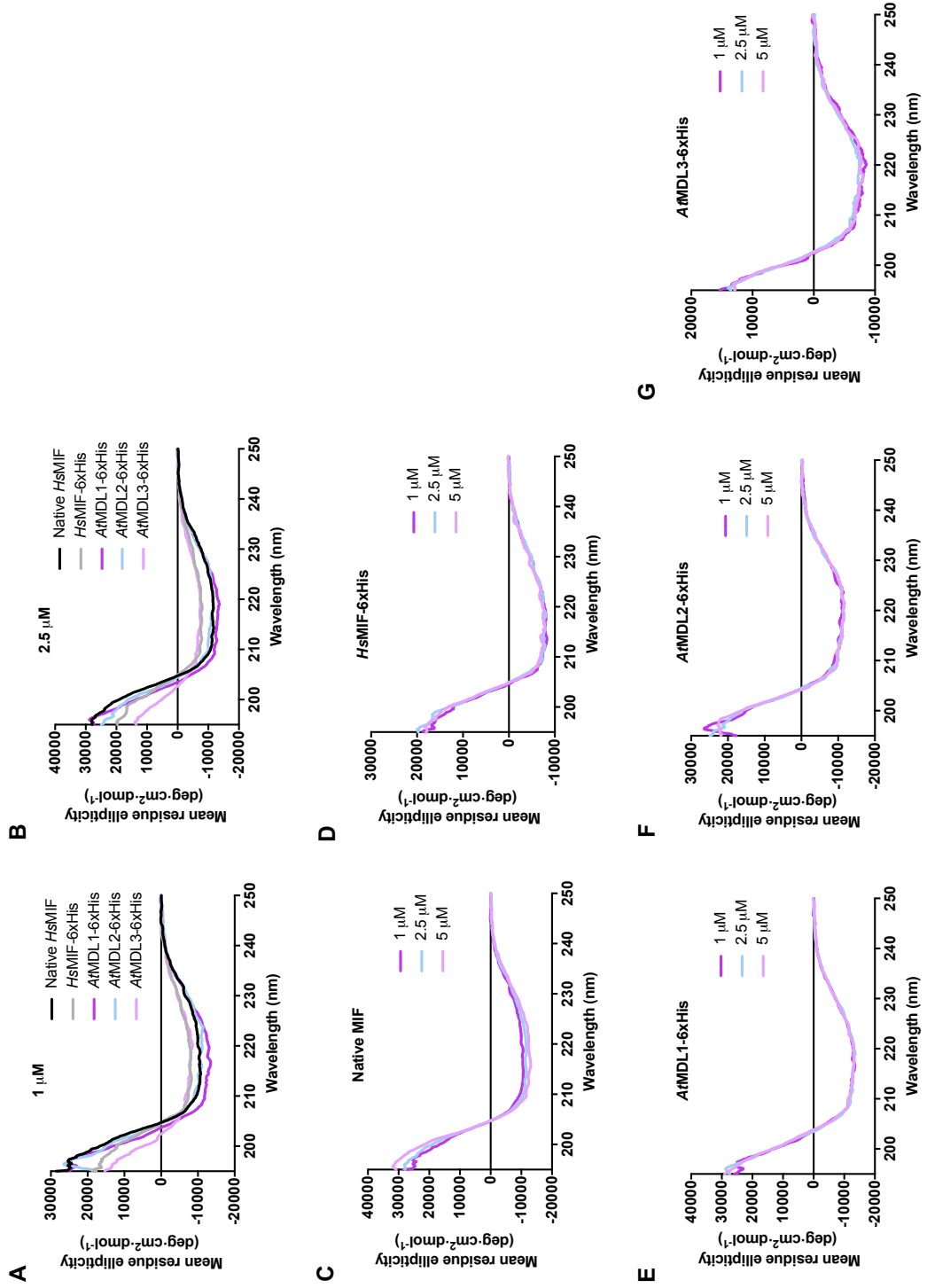
Supplementary Figure 1. Sinitiski et al. 2019



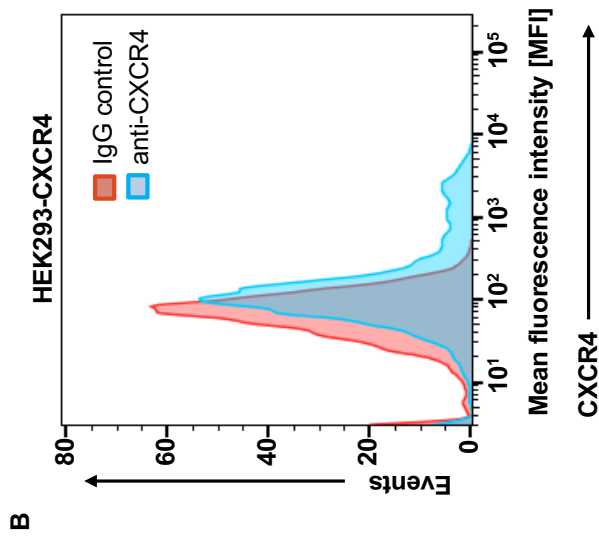
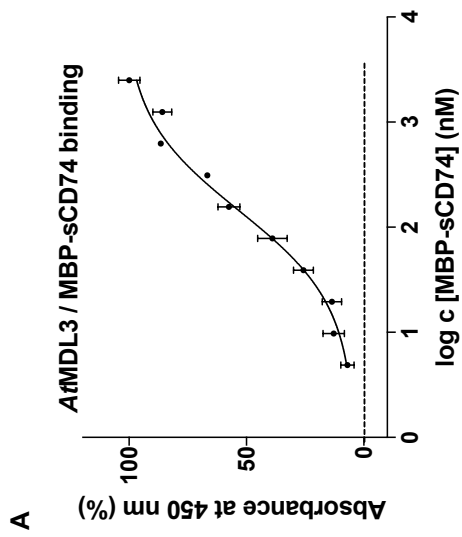
Supplementary Figure 2. Sinitiski et al. 2019



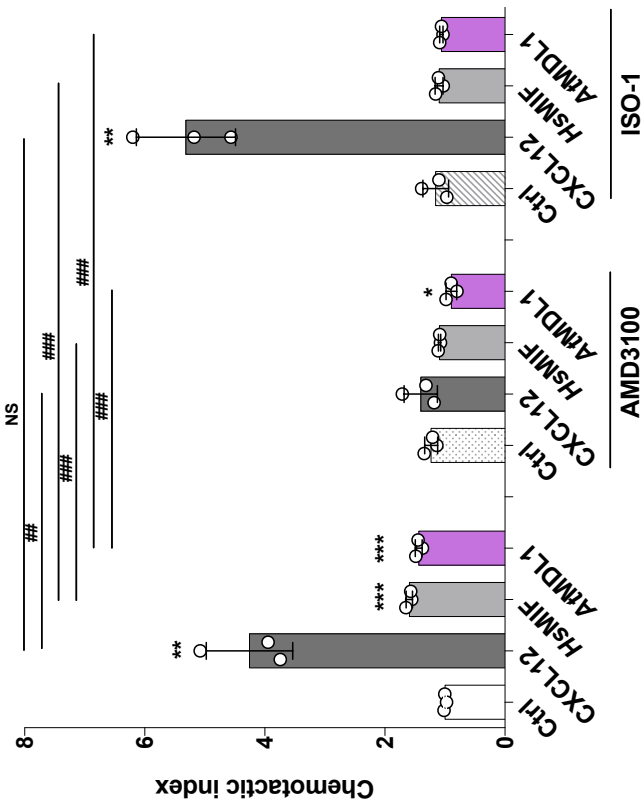
Supplementary Figure 3. Sinitski et al. 2019



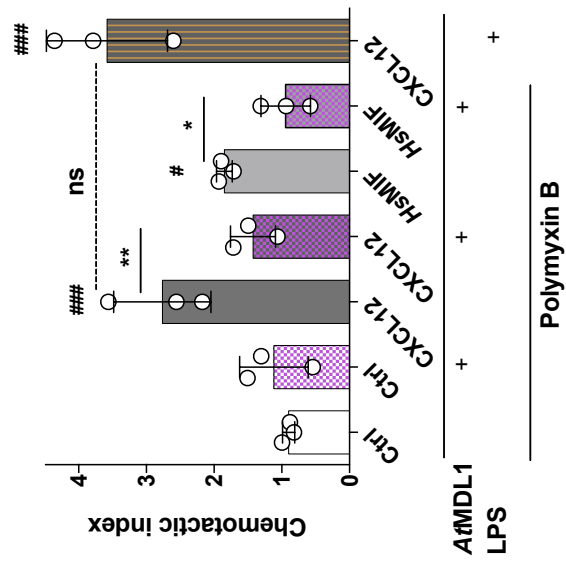
Supplementary Figure 4. Sinitiski et al. 2019



Supplementary Figure 5. Sinitski et al. 2019



Supplementary Figure 6. Sinitiski et al. 2019



Supplementary Table 1. Characteristics of the recombinant proteins used in this study.

Organism	Protein	Epitope tag	Amino acid sequence identity with naïve HsMIF	Molecular mass (Da) ^a	Isoelectric point (pI) ^a	UniProt accession number	ENA accession number
<i>Homo sapiens</i>	HsMIF	C-terminal -6xHis	99%	13410.23	7.50	P14174	CAA80598.1
<i>Arabidopsis thaliana</i>	AAMD1	C-terminal -6xHis	33%	13258.16	6.04	Q9LU69	BAC43697.1
<i>Arabidopsis thaliana</i>	AAMD2	C-terminal -6xHis	30%	13044.85	6.69	Q9M011	AED90371.1
<i>Arabidopsis thaliana</i>	AAMD3	C-terminal -6xHis	27%	13144.22	8.44	Q8LG92	BAC42273.1

^a including hexahistidine tag

Supplementary Table 2. Purification characteristics of recombinant 6xHis-tagged HsMIF and AAMD proteins.

Protein	Protein content in lysate (mg) / % purity	Protein content after IMAC ^a (mg) / % purity	Protein content after SEC ^b (mg) / % purity	Protein content after filtration ^c (mg) / % purity	Endotoxin content in final solution (pg/μg protein)
HsMIF-6xHis	93.2 / 10-15%	8.0 / 80-90%	4.5 / 95-98%	4.5 / 95-98%	11.3
AAMD1-6xHis	112.1 / 10-15%	12.5 / 80-90%	8.0 / 95-98%	8.0 / 95-98%	6.8
AAMD2-6xHis	86.3 / 10-15%	8.1 / 80-90%	6.5 / 95-98%	6.5 / 95-98%	9.3
AAMD3-6xHis	91.4 / 10-15%	1.1 / 80-90%	0.6 / 95-98%	0.6 / 95-98%	9.5

^a IMAC, immobilized metal affinity chromatography

^b SEC, size exclusion chromatography

^c Sterile filtration through a 0.2 μm pore size filter device

Supplementary Table 3. Secondary structure contents of recombinant 6xHis-tagged HsMIF and AAMD1 proteins as derived by deconvolution of the circular dichroism spectroscopy data.

Protein	α -helix (%)	β -strand (%)	β -turn (%)	β -strand / β -turn (%)	Unordered (%)	NMRSD ^a
Native HsMIF ^b	44.7	27.8	20.8	48.6	6.8	0.090
HsMIF-6xHis	27.6	32.8	21.8	54.6	17.7	0.070
AAMD1-6xHis	36.6	27.6	21.6	49.2	14.0	0.049
AAMD2-6xHis	36.2	30.5	17.0	47.5	16.2	0.072
AAMD3-6xHis	20.2	31.3	18.6	49.9	29.9	0.066

^a NMRSD (normalized root mean square deviation) of fits

^b The data for native HsMIF was published previously (1) and is included for comparison

Supplementary Table 4. Primers used for the cloning of the recombinant *AtMDLs*.

Target gene	NCBI reference sequence	Primer name	Primer sequence (5' to 3')
HsMIF	NP_002406.1	Ndel-HsMIF_Fwd	GAACATATGCCGATGTTTCATCGTAAAC
		HsMIF-XhoI_Rev	GTTCTCGAGGGCGAAGGTGGAGTTG
<i>AtMDL1</i> (At5g57170.1)	NM_125099.4	Ndel- <i>AtMDL1</i> _Fwd	GGCATA TGCCCACTTTGAATCTC
		<i>AtMDL1</i> -XhoI_Rev	CGGCTCGAGGAAAGTTGATCCATTGTAACC
		<i>AtMDL1</i> _mut_Fwd	GAGGAACCTGCTGCGTATGGAGAATTGATATC
		<i>AtMDL1</i> _mut_Rev	GATATCAATTCTCCATACGCAGCAGGTTCCCTC
<i>AtMDL2</i> (At5g01650.1)	NM_120243.4	Ndel- <i>AtMDL2</i> _Fwd	GAACATATGCCGTGCCTCAACCTCTCC
		<i>AtMDL2</i> -XhoI_Rev	CAACTCGAGAAAGAGTCGCCCCGTTCCAACC
<i>AtMDL3</i> (At3g51660.1)	NM_115025.4	Ndel- <i>AtMDL3</i> _Fwd	GCCCATA TGCCCTTGCTTTTACATTAC
		<i>AtMDL3</i> -XhoI_Rev	CGGCTCGAGAAGTTTAGAAGGAAGAGGCAAAG
		<i>AtMDL3</i> _mut_Fwd	CAAAGAAGCAGCTGCGTATGCAGAGATTGTGTC
		<i>AtMDL3</i> _mut_Rev	GACACAATCTCTGCATACGCAGCTGCTTCTTTG

References cited in Supplementary Information:

1. Lacy, M., Kontos, C., Brandhofer, M., Hille, K., Groning, S., Sinitski, D., Bourilhon, P., Rosenberg, E., Krammer, C., Thavayogarah, T., Pantouris, G., Bakou, M., Weber, C., Lolis, E., Bernhagen, J., and Kapurniotu, A. (2018) Identification of an Arg-Leu-Arg tripeptide that contributes to the binding interface between the cytokine MIF and the chemokine receptor CXCR4. *Sci Rep* **8**, 5171

**corresponds to reference 46 of the main manuscript*

A.2.3. Supplementary data for manuscript by Brandhofer et al., 2022

bioRxiv preprint doi: <https://doi.org/10.1101/2021.11.26.470090>; this version posted February 24, 2022. The copyright holder for this preprint (which was not certified by peer review) is the author/funder, who has granted bioRxiv a license to display the preprint in perpetuity. It is made available under aCC-BY-NC-ND 4.0 International license.

1 **Supplementary figure legends**

2

3 **Supplementary Figure 1.** Additional data for chemokine protein array. (A) Negative control
4 membrane related to the experiment in **Figure 1**, incubated in buffer at pH 8.0 without biotin-
5 MIF. (B) Close-up of membrane from a chemokine protein array experiment with a focus on
6 CXCL4 and CXCL4L1. The membrane was incubated with biotin-MIF and the incubation was
7 performed at pH 6.0.

8

9 **Supplementary Figure 2.** Investigation of the MIF/CXCL4L1 interaction interface and *in*
10 *silico* studies. (A) CelluSpot peptide array experiments, where overlapping peptides of
11 CXCL4 (*left*) and CXCL4L1 (*right*) were spotted on an array and probed with biotin-MIF.
12 Chemiluminescence signal intensity indicates binding of biotin-MIF to the respective peptide.
13 Arrows indicate peptides of interest that are most likely to be involved in the interaction with
14 MIF. (B) Sequences of peptides identified in **A** are highlighted in the 3D structure of
15 monomeric CXCL4 and CXCL4L1, showing their localization in the folded proteins. For both
16 chemokines, these peptides of interest represent almost identical amino acid sequences,
17 corresponding to highly similar regions of the protein. This indicates that not only the
18 sequence but also the three-dimensional conformation of the chemokines might play a role in
19 the interaction with MIF. Amino acid residues, in which CXCL4L1 differs from CXCL4 are in
20 italics. PyMOL was used to visualize a CXCL4 (PDB ID: 1F9Q Chain A) and CXCL4L1
21 monomer (PDB ID: 4HSV Chain A). (C) To visualize the proposed MIF/CXCL4L1 complex,
22 an unbiased *in silico* protein-protein docking approach was taken. The ClusPro 2.0
23 webserver was used to simulate a complex consisting of both a MIF and CXCL4L1
24 monomer. Depicted here is the highest-ranking docking result, with peptides identified in **A** to
25 be potentially part of the interaction interface highlighted in CXCL4L1. According to this *in*
26 *silico* prediction, they are partially directed towards MIF, allowing parts of their sequences
27 being involved in complex formation. PyMOL was used to calculate the surface charge
28 distribution of these proteins (red: negatively charged; blue: positively charged), revealing an

44

bioRxiv preprint doi: <https://doi.org/10.1101/2021.11.26.470090>; this version posted February 24, 2022. The copyright holder for this preprint (which was not certified by peer review) is the author/funder, who has granted bioRxiv a license to display the preprint in perpetuity. It is made available under aCC-BY-NC-ND 4.0 International license.

1 area of opposite charges in the proposed contact region of MIF and CXCL4L1 that partially
2 matches the peptide array results.

3

4 **Supplementary Figure 3.** Effects on cell migration in Jurkat T cells and microglia. (A) Effect
5 of CXCL4L1 on MIF-mediated chemotaxis of Jurkat T cells as analyzed in a Transwell
6 migration assay. Used concentrations: MIF: 16 nM, CXCL4L1: 32 nM; Data is presented as
7 mean \pm SD. n = 2-4 independent experiments. (B) Same as (A), except that co-incubation
8 with CXCL4 was analyzed. Data is presented as mean \pm SD. n = 4 independent experiments
9 with duplicates each. (C) Quantification of murine microglia motility, based on the
10 accumulated distance of GFP-positive microglia tracked during live cell imaging (n = 5). MIF
11 was used at a concentration of 8 nM, the soluble CXCR4-mimicking peptide msR4M-L1 at 40
12 nM and the cognate ligand of CXCR4, CXCL12, at 16 nM. Data presented as mean \pm SD.
13 Statistical significance: *, P < 0.05; **, P < 0.01; ***, P < 0.005; ****, P < 0.0001.

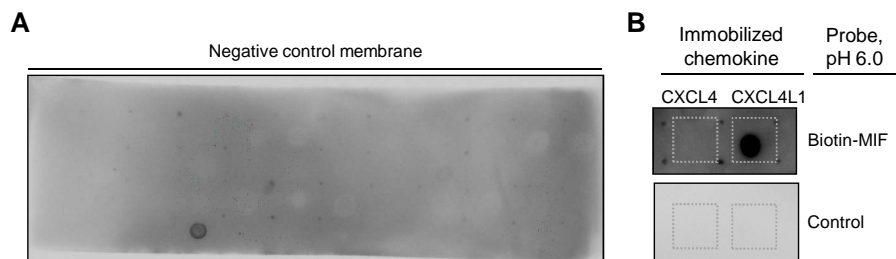
14

15 **Supplementary Figure 4.** Quantification of mean thrombus sizes from **Figure 5A**, showing a
16 trend for CXCL4L1 inhibiting the MIF-mediated increase in thrombus size in samples, in
17 which MIF and CXCL4L1 were pre-incubated together.

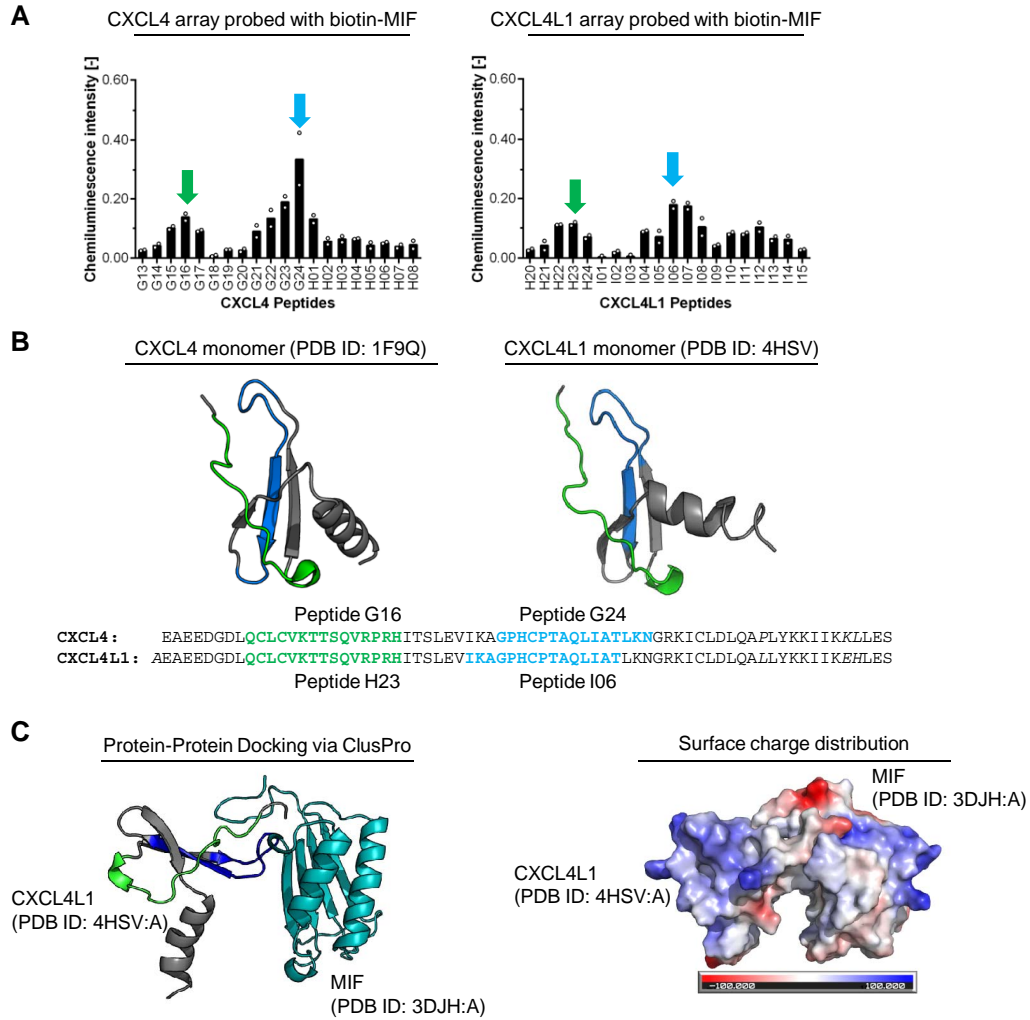
18

A. Appendix

bioRxiv preprint doi: <https://doi.org/10.1101/2021.11.26.470090>; this version posted February 24, 2022. The copyright holder for this preprint (which was not certified by peer review) is the author/funder, who has granted bioRxiv a license to display the preprint in perpetuity. It is made available under aCC-BY-NC-ND 4.0 International license.

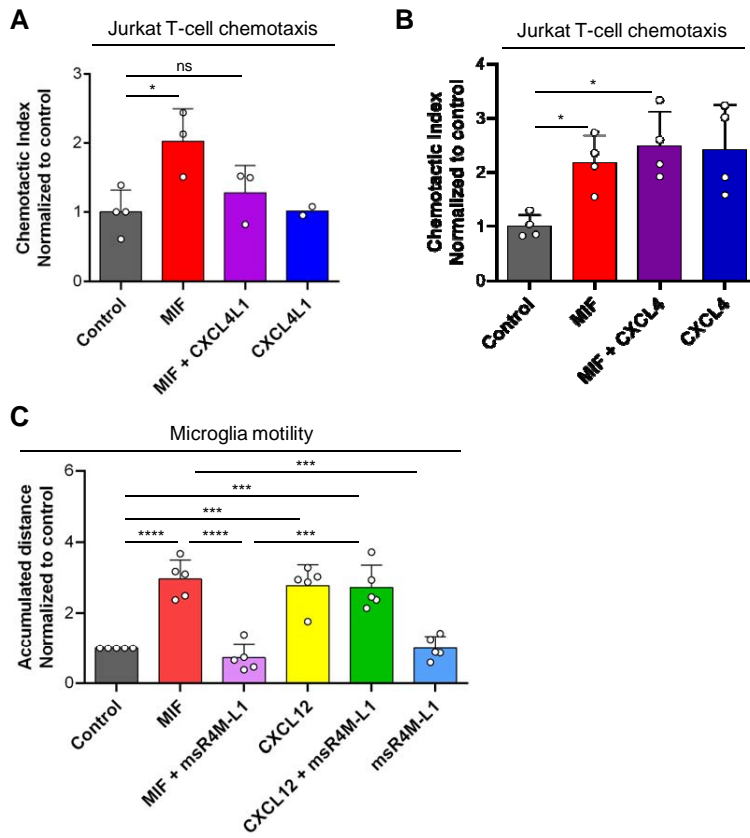


bioRxiv preprint doi: <https://doi.org/10.1101/2021.11.26.470090>; this version posted February 24, 2022. The copyright holder for this preprint (which was not certified by peer review) is the author/funder, who has granted bioRxiv a license to display the preprint in perpetuity. It is made available under aCC-BY-NC-ND 4.0 International license.

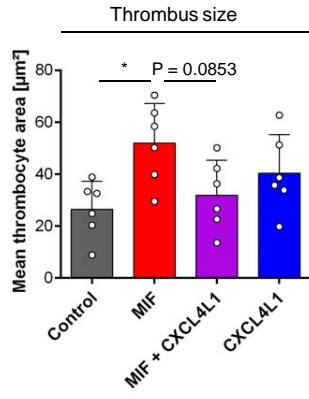


A. Appendix

bioRxiv preprint doi: <https://doi.org/10.1101/2021.11.26.470090>; this version posted February 24, 2022. The copyright holder for this preprint (which was not certified by peer review) is the author/funder, who has granted bioRxiv a license to display the preprint in perpetuity. It is made available under aCC-BY-NC-ND 4.0 International license.



bioRxiv preprint doi: <https://doi.org/10.1101/2021.11.26.470090>; this version posted February 24, 2022. The copyright holder for this preprint (which was not certified by peer review) is the author/funder, who has granted bioRxiv a license to display the preprint in perpetuity. It is made available under aCC-BY-NC-ND 4.0 International license.



References

- [1] S. Bi and V. Sourjik. “Stimulus sensing and signal processing in bacterial chemotaxis”. In: *Curr Opin Microbiol* 45 (2018), pp. 22–29. DOI: 10.1016/j.mib.2018.02.002.
- [2] J. E. Haber. “Mating-type genes and MAT switching in *Saccharomyces cerevisiae*”. In: *Genetics* 191.1 (2012), pp. 33–64. DOI: 10.1534/genetics.111.134577.
- [3] B. Alberts, D. Bray, A. Johnson, J. Lewis, M. Raff, K. Roberts, and P. Walter. *Lehrbuch der Molekularen Zellbiologie*. Ed. by K. Simons and T. Kurzchalia. Vol. XXIV. Wiley-VCH, 1999. ISBN: 9783527301010.
- [4] M. T. Madigan and J. M. Martinko. *Brock Mikrobiologie*. Ed. by M. Thomm. 11th ed. Pearson Studium, 2006. ISBN: 9783827371874.
- [5] C. A. Dinarello. “Historical insights into cytokines”. In: *Eur J Immunol* 37 Suppl 1 (2007), S34–45. DOI: 10.1002/eji.200737772.
- [6] A. Bagorda and C. A. Parent. “Eukaryotic chemotaxis at a glance”. In: *J Cell Sci* 121.Pt 16 (2008), pp. 2621–4. DOI: 10.1242/jcs.018077.
- [7] M. D. Turner, B. Nedjai, T. Hurst, and D. J. Pennington. “Cytokines and chemokines: At the crossroads of cell signalling and inflammatory disease”. In: *Biochim Biophys Acta* 1843.11 (2014), pp. 2563–2582. DOI: 10.1016/j.bbamcr.2014.05.014.
- [8] J. Parkin and B. Cohen. “An overview of the immune system”. In: *Lancet* 357.9270 (2001), pp. 1777–89. DOI: 10.1016/S0140-6736(00)04904-7.
- [9] B. Moser and K. Willmann. “Chemokines: role in inflammation and immune surveillance”. In: *Ann Rheum Dis* 63 Suppl 2 (2004), pp. ii84–ii89. DOI: 10.1136/ard.2004.028316.
- [10] I. F. Charo and R. M. Ransohoff. “The many roles of chemokines and chemokine receptors in inflammation”. In: *N Engl J Med* 354.6 (2006), pp. 610–21. DOI: 10.1056/NEJMra052723.
- [11] X. Wang, J. S. Sharp, T. M. Handel, and J. H. Prestegard. “Chemokine oligomerization in cell signaling and migration”. In: *Prog Mol Biol Transl Sci* 117 (2013), pp. 531–78. DOI: 10.1016/B978-0-12-386931-9.00020-9.
- [12] L. Rajagopalan and K. Rajarathnam. “Structural basis of chemokine receptor function—a model for binding affinity and ligand selectivity”. In: *Biosci Rep* 26.5 (2006), pp. 325–39. DOI: 10.1007/s10540-006-9025-9.
- [13] M. C. Miller and K. H. Mayo. “Chemokines from a Structural Perspective”. In: *Int J Mol Sci* 18.10 (2017). DOI: 10.3390/ijms18102088.
- [14] X. Blanchet, M. Langer, C. Weber, R. R. Koenen, and P. von Hundelshausen. “Touch of chemokines”. In: *Front Immunol* 3 (2012), p. 175. DOI: 10.3389/fimmu.2012.00175.
- [15] H. Nomiya, N. Osada, and O. Yoshie. “Systematic classification of vertebrate chemokines based on conserved synteny and evolutionary history”. In: *Genes Cells* 18.1 (2013), pp. 1–16. DOI: 10.1111/gtc.12013.

References

- [16] F. Bachelierie, A. Ben-Baruch, A. M. Burkhardt, C. Combadiere, J. M. Farber, G. J. Graham, R. Horuk, A. H. Sparre-Ulrich, M. Locati, A. D. Luster, A. Mantovani, K. Matsushima, P. M. Murphy, R. Nibbs, H. Nomiyama, C. A. Power, A. E. Proudfoot, M. M. Rosenkilde, A. Rot, S. Sozzani, M. Thelen, O. Yoshie, and A. Zlotnik. “International Union of Basic and Clinical Pharmacology. [corrected]. LXXXIX. Update on the extended family of chemokine receptors and introducing a new nomenclature for atypical chemokine receptors”. In: *Pharmacol Rev* 66.1 (2014), pp. 1–79. DOI: 10.1124/pr.113.007724.
- [17] L. Schrödinger. “The PyMOL Molecular Graphics System, Version 1.8”. Nov. 2015.
- [18] I. Clark-Lewis, K. S. Kim, K. Rajarathnam, J. H. Gong, B. Dewald, B. Moser, M. Baggiolini, and B. D. Sykes. “Structure-activity relationships of chemokines”. In: *J Leukoc Biol* 57.5 (1995), pp. 703–11. DOI: 10.1002/jlb.57.5.703.
- [19] W. G. Liang, C. G. Triandafillou, T. Y. Huang, M. M. Zulueta, S. Banerjee, A. R. Dinner, S. C. Hung, and W. J. Tang. “Structural basis for oligomerization and glycosaminoglycan binding of CCL5 and CCL3”. In: *Proc Natl Acad Sci U S A* 113.18 (2016), pp. 5000–5. DOI: 10.1073/pnas.1523981113.
- [20] M. J. Stone, J. A. Hayward, C. Huang, E. H. Z, and J. Sanchez. “Mechanisms of Regulation of the Chemokine-Receptor Network”. In: *Int J Mol Sci* 18.2 (2017). DOI: 10.3390/ijms18020342.
- [21] K. H. Mayo and M. J. Chen. “Human platelet factor 4 monomer-dimer-tetramer equilibria investigated by 1H NMR spectroscopy”. In: *Biochemistry* 28.24 (1989), pp. 9469–78. DOI: 10.1021/bi00450a034.
- [22] Y. P. Chen, H. L. Wu, K. Boye, C. Y. Pan, Y. C. Chen, N. Pujol, C. W. Lin, L. Y. Chiu, C. Billottet, I. D. Alves, A. Bikfalvi, and S. C. Sue. “Oligomerization State of CXCL4 Chemokines Regulates G Protein-Coupled Receptor Activation”. In: *ACS Chem Biol* 12.11 (2017), pp. 2767–2778. DOI: 10.1021/acscchembio.7b00704.
- [23] J. J. Ziarek, A. B. Kleist, N. London, B. Raveh, N. Montpas, J. Bonnetterre, G. St-Onge, C. J. DiCosmo-Ponticello, C. A. Koplinski, I. Roy, B. Stephens, S. Thelen, C. T. Veldkamp, F. D. Coffman, M. C. Cohen, M. B. Dwinell, M. Thelen, F. C. Peterson, N. Heveker, and B. F. Volkman. “Structural basis for chemokine recognition by a G protein-coupled receptor and implications for receptor activation”. In: *Sci Signal* 10.471 (2017). DOI: 10.1126/scisignal.aah5756.
- [24] D. F. Legler and M. Thelen. “New insights in chemokine signaling”. In: *F1000Res* 7 (2018), p. 95. DOI: 10.12688/f1000research.13130.1.
- [25] A. Jansma, T. M. Handel, and D. J. Hamel. “Chapter 2 Homo- and Hetero-Oligomerization of Chemokines”. In: *Chemokines, Part B*. Vol. 461. Methods in Enzymology. Academic Press, 2009, pp. 31–50. DOI: [https://doi.org/10.1016/S0076-6879\(09\)05402-0](https://doi.org/10.1016/S0076-6879(09)05402-0).
- [26] P. von Hundelshausen, S. M. Agten, V. Eckardt, X. Blanchet, M. M. Schmitt, H. Ippel, C. Neideck, K. Bidzhekov, J. Leberzammer, K. Wichapong, A. Faussner, M. Drechsler, J. Grommes, J. P. van Geffen, H. Li, A. Ortega-Gomez, R. T. Megens, R. Naumann, I. Dijkgraaf, G. A. Nicolaes, Y. Doring, O. Soehnlein, E. Lutgens, J. W. Heemskerk, R. R. Koenen, K. H. Mayo, T. M. Hackeng, and C. Weber. “Chemokine interactome mapping enables tailored intervention in acute and chronic inflammation”. In: *Sci Transl Med* 9.384 (2017). DOI: 10.1126/scitranslmed.aah6650.

- [27] S. Massena, G. Christoffersson, E. Hjertstrom, E. Zcharia, I. Vlodaysky, N. Ausmees, C. Rolny, J. P. Li, and M. Phillipson. “A chemotactic gradient sequestered on endothelial heparan sulfate induces directional intraluminal crawling of neutrophils”. In: *Blood* 116.11 (2010), pp. 1924–31. DOI: 10.1182/blood-2010-01-266072.
- [28] M. Sarris, J. B. Masson, D. Maurin, L. M. Van der Aa, P. Boudinot, H. Lortat-Jacob, and P. Herbomel. “Inflammatory chemokines direct and restrict leukocyte migration within live tissues as glycan-bound gradients”. In: *Curr Biol* 22.24 (2012), pp. 2375–82. DOI: 10.1016/j.cub.2012.11.018.
- [29] J. D. van Buul and P. L. Hordijk. “Signaling in leukocyte transendothelial migration”. In: *Arterioscler Thromb Vasc Biol* 24.5 (2004), pp. 824–33. DOI: 10.1161/01.ATV.0000122854.76267.5c.
- [30] A. E. Proudfoot, T. M. Handel, Z. Johnson, E. K. Lau, P. LiWang, I. Clark-Lewis, F. Borlat, T. N. Wells, and M. H. Kosco-Vilbois. “Glycosaminoglycan binding and oligomerization are essential for the in vivo activity of certain chemokines”. In: *Proc Natl Acad Sci U S A* 100.4 (2003), pp. 1885–90. DOI: 10.1073/pnas.0334864100.
- [31] A. Mantovani, R. Bonecchi, and M. Locati. “Tuning inflammation and immunity by chemokine sequestration: decoys and more”. In: *Nat Rev Immunol* 6.12 (2006), pp. 907–18. DOI: 10.1038/nri1964.
- [32] G. S. Kuschert, A. J. Hoogewerf, A. E. Proudfoot, C. W. Chung, R. M. Cooke, R. E. Hubbard, T. N. Wells, and P. N. Sanderson. “Identification of a glycosaminoglycan binding surface on human interleukin-8”. In: *Biochemistry* 37.32 (1998), pp. 11193–201. DOI: 10.1021/bi972867o.
- [33] A. E. Proudfoot. “Chemokines and Glycosaminoglycans”. In: *Front Immunol* 6 (2015), p. 246. DOI: 10.3389/fimmu.2015.00246.
- [34] A. Rot. “Neutrophil attractant/activation protein-1 (interleukin-8) induces in vitro neutrophil migration by haptotactic mechanism”. In: *Eur J Immunol* 23.1 (1993), pp. 303–6. DOI: 10.1002/eji.1830230150.
- [35] Z. Johnson, M. H. Kosco-Vilbois, S. Herren, R. Cirillo, V. Muzio, P. Zarin, M. Carbonatto, M. Mack, A. Smailbegovic, M. Rose, R. Lever, C. Page, T. N. Wells, and A. E. Proudfoot. “Interference with heparin binding and oligomerization creates a novel anti-inflammatory strategy targeting the chemokine system”. In: *J Immunol* 173.9 (2004), pp. 5776–85. DOI: 10.4049/jimmunol.173.9.5776.
- [36] J. H. Kuo, Y. P. Chen, J. S. Liu, A. Dubrac, C. Quemener, H. Prats, A. Bikfalvi, W. G. Wu, and S. C. Sue. “Alternative C-terminal helix orientation alters chemokine function: structure of the anti-angiogenic chemokine, CXCL4L1”. In: *J Biol Chem* 288.19 (2013), pp. 13522–33. DOI: 10.1074/jbc.M113.455329.
- [37] G. J. Graham, T. M. Handel, and A. E. I. Proudfoot. “Leukocyte Adhesion: Reconceptualizing Chemokine Presentation by Glycosaminoglycans”. In: *Trends Immunol* 40.6 (2019), pp. 472–481. DOI: 10.1016/j.it.2019.03.009.
- [38] K. Rajarathnam and U. R. Desai. “Structural Insights Into How Proteoglycans Determine Chemokine-CXCR1/CXCR2 Interactions: Progress and Challenges”. In: *Frontiers in Immunology* 11 (2020), p. 660. DOI: 10.3389/fimmu.2020.00660.

References

- [39] S. Alampour-Rajabi, O. El Bounkari, A. Rot, G. Muller-Newen, F. Bachelierie, M. Gawaz, C. Weber, A. Schober, and J. Bernhagen. "MIF interacts with CXCR7 to promote receptor internalization, ERK1/2 and ZAP-70 signaling, and lymphocyte chemotaxis". In: *FASEB J* 29.11 (2015), pp. 4497–511. DOI: 10.1096/fj.15-273904.
- [40] M. Chatterjee, O. Borst, B. Walker, A. Fotinos, S. Vogel, P. Seizer, A. Mack, S. Alampour-Rajabi, D. Rath, T. Geisler, F. Lang, H. F. Langer, J. Bernhagen, and M. Gawaz. "Macrophage migration inhibitory factor limits activation-induced apoptosis of platelets via CXCR7-dependent Akt signaling". In: *Circ Res* 115.11 (2014). DOI: 10.1161/CIRCRESAHA.115.305171.
- [41] C. E. Hughes and R. J. B. Nibbs. "A guide to chemokines and their receptors". In: *FEBS J* 285.16 (2018), pp. 2944–2971. DOI: 10.1111/febs.14466.
- [42] A. Zernecke and C. Weber. "Chemokines in atherosclerosis: proceedings resumed". In: *Arterioscler Thromb Vasc Biol* 34.4 (2014), pp. 742–50. DOI: 10.1161/ATVBAHA.113.301655.
- [43] A. Glabinski, M. Jalosinski, and R. M. Ransohoff. "Chemokines and chemokine receptors in inflammation of the CNS". In: *Expert Rev Clin Immunol* 1.2 (2005), pp. 293–301. DOI: 10.1586/1744666X.1.2.293.
- [44] D. P. Ramji and T. S. Davies. "Cytokines in atherosclerosis: Key players in all stages of disease and promising therapeutic targets". In: *Cytokine Growth Factor Rev* 26.6 (2015), pp. 673–85. DOI: 10.1016/j.cytogfr.2015.04.003.
- [45] J. Duchene and P. von Hundelshausen. "Platelet-derived chemokines in atherosclerosis". In: *Hamostaseologie* 35.2 (2015), pp. 137–41. DOI: 10.5482/HAM0-14-11-0058.
- [46] C. Weber and H. Noels. "Atherosclerosis: current pathogenesis and therapeutic options". In: *Nat Med* 17.11 (2011), pp. 1410–22. DOI: 10.1038/nm.2538.
- [47] N. Schwarz, J. Pruessmeyer, F. M. Hess, D. Drey Mueller, E. Pantaler, A. Koelsch, R. Windoffer, M. Voss, A. Sarabi, C. Weber, A. S. Sechi, S. Uhlig, and A. Ludwig. "Requirements for leukocyte transmigration via the transmembrane chemokine CX3CL1". In: *Cell Mol Life Sci* 67.24 (2010), pp. 4233–48. DOI: 10.1007/s00018-010-0433-4.
- [48] L. Landsman, L. Bar-On, A. Zernecke, K. W. Kim, R. Krauthgamer, E. Shagdarsuren, S. A. Lira, I. L. Weissman, C. Weber, and S. Jung. "CX3CR1 is required for monocyte homeostasis and atherogenesis by promoting cell survival". In: *Blood* 113.4 (2009), pp. 963–72. DOI: 10.1182/blood-2008-07-170787.
- [49] G. E. White and D. R. Greaves. "Fractalkine: one chemokine, many functions". In: *Blood* 113.4 (2009), pp. 767–8. DOI: 10.1182/blood-2008-11-189860.
- [50] G. Domschke and C. A. Gleissner. "CXCL4-induced macrophages in human atherosclerosis". In: *Cytokine* 122 (2019), p. 154141. DOI: 10.1016/j.cyto.2017.08.021.
- [51] S. A. Luther and J. G. Cyster. "Chemokines as regulators of T cell differentiation". In: *Nat Immunol* 2.2 (2001), pp. 102–7. DOI: 10.1038/84205.
- [52] P. M. Murphy, M. Baggiolini, I. F. Charo, C. A. Hébert, R. Horuk, K. Matsushima, L. H. Miller, J. J. Oppenheim, and C. A. Power. "International Union of Pharmacology. XXII. Nomenclature for Chemokine Receptors". In: *Pharmacological Reviews* 52.1 (2000), pp. 145–176.

- [53] N. R. Latorraca, A. J. Venkatakrishnan, and R. O. Dror. “GPCR Dynamics: Structures in Motion”. In: *Chem Rev* 117.1 (2017), pp. 139–155. DOI: 10.1021/acs.chemrev.6b00177.
- [54] I. Kufareva, C. L. Salanga, and T. M. Handel. “Chemokine and chemokine receptor structure and interactions: implications for therapeutic strategies”. In: *Immunol Cell Biol* 93.4 (2015), pp. 372–83. DOI: 10.1038/icb.2015.15.
- [55] A. B. Kleist, A. E. Getschman, J. J. Ziarek, A. M. Nevins, P. A. Gauthier, A. Chevigne, M. Szpakowska, and B. F. Volkman. “New paradigms in chemokine receptor signal transduction: Moving beyond the two-site model”. In: *Biochem Pharmacol* 114 (2016), pp. 53–68. DOI: 10.1016/j.bcp.2016.04.007.
- [56] L. Martínez-Muñoz, R. Villares, J. L. Rodríguez-Fernández, J. M. Rodríguez-Frade, and M. Mellado. “Remodeling our concept of chemokine receptor function: From monomers to oligomers”. In: *J Leukoc Biol* 104.2 (2018), pp. 323–331. DOI: 10.1002/JLB.2MR1217-503R.
- [57] A. Levoye, K. Balabanian, F. Baleux, F. Bachelierie, and B. Lagane. “CXCR7 heterodimerizes with CXCR4 and regulates CXCL12-mediated G protein signaling”. In: *Blood* 113.24 (2009), pp. 6085–93. DOI: 10.1182/blood-2008-12-196618.
- [58] A. Mantovani. “The chemokine system: redundancy for robust outputs”. In: *Immunol Today* 20.6 (1999), pp. 254–7. DOI: 10.1016/S0167-5699(99)01469-3.
- [59] M. Déruaz, A. Frauenschuh, A. L. Alessandri, J. M. Dias, F. M. Coelho, R. C. Russo, B. R. Ferreira, G. J. Graham, J. P. Shaw, T. N. Wells, M. M. Teixeira, C. A. Power, and A. E. Proudfoot. “Ticks produce highly selective chemokine binding proteins with antiinflammatory activity”. In: *J Exp Med* 205.9 (2008), pp. 2019–31. DOI: 10.1084/jem.20072689.
- [60] S. S. Denisov, J. H. Ippel, A. C. A. Heinzmann, R. R. Koenen, A. Ortega-Gomez, O. Soehnlein, T. M. Hackeng, and I. Dijkgraaf. “Tick saliva protein Evasin-3 modulates chemotaxis by disrupting CXCL8 interactions with glycosaminoglycans and CXCR2”. In: *J Biol Chem* 294.33 (2019), pp. 12370–12379. DOI: 10.1074/jbc.RA119.008902.
- [61] P. M. Murphy. “Viral exploitation and subversion of the immune system through chemokine mimicry”. In: *Nat Immunol* 2.2 (2001), pp. 116–22. DOI: 10.1038/84214.
- [62] A. Alcami. “Viral mimicry of cytokines, chemokines and their receptors”. In: *Nat Rev Immunol* 3.1 (2003), pp. 36–50. DOI: 10.1038/nri980.
- [63] A. Steen, O. Larsen, S. Thiele, and M. M. Rosenkilde. “Biased and g protein-independent signaling of chemokine receptors”. In: *Front Immunol* 5 (2014), p. 277. DOI: 10.3389/fimmu.2014.00277.
- [64] D. S. Eiger, N. Boldizsar, C. C. Honeycutt, J. Gardner, and S. Rajagopal. “Biased agonism at chemokine receptors”. In: *Cell Signal* 78 (2021), p. 109862. DOI: 10.1016/j.cellsig.2020.109862.
- [65] R. R. Koenen and C. Weber. “Therapeutic targeting of chemokine interactions in atherosclerosis”. In: *Nat Rev Drug Discov* 9.2 (2010), pp. 141–53. DOI: 10.1038/nrd3048.
- [66] P. von Hundelshausen, R. R. Koenen, M. Sack, S. F. Mause, W. Adriaens, A. E. Proudfoot, T. M. Hackeng, and C. Weber. “Heterophilic interactions of platelet factor 4 and RANTES promote monocyte arrest on endothelium”. In: *Blood* 105.3 (2005), pp. 924–30. DOI: 10.1182/blood-2004-06-2475.

References

- [67] S. Paoletti, V. Petkovic, S. Sebastiani, M. G. Danelon, M. Ugucioni, and B. O. Gerber. “A rich chemokine environment strongly enhances leukocyte migration and activities”. In: *Blood* 105.9 (2005), pp. 3405–12. DOI: 10.1182/blood-2004-04-1648.
- [68] S. E. Crown, Y. Yu, M. D. Sweeney, J. A. Leary, and T. M. Handel. “Heterodimerization of CCR2 chemokines and regulation by glycosaminoglycan binding”. In: *J Biol Chem* 281.35 (2006), pp. 25438–46. DOI: 10.1074/jbc.M601518200.
- [69] R. R. Koenen, P. von Hundelshausen, I. V. Nesmelova, A. Zernecke, E. A. Liehn, A. Sarabi, B. K. Kramp, A. M. Piccinini, S. R. Paludan, M. A. Kowalska, A. J. Kungl, T. M. Hackeng, K. H. Mayo, and C. Weber. “Disrupting functional interactions between platelet chemokines inhibits atherosclerosis in hyperlipidemic mice”. In: *Nat Med* 15.1 (2009), pp. 97–103. DOI: 10.1038/nm.1898.
- [70] J. Grommes, J. E. Alard, M. Drechsler, S. Wantha, M. Morgelin, W. M. Kuebler, M. Jacobs, P. von Hundelshausen, P. Markart, M. Wygrecka, K. T. Preissner, T. M. Hackeng, R. R. Koenen, C. Weber, and O. Soehnlein. “Disruption of platelet-derived chemokine heteromers prevents neutrophil extravasation in acute lung injury”. In: *Am J Respir Crit Care Med* 185.6 (2012), pp. 628–36. DOI: 10.1164/rccm.201108-15330C.
- [71] S. M. Agten, R. R. Koenen, H. Ippel, V. Eckardt, P. von Hundelshausen, K. H. Mayo, C. Weber, and T. M. Hackeng. “Probing Functional Heteromeric Chemokine Protein-Protein Interactions through Conformation-Assisted Oxime Ligation”. In: *Angew Chem Int Ed Engl* 55.48 (2016), pp. 14963–14966. DOI: 10.1002/anie.201607036.
- [72] I. V. Nesmelova, Y. Sham, J. Gao, and K. H. Mayo. “CXC and CC chemokines form mixed heterodimers: association free energies from molecular dynamics simulations and experimental correlations”. In: *J Biol Chem* 283.35 (2008), pp. 24155–66. DOI: 10.1074/jbc.M803308200.
- [73] R. P. Bhusal, J. R. O. Eaton, S. T. Chowdhury, C. A. Power, A. E. I. Proudfoot, M. J. Stone, and S. Bhattacharya. “Evasins: Tick Salivary Proteins that Inhibit Mammalian Chemokines”. In: *Trends Biochem Sci* 45.2 (2020), pp. 108–122. DOI: 10.1016/j.tibs.2019.10.003.
- [74] M. E. Bianchi. “HMGB1 loves company”. In: *Journal of Leukocyte Biology* 86.3 (2009), pp. 573–576. DOI: 10.1189/jlb.1008585.
- [75] M. Schiraldi, A. Raucci, L. M. Muñoz, E. Livoti, B. Celona, E. Venereau, T. Apuzzo, F. De Marchis, M. Pedotti, A. Bachi, M. Thelen, L. Varani, M. Mellado, A. Proudfoot, M. E. Bianchi, and M. Ugucioni. “HMGB1 promotes recruitment of inflammatory cells to damaged tissues by forming a complex with CXCL12 and signaling via CXCR4”. In: *The Journal of Experimental Medicine* 209.3 (2012), pp. 551–563. DOI: 10.1084/jem.20111739.
- [76] V. Cecchinato, G. D’Agostino, L. Raeli, and M. Ugucioni. “Chemokine interaction with synergy-inducing molecules: fine tuning modulation of cell trafficking”. In: *J Leukoc Biol* 99.6 (2016), pp. 851–5. DOI: 10.1189/jlb.1MR1015-457R.
- [77] J.-E. Alard. “Recruitment of classical monocytes can be inhibited by disturbing heteromers of neutrophil HNP1 and platelet CCL5”. In: *Science Translational Medicine* (2015).

- [78] V. Eckardt, M. C. Miller, X. Blanchet, R. Duan, J. Leberzammer, J. Duchene, O. Soehnlein, R. T. Megens, A. K. Ludwig, A. Dregni, A. Faussner, K. Wichapong, H. Ippel, I. Dijkgraaf, H. Kaltner, Y. Doring, K. Bidzhekov, T. M. Hackeng, C. Weber, H. J. Gabius, P. von Hundelshausen, and K. H. Mayo. “Chemokines and galectins form heterodimers to modulate inflammation”. In: *EMBO Rep* 21.4 (2020), e47852. DOI: 10.15252/embr.201947852.
- [79] A. Kapurniotu, O. Gokce, and J. Bernhagen. “The Multitasking Potential of Alarmins and Atypical Chemokines”. In: *Front Med (Lausanne)* 6 (2019), p. 3. DOI: 10.3389/fmed.2019.00003.
- [80] B. Degryse and M. de Virgilio. “The nuclear protein HMGB1, a new kind of chemokine?” In: *FEBS Lett* 553.1-2 (2003), pp. 11–7. DOI: 10.1016/s0014-5793(03)01027-5.
- [81] K. Zhang, S. Shi, and W. Han. “Research progress in cytokines with chemokine-like function”. In: *Cell Mol Immunol* 15.7 (2018), pp. 660–662. DOI: 10.1038/cmi.2017.121.
- [82] J. R. David. “Delayed hypersensitivity in vitro: its mediation by cell-free substances formed by lymphoid cell-antigen interaction”. In: *Proceedings of the National Academy of Sciences of the United States of America* 56.1 (1966), pp. 72–77. DOI: 10.1073/pnas.56.1.72.
- [83] B. R. Bloom and B. Bennet. “Mechanism of a reaction in vitro associated with delayed-type hypersensitivity”. In: *Science* 153.3731 (1966), pp. 80–82. DOI: 10.1126/science.153.3731.80.
- [84] M. Merk, S. Zierow, L. Leng, R. Das, X. Du, W. Schulte, J. Fan, H. Lue, Y. Chen, H. Xiong, F. Chagnon, J. Bernhagen, E. Lolis, G. Mor, O. Lesur, and R. Bucala. “The D-dopachrome tautomerase (DDT) gene product is a cytokine and functional homolog of macrophage migration inhibitory factor (MIF)”. In: *Proceedings of the National Academy of Sciences* 108.34 (2011), E577–E585-E577–E585.
- [85] A. Sparkes, P. De Baetselier, K. Roelants, C. De Trez, S. Magez, J. A. Van Ginderachter, G. Raes, R. Bucala, and B. Stijlemans. “The non-mammalian MIF superfamily”. In: *Immunobiology* 222.3 (2017), pp. 473–482. DOI: 10.1016/j.imbio.2016.10.006.
- [86] H. Sugimoto, M. Taniguchi, A. Nakagawa, I. Tanaka, M. Suzuki, and J. Nishihira. “Crystal structure of human D-dopachrome tautomerase, a homologue of macrophage migration inhibitory factor, at 1.54 Å resolution”. In: *Biochemistry* 38.11 (1999), pp. 3268–79. DOI: 10.1021/bi982184o.
- [87] M. Merk, R. A. Mitchell, S. Endres, and R. Bucala. “D-dopachrome tautomerase 1 (D-DT or MIF-2): Doubling the MIF cytokine family”. In: *Cytokine* 59.1 (2012), pp. 10–17.
- [88] T. Calandra and T. Roger. “Macrophage Migration Inhibitory Factor: A Regulator Of Innate Immunity”. In: *Nature Reviews Immunology* 3.10 (2003), pp. 791–800. DOI: 10.1038/nri1200.
- [89] J. Bernhagen, T. Calandra, R. A. Mitchell, S. B. Martin, K. J. Tracey, W. Voelter, K. R. Manogue, A. Cerami, and R. Bucala. “MIF is a pituitary-derived cytokine that potentiates lethal endotoxaemia”. In: *Nature* 365 (1993), pp. 756–759.
- [90] R. Bucala. “MIF rediscovered: cytokine, pituitary hormone, and glucocorticoid-induced regulator of the immune response”. In: *The FASEB Journal* 10.14 (1996), pp. 1607–1613. DOI: 10.1096/fasebj.10.14.9002552.

References

- [91] H.-W. Sun, J. Bernhagen, R. Bucala, and E. Lolis. “Crystal structure at 2.6-Å resolution of human macrophage migration inhibitory factor”. In: *Proceedings of the National Academy of Sciences* 93 (1996), pp. 5191–5196.
- [92] P. Mühlhahn, J. Bernhagen, M. Czisch, J. Georgescu, C. Renner, A. Ross, R. Bucala, and T. A. Holak. “NMR characterization of structure, backbone dynamic, and glutathione binding of the human macrophage migration inhibitory factor (MIF)”. In: *Protein Science* 5 (1996), pp. 2095–2103.
- [93] R. Mischke, R. Kleemann, H. Brunner, and J. Bernhagen. “Cross-linking and mutational analysis of the oligomerization state of the cytokine macrophage migration inhibitory factor (MIF)”. In: *FEBS Letters* 427.1 (1998), pp. 85–90. DOI: 10.1016/s0014-5793(98)00400-1.
- [94] E. J. Lolis and R. Bucala. “Macrophage migration inhibitory factor”. In: *Expert Opinion on Therapeutic Targets* 7.2 (2003), pp. 153–164. DOI: 10.1517/14728222.7.2.153.
- [95] G. V. Crichlow, J. B. Lubetsky, L. Leng, R. Bucala, and E. J. Lolis. “Structural and kinetic analyses of macrophage migration inhibitory factor active site interactions”. In: *Biochemistry* 48.1 (2009), pp. 132–9. DOI: 10.1021/bi8014423.
- [96] H. Lue, R. Kleemann, T. Calandra, T. Roger, and J. Bernhagen. “Macrophage migration inhibitory factor (MIF): mechanisms of action and role in disease”. In: *Microbes and Infection* 4.4 (2002), pp. 449–460. DOI: 10.1016/s1286-4579(02)01560-5.
- [97] T. Strussmann, S. Tillmann, T. Wirtz, R. Bucala, P. von Hundelshausen, and J. Bernhagen. “Platelets are a previously unrecognised source of MIF”. In: *Thromb Haemost* 110.5 (2013), pp. 1004–13. DOI: 10.1160/TH13-01-0049.
- [98] T. Calandra, J. Bernhagen, R. A. Mitchell, and R. Bucala. “The Macrophage Is an Important and Previously Unrecognized Source of Macrophage Migration Inhibitory Factor”. In: *Journal of Experimental Medicine* 179 (1994), pp. 1895–1902.
- [99] T. Calandra, L. A. Spiegel, C. N. Metz, and R. Bucala. “Macrophage migration inhibitory factor is a critical mediator of the activation of immune cells by exotoxins of Gram-positive bacteria”. In: *Proceedings of the National Academy of Sciences of the United States of America* 95 (1998), pp. 11383–11388.
- [100] T. H. Wirtz, S. Tillmann, T. Strussmann, S. Kraemer, J. W. Heemskerk, O. Grottko, M. Gawaz, P. von Hundelshausen, and J. Bernhagen. “Platelet-derived MIF: a novel platelet chemokine with distinct recruitment properties”. In: *Atherosclerosis* 239.1 (2015), pp. 1–10. DOI: 10.1016/j.atherosclerosis.2014.12.039.
- [101] W. Dankers, M. A. Hasnat, V. Swann, A. Alharbi, J. P. Lee, M. A. Cristofaro, M. P. Gantier, S. A. Jones, E. F. Morand, J. K. Flynn, and J. Harris. “Necrotic cell death increases the release of macrophage migration inhibitory factor by monocytes/macrophages”. In: *Immunol. Cell Biol.* 98.9 (2020), pp. 782–790. DOI: 10.1111/imcb.12376.
- [102] A. Hoffmann and J. Bernhagen. “Revisiting the secretion mechanism(s) of macrophage migration inhibitory factor – welcome to the “UPS club””. In: *Immunol. Cell Biol.* 98.9 (2020), pp. 704–708. DOI: 10.1111/imcb.12388.
- [103] O. Flieger, A. Engling, R. Bucala, H. Lue, W. Nickel, and J. Bernhagen. “Regulated secretion of macrophage migration inhibitory factor is mediated by a non-classical pathway involving an ABC transporter”. In: *FEBS Letters* 551 (2003), pp. 78–86.

- [104] H. Lue, M. T. Thiele, J. Franz, E. Dahl, S. Speckgens, L. Leng, G. Fingerle-Rowson, R. Bucala, B. Lüscher, and J. Bernhagen. “Macrophage migration inhibitory factor (MIF) promotes cell survival by activation of the Akt pathway and role for CSN5/JAB1 in the control of autocrine MIF activity”. In: *Oncogene* 26.35 (2007), pp. 5046–5059. DOI: 10.1038/sj.onc.1210318.
- [105] M. Merk, J. Baugh, S. Zierow, L. Leng, U. Pal, S. J. Lee, A. D. Ebert, Y. Mizue, J. O. Trent, R. Mitchell, W. Nickel, P. B. Kavathas, J. Bernhagen, and R. Bucala. “The Golgi-Associated Protein p115 Mediates the Secretion of Macrophage Migration Inhibitory Factor”. In: *The Journal of Immunology* 182.11 (2009), pp. 6896–6906. DOI: 10.4049/jimmunol.0803710.
- [106] T. Calandra, J. Bernhagen, C. N. Metz, L. A. Spiegel, M. Bacher, T. Donnelly, A. Cerami, and R. Bucala. “MIF as a glucocorticoid-induced modulator of cytokine production”. In: *Nature* 377 (1995), pp. 68–71.
- [107] T. Calandra, B. Echtenacher, D. Le Roy, J. Pugin, C. N. Metz, L. Hültner, D. Heumann, D. Männel, and M. P. Richard Bucala. “Protection from septic shock by neutralization of macrophage migration inhibitory factor”. In: *Nature Medicine* 6.2 (2000), pp. 164–170. DOI: 10.1038/72262.
- [108] E. F. Morand, M. Leech, and J. Bernhagen. “MIF: a new cytokine link between rheumatoid arthritis and atherosclerosis”. In: *Nature Reviews Drug Discovery* 5 (2006), pp. 399–410.
- [109] S. Tillmann, J. Bernhagen, and H. Noels. “Arrest functions of the MIF ligand/receptor axes in atherogenesis”. In: *Frontiers in Immunology* 4 (2013), pp. 1–19. DOI: 10.3389/fimmu.2013.00115.
- [110] M. Sauler, R. Bucala, and P. J. Lee. “Role of macrophage migration inhibitory factor in age-related lung disease”. In: *Am J Physiol Lung Cell Mol Physiol* 309.1 (2015), pp. L1–10. DOI: 10.1152/ajplung.00339.2014.
- [111] H. Conroy, L. Mawhinney, and S. C. Donnelly. “Inflammation and cancer: macrophage migration inhibitory factor (MIF) – the potential missing link”. In: *QJM: An International Journal of Medicine* 103.11 (2010), pp. 831–836. DOI: 10.1093/qjmed/hcq148.
- [112] L. Leng, C. N. Metz, Y. Fang, Y. Xu, S. Donnelly, J. Baugh, T. Delohery, Y. Chen, R. A. Mitchell, and R. Bucala. “MIF Signal Transduction Initiated by Binding to CD74”. In: *The Journal of Experimental Medicine* 197.11 (2003), pp. 1467–1476. DOI: 10.1084/jem.20030286.
- [113] J. Bernhagen, R. Krohn, H. Lue, J. L. Gregory, A. Zerneck, R. R. Koenen, M. Dewor, I. Georgiev, A. Schober, L. Leng, T. Kooistra, G. Fingerle-Rowson, P. Ghezzi, R. Kleemann, S. R. McColl, R. Bucala, M. J. Hickey, and C. Weber. “MIF is a noncognate ligand of CXC chemokine receptors in inflammatory and atherogenic cell recruitment”. In: *Nature Medicine* 13.5 (2007), pp. 587–596.
- [114] R. Busch, C. H. Rinderknecht, S. Roh, A. W. Lee, J. J. Harding, T. Burster, T. M. C. Hornell, and E. D. Mellins. “Achieving stability through editing and chaperoning: regulation of MHC class II peptide binding and expression”. In: *Immunological Reviews* 207.1 (2005), pp. 242–260.
- [115] C. Henne, F. Schwenk, N. Koch, and P. Möller. “Surface expression of the invariant chain (CD74) is independent of concomitant expression of major histocompatibility complex class II antigens”. In: *Immunology* 84.2 (1995), pp. 177–182.

References

- [116] A. Zerneck, J. Bernhagen, and C. Weber. “Macrophage Migration Inhibitory Factor in Cardiovascular Disease”. In: *Circulation* 117.12 (2008), pp. 1594–1602. DOI: 10.1161/CIRCULATIONAHA.107.729125.
- [117] P. V. Tilstam, D. Qi, L. Leng, L. Young, and R. Bucala. “MIF family cytokines in cardiovascular diseases and prospects for precision-based therapeutics”. In: *Expert Opin Ther Targets* 21.7 (2017), pp. 671–683. DOI: 10.1080/14728222.2017.1336227.
- [118] M. Chatterjee, P. Seizer, O. Borst, T. Schonberger, A. Mack, T. Geisler, H. F. Langer, A. E. May, S. Vogel, F. Lang, and M. Gawaz. “SDF-1alpha induces differential trafficking of CXCR4-CXCR7 involving cyclophilin A, CXCR7 ubiquitination and promotes platelet survival”. In: *FASEB J* 28.7 (2014), pp. 2864–78. DOI: 10.1096/fj.14-249730.
- [119] S. Raffei, B. Gui, J. Wu, X. S. Liu, A. S. Kibel, and L. Jia. “Targeting the MIF/CXCR7/AKT Signaling Pathway in Castration-Resistant Prostate Cancer”. In: *Mol Cancer Res* 17.1 (2019), pp. 263–276. DOI: 10.1158/1541-7786.MCR-18-0412.
- [120] A. Burger-Kentscher, H. Göbel, R. Kleemann, A. Zerneck, R. Bucala, L. Leng, D. Finkelmeier, G. Geiger, H. E. Schaefer, A. Schober, C. Weber, H. Brunner, H. Rütten, C. Ihling, and J. B. Bernhagen. “Reduction of the aortic inflammatory response in spontaneous atherosclerosis by blockade of macrophage migration inhibitory factor (MIF)”. In: *Atherosclerosis* 184.1 (2006), pp. 28–38. DOI: 10.1016/j.atherosclerosis.2005.03.028.
- [121] D. Sinitski, C. Kontos, C. Krammer, Y. Asare, A. Kapurniotu, and J. Bernhagen. “Macrophage Migration Inhibitory Factor (MIF)-Based Therapeutic Concepts in Atherosclerosis and Inflammation”. In: *Thromb Haemost* 119.4 (2019), pp. 553–566. DOI: 10.1055/s-0039-1677803.
- [122] C. Krammer, C. Kontos, M. Dewor, K. Hille, B. Dalla Volta, O. El Bounkari, K. Tas, D. Sinitski, M. Brandhofer, R. T. A. Megens, C. Weber, J. R. Schultz, J. Bernhagen, and A. Kapurniotu. “A MIF-derived cyclopeptide that inhibits MIF binding and atherogenic signaling via the chemokine receptor CXCR2”. In: *Chembiochem* (2020). DOI: 10.1002/cbic.202000574.
- [123] C. Kontos, O. El Bounkari, C. Krammer, D. Sinitski, K. Hille, C. Zan, G. Yan, S. Wang, Y. Gao, M. Brandhofer, R. T. A. Megens, A. Hoffmann, J. Pauli, Y. Asare, S. Gerra, P. Bourilhon, L. Leng, H. H. Eckstein, W. E. Kempf, J. Pelisek, O. Gokce, L. Maegdefessel, R. Bucala, M. Dichgans, C. Weber, A. Kapurniotu, and J. Bernhagen. “Designed CXCR4 mimic acts as a soluble chemokine receptor that blocks atherogenic inflammation by agonist-specific targeting”. In: *Nat Commun* 11.1 (2020), p. 5981. DOI: 10.1038/s41467-020-19764-z.
- [124] C. Stoppe, L. Averdunk, A. Goetzenich, J. Soppert, A. Marlier, S. Kraemer, J. Vieten, M. Coburn, A. Kowark, B. S. Kim, G. Marx, S. Rex, A. Ochi, L. Leng, G. Moeckel, A. Linkermann, O. El Bounkari, A. Zarbock, J. Bernhagen, S. Djudjaj, R. Bucala, and P. Boor. “The protective role of macrophage migration inhibitory factor in acute kidney injury after cardiac surgery”. In: *Sci Transl Med* 10.441 (2018). DOI: 10.1126/scitranslmed.aan4886.
- [125] T. Rassaf, C. Weber, and J. Bernhagen. “Macrophage migration inhibitory factor in myocardial ischaemia/reperfusion injury”. In: *Cardiovasc Res* 102.2 (2014), pp. 321–8. DOI: 10.1093/cvr/cvu071.

- [126] D. Heinrichs, M. L. Berres, M. Coeuru, M. Knauel, A. Nellen, P. Fischer, C. Philippeit, R. Bucala, C. Trautwein, H. E. Wasmuth, and J. Bernhagen. “Protective role of macrophage migration inhibitory factor in nonalcoholic steatohepatitis”. In: *FASEB J* 28.12 (2014), pp. 5136–47. DOI: 10.1096/fj.14-256776.
- [127] D. Heinrichs, E. F. Brandt, P. Fischer, J. Kohncke, T. H. Wirtz, N. Guldiken, S. Djudjaj, P. Boor, D. Kroy, R. Weiskirchen, R. Bucala, H. E. Wasmuth, P. Strnad, C. Trautwein, J. Bernhagen, and M. L. Berres. “Unexpected Pro-Fibrotic Effect of MIF in Non-Alcoholic Steatohepatitis Is Linked to a Shift in NKT Cell Populations”. In: *Cells* 10.2 (2021). DOI: 10.3390/cells10020252.
- [128] E. Rosengren, R. Bucala, P. Aman, L. Jacobsson, G. Odh, C. N. Metz, and H. Rorsman. “The Immunoregulatory Mediator Macrophage Migration Inhibitory Factor (MIF) Catalyzes a Tautomerization Reaction”. In: *Molecular Medicine* 2.1 (1996), pp. 143–149.
- [129] R. Kleemann, A. Kapurniotu, R. W. Frank, A. Gessner, R. Mischke, O. Flieger, S. Juttner, H. Brunner, and J. Bernhagen. “Disulfide analysis reveals a role for macrophage migration inhibitory factor (MIF) as thiol-protein oxidoreductase”. In: *Journal of Molecular Biology* 280.1 (1998), pp. 85–102.
- [130] A. Hermanowski-Vosatka, S. S. Mundt, J. M. Ayala, S. Goyal, W. A. Hanlon, R. M. Czerwinski, S. D. Wright, and C. P. Whitman. “Enzymatically Inactive Macrophage Migration Inhibitory Factor Inhibits Monocyte Chemotaxis and Random Migration”. In: *Biochemistry* 38.39 (1999), pp. 12841–12849. DOI: 10.1021/bi991352p.
- [131] G. Fingerle-Rowson, D. R. Kaleswarapu, C. Schlander, N. Kabgani, T. Brocks, N. Reinart, R. Busch, A. Schutz, H. Lue, X. Du, A. Liu, H. Xiong, Y. Chen, A. Nemajerova, M. Hallek, J. Bernhagen, L. Leng, and R. Bucala. “A tautomerase-null macrophage migration-inhibitory factor (MIF) gene knock-in mouse model reveals that protein interactions and not enzymatic activity mediate MIF-dependent growth regulation”. In: *Mol Cell Biol* 29.7 (2009), pp. 1922–32. DOI: 10.1128/MCB.01907-08.
- [132] G. Pantouris, M. A. Syed, C. Fan, D. Rajasekaran, T. Y. Cho, J. Rosenberg E. M., R. Bucala, V. Bhandari, and E. J. Lolis. “An Analysis of MIF Structural Features that Control Functional Activation of CD74”. In: *Chem Biol* 22.9 (2015), pp. 1197–205. DOI: 10.1016/j.chembiol.2015.08.006.
- [133] D. Rajasekaran, S. Groning, C. Schmitz, S. Zierow, N. Drucker, M. Bakou, K. Kohl, A. Mertens, H. Lue, C. Weber, A. Xiao, G. Luker, A. Kapurniotu, E. Lolis, and J. Bernhagen. “Macrophage Migration Inhibitory Factor-CXCR4 Receptor Interactions: EVIDENCE FOR PARTIAL ALLOSTERIC AGONISM IN COMPARISON WITH CXCL12 CHEMOKINE”. In: *J Biol Chem* 291.30 (2016), pp. 15881–95. DOI: 10.1074/jbc.M116.717751.
- [134] T. Kok, A. A. Wasiel, R. H. Cool, B. N. Melgert, G. J. Poelarends, and F. J. Dekker. “Small-molecule inhibitors of macrophage migration inhibitory factor (MIF) as an emerging class of therapeutics for immune disorders”. In: *Drug Discov Today* 23.11 (2018), pp. 1910–1918. DOI: 10.1016/j.drudis.2018.06.017.
- [135] J. Matsunaga, D. Sinha, L. Pannell, C. Santis, F. Solano, G. J. Wistow, and V. J. Hearing. “Enzyme activity of macrophage migration inhibitory factor toward oxidized catecholamines”. In: *J Biol Chem* 274.6 (1999), pp. 3268–71. DOI: 10.1074/jbc.274.6.3268.

References

- [136] F. Solano, V. J. Hearing, and J. C. García-Borrón. “Neurotoxicity due to o-quinones: neuromelanin formation and possible mechanisms for o-quinone detoxification”. In: *Neurotox Res* 1.3 (2000), pp. 153–69. DOI: 10.1007/BF03033287.
- [137] C. Weber, S. Krämer, M. Drechsler, H. Lue, R. R. Koenen, A. Kapurniotu, A. Zerneck, and J. Bernhagen. “Structural determinants of MIF functions in CXCR2-mediated inflammatory and atherogenic leukocyte recruitment”. In: *PNAS* 105.42 (2008), pp. 16278–16283. DOI: 10.1073/pnas.0804017105.
- [138] S. Kraemer, H. Lue, A. Zerneck, A. Kapurniotu, E. Andreetto, R. Frank, B. Lennartz, C. Weber, and J. Bernhagen. “MIF-chemokine receptor interactions in atherogenesis are dependent on an N-loop-based 2-site binding mechanism”. In: *The FASEB Journal* 25.3 (2011), pp. 894–906. DOI: 10.1096/fj.10-168559.
- [139] L. Xu, Y. Li, D. Li, P. Xu, S. Tian, H. Sun, H. Liu, and T. Hou. “Exploring the binding mechanisms of MIF to CXCR2 using theoretical approaches”. In: *Phys Chem Chem Phys* 17.5 (2015), pp. 3370–82. DOI: 10.1039/c4cp05095a.
- [140] R. Panstruga, K. Baumgarten, and J. Bernhagen. “Phylogeny and evolution of plant macrophage migration inhibitory factor/D-dopachrome tautomerase-like proteins”. In: *BMC Evol Biol* 15 (2015), p. 64. DOI: 10.1186/s12862-015-0337-x.
- [141] C. Michelet, E. G. J. Danchin, M. Jaouannet, J. Bernhagen, R. Panstruga, K. H. Kogel, H. Keller, and C. Coustau. “Cross-Kingdom Analysis of Diversity, Evolutionary History, and Site Selection within the Eukaryotic Macrophage Migration Inhibitory Factor Superfamily”. In: *Genes (Basel)* 10.10 (2019). DOI: 10.3390/genes10100740.
- [142] M. Jaouannet, A. S. Pavaux, S. Pagnotta, O. Pierre, C. Michelet, S. Marro, H. Keller, R. Lemee, and C. Coustau. “Atypical Membrane-Anchored Cytokine MIF in a Marine Dinoflagellate”. In: *Microorganisms* 8.9 (2020). DOI: 10.3390/microorganisms8091263.
- [143] D. C. Jaworski, A. Jasinkas, C. N. Metz, R. Bucala, and A. G. Barbour. “Identification and characterization of a homologue of the pro-inflammatory cytokine Macrophage Migration Inhibitory Factor in the tick, *Amblyomma americanum*”. In: *Insect Molecular Biology* 10.4 (2001), pp. 323–331. DOI: 10.1046/j.0962-1075.2001.00271.x.
- [144] D. Kamir, S. Zierow, L. Leng, Y. Cho, Y. Diaz, J. Griffith, C. McDonald, M. Merk, R. A. Mitchell, J. Trent, Y. Chen, Y. K. Kwong, H. Xiong, J. Vermeire, M. Cappello, D. McMahon-Pratt, J. Walker, J. Bernhagen, E. Lolis, and R. Bucala. “A *Leishmania* ortholog of macrophage migration inhibitory factor modulates host macrophage responses”. In: *J Immunol* 180.12 (2008), pp. 8250–61. DOI: 10.4049/jimmunol.180.12.8250.
- [145] S. Ghosh, N. Jiang, L. Farr, R. Ngoben, and S. Moonah. “Parasite-Produced MIF Cytokine: Role in Immune Evasion, Invasion, and Pathogenesis”. In: *Front Immunol* 10 (2019), p. 1995. DOI: 10.3389/fimmu.2019.01995.
- [146] D. Sinitski, K. Gruner, J. Bernhagen, and R. Panstruga. “Studying Plant MIF/D-DT-Like Genes and Proteins (MDLs)”. In: *Macrophage Migration Inhibitory Factor: Methods and Protocols*. Ed. by J. Harris and E. F. Morand. New York, NY: Springer US, 2020, pp. 249–261. ISBN: 978-1-4939-9936-1. DOI: 10.1007/978-1-4939-9936-1_22.
- [147] R. Bucala. “A most interesting factor”. In: *Nature* 408 (2000), pp. 146–147.

- [148] Z. Feng, G. R. Dubyak, X. Jia, J. T. Lubkowski, and A. Weinberg. “Human beta-defensin-3 structure motifs that are important in CXCR4 antagonism”. In: *FEBS J* 280.14 (2013), pp. 3365–75. DOI: 10.1111/febs.12328.
- [149] K. Gruner, F. Leissing, D. Sinitski, H. Thieron, C. Axstmann, K. Baumgarten, A. Reinstadler, P. Winkler, M. Altmann, A. Flatley, M. Jaouannet, K. Zienkiewicz, I. Feussner, H. Keller, C. Coustau, P. Falter-Braun, R. Feederle, J. Bernhagen, and R. Panstruga. “Chemokine-like MDL proteins modulate flowering time and innate immunity in plants”. In: *J Biol Chem* (2021), p. 100611. DOI: 10.1016/j.jbc.2021.100611.
- [150] M. Brandhofer, A. Hoffmann, X. Blanchet, E. Siminkovitch, A.-K. Rohlfing, O. E. Bounkari, J. A. Nestele, A. Bild, C. Kontos, K. Hille, V. Rohde, A. Fröhlich, J. Golemi, O. Gokce, C. Krammer, P. Scheiermann, N. Tsilimparis, W. E. Kempf, L. Maegdefessel, R. T. Megens, H. Ippel, R. R. Koenen, K. H. Mayo, M. Gawaz, A. Kapurniotu, C. Weber, P. von Hundelshausen, and J. Bernhagen. “Heterocomplexes between the Atypical Chemokine MIF and the CXC-Motif Chemokine CXCL4L1 Regulate Inflammation and Thrombus Formation”. In: *bioRxiv (Preprint)* (2022). DOI: 10.1101/2021.11.26.470090.
- [151] H. Jung, T. Kim, H. Z. Chae, K. T. Kim, and H. Ha. “Regulation of macrophage migration inhibitory factor and thiol-specific antioxidant protein PAG by direct interaction”. In: *J Biol Chem* 276.18 (2001), pp. 15504–10. DOI: 10.1074/jbc.M009620200.
- [152] P. Artimo, M. Jonnalagedda, K. Arnold, D. Baratin, G. Csardi, E. de Castro, S. Duvaud, V. Flegel, A. Fortier, E. Gasteiger, A. Grosdidier, C. Hernandez, V. Ioannidis, D. Kuznetsov, R. Liechti, S. Moretti, K. Mostaguir, N. Redaschi, G. Rossier, I. Xenarios, and H. Stockinger. “ExpASY: SIB bioinformatics resource portal”. In: *Nucleic Acids Res* 40.Web Server issue (2012), W597–603. DOI: 10.1093/nar/gks400.
- [153] J. Bernhagen, R. A. Mitchell, T. Calandra, W. Voelter, A. Cerami, and R. Bucala. “Purification, Bioactivity, and Secondary Structure Analysis of Mouse and Human Macrophage Migration Inhibitory Factor (MIF)”. In: *Biochemistry* 33 (1994), pp. 14144–14155.
- [154] A. Sarabi, B. K. Kramp, M. Drechsler, T. M. Hackeng, O. Soehnlein, C. Weber, R. R. Koenen, and P. Von Hundelshausen. “CXCL4L1 inhibits angiogenesis and induces undirected endothelial cell migration without affecting endothelial cell proliferation and monocyte recruitment”. In: *J Thromb Haemost* 9.1 (2011), pp. 209–19. DOI: 10.1111/j.1538-7836.2010.04119.x.
- [155] M. M. Bradford. “A Rapid and Sensitive Method for the Quantitation of Microgram Quantities of Protein Utilizing the Principle of Protein-Dye Binding”. In: *Analytical Biochemistry* 72 (1976), pp. 248–254. DOI: 10.1006/abio.1976.9999.

Acknowledgements

As scientific progress is rarely achieved without a collaborative, multidisciplinary environment, fostering both scientific as well as personal interactions, I would like to express my gratitude towards a number of persons, who were involved in this work and made it possible:

First of all, I would like to thank Prof. Dr. rer. nat. Jürgen Bernhagen for his supervision and support during my work in his lab, here in Munich as well as back in Aachen where I first joined the group for my Master Thesis. I could not have imagined, back then when I started working on MIF, that later on I would stay to pursue a doctoral degree, let alone that this path would also lead me back home to Bavaria. I appreciate the opportunity to be involved in many interesting projects, but also for the experience that came with relocating the lab – starting with only a few people initially, watching the group grow and develop over the years.

Furthermore, large thanks go to my colleagues in the Bernhagen as well as Gökce Lab, whom I shared many years and experiences at the bench with, for countless discussions, exchange of advice and keeping me motivated. First to mention here are Adrian Hoffmann and the whole “*Interacteam*”, Elena Siminkovitch and Vanessa Rohde, who offered their hands and minds to help pushing the interactome project forward, investigating multiple interaction partners apart from CXCL4L1 in their work. But also other current and former lab members shall be mentioned here – to name a few, in no particular order: Dzmitry Sinitski (my long-year desk- and benchmate, full of words, ideas and a unique mindset), Simona Gerra (Thank you not only for the support and personal discussions, but also for your constant fight with the ÄKTA to purify all the MIF that we needed!), Omar El Bounkari (another familiar face from Aachen, providing ideas, help and both challenging and insightful discussions), and many more. You all made my time here into the unique experience that it was!

I also want to thank external collaboration partners and colleagues that played pivotal roles in this work: Xavier Blanchet, who initially helped out with a side project that soon developed into a – sometimes challenging but always fascinating – main project, taught us how (and from whom) best to isolate thrombocytes and somehow always pulled out materials and reagents from some hidden drawers when our stocks ran dry. Here I should also thank Christos Kontos, who provided not only technical expertise – like when troubleshooting issues with HPLC columns or checking for unwanted methionines on MIF – during this journey Odyssey, but also a sprinkle of Greek mythology and various peptides to keep us busy.

Apart from my colleagues, most importantly my gratitude belongs to my dear parents, Christine and Paul Brandhofer. While I cannot tell what may initially have ignited my interest in science, way back in my childhood, I *do* know it was thanks to them that this spark could grow – ultimately leading to me now writing these lines while finalizing my PhD thesis. Thank you, for always being there for me during this journey and throughout my life!

At this point I would also like to express my gratitude to Christian Sachs, for standing by my side and encouraging me during this exciting – and sometimes challenging – period, both in Jülich and Munich (and in between), keeping me going.

Last but certainly not least, I'd like to thank all my friends who supported me during the time of this work, no matter the distance and circumstances.

Curriculum Vitæ

Personal Information

Full name: Markus Brandhofer

Place of birth: Munich

Professional Experience

- 2016.04–2021.09** Research staff member and doctoral candidate Munich
Department of Vascular Biology (Group of Prof. Bernhagen)
Institute for Stroke and Dementia Research (ISD), LMU Klinikum
- 2014.11–2016.04** Research staff member and doctoral candidate Aachen
Institute for Biochemistry and Molecular Cell Biology (Group of Prof. Bernhagen)
RWTH Aachen University
- 2014.06–2014.09** Student assistant Aachen
At the Institute for Biochemistry and Molecular Cell Biology, RWTH Aachen University:
Supervision of practical courses in biochemistry for medical students.

Education

- 2014–2022** Doctoral studies (Dr. rer. nat.) Munich, Aachen
Ludwig-Maximilians-University (LMU) Munich
Faculty of Medicine, Department of Vascular Biology at the Institute for Stroke and Dementia Research (ISD). Initially started at the Institute for Biochemistry and Molecular Cell Biology at RWTH Aachen University, moved with Professor's lab to LMU Munich.
Thesis: "*Interactions between MIF-family proteins and the classical chemokine ligand/receptor network*"
- 2012–2014** **Master of Science**, Biotechnology Jülich
FH Aachen University of Applied Sciences
Thesis: "*Influence of the cytokine MIF on the expression of Gpr25 in the liver*" (official title was in German), performed at the Institute for Biochemistry and Molecular Cell Biology at RWTH Aachen University.
- 2009–2012** **Bachelor of Science**, Biotechnology Jülich
FH Aachen University of Applied Sciences
Thesis: "*Generation and characterization of DHS-overexpressing plants (Arabidopsis thaliana (L.) HEYNH.)*" (official title was in German), performed at the Growth and Metabolism Research Group, Institute for Bio- and Geosciences 2 – Plant Sciences at Forschungszentrum Jülich GmbH.

2005–2009 Biotechnology (Dipl.-Ing. (FH) studies, discontinued and resumed at Freising
FH Aachen University of Applied Sciences.)
Weihenstephan-Triesdorf University of Applied Sciences

Awards & Other Activities

2021.10.21 m⁴ Award 2021 – Project SELECKREM Munich
Won the m⁴ Award competition for start-up pre-seed funding of the Bavarian Ministry
of Economic Affairs, Regional Development and Energy, supported by the Bio^M Biotech
Network, as part of the SELECKREM project team with Prof. Dr. J. Bernhagen, Prof. Dr.
A. Kapurniotu and C. Kontos.

2021.10.19 Poster Competition Award Venice
9th Cardiac Regeneration and Vascular Biology Conference

2007.03–2007.07 Internship Dr. Graner & Partner GmbH Munich
Laboratory for chemical-physical and microbiological analysis and bureau of expertise

Trainings & Certificates

“*FELASA B Course*” on laboratory animal science and experimentation
(RWTH Aachen University)


Qualification for Project Lead in Biosafety matters according to German GenTSV
(KölnPUB e.V., Frechen, “Projektleiterkurs”)


DGQ seminar regarding statistical sample inspection
(German Association for Quality, “Statistische Lieferantenbewertung”)

Social Media Profiles

 [researchgate.net/profile/Markus_Brandhofer](https://www.researchgate.net/profile/Markus_Brandhofer)

 twitter.com/M_Brandhofer

 [linkedin.com/in/Markus-Brandhofer](https://www.linkedin.com/in/Markus-Brandhofer)

 [xing.com/profile/Markus_Brandhofer](https://www.xing.com/profile/Markus_Brandhofer)